Anthraniloyl-derived Nucleotides as potent and selective Adenylyl Cyclase Inhibitors

Dissertation

Zur Erlangung des Doktorgrades der Naturwissenschaften

(Dr. rer. nat.)

an der Fakultät für Chemie und Pharmazie

der Universität Regensburg

vorgelegt von

Jens Geduhn

aus Cloppenburg

2009

The experimental part of this work was carried out between March 2005 and October 2008 at the Institute for Organic Chemistry and the Department of Pharmacology and Toxicology at the University of Regensburg under the supervision of Prof. Dr. B. König and Prof. Dr. R. Seifert.

The PhD – thesis was submitted on: 27. March 2009

The colloquium took place on: 30. April 2009

Board of Examiners: Prof. Dr. J. Schlossmann   (Chairman)

Prof. Dr. B. König   (1st Referee)

Prof. Dr. R. Seifert   (2nd Referee)

Prof. Dr. G. Schmeer   (Examiner)

Danksagung

Mein persönlicher Dank gilt meiner Frau Sonja für ihre Liebe, ihre Unterstützung und ihr Verständnis zu jeder Zeit und unserem Sonnenschein Sophie Marie danke ich dafür, die Welt mit neuen Augen zu sehen.

Zuletzt, aber vor allem, danke ich meiner Familie für ihre großartige Unterstützung und den großen Rückhalt während meines gesamten Studiums.

Ein Gelehrter in seinem Laboratorium ist nicht nur ein Techniker,

er steht vor den Naturgesetzen wie ein Kind vor der Märchenwelt.

Marie Curie

In memoriam patris mei.

Für Sonja

&

Sophie Marie

Table of Contents

I. Adenylyl Cyclases

1. General Introduction

1.1 Mammalian Adenylyl Cyclases

In intracellular signaling pathways adenosine 3',5'-cyclic monophosphate (cAMP) is a key player as second messenger in the response to first messenger signaling molecules such as neurotransmitters, hormones, and odorants. Until recently, the signaling by this archetypal second messenger was considered to be understood and straightforward, but fifty years after its discovery by Earl Sutherland cAMP regulation has become very complex. By direct activation of nucleotide-gated ion channels and stimulation of protein phosphorylation via activation of protein kinase A (PKA), cAMP is known to be involved in modulation of membrane potential and the rate of cell division[1,2,3]. Independently of any phosphorylation, cAMP also induces protein-protein interactions, *e.g.* in signaling of Rap1 proteins[4,5]. The high complexity of synthesis and degradation of the second messenger is also due to a multiplicity of phosphodiesterases and adenylyl cyclase (AC) isoforms.

The modulation of AC activity is the key step in intracellular cAMP regulation by extracelluar stimuli. In mammals, the major ACs are integral plasma-membrane proteins; they catalyze the synthesis of cAMP and pyrophosphate (PP_i) by conversion of adenosine 5'-triphosphate (ATP)[6,7,8]. ACs act as effector enzymes integrating extracelluar signals by G-protein coupled receptors (GPCRs) to a variety of intracellular signaling pathways[9,10]. The classic receptor-G-protein-AC signal transduction cascade is characterized by a large excess of G-proteins compared to receptor and effector molecules (**Fig. 1**). Therefore, G-proteins are the major amplification factor of the GPCR signal[11,12] and the AC molecules are the limiting component for maximum second messenger production in response to hormone stimulation[10,13]. Although ACs do not contribute extensively to the amplification of intracellular signaling, they participate in diverse manners to integrate signaling pathways and cross-talks in different cell systems[14,15].

Once, in 1968, the signal cascade proposed by Robinson *et al.* was considered to be simple[2], but today, the growth in knowledge about ACs and stoichiometric relationships between the membranous components leads to better understanding of this fundamental area of pharmacological research.

Fig. 1. Transmembrane signal transduction
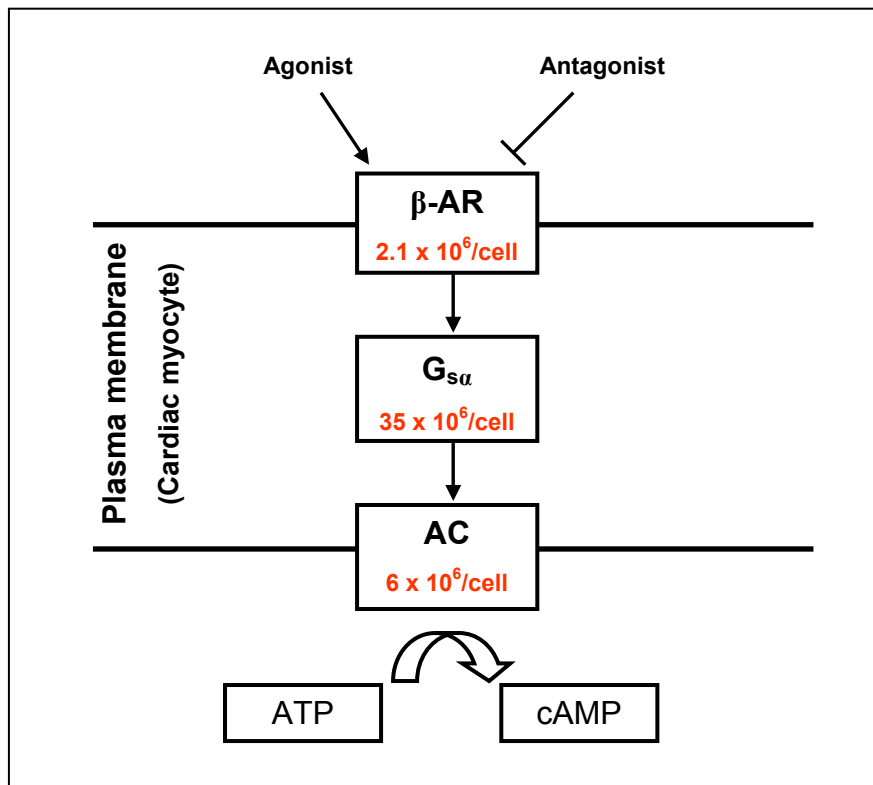
Stoichiometric relationship of receptor-G-protein-effector molecules in the β-adrenergic-receptor mediated signal transduction was adapted based on the results of Post *et. al.*[11,12]. The basic transmembrane signal transduction cascade (GPCR – G-protein – AC) is shown by the receptor (2.1 x 10^6 β-AR molecules/cell), $G_{s\alpha}$ in large excess (35 x 10^6 molecules/cell), and AC protein (6 x 10^6 AC molecules/cell). Based on these results similar ratios were hypothesized for other signaling systems[12].

Structure of adenylyl cyclases

After the first cloning of a mammalian adenylyl cyclase gene by Krupinski *et al.*, so far, nine closely related isoforms of membrane-bound ACs (mACs) and one soluble form (sAC) have been cloned and characterized in mammals[15,16,17,18]. Although each AC isoform exhibits its own tissue distribution and special biochemical properties, they all share the same three-dimensional structure with a large homology in their amino acid sequence[8,19,20]. All mACs consist of two hydrophobic stretches with six proposed α-helices each (M1 and M2) in the plasma membrane and of two cytoplasmatic domains C1 and C2 forming together the catalytical core of ACs (**Fig. 2**). These intracellular domains are further divided into "a" and "b" subdomains[21]. The units of $C1_a$ and $C2_a$ are responsible for ATP binding and catalysis as assessed by systematic mutational analysis[19]. Moreover, the ~230 amino acid long region of $C1_a$ and $C2_a$ shares 50 % to 90 % high sequence homology

among different AC isoforms. The subdomains $C1_b$ and $C2_b$ display less conserved regions among mammalian ACs. Recent studies may serve for better understanding of these subunits, proposing a role as isoform-specific regulatory domains, especially for $C1_b$[22]. The knowledge about the transmembrane domains is still rather limited with the exception of their membrane anchoring function and coordination of C1/C2 interaction[6,23].

It should be noted that the soluble AC isoform in mammals is structurally different from membranous ACs and related to cyanobacterial ACs[15,24]. Interestingly, inhibition of sAC may be useful as male contraceptives, because sAC is important for spermatocyte function[25].

Fig. 2. Structure of membranous adenylyl cyclases
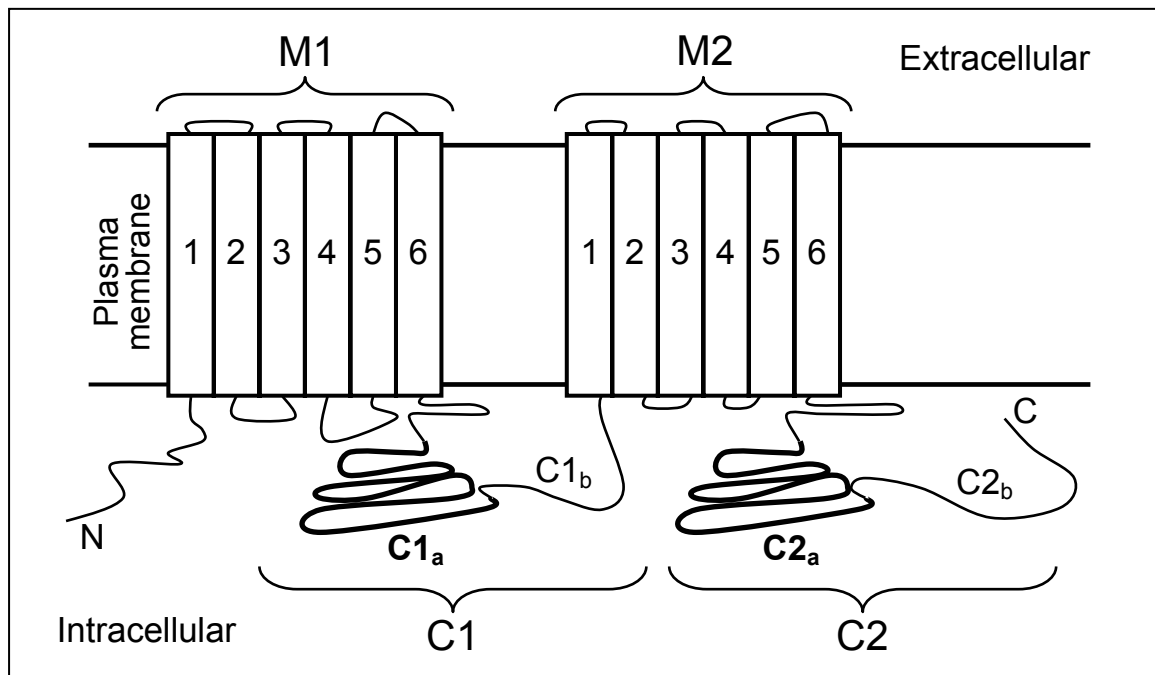
Schematic model of the proposed structure of membrane-bound adenylyl cyclase[6,19,23] shows the N-terminus (N), two hydrophobic domains (M1 and M2) with six transmembrane spans each, two cytosolic domains (C1 and C2) and the C-terminus (C). The intracellular domains are further divided into $C1_a$/$C1_b$ and $C2_a$/$C2_b$. The catalytical core is formed by $C1_a$ and $C2_a$.

Tissue distribution and (patho)physiological functions

Due to low expression levels of mACs and the lack of high-quality antibodies, the exact determination of the tissue distribution of AC isoforms is difficult to assess. Although each mAC isoform exhibit its own unique form of tissue distribution in terms of mRNA, some overlap is observed. All mammalian AC isoforms are expressed in the central nervous system, and especially mACs 1, 2, and 8 are mainly expressed in the brain[26] and implicated in synaptic plasticity, memory, learning, and long-term potentiation (LTP)[27]. Furthermore, AC2 is predominantly expressed in the lungs. For olfaction, the major AC isoform in the olfactory neuroepithelium is AC3[28]. Interestingly, AC5 and AC6 are equally expressed in the heart at birth, but in adulthood AC5 becomes the major cardiac isoform[29]. Moreover, a further specific tissue distribution of AC5 and AC6 was observed in the kidney, mainly in the *Medulla renalis*[30]. The other mACs 4, 7, and 9 are widely expressed in several tissues, like brain, lung, kidney, or liver[31].

Knockout (KO) and transgenic animal models for AC research are feasible tools to assess the functional relevance of specific isoform expression in different tissues[32]. The results of KO-studies may be discussed controversially, *i.e.* AC1-KO mice showed impaired cerebellar LTP and somatosensory cortex development[33]. In contrast, the AC1-KO mice were protected against neuronal toxicity by ionotropic glutamate receptors[34]. Accordance is achieved to large extent for AC5-KO results. In a model of heart failure, AC5-KO improves heart function[35]. Furthermore, these mice were protected against stress and showed reduced chronic pain responses as well as increased longevity[36]. Thus, AC1/5 inhibitors may be useful drugs for the treatment of various age-related ailments including heart failure, neurodegenerative diseases, stroke and chronic pain[37].

Finally, experiments with AC3-KO mice indicated anosmia[38] and AC8-KO mice revealed altered stress-induced anxiety responses[39]. So far, no experiments with AC4 and AC9 KO mice are reported.

AC regulation mechanisms

Overall, the regulation mechanisms of ACs are not simple and straightforward. In fact, in detail, the modulations are very diverse and complex due to the different regulatory properties of each AC isoform[19,40]. The best understood mechanism of AC

regulation is characterized by agonist activated GPCRs and subsequent stimulation of $G_{s\alpha}$[41]. Although this signaling pathway is a common regulatory mechanism for activation of all AC isoforms, the affinity for $G_{s\alpha}$ is different for each isoform. A very potent and direct activator of mACs 1 – 8 is the diterpene forskolin (FS) from the roots of the Indian plant *Coleus forskohlii*[40,42], but AC9 is not activated by FS[43].

G-proteins are also modulators for AC inhibition in an isozyme-specific manner, *i.e.* $G_{i\alpha}$ inhibits AC5, AC6 and calmodulin-stimulated AC1[44]. AC2 is not influenced by $G_{i\alpha}$[45]. The $\beta\gamma$-subunits of G-proteins exhibit an inhibitory effect on ACs 1, 5, and 6, but a stimulatory effect on ACs 2, 4, and 7[18]. Protein kinases are a further instrument in AC regulation. Due to direct phosphorylation by cAMP-dependant protein kinase, AC5 and AC6 are inhibited. AC phosphorylation by PKA disrupts binding of $G_{s\alpha}$ to AC, causing inactivation[46].

In contrast to PKA, protein kinase C (PKC) activates several AC isoforms (ACs 1, 2, 3, 5 and 7). The stimulatory effect of PKC-mediated phosphorylation on the activity of these specific ACs is synergistic with the stimulation by FS and $G_{s\alpha}$[15]. However, the activity of $G_{s\alpha}$-stimulated AC4 and AC6 is reduced by PKC[47]. Moreover, the divalent cations of Mg^{2+} and Mn^{2+} exhibit different stimulatory effects on all mAC isoforms[48]. Another important divalent cation, especially in complex with calmodulin (CaM), is Ca^{2+}. The Ca^{2+}/CaM complex directly activates AC isoforms 1, 3, and 8 by a putative binding site located closely to the catalytical core of ACs[49] and integrates into a high synergism with $G_{s\alpha}$ stimulation[50]. In contrast, the closely related isoforms of AC5 and AC6 are inhibited by physiological concentrations of Ca^{2+}-ions in submircomolar concentrations. All other AC isoforms are inhibited by supraphysiological Ca^{2+} levels (submillimolar concentrations)[51]. Because of the different patterns of regulation and specificity of the regulatory mechanism, individual AC isoforms are relevant in specific tissues and subcellular localization. Thus, the most abundant mAC isoforms in the brain are Ca^{2+}/CaM-activated ACs facilitating distribution of signals mediated by cAMP. ACs 1 and 8 play an important role in memory function and LTP[9,52]. In comparison to CaM-activated ACs, AC5 and AC6, mainly expressed in the heart, are inhibited by Ca^{2+}. AC activation is followed by activation of L-type Ca^{2+} channels and an increase of intracellular Ca^{2+} concentrations in the heart. This increase of Ca^{2+} displays a downstream and negative feedback in regulatory mechanism in AC catalysis.

Catalytic mechanism of mACs

Crystallographic and mutational studies have shown the fundamental requirement of the cytosolic domains C1 and C2 for maximum AC catalysis in the presence of activators like FS and $G_{s\alpha}$.(**Fig. 3**)[53].

Fig. 3. Crystal structure of catalytic domains VC1 and IIC2
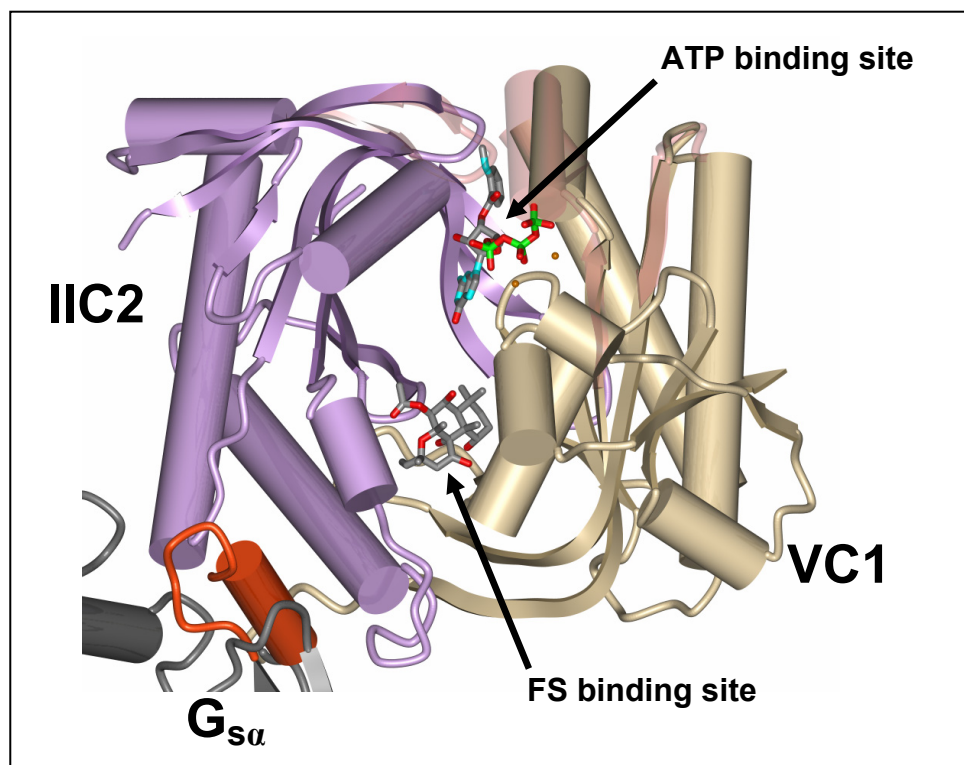
Crystallography of catalytic domains of C1 from AC5 (VC1) and C2 from AC2 (IIC2) together with $G_{s\alpha}$ adapted from Mou *et al*.[53]. The VC1 and IIC2 domains are colored tan and mauve, $G_{s\alpha}$ is shown as a red cylinder. FS and the ATP substrate analog MANT-GTP are drawn as stick models. The two Mn^{2+} ions are shown as metallic orange spheres.

Although the two domains C1 and C2 are very homologous to each other, they possess different functional properties[54]. The interface between C1/C2 domains is formed by interacting polar and charged regions. In the C2 domain asparagine 1025 and aspartic acid 1029 are the two most crucial amino acid residues for catalysis identified by mutagenesis and kinetic studies. However, these two amino acids are not conserved in the C1 domain, e.g. exchange by tyrosine for Asp1025[55]. Mutation of Asp354 in AC1 leads to almost complete loss of catalytical activity[19]. In addition, Lys1067 (AC2) located in the carboxyl-terminal region, is a further crucial amino acid and confers specificity to adenine[56]. Recent studies illustrate that mutations of some

residues at C2 (Ile1010Met, Lys1014Asn, Pro1015Glu, AC5) leading to constitutive activation of AC and increased association of C1/C2[57,58]. The precise alignment of these residues forming the catalytic core is required for substrate binding (ATP) and catalysis (cAMP formation). Thus, different AC regulators change the relative orientation of C1/C2 and the position of these active site residues within the catalytical binding pocket. A model for the enzymatic mechanism of AC was firstly proposed by Tang and Hurley[8]. They hypothesized that AC cycles between several conformational states (**Fig. 4**).

Fig. 4. Proposed model of the catalytic cycle of AC
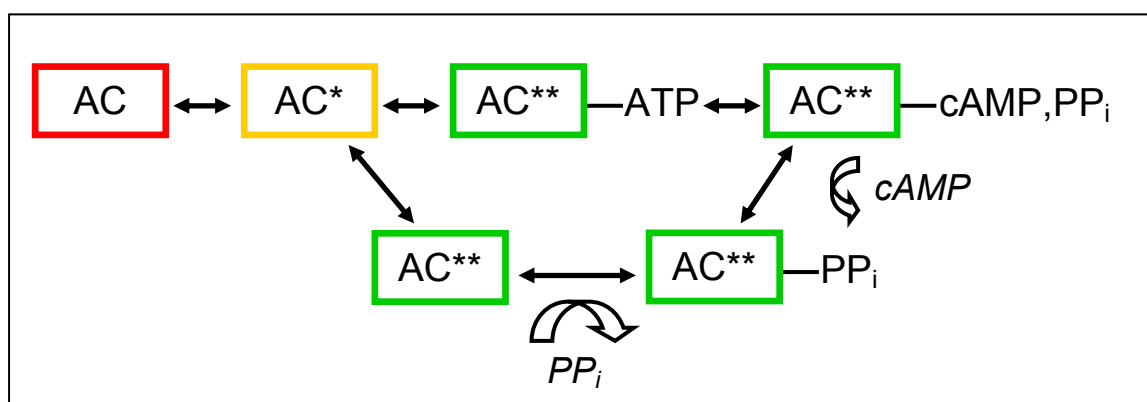
A schematic representation of the proposed catalytic cycle of AC adapted from Tang and Hurley is shown[8]. Activators cause conformational change in the enzyme to go from the inactive (AC) to the substrate-free activated state (AC*). In its active state, the enzyme is inactive for catalysis, but open for the substrate ATP. ATP binding leads to further conformational changes. Now, this active substrate-bound state (AC**-ATP) allows the catalytic reaction to cAMP and pyrophosphate (PP_i) (AC** - cAMP, PP_i) in the closed conformation. After catalysis and release of the products (cAMP followed by PP_i) AC returns to the substrate-free activated state (AC** and AC*) and eventually to its ground state (AC).

The model includes at least three conformational states, *i.e.* an inactive state (AC), a substrate-free activated state (AC*), and a substrate/product-bound state (AC**-ATP and AC**-cAMP, PP_i). ACs convert ATP to cAMP without a covalently enzyme-bound intermediate with turnover numbers of 1 to 100 sec^{-1} [59]. The enzymatic reaction is sequential and bireactant requiring Mg^{2+}-ATP and free Mg^{2+} [60]. The key step in the reaction mechanism proceeds by the inversion of configuration at the α-phosphate, consistent with a direct in-line displacement of pyrophosphate by attack of the 3'-OH on the α-phosphate[59]. The catalytic cycle is proposed as follows: the catalytic region (C1/C2) of AC undergoes a conformational transition (AC→AC*) that is promoted by

activators like FS or $G_{s\alpha}$, or is blocked by inhibitors like $G_{i\alpha}$. Although with ~10-fold lower affinity than for ATP, AC binds to GTP, but it is not used as a substrate. Therefore, substrate binding (ATP) has to induce a further conformational change (AC*→AC**) which enables the enzyme to confirm its substrate (proof reading) and proceed through catalysis. After the conversion, the AC* state could reform either before or after release of the product. The release of cAMP first may be favorable. Further structural characterization of the conformational changes on activation and during the enzyme reaction cycle will be critically important.

Furthermore, AC may exist in different catalytic, inactive, and transitional states of conformation[8,58]. Stabilization of different conformations of AC may significantly change the binding mode of ATP and in consequence the catalytic activity of AC in an isozyme-specific manner. Nevertheless, the precise molecular mechanism of AC catalysis is still incomplete understood, due to the lack of crystallographic structures of holo ACs with substrate or substrate analogs.

1.2 Bacterial Adenylyl Cyclases

Exotoxin AC of *Bordetella pertussis* (CyaA)

Expression of ACs is not limited to mammals and extended to other organisms like bacteria[8]. Interestingly, mammalian sAC exhibit high homology to AC of cyanobacteria[15,24]. In the evolutionary perspective, ACs of bacteria are the ancestors of mammalian second messenger signaling systems. Especially, cyanobacteria and their precursors are known to be one of the oldest species populated on Earth, dating back to more than three billion years[61]. Beside the appearance of intracellular ACs in bacteria, secretions of some bacteria contain exotoxin ACs as well. One representative AC exotoxin is CyaA of *Bordetella pertussis*, the bacterium causing whooping cough, a highly contagious acute disease of the respiratory tract[62,63].

Whooping cough (or pertussis) is both, the name and the most dominant symptom of this illness affecting young infants most severely. According to the literature, the first description of a whooping cough epidemic in France was in 1578 by Guillaume de Baillou[64]. Other descriptions like the *Perinthus cough* go back to Hippocrates (around 400 B.C.) and may also indicate whooping cough[65]. The clinical course is divided into three stages. After the incubation period (5 to 10 days) the illness starts with the catarrhal phase and lasts usually 1 to 2 weeks characterized by low-grade fever, rhinorrhea and progressive cough. The subsequent stage is determined by the paroxysmal phase (several weeks), causing severe spasmodic cough episodes with a characteristic whoop with cyanosis and vomiting. In between the attacks the patients often perform normally. Paroxysmal attacks occur more frequently at night with an average of 15 attacks per 24 hours. Although young infants (under 6 months of age) may not have the strength to whoop, they could exhibit paroxysms of coughing. A further risk of an absent cough is displayed by spells of apnoea[66]. The third and last phase of reconvalescence (1 to 3 weeks) is characterized by a continuous decline of the cough before the patient returns to normal. However, paroxysms could recur with subsequent respiratory infections for many months after the onset of pertussis. In general, fever only occurs minimally in the course of infection.

Infection results in colonization and rapid multiplication of *Bordetella pertussis* on the mucous membranes of the respiratory tract. The immobile and aerobic bacterium produces a number of virulence factors, which includes adenylyl cyclase toxin

(CyaA), pertussis toxin, filamentous haemagglutinin, fimbriae, tracheal cytotoxin, pertactin and dermonecrotic toxin. The *bvg* locus regulates the expression of these factors and assures the compound synthesis in response to certain environmental stimuli[67].

The key virulence factor of *Bordetella pertussis* is represented by the adenylyl cyclase toxin CyaA[62,63]. The exotoxin consists of 1706 amino acids and is divided into two functional parts. The N-terminal domain (400 amino acids) contains the active center for catalysis and the 1300 amino acid C-terminal domain interacts with eukaryotic host cells for delivery of the catalytic domain into the cytosol[68]. Moreover, the C-terminal residue possesses low hemolytic activity[63]. The endogenous calcium sensor calmodulin (CaM) activates CyaA toxin with high affinity by forming salt bridges, hydrogen bonds, and hydrophobic interactions[69]. After activation of the bacterial adenylyl cyclase a massive production of the second messenger cAMP from ATP is catalyzed[70]. The supraphysiological level of cAMP disrupts the endogenous signal transduction, inhibits phagocyte function, and facilitates respiratory tract infection by *Bordetella pertussis*[71]. Substrate analogs of ATP may be used to inhibit the catalytic activity of CyaA[72] and prophylaxis of *Bordetella pertussis* infection.

20 – 40 million cases of pertussis infections are diagnosed per year world-wide, with a 90% ratio of occurrence in developing countries and estimated 200,000 – 400,000 fatalities each year[73]. However, over the last decade many industrial nations observe a re-emergence of whooping cough, even in countries with high vaccination coverage. Older children and adults are susceptible to be infected again because of waning naturally derived and vaccine-induced immunity. Thus, infection frequency is probably highest in adolescents and adults and in consequence those age groups are the main source of infection for infants[62]. In combination with an increase in tiredness for primary vaccination of infants and secondary vaccination of adults, this fact is alarming[74]. For classical antibiotic therapy drugs like azithromycin and clarithromycin are recommended.

Nevertheless, toxemia and antibiotic-resistant strains of conventional antibiotic treatment set application limits, demanding more effective drugs for the prophylaxis of whooping cough.

Exotoxin AC of *Bacillus anthracis* (Edema factor)

Another interesting field of research is the AC exotoxin edema factor (EF) of the bacterium *Bacillus anthracis*[75]. This bacterium causes the infectious disease of anthrax in humans and animals[76]. Bacillus anthracis is one of only a few bacteria forming long-lived spores[75], which could survive for many decades or even centuries in a hostile environment. Thus, herbivorous mammals like cloven-hoofed animals are probably infected by ingesting or inhaling the spores while eating grass. Humans can also be infected by the bacilli by three different modes (ingestion, inhalation, cutaneous lesions), causing distinct clinical symptoms based on its site of entry. If bacteria enter a cut or abrasion on the skin, cutaneous anthrax (the most common type) includes symptoms of a raised, itchy blister which eventually becomes a painless necrotic ulcer. This type of anthrax responds well to early therapy with antibiotics. Gastrointestinal anthrax is rare, but humans can acquire this form from eating meat contaminated with *Bacillus anthracis* or their spores. Typical symptoms are stomach pain, bloody diarrhea, nausea, and blood vomit. After the invasion of the bowel system the bacteria spread through the bloodstream throughout the body. Compared to cutaneous anthrax, gastrointestinal anthrax therapy is less successful and results in a mortality rate of 25 % to 60 %. The least common but most threatening infection pathway is by inhalation. This type of anthrax has also been called wool sorter's disease because it is an occupational hazard for people who sort wool, inhaling spore-bearing dust. Spores are further transported through the air passages into the alveoli in the lungs. Picked up by macrophages, the bacilli enter the lymph nodes in the central chest cavity, where the spores transform into active reproducing bacteria. The respiratory infection with cold or flu-like symptoms is rarely treated efficiently, causing death rate of nearly 100 %[77]. A lethal infection is reported by inhalation of about 2,500 – 55,000 spores[78], depending on the host species. Moreover, this type of infection is disreputably used in biological warfare[79] and in terroristic attacks[80].

The discovery of *Bacillus anthracis* is based on the research of the German physician Robert Koch in the 1870s, who was the first to draw the conclusion that a bacterium causes a disease in mammals. The scientist cultivated the anthrax organisms taken from dead farm animals on microscopic slides and demonstrated the relation between bacillus and disease by the growing bacteria into long filaments.

The gram-positive *Bacillus anthracis* exerts its deleterious effects by production of

three major exotoxins: EF, protective antigen, and lethal factor[75]. EF and lethal factor enter host cells via a complex with membrane-associated protective antigen, which acts as a pH-dependent protein transporter. Lethal factor, a specific zinc-metalloprotease, inactivates mitogen-activated protein kinase[81]. EF possesses ~800 amino acid residues and an apparent molecular mass of ~89 kDa and is a CaM-dependent AC[82]. After entering host cells, EF forms a complex with CaM, the mammalian regulatory protein, (as described before with CyaA toxin), that mediates many aspects of calcium-regulated signaling[83]. The binding of CaM induces a major conformational change in the catalytic domain of EF[82]. This rearrangement renders EF highly efficient at catalyzing the conversion of ATP into cAMP, disrupting intracellular signaling pathways through excessive activation of cAMP-dependent signaling pathways[84]. Thus, EF mediates the efflux of water out of the cells, resulting in edema (explanation for the name: edema factor).

In spite of limitations in antibiotic treatment the disruption of the infection cascade by inhibition of EF[72b] is a feasible tool to prevent the massive onset of anthrax. The impairment of the second messenger signaling is an entirely new approach in finding new drugs against exotoxins like EF.

1.3 Research aims in this thesis

The aim of our studies presented in this thesis was initially the synthesis of ATP substrate analogs based on methylanthraniloyl-derived nucleotides as high potent AC inhibitors. Moreover, newly synthesized compounds were characterized on mammalian ACs 1, 2 and 5 and bacterial AC toxin CyaA, regarding inhibition potency and selectivity by pharmacological AC assays to validate this enzymes as potential drug targets. For better understanding of the catalytic site and mode of action for AC inhibition, fluorescence spectroscopy, crystallography and molecular modeling support our investigations.

2. References

[1] Dumont, J. E.; Jauniaux, J. C.; Roger, P. P. *Trends Biochem. Sci.* **1989**, *14*, 67

[2] Robison, G. A.; Butcher, R. W.; Sutherland, E. W. *Annu. Rev. Biochem.* **1968**, *37*, 149

[3] Rodbell, M. *Nature* **1980**, *284*, 17

[4] De Rooij, J.; Zwartkruis, F. J.; Verheijen, M. H.; Cool, R. H.; Nijman, S. M.; Wittinghofer, A.; Bos, J. L. *Nature* **1998**, *396*, 474

[5] Kawasaki, H.; Springett, G. M.; Mochizuki, N.; Toki, S.; Nakaya, M.; Matsuda, M.; Housman, D. E.; Graybiel, A. M. *Science*, **1998**, *282*, 2275

[6] Hurley, J. H. *Curr. Opin. Struct. Biol.* **1998**, *8*, 770

[7] Ishikawa, Y.; Homcy, C. J. *Circ. Res* **1997**, *80*, 297

[8] Tang, W. J.; Hurley, J. H. *Mol. Pharmacol.* **1998**, *54*, 231

[9] Cooper, D. M.; Mons, N.; Karpen, J. W. *Nature* **1995**, *374*, 421

[10] Defer, N.; Best-Belpomme, M.; Hanoune, J. *Am. J. Physiol. Renal. Physiol.* **2000**, *279*, F400

[11] Alousi, A. A.; Jasper, J. R.; Insel, P. A.; Motulsky, H. J. *Faseb J.* **1991**, *5*, 2300

[12] Post, S. R.; Hilal-Dandan, R.; Urasawa, K.; Brunton, L. L.; Insel, P. A. *Biochem. J.* **1995**, *311*, 75

[13] (a) Gao, M.; Ping, P.; Post, S.; Insel, P. A.; Tang, R.; Hammond, H. K. *Proc. Natl. Acad. Sci. USA* **1998**, *95*, 1038; (b) MacEwan, D. J.; Kim, G. D.; Milligan; G. *Biochem. J.* **1996**, *318*, 1033

[14] (a) Iyengar, R. *Faseb J.* **1993**, *7*, 768; (b) Iyengar, R. *Science* **1996**, *271*, 461

[15] Sunahara, R. K.; Dessauer, C. W.; Gilman, A. G. *Annu. Rev. Pharmacol. Toxicol.* **1996**, *36*, 461

[16] Feinstein, P. G.; Schrader, K. A.; Bakalyar, H. A.; Tang, W. J.; Krupinski, J.; Gilman, A. G.; Reed, R. R. *Proc. Natl. Acad. Sci. USA* **1991**, *88*, 10173

[17] Krupinski, J.; Coussen, F.; Bakalyar, H. A.; Tang, W. J.; Feinstein, P. G.; Orth, K.; Slaughter, C.; Reed, R. R.; Gilman, A. G. *Science* **1989**, *244*, 1558

[18] Tang, W. J.; Gilman, A. G. *Science* **1991**, *254*, 1500

[19] Tang, W. J.; Gilman, A. G. *Cell* **1992**, *70*, 869; Tang, W. J.; Gilman, A. G. *Science* **1995**, *268*, 1769

[20] Yan, S. Z.; Hahn, D.; Huang, Z. H.; Tang, W. J. *J. Biol. Chem.* **1996**, *271*, 10941

[21] (a) Zhang, G.; Liu, Y.; Qin, J.; Vo, B.; Tang, W. J.; Ruoho, A. E.; Hurley, J. H. *Protein Sci.* **1997**, *6*, 903; (b) Zhang, G.; Liu, Y.; Ruoho, A. E.; Hurley, J. H. *Nature* **1997**, *386*, 247

[22] (a) Beeler, J. A.; Yan, S. Z.; Bykov, S.; Murza, A.; Asher, S.; Tang, W. J. *Biochemistry* **2004**, *43*, 15463; (b) Yan, S. Z.; Beeler, J. A.; Chen, Y.; Shelton, R. K.; Tang, W. J. *J. Biol. Chem.* **2001**, *276*, 8500

[23] Hanoune, J.; Pouille, Y.; Tzavara, E.; Shen, T.; Lipskaya, L; Miyamoto, N; Suzuki, Y.; Defer, N. *Mol. Cell. Endocrinol.* **1997**, *128*, 179

[24] (a) Johnson, R. A.; Shoshani, I. *J. Biol. Chem.* **1990**, *265*, 11595; (b) Patel, T. B.; Du, Z.; Pierre, S.; Cartin, L.; Scholich, K. *Gene* (*Amst.*) **2001**, *269*, 13

[25] Chen, Y.; Cann, M. J.; Litvin, T. N.; Iourgenko, V.; Sinclair, M. L.; Levin, L. R.; Buck, J. *Science* **2000**, *289*, 625

[26] (a) Matsuoka, I.; Giuili, G.; Poyard, M.; Stengel, D.; Parma, J.; Guellaen, G.; Hanoune J. *J. Neurosci.* **1992**, *12*, 3350; (b) Stengel, D.; Parma, J.; Gannage, M. H.; Roeckel, N.; Mattei, M. G.; Barouki, R.; Hanoune, J. *Hum. Genet.* **1992**, *90*, 126

[27] (a) Xia, Z.; Storm, D. R. *Curr. Opin. Neurobiol.* **1997**, *7*, 391; (b) Xia, Z. G.; Refsdal, C. D.; Merchant, K. M.; Dorsa, D. M.; Storm, D. R. *Neuron* **1991**, *6*, 431

[28] Choi, E. J.; Xia, Z.; Storm, D. R. *Biochemistry* **1992**, *31*, 6492

[29] (a) Ishikawa, Y. *J. Cardiovasc. Pharmacol.* **2003**, *41*, Suppl 1, S1; (b) Ishikawa, Y.; Katsushika, S.; Chen, L.; Halnon, N. J.; Kawabe, J.; Homcy, C. J. *J. Biol. Chem.* **1992**, *267*, 13553; (c) Katsushika, S.; Chen, L.; Kawabe, J.; Nilakantan, R.; Halnon, N. J.; Homcy, C. J.; Ishikawa, Y. *Proc. Natl. Acad. Sci. USA* **1992**, *89*, 8774

[30] Shen, T.; Suzuki, Y.; Poyard, M.; Miyamoto, N.; Defer, N.; Hanoune, J. *Am. J. Physiol.* **1997**, *273*, C323

[31] (a) Gao, B. N.; Gilman, A. G. *Proc. Natl. Acad. Sci. USA* **1991**, *88*, 10178; (b) Hacker, B. M.; Tomlinson, J. E.; Wayman, G. A.; Sultana, R.; Chan, G.; Villacres, E.; Disteche, C.; Storm, D. R. *Genomics* **1998**, *50*, 97; (c) Krupinski, J.; Lehman, T. C.; Frankenfield, C. D.; Zwaagstra, J. C.; Watson, P. A.; *J. Biol. Chem.* **1992**, *267*, 24858; (d) Watson, P. A.; Krupinski, J.; Kempinski, A. M.; Frankenfield, C. D. *J. Biol. Chem.* **1994**, *269*, 28893

[32] Patel, T. B.; Du, Z.; Pierre, S.; Cartin, L.; Scholich, K. *Gene* **2001**, *269*, 13

33 (a) Abdel-Majid, R. M.; Leong, W. L.; Schalkwyk, L. C.; Smallman, D. S.; Wong, S. T.; Storm, D. R.; Fine, A.; Dobson, M. J.; Guernsey, D. L.; Neumann, P. E. *Nat. Genet.* **1998**, *19*, 289; (b) Storm, D. R.; Hansel, C.; Hacker, B.; Parent, A.; Linden, D. J. *Neuron* **1998**, *20*, 1199; (c) Villacres, E. C.; Wong, S. T.; Chavkin, C.; Storm, D. R. *J. Neurosci.* **1998**, *18*, 3186

34 (a) Watts, V. J. *Mol. Interv.* **2007**, *7*, 70; (b) Wang, H.; Gong, B.; Vadakkan, K. I.; Toyoda, H.; Kaang, B. K.; Zhuo, M. *J. Biol. Chem.* **2007**, *282*, 1507

35 (a) Okumura, S.; Kawabe, J.; Yatani, A.; Takagi, G.; Lee, M. C.; Hong, C.; Liu, J.; Takagi, I.; Sadoshima, J.; Vatner, D. E.; Vatner, S. F.; Ishikawa, Y. *Circ. Res.* **2003**, *93*, 364; (b) Okumura, S.; Takagi, G.; Kawabe, J.; Yang, G.; Lee, M. C.; Hong, C.; Liu, J.; Vatner, D. E.; Sadoshima, J.; Vatner, S. F.; Ishikawa, Y. *Proc. Natl. Acad. Sci. USA* **2003**, *100*, 9986

36 (a) Yan, L.; Vatner, D. E.; O'Connor, J. P.; Ivessa, A.; Ge, H.; Chen, W.; Hirotani, S.; Ishikawa, Y.; Sadoshima, J.; Vatner, S. F. *Cell* **2007**, *130*, 247; (b) Tang, T.; Lai, N. C.; Roth, D. M.; Drumm J., Guo, T.; Lee, K. W.; Han, P. L.; Dalton, N.; Gao, M. H. *Basic. Res. Cardiol.* **2006**, *101*, 117; (c) Okumura, S.; Vatner, D. E.; Kurotani, R.; Bai, Y.; Gao, S.; Yuan, Z.; Iwatsubo, K.; Ulucan, C.; Kawabe, J.; Ghosh, K.; Vatner, S. F.; Ishikawa, Y. *Circulation* **2007**, *116*, 1776, (d) Kim, K. S.; Kim, J.; Back, S. K.; Im, J. Y.; Na, H. S.; Han, P. L. *Genes Brain Behav.* **2007**, *6*, 120; (e) Chester, J. A.; Watts, V. J. *Sci. STKE* **2007**, *413*, pe64

37 (a) Onda, T.; Hashimoto, Y.; Nagai, M.; Kuramochi, H.; Saito, S.; Yamazaki, H.; Toya, Y.; Sakai, I.; Homcy, C. J.; Nishikawa, K.; Ishikawa, Y. *J. Biol. Chem.* **2001**, *276*, 47785; (b) Watts, V. J. *Mol. Interv.* **2007**, *7*, 70; (c) Okumura, S.; Takagi, G.; Kawabe, J.; Yang, G.; Lee, M. C.; Hong, C.; Liu, J.; Vatner, D. E.; Sadoshima, J.; Vatner, S. F.; Ishikawa, Y. *Proc. Natl. Acad. Sci. USA* **2003**, *100*, 9986; (d) Yan, L.; Vatner, D. E.; O'Connor, J. P.; Ivessa, A.; Ge, H.; Chen, W.; Hirotani, S.; Ishikawa, Y.; Sadoshima, J.; Vatner, S. F. *Cell* **2007**, *130*, 247; (e) Rottländer, D.; Matthes, J.; Vatner, S. F.; Seifert, R.; Herzig, S. *J. Pharmacol. Exp. Ther.* **2007**, *321*, 608

38 Wong, S. T.; Trinh, K.; Hacker, B.; Chan, G. C.; Lowe, G.; Gaggar, A.; Xia, Z.; Gold, G. H.; Storm, D. R. *Neuron* **2000**, *27*, 487

39 Schaefer, M. L.; Wong, S.T.; Wozniak, D. F.; Muglia, L. M.; Liauw, J. A.; Zhuo, M.; Nardi, A.; Hartman, R. E.; Vogt, S. K.; Luedke, C. E.; Storm, D. R.; Muglia, L. J. *J. Neurosci.* **2000**, *20*, 4809

40 Hanoune, J.; Defer, N. *Annu. Rev. Pharmacol. Toxicol.* **2001**, *41*, 145

[41] Sunahara, R. K.; Dessauer, C. W.; Whisnant, R. E.; Kleuss, C.; Gilman, A. G. *J. Biol. Chem.* **1997**, *272*, 22265

[42] (a) Chen, Y.; Wenig, G.; Li, J.; Harry, A.; Pieroni, J.; Dingus, J.; Hildebrandt, J. D.; Guarnieri, F.; Weinstein, H.; Iyengar, R. *Proc. Natl. Acad. Sci. USA* **1997**, *94*, 2711; (b) Harry, A.; Chen, Y.; Magnusson, R.; Iyengar, R.; Weng, G. *J. Biol. Chem.* **1997**, *272*, 19017; (c) Pinto, C.; Papa, D.; Hübner, M.; Mou, T. C.; Lushington, G. H.; Seifert, R. *J. Pharmacol. Exp. Ther.* **2008**, *325*, 27;

[43] (a) Seamon, K.; Daly, J. W. *J. Biol. Chem.* **1981**, *256*, 9799; (b) Seamon, K. B.; Daly, J. W.; Metzger, H.; de Souza, N. J.; Reden, J. *J. Med. Chem.* **1983**, *26*, 436; (c) Yan, S. Z.; Huang, Z. H.; Andrews, R. K.; Tang W. J. *Mol. Pharmacol.* **1998**, *53*, 182

[44] Taussig, R.; Iniguez-Lluhi, J. A.; Gilman, A. G. *Science* **1993**, *261*, 218

[45] Lustig, K. D.; Conklin, B. R.; Herzmark, P.; Taussig, R.; Bourne, H. R. *J. Biol. Chem.* **1993**, *268*, 13900

[46] Iwami, G.; Kawabe, J.; Ebina, T.; Cannon, P. J.; Homcy, C. J.; Ishikawa, Y. *J. Biol. Chem.* **1995**, *270*, 12481

[47] Kawabe, J.; Iwami, G.; Ebina, T.; Ohno, S.; Katada, T.; Ueda, Y.; Homcy, C. J.; Ishikawa, Y. *J. Biol. Chem.* **1994**, *269*, 16554

[48] Somkuti, S. G.; Hildebrandt, J. D.; Herberg, J. T.; Iyengar, R. *J. Biol. Chem.* **1982**, *257*, 6387

[49] Vorherr, T.; Knopfel, L.; Hofmann, F.; Mollner, S.; Pfeuffer, T.; Carafoli, E. *Biochemistry* **1993**, *32*, 6081

[50] Wayman, G. A.; Impey, S.; Wu, Z.; Kindsvogel, W.; Prichard, L.; Storm, D. R. *J. Biol. Chem.* **1994**, *269*, 25400

[51] (a) Chabardes, D.; Elalouf, J. M.; Aarab, L. *Nephrologie* **1999**, *20*, 193; (b) Chabardes, D.; Imbert-Teboul, M.; Elalouf, J. M. *Cell Signal* **1999**, *11*, 651; (c) Cooper, D. M. *Biochem. J.* **1991**, *278*, 903; (d) Guillou, J. L.; Nakata, H.; Cooper, D. M.; *J. Biol. Chem.* **1999**, *274*, 35539

[52] (a) Mons, N.; Cooper, D. M. *Trends Neurosci.* **1995**, *18*, 536; (b) Mons, N.; Harry, A.; Dubourg, P.; Premont, R. T.; Iyengar, R.; Cooper, D. M. *Proc. Natl. Acad. Sci. USA* **1995**, *92*, 8473

[53] Mou, T. C.; Gille, A.; Fancy, D. A.; Seifert, R.; Sprang, S. R. *J. Biol. Chem.* **2005**, *280*, 7253

54   (a) Whisnant, R. E.; Gilman, A. G.; Dessauer, C. W. *Proc. Natl. Acad. Sci. USA* **1996**, *93*, 6621; (b) Zhang, G.; Liu, Y.; Qin, J.; Vo, B.; Tang, W. J.; Ruoho, A. E.; Hurley, J. H. *Protein Sci.* **1997**, *6*, 903

55   Yan, S. Z.; Huang, Z. H.; Shaw, R. S.; Tang, W. J. *J. Biol. Chem.* **1997**, *272*, 12342

56   (a) Tesmer, J. J.; Sunahara, R. K.; Gilman, A. G.; Sprang, S. R. *Science* **1997**, *278*, 1907; (b) Liu, Y.; Ruoho, A. E.; Rao, V. D.; Hurley, J. H. *Proc. Natl. Acad. Sci. USA* **1997**, *94*, 13414

57   Hatley, M. E.; Benton, B. K.; Xu, J.; Manfredi J. P.; Gilman, A. G.; Sunahara, R. K. *J. Biol. Chem.* **2000**, *275*, 38626

58   Yoo, B.; Iyengar, R.; Chen, Y. *J. Biol. Chem.* **2004**, *279*, 13925

59   (a) Eckstein, F.; Romaniuk, P. J.; Heideman, W.; Storm, D. R. *J. Biol. Chem.* **1981**, *256*, 9118; (b) Dessauer, C. W.; Gilman, A. G. *J. Biol. Chem.* **1996**, *271*, 16967

60   (a) Garbers, D. L.; Johnson, R. A. *J. Biol. Chem.* **1975**, *250*, 8449; (b) Somkuti, S. G.; Hildebrandt, J. D.; Herberg, J. T.; Iyengar, R. *J. Biol. Chem.* **1982**, *257*, 6387

61   Olson, J. M. *Photosynth. Res.* **2006**, *88*, 109

62   Versteegh, F. G. A.; Schellekens, J. F. P.; Fleer, A.; Roord, J. *Rev. Med. Microbiol.* **2005**, *16*, 79

63   Mattoo, S.; Foreman-Wykert, A. K.; Cotter, P. A.; Miller, J. F. *Front Biosci.* **2001**, *6*, e168

64   Baillou, G.: Constitutio aestiva. In: *RH Major: Classic description of disease*. Charles C. Thomas, Springfield Ill., **1965**, 3rd ed., 6th print, pp 210-212

65   Kohn, G. C.: Cough of Perinthus. In: *The Wordsworth encyclopedia of plague and pestilence*, Wordsworth edition Ltd., Hertfordshire **1998**, p 66

66   Christie, C. D. C.; Baltimore, R. S. *Am. J. Dis. Child.* **1989**,*143*, 1199

67   (a) Hewlett, E. L. *Ped. Infect. Dis. J.* **1997**, *16*, 78; (b) Madan Babu, M.; Bhargavi, J.; Ranajeet Singh Saund; Kumar Singh, S. *Curr. Science* **2001**, *80*, 1512

68   (a) Confer, D. L.; Eaton, J. W. *Science*, **1982**, *217*, 948; (b) Hewlett, E. L.; Gordon, V. M.; McCaffery, J. D.; Sutherland, W. M.; Gray, M. C. *J. Biol. Chem.* **1989**, *264*, 19379; (c) Ladant, D.; Ullmann, A. *Trends Microbiol.* **1999**, *7*, 172

69   Guo, Q.; Shen, Y.; Lee, Y. S.; Gibbs, C. S.; Mrksich, M.; Tang, W. J. *EMBO J.* **2005**, *24,* 3190

[70] (a) Mock, M.; Ullmann, A. *Trends Microbiol.* **1993**, *1*, 187; (b) Ahuja, N.; Kumar, P.; Bhatnagar, R. *Crit. Rev. Microbiol.* **2004**, *30*, 187; (c) Shen, Y.; Lee, Y. S.; Soelaiman, S.; Bergson P.; Lu, D.; Chen, A.; Beckingham, K.; Grabarek, Z.; Mrksich, M.; Tang, W. J. *EMBO J.* **2002**, *21*, 6721

[71] (a) Boyd, A. P.; Ross P. J.; Conroy, H.; Mahon, N.; Lavelle, E. C.; Mills, K. H. *J. Immunol.* **2005**, *175*, 730; (b) Carbonetti, N. H.; Artamonova, G. V.; Andreasen, C.; Bushar, N. *Infect. Immun.* **2005**, *73*, 2698; (c) Hewlett, E. L.; Donato, G. M.; Gray, M. C. *Mol. Microbiol.* **2006**, *59*, 447

[72] (a) Soelaiman, S.; Wei, B. Q.; Bergson, P.; Lee, Y. S.; Shen, Y.; Mrksich, M.; Shoichet, B. K.; Tang, W. J. *J. Biol. Chem.* **2003**, *278*, 25990; (b) Gille, A.; Lushington, G. H.; Mou, T. C.; Doughty, M. B.; Johnson, R. A.; Seifert, R. *J. Biol. Chem.* **2004**, *279*, 19955; (c) Johnson, R. A.; Shoshani, I. *J. Biol. Chem.* **1990**, *265*, 11595

[73] (a) WHO-Weekly Epidemiological Record*,* **1999**, *74*, 137; (b) WHO-Weekly Epidemiological Record*,* **2005**, *80*, 29

[74] http://www.auswaertiges-amt.de/diplo/de/Laenderinformationen/01-Laender /Gesundheitsdienst/Symposien/XIII/Uebersicht.html; XIII. Symposium Reise- und Impfmedizin-Internationale Gesundheit im Auswärtigen Amt am 25./26. April **2008**, Dr. Martina Littmann, Pertussis – wieder ein Thema?

[75] Jedrzejas, M. J. *Crit. Rev. Biochem. Mol. Biol.* **2002**, *37*, 339

[76] Hanna, P. *Curr. Top. Microbiol*. **1998**, *225*, 13

[77] Holty, J. E. C.; Bravata, D. M.; Hau, L.; Olshen, R. A.; McDonald, K. M.; Owens, D. K. *Ann. Intern. Med.* **2006**; *144*, 270

[78] Inglesby, T. V.; Henderson, D. A.; Barlett, J. G.; Ascher, M. S.; Eitzen, E.; Friedlander, A. M.; Hauer, J.; McDade, J.; Osterholm, M. T.; O'Toole, T.; Parker, G.; Perl, T. M.; Russell, P. K.; Tonat, K. *JAMA* **1999**, *281*, 1735

[79] Meselon, M.; Guillemin, J.; Hugh-Jones, M.; Langmuir, A.; Popova, I.; Shelokov, A.; Yampolskaya, O. *Science* **1994**, *266*, 1202

[80] Atlas, R. M. *Annu. Rev. Microbiol.* **2002**, *56*, 167

[81] Hong, J.; Beeler, J.; Zhukovskaya, N. L.; He, W.; Tang, W. J.; Rosner, M. R. *Biochem. Biophys. Res. Commun.* **2005**, *335*, 850

[82] Drum, C. L.; Yan, S. Z.; Bard, J.; Shen, Y. Q.; Lu, D.; Soelaiman, S.; Grabarek, Z.; Bohm, A; Tang, W. J. *Nature* **2002**, *415*, 396

[83] Shen, Y.; Lee, Y. S.; Soelaiman, S.; Bergson, P.; Lu, D.; Chen, A.; Beckingham, K.; Grabarek, Z.; Mrksich, M.; Tang, W. J. *EMBO J.* **2002**, *21*, 6721

[84] Shen, Y.; Zhukovskaya, N. L.; Guo, Q.; Florián, J.; Tang, W. J. *EMBO J.* **2005**, *24*, 929

II. Potent inhibition of mammalian adenylyl cyclases by anthraniloyl-derived nucleotides[φζ]

1. Introduction

Mammals express nine membranous AC isoforms that play an important role in signal transduction[1,2]. ACs are activated by the G-protein G_s *via* receptors for hormones and neurotransmitters and catalyze the production of the second messenger cAMP.

ACs 1-8 are also activated by the diterpene, forskolin (FS)[1-3]. The analysis of AC knock-out mice provided important insights into the function of specific AC isoforms and potential therapeutic applications of AC inhibitors[2b]. Currently, there is much interest in ACs 1 and 5. Specifically, AC1 knock-out mice are protected against neuronal toxicity mediated by ionotropic glutamate receptors[4,5]. AC5 knock-out mice are protected against heart failure and stress and show reduced chronic pain responses as well as increased longevity[6,7,8]. Thus, AC1/5 inhibitors may be useful drugs for the treatment of various age-related ailments including heart failure, neurodegenerative diseases, stroke and chronic pain[6,9,10]. 2',3'-O-(N-Methylanthraniloyl) (MANT)-substituted nucleotides are competitive AC inhibitors[11,12]. ACs 1 and 5 are more sensitive to inhibition by MANT-nucleotides than AC2[12]. MANT-GTPγS inhibits recombinant ACs 1 and 5 expressed in Sf9 insect cells with K_i values of ~30 – 60 nM[12] and blocks activation of voltage-dependent calcium channels in cardiomyocytes via AC5[10].

Moreover, MANT-nucleotides are fluorescence probes[13]. In the presence of forskolin, MANT-nucleotides promote assembly of the purified catalytic subunits of mammalian AC (C1 subunit of AC5 (VC1) and C2 subunit of AC2 (IIC2)), giving rise to a direct MANT-nucleotide fluorescence increase and FRET between Trp1020 in IIC2 and the MANT-group[14,15]. Enzymatic, fluorescence, crystallographic and molecular modeling studies showed that ACs exhibit a high degree of conformational flexibility, allowing the catalytic site to accommodate structurally diverse bases[12,16,17].

The aim of the present study was to identify even more potent AC1/5 inhibitors than

MANT-GTPγS and to better understand their mechanism of action. To achieve the aim, we examined the effects of 21 (M)ANT-nucleotides on recombinant ACs 1, 2, and 5 expressed in Sf9 insect cells (**Fig. 1**).

In addition, we examined the interactions of (M)ANT-nucleotides with VC1/IIC2 in terms of enzyme inhibition, co-crystallography, and fluorescence spectroscopy. It would have been desirable to examine the homologous C1 and C2 subunits from ACs 1, 2 and 5, but to this end, we have not yet achieved this ambitious goal (data not shown). Nonetheless, in view of the high degree of homology of the catalytic C1 and C2 subunits of ACs 1, 2 and 5, respectively[1,14], the VC1/IIC2 system is a valid general model for membranous ACs.

In 2',3'-MANT-nucleotides, the MANT-group spontaneously isomerizes between the 2'- and 3'-position of the ribosyl residue[13]. Therefore, we also studied the defined 3'-MANT-2'-d- and 2'-MANT-3'-d-isomers of MANT-GTP (**2** and **3**) and MANT-ATP (**6** and **7**). Moreover, given the high affinity of MANT-ITPγS (**9**) for AC5 (K_i = 31 nM)[12], we studied MANT-ITP (**8**), differing from MANT-GTP (**1**) only by the lack of a NH_2-group at C2 of the purine ring. For comparison, we studied MANT-XTP (**10**) which inhibits VC1/IIC2 (also briefly referred to as C1/C2) much less potently than MANT-GTP[14]. Considering the relatively high potency of 2',3'-*O*-(2,4,6-trinitrophenyl)-UTP and 2',3'-*O*-(2,4,6-trinitrophenyl)-CTP for VC1/IIC2 (K_i ~100 – 300 nM)[15], we examined the interaction of C1/C2 with MANT-UTP (**11**) and MANT-CTP (**12**) as well. ANT-nucleotides differ from MANT-nucleotides by the lack of the methyl group at the anthraniloyl residue and were used for the fluorescence analysis of various proteins[13]. Therefore, we included various ANT-nucleotides (**14** and **15**, **21**) into our studies. Finally, the length of the polyphosphate tail critically determines the affinity of AC for 2',3'-substituted nucleotides[12]. Thus, we examined several (M)ANT-NDPs (**15 – 19**) and (M)ANT-NMPs (**20**, **21**), too.

Fig. 1. General structure of 2',3'-ribosyl modified nucleotides

Bases:

guanine   adenine   hypoxanthine

xanthine   uracil   cytosine

MANT: ANT:
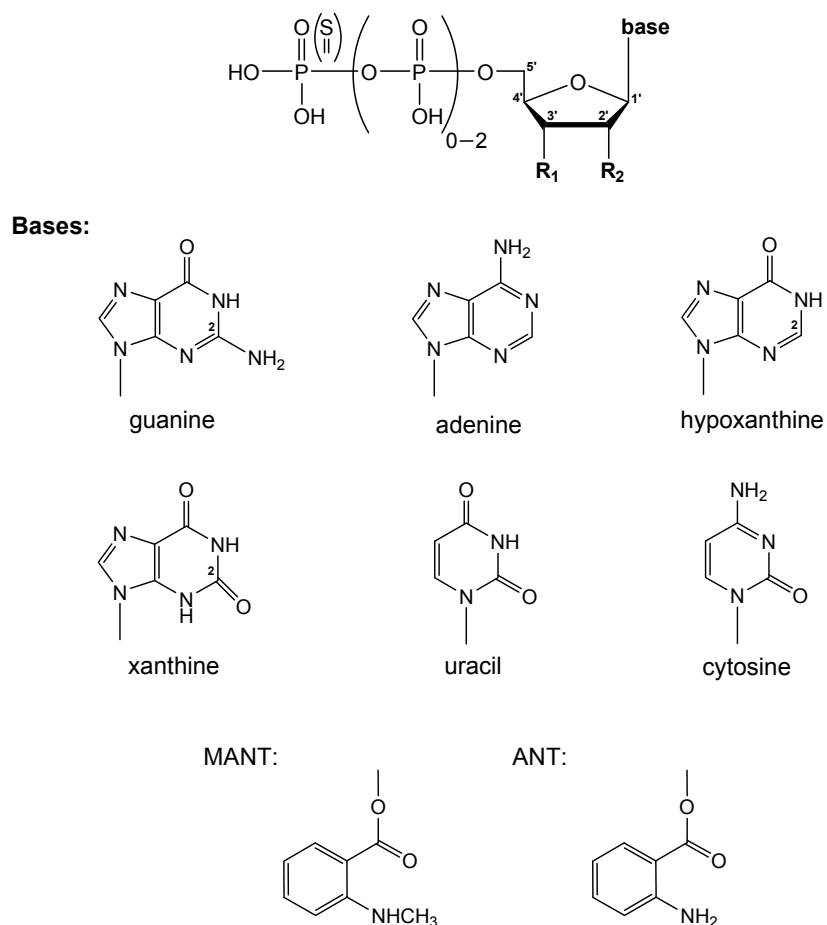
	(M)ANT- nucleotide	R_1	R_2
1	MANT-GTP	MANT / OH	
2	3'-MANT-2'-d-GTP	MANT	H
3	2'-MANT-3'-d-GTP	H	MANT
4	MANT-GTPγS	MANT / OH	
5	MANT-ATP	MANT / OH	
6	3'-MANT-2'-d-ATP	MANT	H
7	2'-MANT-3'-d-ATP	H	MANT
8	MANT-ITP	MANT / OH	
9	MANT-ITPγS	MANT / OH	
10	MANT-XTP	MANT / OH	
11	MANT-UTP	MANT / OH	
12	MANT-CTP	MANT / OH	
14	ANT-ATP	ANT / OH	
15	ANT-ADP	ANT / OH	
16	MANT-ADP	MANT / OH	
17	MANT-IDP	MANT / OH	
18	MANT-UDP	MANT / OH	
19	MANT-CDP	MANT / OH	
20	MANT-IMP	MANT / OH	
21	ANT-IMP	ANT / OH	

Represented are the three pharmacophores contributing to the inhibitor potencies of these nucleotides, *i.e.* the base, the phosphate chain and the (M)ANT-group. Nucleotides differed from each other in the base (guanine, hypoxanthine, xanthine, adenine, uracil and cytidine), γ-phosphate chain substitution (phosphate or thiophosphate), phosphate chain length (5'-triphosphate, 5'-diphosphate, 5'-monophosphate analogs), ribosyl substituent (MANT or ANT), and in the position of the MANT-group (2'- and 3'-MANT).

2.   Materials and Methods

2.1. Materials

Mono-substituted (M)ANT-NTPs of MANT-ATP (**5**), MANT-ITP (**8**), MANT-UTP (**11**), MANT-CTP (**12**), ANT-ATP (**14**), and MANT-NDPs of ANT-ADP (**15**), MANT-ADP (**16**), MANT-IDP (**17**), MANT-UDP (**18**), MANT-CDP (**19**), and MANT-NMPs of MANT-IMP (**20**), ANT-IMP (**21**) were synthesized according to Hiratsuka[18] as previously described[19,20]. Under the basic reaction conditions (M)ANT-NTP derivatives were partially decomposed to its corresponding diphosphates. Because of their putative inhibitory effects they were isolated as well. For detailed description of synthesis and purification see Experimental section.

MANT-GTP (**1**), 3'-MANT-2'-d-GTP (**2**), 2'-MANT-3'-d-GTP (**3**), MANT-GTPγS (**4**), 3'-MANT-2'-d-ATP (**6**), 2'-MANT-3'-d-ATP (**7**), MANT-ITPγS (**9**), MANT-XTP (**10**), and ANT-GTP (**14**) were obtained from Jena Bioscience, Jena, Germany. Methylisatoic anhydride, isatoic anhydride, ATP, ITP, CTP, UTP, IMP and bovine serum albumin, fraction V, highest quality, were purchased from Sigma-Aldrich (Seelze, Germany). $MnCl_2$ tetrahydrate (highest quality) and Aluminum oxide 90 active, (neutral, activity 1; particle size, 0.06 - 0.2 mm) were from MP Biomedicals (Eschwege, Germany). [α-^{32}P]ATP (800 Ci/mmol) was purchased from PerkinElmer, Rodgau Jügesheim, Germany. Forskolin was supplied by LC Laboratories (Woburn, MA). For all experiments double-distilled water was used. Catalytic AC subunits VC1 and IIC2 and GTPγS activated $G_{sα}$ ($G_{sα\text{-}GTPγS}$) were expressed and purified as described[21].

2.2   Cell culture and membrane preparation

Cell culture and membrane preparation were performed as previously described[22]. Briefly, Sf9 cells were cultured in SF 900 II medium supplemented with 5 % (vol/vol) fetal bovine serum and 0.1 mg/ml gentamicin. High-titer baculoviruses for ACs 1, 2 and 5 were generated through two sequential amplification steps as previously described[12,22]. In each amplification step the supernatant fluid was harvested and stored under light protection at 4 °C. For membrane preparation Sf9 cells (3.0 x 10^6 cells/ml) were infected with corresponding baculovirus encoding different mammalian ACs (1:100 dilutions of high-titer virus) and cultured for 48 hours. Membranes expressing each construct and membranes from uninfected Sf9 cells were prepared

as described[22]. Briefly, cells were harvested and cell suspensions were centrifuged for 10 min at 1,000 x g at 4 °C. Pellets were resuspended in 10 ml of lysis buffer (1 mM EDTA, 0.2 mM phenylmethylsulfonylfluoride, 10 µg/ml leupeptine and 10 µg/ml benzamide, pH 7.4). Thereafter, cells were lyzed with 20 – 25 strokes using a Dounce homogenizer. The resultant cell fragment suspension was centrifuged for 5 min at 500 x g and 4 °C to sediment nuclei. The cell membrane-containing supernatant suspension was transferred into 30 ml tubes and centrifuged for 20 min at 30,000 x g and 4 °C. The supernatant fluid was discarded and cell pellets were discarded and cell pellets were resuspended in buffer consisting of 75 mM Tris/HCl, 12.5 mM $MgCl_2$, and 1mM EDTA, pH 7.4. Membrane aliquots of 1 ml were prepared, stored at -80 °C and protein concentration for each membrane preparation was determined using the Bio-Rad DC protein assay kit (Bio-Rad, Hercules, CA).

2.3 AC activity assay

AC activity in Sf9 membranes expressing ACs 1, 2 or 5 was determined essentially as described in the literature[12]. Before starting experiments, membranes were sedimented by a 15 min centrifugation at 4 °C and 15,000 x g and resuspended in 75 mM Tris/HCl, pH 7.4. Reaction mixtures (50 µl, final volume) contained 20 – 40 µg of membrane protein, 40 µM ATP/Mn^{2+} plus 5 mM $MnCl_2$, 100 µM FS, 10 µM GTPγS and (M)ANT-nucleotides at concentrations from 0.1 nM to 1 mM as appropriate to obtain saturated inhibition curves. Following a 2 min pre-incubation at 37 °C, reactions were initiated by adding 20 µl of reaction mixture containing (final) 1.0 - 1.5 µCi/tube [α-^{32}P]ATP and 0.1 mM cAMP. AC assays were conducted in the absence of an NTP-regenerating system to allow for the analysis of (M)ANT-NDPs that could otherwise be phosphorylated to the corresponding (M)ANT-NTPs[12]. For the determination of K_m values, reactions mixtures contained 20 µM – 1 mM ATP/Mn^{2+} as substrate[12]. Reactions were conducted for 20 min at 37 °C and were terminated by adding 20 µl of 2.2 N HCl. Denatured protein was precipitated by a 1 min centrifugation at 25 °C and 15,000 x g. Sixty µl of the supernatant fluid were applied onto disposable columns filled with 1.3 g neutral alumina. [^{32}P]cAMP was separated from [α-^{32}P]ATP by elution of [^{32}P]cAMP with 4 ml of 0.1 M ammonium acetate, pH 7.0. Recovery of [^{32}P]cAMP was ~80 % as assessed with [^{3}H]cAMP as standard. Blank values were approximately 0.02 % of the total added amount of [α-^{32}P]ATP; substrate turnover was < 3 % of the total added [α-^{32}P]ATP. Samples

collected in scintillation vials were filled up with 10 ml of double-distilled water and Čerenkov radiation was measured in a Tri-Carb 2800TR liquid scintillation analyzer (PerkinElmer Life and Analytical Sciences).

For experiments with purified catalytic AC subunits, reaction mixtures contained 100 µM ATP/Mn^{2+}, 10 mM $MnCl_2$ and (M)ANT-nucleotides at concentrations from 0.1 nM to 1 mM as appropriate to obtain saturated inhibition curves. For experiments with $G_{s\alpha\text{-GTP}\gamma S}$, assay tubes contained VC1 (3 nM), IIC2 (15 nM) and $G_{s\alpha\text{-GTP}\gamma S}$ (51 nM). Reactions were conducted in the presence of 100 µM FS. Following a 2 min pre-incubation at 30 °C, reactions were initiated by adding 20 µl of reaction mixture containing (final) 1.0 µCi/tube [α-^{32}P]ATP, 0.1 mM cAMP and 100 mM KCl in 25 mM HEPES/NaOH, pH 7.4. AC assays were conducted in the absence of an NTP-regenerating system to allow for the analysis of 2',3'-substituted (M)ANT-NDPs that could otherwise be phosphorylated to the corresponding (M)ANT-NTPs[12]. Reactions were conducted for 10 – 20 min at 30 °C.

Free concentrations of divalent cations were calculated with Win-MaxC (http://www.stanford.edu/_cpatton/maxc.html). Competition isotherms were analyzed by non-linear regression using the Prism 4.0 software (GraphPad, San Diego, CA). K_m values were 120 µM (AC1), 100 µM (AC2), 70 µM (AC5) and were taken from Gille *et al.*[12] for mAC. K_m value for catalytic subdomains VC1/IIC2 was 430 µM (Mn^{2+}+FS+$G_{s\alpha\text{-GTP}\gamma S}$), determined in a previous study[14].

2.4 Crystallographic studies

In analogy to previous crystallographic studies with catalytical subunits of VC1/IIC2 with MANT-GTP[14] as ATP substrate analog, we investigated in a further co-crystal with MANT-ITP to explain its high potency for AC inhibition. For this thesis the crystallographic data is only presented in the discussion part (*4. Discussion and Conclusion*; page 30). For details of generating the crystallographic data please contact Melanie Hübner, Department of Pharmacology and Toxicology, University of Regensburg, Germany.

3. Results

3.1 Inhibition of the catalytic activity of recombinant ACs 1, 2 and 5 by (M)ANT-nucleotides

In agreement with previous data[12], MANT-GTPγS (**4**) and MANT-ITPγS (**9**) were similarly potent AC5 inhibitors (**Table 1**). Whereas substitution of the γ-thiophosphate by a γ-phosphate decreased potency in case of guanine nucleotide (**4**→**1**), this substitution increased potency in case of inosine nucleotides (**9**→**8**) by more than 25-fold, yielding MANT-ITP.

MANT-UTP was similarly potent as MANT-GTP, whereas introduction of adenine (**5**) or cytosine (**12**) decreased affinity for AC5 by 3- to 5-fold relative to guanine (**1**). Among all bases studied, xanthine (**10**) conferred the lowest inhibitor potency to MANT-NTPs. In case of guanine, both the 3'-MANT-2'-d-substitution (**2**) and the 2'-MANT-3'-d-substitution (**3**) substantially reduced inhibitor potency, whereas in case of adenine, only the 3'-MANT-2'-d-substitution (**6**) decreased inhibitor potency. Exchange of the MANT-group for an ANT-group had little effect on inhibitor potency (**5**→**14**, **15**→**16** and **20**→**21**). Deletion of the γ-phosphate reduced inhibitor affinity 5- to 30-fold (**5**→**16**, **8**→**17**, **11**→**18** and **12**→**19**) and deletion of the β-phosphate reduced inhibitor affinity almost 150-fold (**17**→**20**). Overall, with the exception of 2'-MANT-3'-d-ATP (**7**), inhibitor affinities at AC1 resembled those at AC5. Inhibitor affinities at AC2 were all lower than at ACs 1 and 5.

Most importantly, MANT-ITP (**8**) inhibited AC2 ~5- to 10-fold less potently than ACs 1 and 5. The generally lower affinities of (M)ANT-nucleotides at AC2 compared to ACs 1 and 5 are in agreement with previous observations[12] and are explained by Ala409Pro- and Val1108Ile exchanges in ACs 1 and 5 versus AC2[14].

Table 1. Inhibition of catalytic activity of recombinant ACs 1, 2, 5 and catalytic subunits of VC1/IIC2 by (M)ANT-nucleotides

	(M)ANT-nucleotide	AC 1 (nM)	AC 2 (nM)	AC 5 (nM)	VC1/IIC2 (nM)
1	MANT-GTP	90 ± 18	610 ± 70	53 ± 12	18 ± 6
2	3'-MANT-2'-d-GTP	270 ± 30	1,300 ± 210	410 ± 35	180 ± 6
3	2'-MANT-3'-d-GTP	1,800 ± 70	8,700 ± 1,800	1,800 ± 100	350 ± 40
4	MANT-GTPγS	63 ± 17	370 ± 80	34 ± 8	24 ± 4
5	MANT-ATP	150 ± 40	330 ± 80	100 ± 30	16 ± 6
6	3'-MANT-2'-d-ATP	320 ± 20	4,800 ± 560	360 ± 54	190 ± 3
7	2'-MANT-3'-d-ATP	470 ± 20	540 ± 20	65 ± 5	90 ± 2
8	MANT-ITP	2.8 ± 0.9	13.5 ± 0.5	1.2 ± 0.1	0.7 ± 0.1
9	MANT-ITPγS	40 ± 11	120 ± 23	32 ± 8	19 ± 3
10	MANT-XTP	1,100 ± 100	3,000 ± 200	1,300 ± 400	1,200 ± 370
11	MANT-UTP	46 ± 4	460 ± 60	32 ± 2	6.1 ± 1.3
12	MANT-CTP	150 ± 30	690 ± 20	150 ± 30	9.2 ± 1.5
14	ANT-ATP	130 ± 20	640 ± 70	120 ± 20	17 ± 2.4
15	ANT-ADP	860 ± 10	2,900 ± 300	640 ± 70	250 ± 12
16	MANT-ADP	1,300 ± 400	2,900 ± 500	790 ± 180	260 ± 40
17	MANT-IDP	39 ± 12	86 ± 9	31 ± 12	n. d.
18	MANT-UDP	390 ± 50	2,700 ± 300	340 ± 10	170 ± 27
19	MANT-CDP	580 ± 10	3,700 ± 400	740 ± 30	140 ± 22
20	MANT-IMP	4,600 ± 400	8,200 ± 800	3,400 ± 200	n. d.
21	ANT-IMP	7,400 ± 1,200	7,500 ± 1,400	4,300 ± 600	n. d.

AC activity in Sf9 membranes and of catalytic subunits of VC1/IIC2 were determined as described in "Materials and Methods". Non-linear regression analysis was used for calculation of K_i values from IC_{50} values. K_i values are given in nanomolar and are the mean values ± SD of 4 – 5 independent experiments performed in triplicates with at least two different membrane preparations (mACs) or two different batches of protein (C1/C2). *n. d.; not determined*.

3.2 Inhibition of the catalytic activity of VC1/IIC2 by (M)ANT-nucleotides

Additionally, the inhibitory effects of selected (M)ANT-nucleotides were determined on the catalytic activity of VC1/IIC2 (**Table 1**). 3'-*O* and 2'-*O*-isomers of both MANT-GTP (**2**, **3**) and MANT-ATP (**6**, **7**) exhibited 5- to 20-fold lower inhibitory potencies for the maximally stimulated VC1/IIC2 than MANT-GTP (**1**) and MANT-ATP (**5**), respectively. These results are in accordance with crystallographic and molecular modelling studies showing that MANT-GTP binds to VC1/IIC2 preferentially as 3'-MANT-isomer and that the 2'-hydroxyl group forms a hydrogen bond with the backbone nitrogen of Asn1025 of IIC2[14,15,17]. Thus, this missing H-bond may explain the lower affinity of **2**, **3**, **6** and **7** relative to **1** and **5**, respectively, for VC1/IIC2. However, hydrophobic interaction between the MANT-group and Ala409, Trp1020, Val413, Leu412, Ala404, and Phe400[12,14,15] in the interface of VC1/IIC2 still confer high-affinity interactions.

2'-MANT-3'-d-GTP (**3**) was 2-fold less potent than the 3'-MANT-2'-d-derivative (**2**). This finding is in accordance with crystallographic data showing that 3'-MANT-GTP is the preferred isomer for binding to VC1/IIC2[14]. Thus, the orientation of the 2'-MANT-derivative into the hydrophobic pocket may be less favorable, resulting in slightly reduced affinity compared with 3'-MANT-GTP. Although previous studies showed that MANT-ATP also binds to VC1/IIC2 preferably as 3'-isomer[15], contrary to MANT-guanine nucleotides **1 – 3** , 3'-MANT-2'-d-ATP (**6**) was less potent than the 2'-MANT-derivative (**7**) at inhibiting VC1/IIC2 catalytic activity. This suggests that in case of a missing hydrogen bond of the free ribosyl hydroxyl group, the adenine nucleotide gains flexibility so that the 2'-MANT-derivative fits into the hydrophobic pocket more favorably than the 3'-MANT-derivative.

MANT-UTP (**11**) and MANT-CTP (**12**) exhibited 2- to 3-fold higher inhibitory potencies at VC1/IIC2 than MANT-GTP (**1**) and MANT-ATP (**5**) under maximally stimulatory conditions. Previous studies showed that MANT-GTP (**1**), MANT-GTPγS (**4**) and MANT-ITPγS (**9**) are similarly potent VC1/IIC2 inhibitors[12]. This study confirms the previous data. In contrast to the MANT-GTP/MANT-GTPγS pair, exchange of the γ-thiophosphate by a phosphate in hypoxanthine nucleotides increased the inhibitory potency by almost 30-fold (**9→8**). Introduction of a keto group at the C2 carbon atom of the purine ring (**8→10**) decreased inhibitor potency several 100-fold which is explained by unfavorable electrostatic repulsion of the keto group with the carbonyl oxygen in Ile1019[14]. The exceptionally high inhibitory potency of

MANT-ITP at VC1/IIC2 fits excellently to the potency of the compound at ACs 1 and 5 (**Table 1**). Deletion of the methyl group from the fluorophore at the 2',3'-*O*-ribosyl substituent in NTPs (compare **5** and **14**) did not largely change their affinity for VC1/IIC2. These data suggest that ANT and MANT-substituted NTPs interact similarly with the hydrophobic pocket in the interface of VC1/IIC2.

Deletion of the γ-phosphate reduced the inhibitory potency of (M)ANT-NDPs ~10- to 80-fold compared to the corresponding (M)ANT-NTPs (compare **14** and **15**, **5** and **16**, **11** and **18**, **12** and **19**). These data are in accordance with crystallographic data demonstrating that the Mn^{2+}-ion in the B-site coordinates with the γ-phosphate of MANT-nucleotides and that deletion of the γ-phosphate destabilizes the polyphosphate chain in its binding site[14,15].

4. Discussion and Conclusion

Recent data from experiments with knock-out animals suggest that dual AC1/5 inhibitors may be useful drugs for several age-related ailments including heart failure and neurodegeneration[6,7,8,23]. In a previous study with 18 MANT-nucleotides we identified MANT-GTP, MANT-GTPγS and MANT-ITPγS as similarly potent AC1/5 inhibitors with K_i values in the 30 – 90 nM range[12]. In the present study, we confirmed those data and studied 14 additional (M)ANT-nucleotides. We identified MANT-ITP as the most potent AC1/5 inhibitor known so far with a K_i value in the 1 – 3 nM range (**Table 1**). MANT-ITP is also a highly potent inhibitor of the purified catalytic AC subunits VC1/IIC2. Possibly, the apparent K_i value of MANT-ITP at VC1/IIC2 is an underestimation of the true K_i value since the enzyme concentration was well above the K_i value of the inhibitor (see Materials and Methods). However, we do not know what fraction of the VC1/IIC2 subunits added to the assay was actually functionally active. The identification of MANT-ITP as a highly potent inhibitor of ACs 1 and 5 provides the basis for the development of a sensitive AC1/5 radioligand binding assay that will facilitate the identification of other potent AC1/5 inhibitors in competition experiments. Hopefully, new inhibitors will exhibit greater selectivity towards other AC isoforms than MANT-ITP, *i.e.* MANT-ITP is just 5-fold less potent at inhibiting AC2 than AC1.

We were particularly interested in learning more about the mechanisms underlying AC inhibition by (M)ANT-nucleotides. Previous studies from our laboratory already

showed that the catalytic site of AC is quite flexible, allowing for the binding of structurally diverse nucleotides[12,14,17]. Therefore, the structure/activity relationships of a series of ribosyl-modified nucleotides were analyzed in terms of VC1/IIC2 inhibition. The nucleotides studied herein varied form each other in their base (purine and pyrimidine), MANT-position (2',3'-isomerization *versus* 3'-MANT-2'-d-substitution and 2'-MANT-3'-d-substitution), type of the fluorophore (MANT and ANT), as well as the length of the polyphosphate chain (triphosphates, diphosphates and monophosphates) (**Fig. 1**). Finally, the exchange of γ-phosphate against γ-thiophosphate was studied. Most of the nucleotides had not yet been analyzed at mammalian ACs in terms of enzyme inhibition. Several nucleotides were synthesized as part of a recently initiated in-house AC inhibitor synthesis program (**5**, **8**, **11**, **12**, **14** **– 21**)[19,20].

The enzymatic data show that several MANT-purine and pyrimidine nucleotides exhibit high inhibitory potencies at recombinant ACs 1, 2 and 5 and VC1/IIC2. In fact, some pyrimidine nucleotides readily surpass purine nucleotides in terms of potency (**Table 1**). These results substantiate the recently elaborated concept[15,17] that due to the conformational flexibility of the catalytic site of VC1/IIC2, ACs can accommodate large chemical alterations in nucleotide inhibitors with regard to the base (**Fig. 1**). As a general rule, the base substituent has relatively little impact on nucleotide-affinity for ACs, *i.e.* both purines and pyrimidines are well tolerated. However, as a most notable exception, an apparently "minor" structural change, namely the deletion of the NH_2 group at C2 of the guanine ring, yielding hypoxanthine, resulted in up to 50-fold increases in potency of MANT-ITP compared to MANT-GTP. For better understanding of these findings we investigated in crystallographic experiments[14] and succeed in obtaining the co-crystal of MANT-ITP in complex with the catalytic subunits of VC1/IIC2 and $G_{s\alpha}$ (**Fig. 2**).

We expected a different binding mode of MANT-ITP to explain its higher potency, compared to previous crystallographic studies with MANT-GTP[14]. After superimposing both structures the overall placement of VC1 and IIC2 did not differ extensively from each other (**Fig. 2C**), the protein residues revealed similar hydrogen bond interactions as well as metal ion interactions with the purine and polyphosphate residues for MANT-ITP in the identical 3'-*O*-isomer conformation (**Fig. 2 B** and **D**). The overall binding constraint of the purine binding pocket may be less favorable for MANT-ITP, due to the lack of hydrogen bonding with Ile1019 (missing NH_2-group in

Fig. 2. Crystal structure of catalytic subunits VC1/IIC2 with MANT-ITP
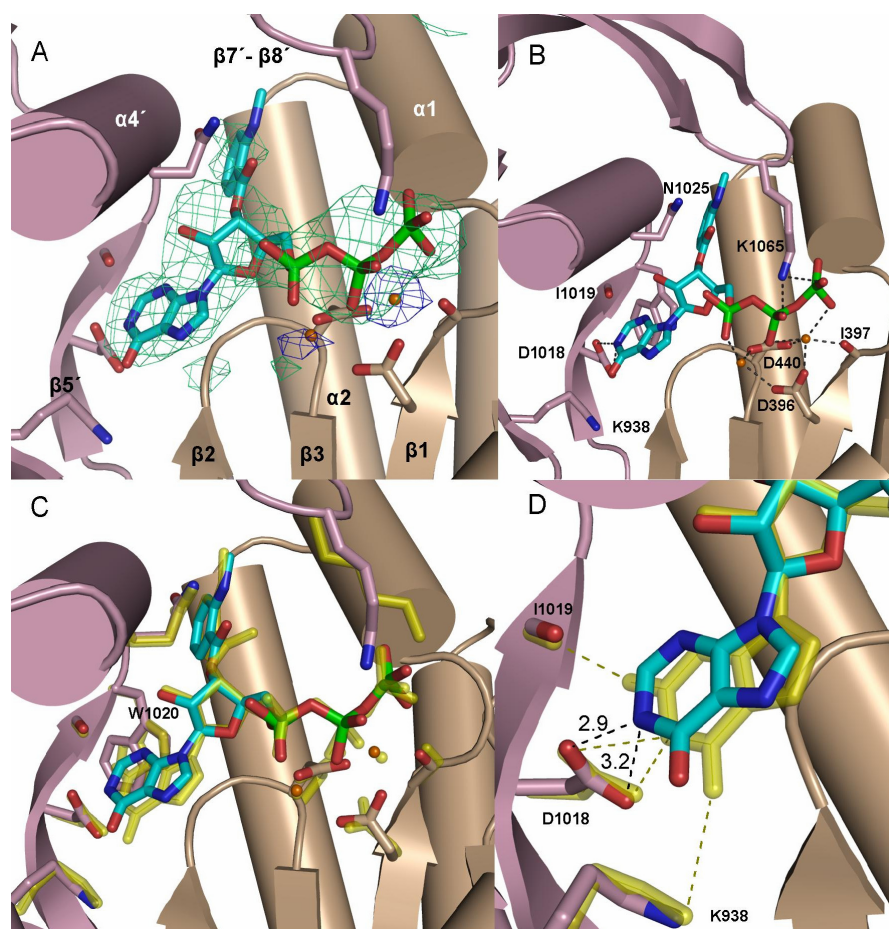
MANT-ITP and two metal ions are bound in the cleft between the soluble C1a and C2a domains. VC1 and IIC2 are colored wheat and violet (A – D). MANT-ITP is shown as stick model, colors of atoms, unless otherwise indicated: lightblue, carbon; darkblue, nitrogen; red, oxygen; green, phosphorus. The two Mn^{2+} ions are shown as orange spheres. A, overview of VC1/IIC2 with electron density for 3'-*O*-MANT-ITP and Mn^{2+}. The secondary structure elements of the complex are labeled as defined previously[24]. B, Detailed view of substrate binding site of VC1/IIC2 with MANT-ITP, two Mn^{2+} ions, and the protein residue, responsible for ligand interaction. The interaction among protein residues and MANT-ITP, Mn^{2+} are shown as gray dashed lines. C, Superimposed crystal structures of 3'-*O*-MANT-ITP and 3'-*O*-MANT-GTP. The derived MANT-ITP crystal structure was superimposed and compared with the crystal structure of MANT-GTP, shown as a transparent yellow stick model (Protein Data Bank code 1TL7)[14]. The protein residues are in almost identical conformation and the inhibitors are situated in the substrate binding pocket in a similar fashion. D, Superimposed purine binding site of 3'-*O*-MANT-ITP and 3'-*O*-MANT-GTP. The interaction of the hypoxanthine ring and guanine ring of MANT-ITP and MANT-GTP are shown as black and olive green dashed lines. The distances of hydrogen bond between the hypoxanthine ring and surrounding protein residues of MANT-ITP are indicated in Å. The hydrogen bond between Ile1019 and the amino group of MANT-GTP is missing in the MANT-ITP structure. Lys938 and the keto function of the hypoxanthine ring are further apart. The hypoxanthine ring has less binding constraint in the purine binding pocket, compared to the guanine ring of MANT-ITP.

the purine residue for MANT-ITP). Moreover, the hydrogen-bond between the keto function of the hypoxanthine ring and Lys938 are further apart (> 3.2 Å). Thus, the catalytic binding pocket offers MANT-ITP more degrees of freedom with less restriction in the binding mode. The higher inhibitor potency of MANT-ITP cannot be readily explained by obvious protein-ligand interactions alone. Residual mobility of the ligand and partial solvation of the binding pocket suggest entropic actions[25,26] as the tip on the scale. Due to the resolution of our crystal structure (3.1 Å), water molecules could not all be assessed by diffraction. Thus, we hypothesize that water molecules could play a crucial role in high affinity binding of MANT-ITP. High resolution crystal structures and isothermal calorimetric titrations may support our hypothesis.

It should be noted that a similarly "minor" structural change in the purine ring as deletion of a NH_2 group, namely exchange against a keto group at C2, yielding xanthine, reduced MANT-nucleotide affinity for ACs and VC1/IIC2 assembly dramatically through impairment of hydrogen bonding and repulsion force within the catalytic site[14]. Modifications of the position of the 2',3'-*O*-ribosyl substituent affected the inhibitory potencies of the ribosyl-modified nucleotides at holo-ACs and VC1/IIC2. Overall, as expected from crystallographic data[14,15], the 3'-MANT-2'-d- and 2'-MANT-3'-d-substitutions of both guanine and adenine nucleotides showed lower inhibitory potencies than their respective 2',3'-MANT-nucleotides (MANT-GTP and MANT-ATP, respectively). However, the impact of the position of the MANT-group (2',3' *vs.* 3'-MANT-2'-d- and 2'-MANT-3'-d-substitution) depended on the base (guanine *vs.* adenine). The enzymatic data showed that based on the overall potency (MANT-GTP >> 3'-MANT-2'-d-GTP > 2'-MANT-3'-d-GTP and MANT-ATP >> 2'-MANT-3'-d-ATP > 3'-MANT-2'-d-ATP) MANT-GTP binds to VC1/IIC2 preferably as 3'-MANT-isomer[14,17]. In contrast, MANT-ATP analogs may favor the 2'-MANT position rather than the 3'-MANT position if hydrogen bonding of the ribosyl hydroxyl group cannot take place. In conclusion, MANT-ITP is the most potent inhibitor of ACs 1, 2 and 5 and VC1/IIC2 identified so far. MANT-ITP can be used as starting point for the preparation of AC radioligands and the synthesis of even more potent and possibly AC isoform-selective inhibitors. Based on our present data, modification of the purine base and introduction of new 2',3'-ribosyl substituents constitute promising future avenues of research to obtain even more potent and selective AC inhibitors.

5. Experimental section

5.1 Synthesis procedure

General protocol of (M)ANT-nucleotide synthesis

(M)ANT-nucleotides were synthesized according to Hiratsuka[18] with modifications. The nucleotide (0.33 mmol, 1 eq) was propounded in a small two-neck round flask and dissolved in a minimum amount of water (3 ml). Under continuous stirring a crystalline preparation of (methyl)isatoic anhydride (0.5 mmol, 1.5 eq) was added. After heating to 38 °C the pH-value was adjusted to 8.6 and maintained by titration of 1 N NaOH solution for 2 hours. The reaction mixture was extracted three times by chloroform (3 x 20 ml; only for MANT-nucleotides). The aqueous phase was dry-frozen. The received foam showed white to brown color and was applied to a long Sephadex® LH-20 column (85 x 2 cm) and subsequently eluted with double-distilled water. The desired product could be detected directly by its blue fluorescence in the collection tubes at λ_{ex} of 366 nm and by TLC. For further purification, reversed-phase preparative HPLC was required to separate (M)ANT-NTP from (M)ANT-NDP. In case of monophosphate derivatives only size-exclusion chromatography was required. After final dry-freezing white solid compounds (purity > 99%) were obtained. For the polyphosphate derivatives yields were determined by analytical HPLC measurements of crude reaction mixtures and correlate with the maximal accessible yield. Because of the time consuming and costly preparative HPLC isolation was stopped after obtaining approximate 5 mg pure compound.

5.2 Analytical procedures

HPLC analysis of (M)ANT-nucleotides

The samples were filtered using a PTFE filter (Chromafil, O-20/15, organic, pore size 0.2 mm; Machery-Nagel, Düren, Germany). A 10 µL sample was analyzed using a HPLC model 1100 (Agilent Technologies, Waldbronn, Germany) fitted with a C18 analytical column (Phenomenex Luna, particle size 3 µm, 150 x 4.60 mm, Aschaffenburg, Germany) and DAD. Data were analyzed using a HPLC-3D ChemStation Rev. A.10.01 [1635]. Gradient elution was performed with 0.05 M ammonium acetate (solvent A) and acetonitrile (solvent B) at a constant flow rate of

1.0 ml/min. A gradient profile with the following proportions of solvent B was applied [t (min), % B]: [0, 5], [10, 5], [30, 45], [40, 80]. The chromatograms were monitored at 220 and 254 nm. In addition, a fluorescence detector was used for the analysis of the fluorescent anthraniloylic compounds at λ_{ex} of 350 nm and λ_{em} of 450 nm.

LC/MS online coupling

All samples were filtered using a PTFE filter and injected into a HPLC model 1100 (Hewlett-Packard, Waldbronn, Germany). The compound to be analyzed was separated by a C18 column (Phenomenex luna, particle size 3 µm, 150 x 2 mm, Aschaffenburg, Germany). A binary eluent mixture consisting of water (10 mM ammonium acetate) (eluent A) and acetonitrile (eluent B) was pumped with a constant flow of 0.3 ml/min. The following gradient profile was used t [min], % B: [0, 5], [10, 5], [30, 45], [40, 80]. The injected volume was 3 µl. The mass of the respective compound was determined with the use of a triple stage mass spectrometer (Finnigan TSQ 7000; Thermo Fisher Scientific, Waltham, MA).

Preparative HPLC

Compound mixtures were dissolved in water (concentration: 30 – 50 mg/ml) and filtered using a PTFE filter. Compounds were separated using a HPLC model 1100 (Agilent Technologies, Waldbronn, Germany) fitted with a C18 preparative column (Phenomenex Luna, particle size 10 µm, 250 x 21.2 mm). Gradient elution was performed with 0.05 M ammonium acetate (solvent A) and acetonitrile (solvent B) at a constant flow rate of 21 ml/min. Due to the goodness of separation injection volumes differed from 10 µl to 60 µl for a run. The chromatograms were monitored at 220 and 254 nm.
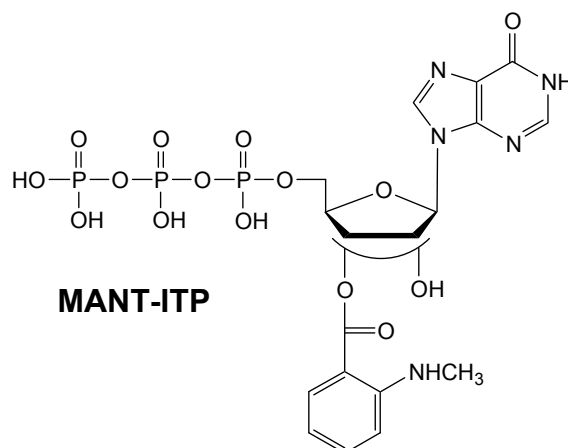
5.3 Synthesized compounds
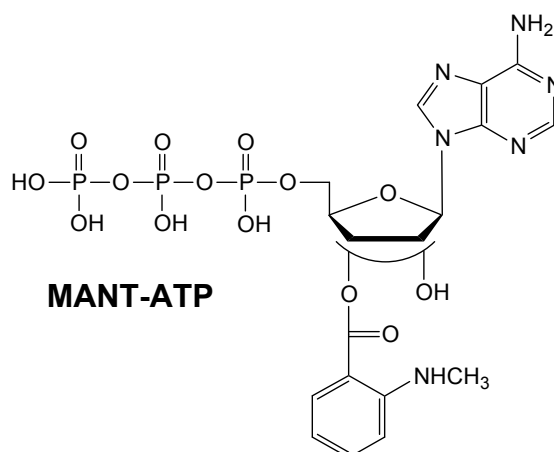
MANT-ATP

MANT-ATP   (*N*-methyl-2'(3')-*O*-anthraniloyl-adenosine-5'-triphosphate)   or
[(2R,3S,4R,5R)-5-(6-aminopurin-9-yl)-4(3)-hydroxy-2-[[hydroxy-(hydroxy-phosphono-
oxyphosphoryl)oxyphosphoryl]oxymethyl]oxolan-3(4)-yl]2-methylaminobenzoate (**5**).

For the procedure see general prescription. 200 mg introduced disodium salt of ATP
led over all purification steps to 41 mg (64 µmol, 19 %) pure product. R_f = 0.26 (1-
propanol:H_2O:NH_3 (32 %) = 2:1:1). HPLC (analytic): R_t = 20.18 min, 20.37 min;
k = 12.83,   12.96;   LC/MS   (ESI, H_2O/CH_3CN):   *m/z* = 658.2   [$M+NH_4^+$]
(R_t = 21.61 min, 21.82 min,   100 %);   (-ESI, H_2O/CH_3CN):   *m/z* = 639.2 [$M-H^-$]
(R_t = 21.60 min, 21.81 min, 100 %); HPLC (preparative), gradient (t [min], % B: [0,
14], [20, 14], [30, 80]): R_t = 10.20 min, 11.46 min; empirical formula: $C_{18}H_{23}N_7O_{15}P_3$;
MW = 640.33

MANT-ITP
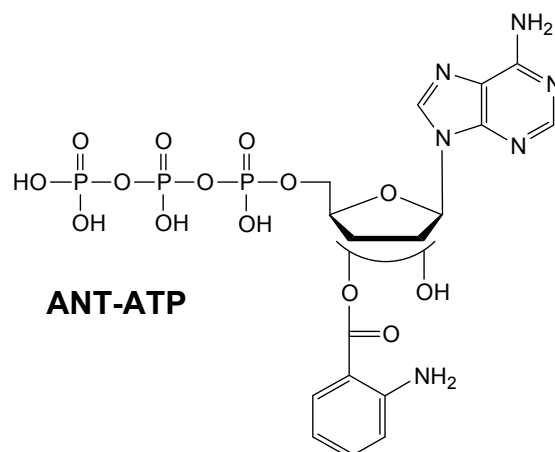
MANT-ITP (*N*-methyl-2'(3')-*O*-anthraniloyl-inosine-5'-triphosphate) or [(2R,3S,4R,5R)-5-(6-oxo-1H-purin-9-yl)-4(3)-hydroxy-2-[[hydroxy-(hydroxy-phosphonooxyphosphoryl)oxyphosphoryl]oxymethyl]oxolan-3(4)-yl]2-methylaminobenzoate (**8**).

189 mg introduced trisodium salt of ITP yielded over all purification steps 39 mg (61 µmol, 18 %) pure product. R_f = 0.31 (1-propanol:H_2O: NH_3 (32 %) = 2:1:1). HPLC (analytic): R_t = 19.74 min, 19.86 min; k = 12.65, 12.73; LC/MS (ESI, H_2O/CH_3CN): *m/z* = 676.2 [M-H+2NH_4^+] (R_t = 20.92 min, 100 %), 659.2 [M+NH_4^+] (R_t = 20.92 min, 80 %); (-ESI, H_2O/CH_3CN): *m/z* = 640.2 [M-H⁻] (R_t = 20.92 min, 100%); HPLC (preparative), gradient (t [min], % B: [0, 14], [20, 14], [30, 80]): R_t = 8.03 min, 8.23 min; empirical formula: $C_{18}H_{22}N_5O_{15}P_3$; MW = 641.31
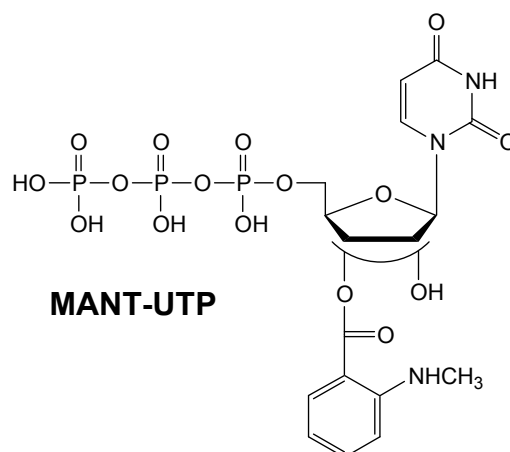

MANT-UTP

MANT-UTP (*N*-methyl-2'(3')-*O*-anthraniloyl-uridine-5'-triphosphate) or [(2R,3S,4R,5R)-5-(2,4-dioxopyrimidin-1-yl)-4(3)-hydroxy-2-[[hydroxy-(hydroxy-phosphonooxyphosphoryl)oxyphosphoryl]oxymethyl]oxolan-3(4)-yl]2-methylaminobenzoate (**11**).

182 mg introduced disodium salt of UTP yielded over all purification steps 32 mg (52 µmol, 15 %) pure product. R_f = 0.21 (1-propanol:H_2O:NH_3 (32 %) = 2:1:1). HPLC (analytic): R_t = 18.78 min, 19.15 min; k = 12.49, 12.75; LC/MS (ESI, H_2O/CH_3CN): *m/z* = 635.2 [M+NH_4^+] (R_t = 19.69 min, 19.88 min, 100 %), 652.2 [M-H+2NH_4^+] (R_t = 20.15 min, 100 %); (-ESI, H_2O/CH_3CN): *m/z* = 616.2 [M-H$^-$] (R_t = 19.53 min, 20.01 min, 100 %); HPLC (preparative), gradient (t [min], % B: [0, 14], [20, 14], [30, 80]): R_t = 6.07 min, 6.79 min; empirical formula: $C_{17}H_{22}N_3O_{16}P_3$; MW = 617.29
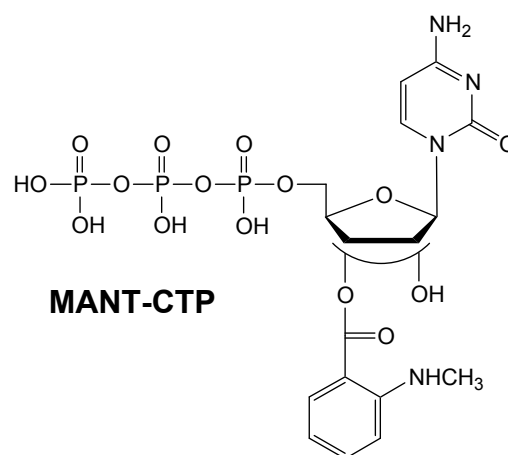
MANT-CTP

MANT-CTP   (*N*-methyl-2'(3')-*O*-anthraniloyl-cytosine-5'-triphosphate)   or [(2R,3S,4R,5R)-5-(4-amino-2-oxopyrimidin-1-yl)-4(3)-hydroxy-2-[[hydroxy-(hydroxy-phosphonooxyphosphoryl)oxyphosphoryl]oxymethyl]oxolan-3(4)-yl]2-methylaminobenzoate (**12**).

200 mg introduced trisodium salt of CTP yielded over all purification steps 30 mg (48 µmol, 14 %) pure product. R_f = 0.24 (1-propanol:H_2O:NH_3 (32 %) = 2:1:1). HPLC (analytic): R_t = 16.86 min, 17.60 min; k = 11.17, 11.70; LC/MS (ESI, H_2O/CH_3CN): *m/z* = 634.2 [M+NH_4^+] (R_t = 12.98 min, 16.98 min, 100 %); (-ESI, H_2O/CH_3CN): *m/z* = 615.2 [M-H$^-$] (R_t = 13.75 min, 17.24 min, 100 %); HPLC (preparative), gradient (t [min], % B: [0, 14], [20, 14], [30, 80]): R_t = 4.08 min, 4.61 min; empirical formula: $C_{17}H_{23}N_4O_{15}P_3$; MW = 616.30

ANT-ATP

ANT-ATP (2'(3')-*O*-anthraniloyl-adenosine-5'-triphosphate) or [(2R,3S,4R, 5R)-5-(6-aminopurin-9-yl)-4(3)-hydroxy-2-[[hydroxy-(hydroxy-phosphonooxy-phosphoryl)oxyphosphoryl]oxymethyl]oxolan-3(4)-yl]2-aminobenzoate (**14**).
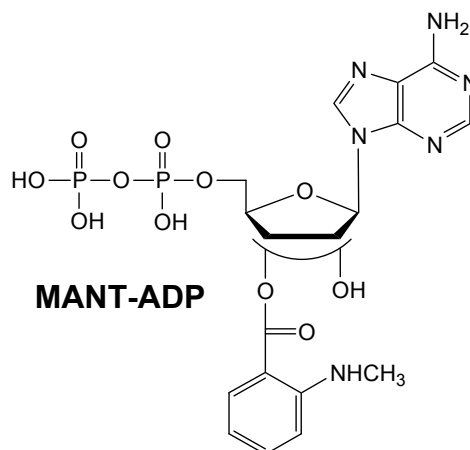
189 mg introduced disodium salt of ATP yielded over all purification steps 59 mg (94 µmol, 26 %) pure product. R_f = 0.24 (1-propanol:H_2O:NH_3 (32 %) = 2:1:1). HPLC (analytic): R_t = 17.44 min; k = 10.07; LC/MS (ESI, H_2O/CH_3CN): *m/z* = 661.3 [M-H+2NH_4^+] (R_t = 18.12 min, 18.32 min, 100 %), 644.2 [M+NH_4^+] (R_t = 18.12 min, 18.32 min, 80 %); (-ESI, H_2O/CH_3CN): *m/z* = 625.2 [M-H$^-$] (R_t = 18.12 min, 18.33 min, 100 %); HPLC (preparative), gradient (t [min], % B: [0, 11], [9, 11], [19, 80]): R_t = 7.07 min, 7.51 min; empirical formula: $C_{17}H_{21}N_6O_{14}P_3$; MW = 626.30
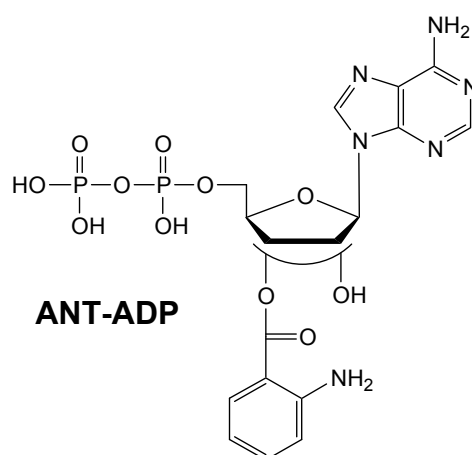
ANT-ADP

ANT-ADP (2'(3')-*O*-anthraniloyl-adenosine-5'-diphosphate) or [(2R,3S,4R,5R)-5-(6-aminopurin-9-yl)-4(3)-hydroxy-2-[(hydroxy-phosphonooxyphosphoryl)oxymethyl]oxolan-3(4)-yl]2-aminobenzoate (**15**).
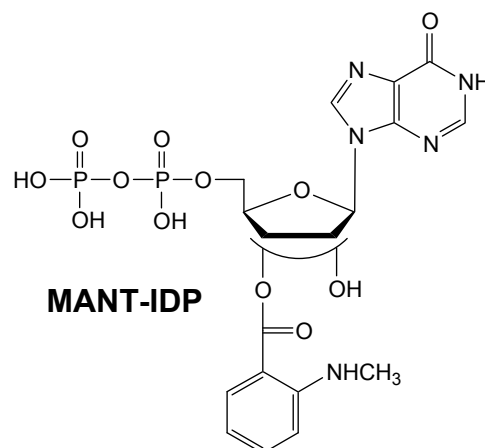
200 mg introduced disodium salt of ADP yielded over all purification steps 8 mg (15 µmol, 4 %) pure product. R_f = 0.27 (1-propanol:H_2O:NH_3 (32 %) = 2:1:1). HPLC

(analytic): R_t = 18.09 min; k = 10.73; LC/MS (ESI, H_2O/CH_3CN): *m/z* = 564.3 [M+NH$_4^+$] (R_t = 18.81 min, 19.04 min, 100 %); (-ESI, H_2O/CH_3CN): *m/z* = 545.2 [M-H$^-$] (R_t = 18.81 min, 19.04 min, 100 %); HPLC (preparative), gradient (t [min], % B: [0, 11], [9, 11], [19, 80]): R_t = 8.99 min; empirical formula: $C_{17}H_{20}N_6O_{11}P_2$; MW = 546.32
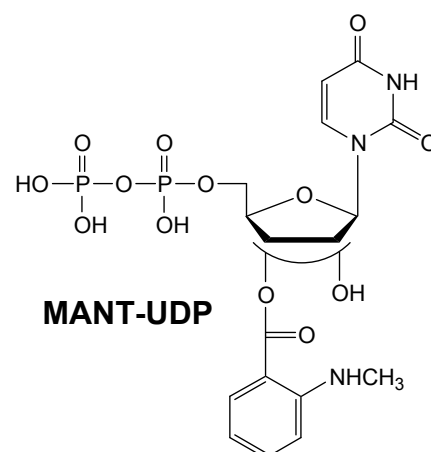

MANT-ADP

MANT-ADP   (*N*-methyl-2'(3')-*O*-anthraniloyl-adenosine-5'-diphosphate)   or [(2R,3S,4R,5R)-5-(6-aminopurin-9-yl)-4(3)-hydroxy-2-[(hydroxy-phosphonooxy phosphoryl)-oxymethyl]oxolan-3(4)-yl]2-methylaminobenzoate (**16**).

For the procedure see general prescription. 200 mg introduced disodium salt of ATP led over all purification steps to 4.7 mg (8.4 µmol, 2.2 %) pure product. R_f = 0.29 (1-propanol:H_2O:NH_3 (32 %) = 2:1:1). HPLC (analytic): R_t = 20.56 min, 20.79 min; k = 13.09, 13.25; LC/MS (ESI, H_2O/CH_3CN): *m/z* = 561.2 [M+H$^+$] (R_t = 22.24 min, 22.41 min, 100 %); (-ESI, H_2O/CH_3CN): *m/z* = 559.2 [M-H$^-$] (R_t = 22.23 min, 22.41 min, 100 %); HPLC (preparative), gradient (t [min], % B: [0, 14], [20, 14], [30, 80]): R_t = 14.56 min, 15.54 min; empirical formula: $C_{18}H_{22}N_6O_{11}P_2$; MW = 560.35

MANT-IDP

MANT-IDP (*N*-methyl-2'(3')-*O*-anthraniloyl-inosine-5'-diphosphate) or [(2R,3S,4R,5R)-5-(6-oxo-1H-purin-9-yl)-4(3)-hydroxy-2-[(hydroxy-phosphonooxy phosphoryl)oxymethyl]oxolan-3(4)-yl]2-methylaminobenzoate (**17**).
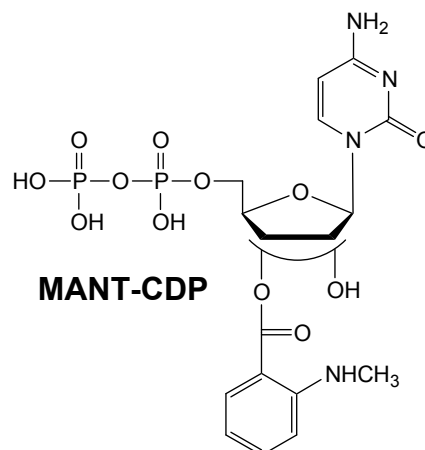
189 mg introduced disodium salt of IDP yielded over all purification steps 15 mg (27 µmol, 7 %) pure product. R_f = 0.35 (1-propanol:H_2O:NH_3 (32 %) = 2:1:1). HPLC (analytic): R_t = 20.34 min, 20.58 min; k = 13.07, 13.23; LC/MS (ESI, H_2O/CH_3CN): *m/z* = 596.3 [M-H+2NH_4^+] (R_t = 21.38 min, 100 %), 579.3 [M+NH_4^+] (R_t = 21.38 min, 70 %); (-ESI, H_2O/CH_3CN): *m/z* = 560.2 [M-H⁻] (R_t = 21.39 min, 21.55 min, 100 %); HPLC (preparative), gradient (t [min], % B: [0, 14], [20, 14], [30, 80]): R_t = 10.62 min, 11.36 min; empirical formula: $C_{18}H_{21}N_5O_{12}P_2$; MW = 561.33

MANT-UDP

MANT-UDP (*N*-methyl-2'(3')-*O*-anthraniloyl-uridine-5'-diphosphate) or [(2R,3S,4R,5R)-5-(2,4-dioxopyrimidin-1-yl)-4(3)-hydroxy-2-[(hydroxy-phosphonooxyphosphoryl)oxymethyl]oxolan-3(4)-yl]2-methylaminobenzoate (**18**).

182 mg introduced disodium salt of UDP yielded over all purification steps 8 mg (15 µmol, 3.8 %) pure product. R_f = 0.25 (1-propanol:H_2O:NH_3 (32 %) = 2:1:1). HPLC

(analytic): R_t = 19.75 min, 19.93 min; k = 13.19, 13.32; LC/MS (ESI, H_2O/CH_3CN): *m/z* = 555.2 [M+NH_4^+] (R_t = 20.64 min, 20.94 min, 100 %), 572.2 [M-H+2NH_4^+] (R_t = 20.64 min, 20.94 min, 40 %); (-ESI, H_2O/CH_3CN): *m/z* = 536.2 [M-H$^-$] (R_t = 20.50 min, 20.78 min, 100 %); HPLC (preparative), gradient (t [min], % B: [0, 14], [20, 14], [30, 80]): R_t = 8.79 min, 9.49 min; empirical formula: $C_{17}H_{21}N_3O_{13}P_2$; MW = 537.31


MANT-CDP

MANT-CDP   (*N*-methyl-2'(3')-*O*-anthraniloyl-cytosine-5'-diphosphate)   or [(2R,3S,4R,5R)-5-(4-amino-2-oxopyrimidin-1-yl)-4(3)-hydroxy-2-[(hydroxy-phosphonooxyphosphoryl)oxymethyl]oxolan-3(4)-yl]2-methylaminobenzoate (**19**).

200 mg introduced disodium salt of CDP yielded over all purification steps 2 mg (3.7 µmol, 1 %) pure product. R_f = 0.28 (1-propanol:H_2O:NH_3 (32 %) = 2:1:1). HPLC (analytic): R_t =18.38 min; k = 12.27; LC/MS (ESI, H_2O/CH_3CN): *m/z* = 554.2 [M+NH_4^+] (R_t = 18.55 min, 100 %); (-ESI, H_2O/CH_3CN): *m/z* = 535.2 [M-H$^-$] (R_t = 18.66 min, 100 %); HPLC (preparative), gradient (t [min], % B: [0, 14], [20, 14], [30, 80]): R_t = 5.80 min; empirical formula: $C_{17}H_{22}N_4O_{12}P_2$; MW = 536.32
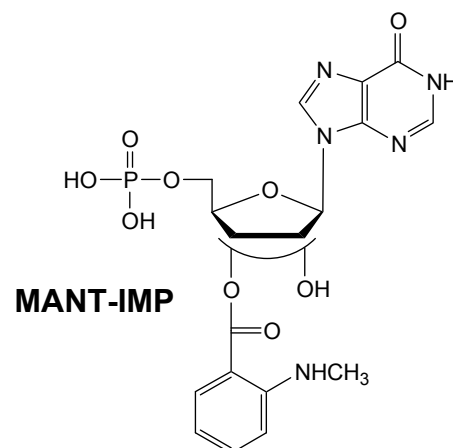
MANT-IMP

MANT-IMP (*N*-methyl-2'(3')-*O*-anthraniloyl-inosine-5'-monophosphate) or [(2R,3S,4R,5R)-5-(6-oxo-1H-purin-9-yl)-4(3)-hydroxy-2-[phosphonooxymethyl] oxolan-3(4)-yl]2-methylaminobenzoate (**20**).

The disodium salt of IMP (100 mg, 0.26 mmol) yielded 34 mg (71 µmol, 27 %) pure product after size-exclusion chromatography. R_f = 0.22 (1-propanol:H_2O:NH_3 (32 %) = 2:1:1). HPLC (analytic): R_t = 21.36 min, 22.08 min; k = 12.68, 13.15; LC/MS (ESI, H_2O/CH_3CN): *m/z* = 499.2 [M+NH_4^+] (R_t = 22.07 min, 22.78 min, 100 %); (-ESI, H_2O/CH_3CN): *m/z* = 480.2 [M-H^-] (R_t = 22.06 min, 22.77 min, 80 %), 540.2 [M+CH_3COO^-] (R_t = 22.06 min, 22.77 min, 100 %); empirical formula: $C_{18}H_{20}N_5O_9P$; MW = 481.35
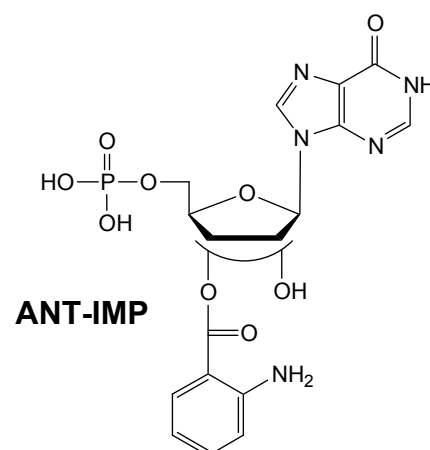
ANT-IMP

ANT-IMP (2'(3')-*O*-anthraniloyl-inosine-5'-monophosphate) or [(2R,3S,4R,5R)-5-(6-oxo-1H-purin-9-yl)-4(3)-hydroxy-2-[phosphonooxymethyl]oxolan-3(4)-yl]2-aminobenzoate (**21**).

The disodium salt of IMP (100 mg, 0.26 mmol) yielded 30 mg (65 µmol, 25 %) pure product after size-exclusion chromatography. R_f = 0.20 (1-propanol:H_2O:NH_3 (32 %)

= 2:1:1). HPLC (analytic): R_t = 17.88 min, 18.82 min; k = 10.72, 11.34; LC/MS (ESI, H_2O/CH_3CN): *m/z* = 485.1 [M+NH$_4^+$] (R_t = 17.75 min, 19.13 min, 100 %); (-ESI, H_2O/CH_3CN): *m/z* = 466.1 [M-H$^-$] (R_t = 17.75 min, 19.13 min, 40 %), 526.2 [M+CH$_3$COO$^-$] (R_t = 17.75 min, 19.13 min, 100 %); empirical formula: $C_{17}H_{18}N_5O_9P$; MW = 467.33

6. References

[1] Sunahara, R. K.; Dessauer, C. W.; Gilman, A. G. *Annu. Rev. Pharmacol. Toxicol.* **1996**, *36*, 461

[2] (a) Tang, W. J.; Hurley, J. H. *Mol. Pharmacol.* **1998**, *54*, 231; (b) Hanoune, J.; Defer, N. *Annu. Rev. Pharmacol. Toxicol.* **2001**, *41*, 145

[3] Pinto, C.; Papa, D.; Hübner, M.; Mou, T. C.; Lushington, G. H.; Seifert, R. *J. Pharmacol. Exp. Ther.* **2008**, *325*, 27

[4] Wang, H.; Gong, B.; Vadakkan, K. I.; Toyoda, H.; Kaang, B. K.; Zhuo, M. *J. Biol. Chem.* **2007**, *282*, 1507

[5] Watts, V. J. *Mol. Interv.* **2007**, *7*, 70

[6] (a) Okumura, S.; Takagi, G.; Kawabe, J.; Yang, G.; Lee, M. C.; Hong, C.; Liu, J.; Vatner, D. E.; Sadoshima, J.; Vatner, S. F.; Ishikawa, Y. *Proc. Natl. Acad. Sci. USA* **2003**, *100*, 9986; (b) Yan, L.; Vatner, D. E.; O'Connor, J. P.; Ivessa, A.; Ge, H.; Chen, W.; Hirotani, S.; Ishikawa, Y.; Sadoshima, J.; Vatner, S. F. *Cell* **2007**, *130*, 247

[7] (a) Kim, K. S.; Kim, J.; Back, S. K.; Im, J. Y.; Na, H. S.; Han, P. L. *Genes Brain Behav.* **2007**, *6*, 120; (b) Tang, T.; Lai, N. C.; Roth, D. M.; Drumm J., Guo, T.; Lee, K. W.; Han, P. L.; Dalton, N.; Gao, M. H. *Basic. Res. Cardiol.* **2006**, *101*, 117

[8] Chester, J. A.; Watts, V. J. *Sci. STKE* **2007**, *413*, pe64

[9] Onda, T.; Hashimoto, Y.; Nagai, M.; Kuramochi, H.; Saito, S.; Yamazaki, H.; Toya, Y.; Sakai, I.; Homcy, C. J.; Nishikawa, K.; Ishikawa, Y. *J. Biol. Chem.* **2001**, *276*, 47785

[10] Rottländer, D.; Matthes, J.; Vatner, S. F.; Seifert, R.; Herzig, S. *J. Pharmacol. Exp. Ther.* **2007**, *321*, 608

[11] Gille, A.; Seifert, R. *J. Biol. Chem.* **2003**, *278*, 12672

[12] Gille, A.; Lushington, G. H.; Mou, T. C.; Doughty, M. B.; Johnson, R. A.; Seifert, R. *J. Biol. Chem.* **2004**, *279*, 19955

[13] Jameson, D. M.; Eccleston, J. F. *Methods Enzymol.* **1997**, *278,* 363

[14] Mou, T. C.; Gille, A.; Fancy, D. A.; Seifert, R.; Sprang, S. R. *J. Biol. Chem.* **2005**, *280*, 7253

[15] Mou, T. C.; Gille, A.; Suryanarayana, S.; Richter, M.; Seifert, R.; Sprang, S. R. *Mol. Pharmacol.* **2006**, *70*, 878

[16] Gille, A.; Guo, J.; Mou, T. C.; Doughty, M. B; Lushington, G. H.; Seifert, R. *Biochem. Pharmacol.* **2005**, *71*, 89

[17] Wang, J. L.; Guo, J. X.; Zhang, Q. Y.; Wu, J. J.; Seifert, R.; Lushington, G. H. *Bioorg. Med. Chem.* **2007**, *15*, 2993

[18] Hiratsuka, T. Biochim. Biophys. Acta **1983**, *742*, 496

[19] Taha, H.; Schmidt, J.; Göttle, M.; Suryanarayana, S.; Shen, Y.; Tang, W. J.; Gille, A.; Geduhn, J.; König, B.; Dove, S.; Seifert, R. *Mol. Pharmacol.* **2009**, *75*, 693

[20] Göttle, M.; Dove, S.; Steindel, P.; Shen, Y.; Tang, W. J.; Geduhn, J.; König, B.; Seifert, R. *Mol. Pharmacol.* **2007**, *72*, 526

[21] Sunahara, R. K.; Dessauer, C. W.; Whisnant, R. E.; Kleuss, C.; Gilman, A. G. *J. Biol. Chem.* **1997**, *272*, 22265

[22] Seifert, R.; Lee, T. W.; Lam, V. T.; Kobilka, B. K. *Eur. J. Biochem.* **1998***, 255,* 369

[23] Okumura, S.; Vatner, D. E.; Kurotani, R.; Bai, Y.; Gao, S.; Yuan, Z.; Iwatsubo, K.; Ulucan, C.; Kawabe, J.; Ghosh, K.; Vatner, S. F.; Ishikawa, Y. *Circulation* **2007**, *116*, 1776

[24] Tesmer, J. J.; Sunahara, R. K.; Gilman, A. G.; Sprang, S. R. *Science* **1997**, *278*, 1907

[25] Gohlke, H.; Klebe, G. *Angew. Chem. Int. Ed.* **2002**, *41*, 2644

[26] Morgan, B. P.; Scholtz, J. M.; Ballinger, M. D.; Zipkin, I. D.; Bartlett, P. A. *J. Am. Chem. Soc.* **1991**, *113*, 297

III. Bis-substituted anthraniloyl-derived nucleotides as potent and selective adenylyl cyclase inhibitors[ψ][ξ]

1. Introduction

Whooping cough is a highly contagious acute disease of the respiratory tract caused by the gram-negative bacterium *Bordetella pertussis*[1,2]. The immobile and aerobic bacterium *Bordetella pertussis* secretes the key virulence factor, the adenylyl cyclase toxin CyaA. The exotoxin consists of 1706 amino acids. The N-terminal domain (400 amino acids) contains the active center for catalysis and the 1300 amino acid C-terminal domain interacts with eukaryotic host cells for delivery of the catalytic domain into the cytosol[3,4,5]. Moreover, the C-terminal residue possesses low hemolytic activity[2].

The endogenous calcium sensor calmodulin (CaM) activates CyaA toxin with high affinity (K_d = 0.2 nM) by forming a large number of salt bridges, hydrogen bonds, and hydrophobic interactions[29]. After activation of the bacterial adenylyl cyclase a massive production of the second messenger cAMP from ATP is catalyzed[6,16]. The supraphysiological level of cAMP disrupts the endogenous signal transduction, inhibits phagocyte function, and facilitates respiratory tract infection by *Bordetella pertussis*[7]. Substrate analogs of ATP may be used to inhibit the catalytic activity of CyaA[8,18,32] and prophylaxis of *Bordetella pertussis* infection (**Fig. 1**). We have discovered *N*-methylanthraniloyl (MANT) substituted nucleotides as competitive inhibitors of mammalian and bacterial ACs, including CyaA[15,18,37]. In addition, 2',3'-(2,4,6-trinitrophenyl) (TNP)-substituted NTPs are valuable compounds for the inhibition and conformational characterization of mammalian[28] and bacterial[15] ACs. Furthermore, adefovir, a drug for the treatment of chronic hepatitis B virus infection, is a potent CyaA inhibitor[16].

In mammals nine closely related membranous AC isoforms (AC1-9) and one soluble AC are expressed[9]. We have employed the cytosolic domains C1 of type 5 AC and C2 of type 2 AC for molecular AC analysis[18,27,28]. We have also reported the crystal structure of CyaA in complex with CaM and 9-[2-(phosphonomethoxy)ethyl]adenine diphosphate (PMEApp)[29], the active metabolite of adefovir. By the combination of

---

[ψ] The results of this chapter are in preparation for publication.

[ξ] Molecular modeling was carried out by Prof. Dr. Stefan Dove, University of Regensburg, Germany.

Fig. 1. Representative AC inhibitors of ATP analogs
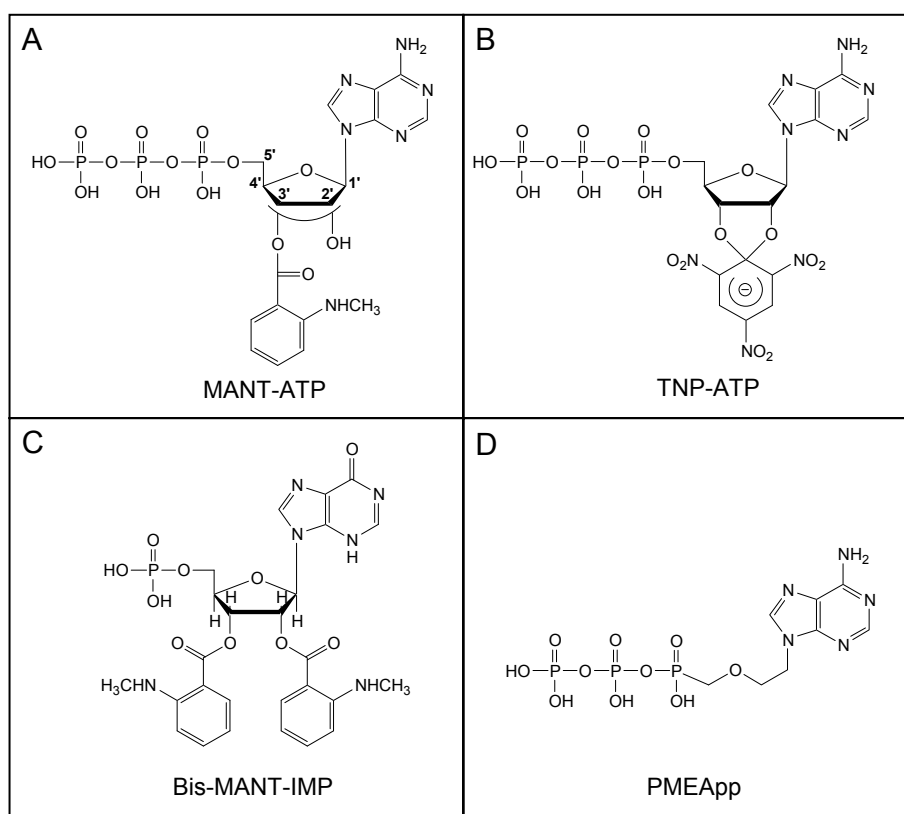
Structures of MANT-ATP (A), TNP-ATP (B), Bis-MANT-IMP (C), PMEApp (D) are shown as representative AC inhibitors. The MANT-group of MANT-ATP is not fixed and undergoes spontaneous isomerization between 2'- and 3'-ribosyl position under physiological pH[23]. For TNP-ATP the TNP-group is fixed to the ribosyl ring via the 2'- and 3'-position, isomerization does not occur at neutral or basic pH[10].

crystallographic and molecular modeling approaches, we investigated in the binding motive of MANT-nucleotides, developing a three-site pharmacophore model for mAC and CyaA with domains for the base, the MANT-group and the polyphosphate chain[11,12,15,28]. Several complementary approaches can be employed for monitoring nucleotide binding to, and conformational changes in, CyaA. MANT- and ANT-nucleotides are environmentally sensitive fluorescent probes displaying increased fluorescence and blue shift of the emission maximum upon exposure to a hydrophobic environment[23,43]. In accordance to the CyaA crystal structure in complex with PMEApp[29] the catalytic site contains the hydrophobic amino acid phenylalanine 306. Nucleotide binding to CyaA allows hydrophobic interactions between the (M)ANT-group and Phe306, resulting in an increased fluorescence signal[13,29]. This observation is supported by the fact that CyaA-Phe306Ala does not increase the fluorescence signal of 3'-ANT-2'd-ATP[29].

Enzymatic, fluorescence, crystallographic and molecular modeling studies showed that the catalytic site of mAC and CyaA exhibit substantial conformational flexibility, accommodating both purine and pyrimidine nucleotides. Nonetheless, the structure/activity relationships of MANT-nucleotides at mAC and CyaA are quite different, offering the opportunity to design potent and selective AC inhibitors[11,12,28]. In our recent study[15], we have shown that the spacious catalytic site of CyaA accommodates a broad variety of 2',3'-substituted nucleotides, even a bis-substituted MANT-nucleotide. Interestingly, Bis-MANT-IMP exhibited higher potency in comparison to the corresponding mono-substituted MANT-nucleotide. This finding was an excellent starting point for the new synthesis of bis-substituted MANT-nucleoside 5'-triphosphates, expecting even higher inhibition potency by the elongation of the polyphosphate tail. The number of phosphate groups critically determines the affinity of AC for 2',3'-substituted nucleotides[11,15].

To the best of our knowledge, bis-substituted (M)ANT-nucleotides have not yet been explicitly described in the literature, although they apparently occurred as side products in the regular synthesis[43] of MANT-nucleotides. In the present study, we expanded the synthesis of bis-substituted (M)ANT-nucleotides (compounds: **17**, **18**, **19**, **28**, **29**, **32**) and synthesized new mono- and bis-substituted anthraniloyl-group derived purine nucleotides (**Fig. 2**). The anthraniloyl (ANT) moiety differ by halogens of chlorine and bromine (**4 – 7**, **14**, **20 – 23**, **30**) and acetylated amino group (**10**, **11**, **26**, **27**) in 5 position of the phenyl ring system. Moreover, substitution at the amino function of the ANT-group lead to propyl (Pr-ANT) derivatives (**8**, **9**, **24**, **25**).

Overall, we prepared 32 compounds in our study to compare 16 pairs of mono- and bis-substituted (M)ANT-nucleotides for their potencies at inhibiting CyaA and mACs and to regard selectivity between mammalian and bacterial AC. So far, highly potent CyaA inhibitors with selectivity towards mammalian ACs are unknown. The insertion of a second fluorophore may result in unexpected fluorescence properties, why we also investigated fluorescence spectroscopy. In addition, the binding mode of representative derivatives was explored by modeling studies.

2. Materials and Methods

2.1. Materials

Mono-substituted (M)ANT-NTPs of MANT-ATP (**1**), MANT-ITP (**2**), MANT-CTP (**3**), MANT-NDPs of MANT-ADP (**12**), MANT-IDP (**13**) and MANT-NMPs of MANT-IMP (**15**), ANT-IMP (**16**) were synthesized as described[14,15].

Synthesis of new compounds of mono- and bis-substituted (M)ANT nucleotides followed the general reaction scheme (**Fig. 2**) to achieve halogen anthraniloylic derived residues of (Bis-)Cl-ANT-ATP (**4**, **20**), (Bis-)Cl-ANT-ITP (**5**, **21**), (Bis-)Br-ANT-ATP (**6**, **22**), (Bis-)Br-ANT-ITP (**7**, **23**), (Bis-)Br-ANT-ADP (**14**, **30**) and propyl anthraniloylic derived residues of (Bis-)Pr-ANT-ATP (**8**, **24**), (Bis-)Pr-ANT-ITP (**9**, **25**) and acetylated amino anthraniloylic derived residues of (Bis-)Ac-NH-ANT-ATP (**10**, **26**), (Bis-)Ac-NH-ANT-ITP (**11**, **27**). Furthermore we generated the bis-substituted derivatives of the known (M)ANT-nucleotides of Bis-MANT-ATP (**17**), Bis-MANT-ITP (**18**), Bis-MANT-CTP (**19**), Bis-MANT-ADP (**28**), Bis-MANT-ADP (**29**), Bis-MANT-IMP (**31**), and Bis-ANT-IMP (**32**).

Under the basic reaction conditions mono- and bis-(M)ANT-NTP derivatives were partially decomposed to its corresponding diphosphates. Because of their putative inhibitory effects they were isolated as well. For more details see Experimental section. Methylisatoic anhydride, isatoic anhydride, chloroisatoic anhydride, bromoisatoic anhydride, aminoisatoic anhydride, ATP, ITP, CTP, IMP and bovine serum albumin, fraction V, highest quality, were purchased from Sigma-Aldrich (Seelze, Germany). $MnCl_2$ tetrahydrate (highest quality) and Aluminum oxide 90 active, (neutral, activity 1; particle size, 0.06 - 0.2 mm) were from MP Biomedicals (Eschwege, Germany). PMEApp was supplied by Gilead Sciences (Foster City, CA). The catalytic domain of *Bacillus pertussis* AC protein (CyaA, amino acids 1–373) was purified as described previously[16]. [α-^{32}P]ATP (800 Ci/mmol) was purchased from PerkinElmer, Rodgau Jügesheim, Germany. Lyophilized calmodulin from bovine brain was from Calbiochem (Darmstadt, Germany). Forskolin was supplied by LC Laboratories (Woburn, MA). For all experiments double-distilled water was used.

**Fig. 2. General reaction scheme for the synthesis of mono- and bis-substituted (M)ANT-nucleotides**
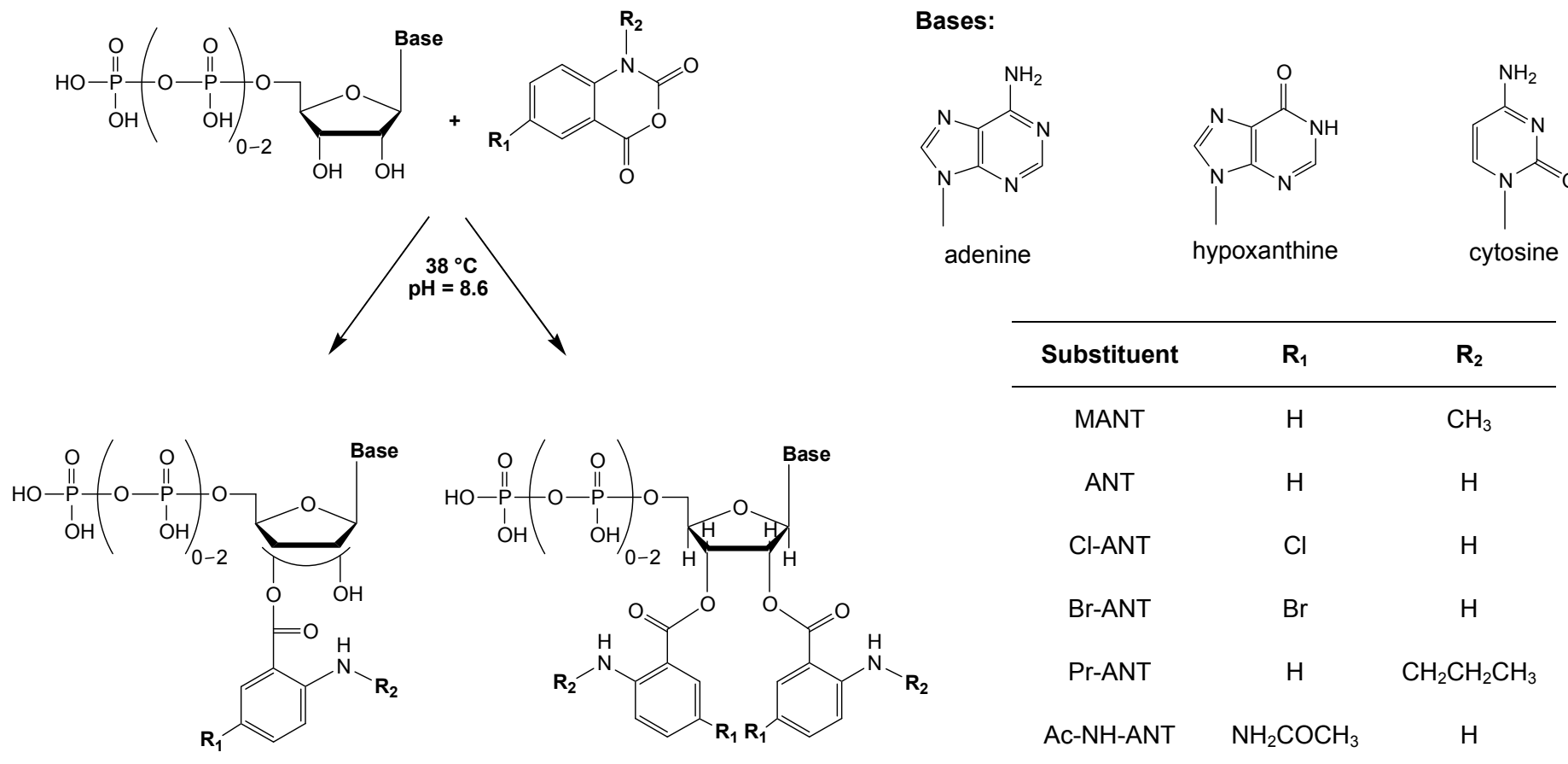
The principle of the one step synthesis of mono- and bis-substituted (M)ANT-nucleotides is shown. The conversion of nucleotide and diversified isatoic anhydride lead to the corresponding acylated nucleotide. 32 compounds were synthesized by variation of phosphate chain length, nucleobase, and anthraniloyl residue (details shown in Experimental section).

2.2 Synthesis of bis-substituted (M)ANT-nucleotides

(M)ANT-nucleotides were synthesized according to Hiratsuka[43] with modifications (details shown in Experimental section). Surprisingly, during the synthesis of MANT-IMP we observed for the first time an intensive new peak at later retention time, when the crude reaction mixture was analyzed by reversed-phase HPLC (**Fig. 3**). Due to the long retention time of the unknown peak, a more lipophilic compound with additional unpolar groups was expected. From our previous studies[14,15] degradation of MANT-NTPs to MANT-NDPs under the basic reaction conditions was known, but a decomposition of inosine 5'-monophosphate was obviously not reasonable. Thus, a further substitution of a second MANT-group was hypothesized. The analysis of LC/MS online coupling corroborated the hypothesis. The esterfication of an additional MANT-group was identified by the mass per charge ratio of 613.2 Da for the negative ESI measurement. The chromatogram of the crude reaction mixture displayed the typical two peak system for the expected *N*-methyl-2'- and 3'-*O*-anthraniloyl nucleotide isomers at a retention time of 21.4 and 22.0 min. Seven minutes later the peak for Bis-MANT-ITP appeared (R_t = 29 min). The high polarity of non-reacted IMP resulted in a fast elution directly after the dead time (minor peak at $R_t < 2$ min). Further peaks are identified for the excess of methylisatoic anhydride (R_t ~17 min) and decomposition product of the nucleoside of hypoxanthine (R_t ~23 min). The assignment of all signals was achieved by LC/MS online coupling. For the

Fig. 3. Analysis of the synthesis of MANT-IMP by HPLC
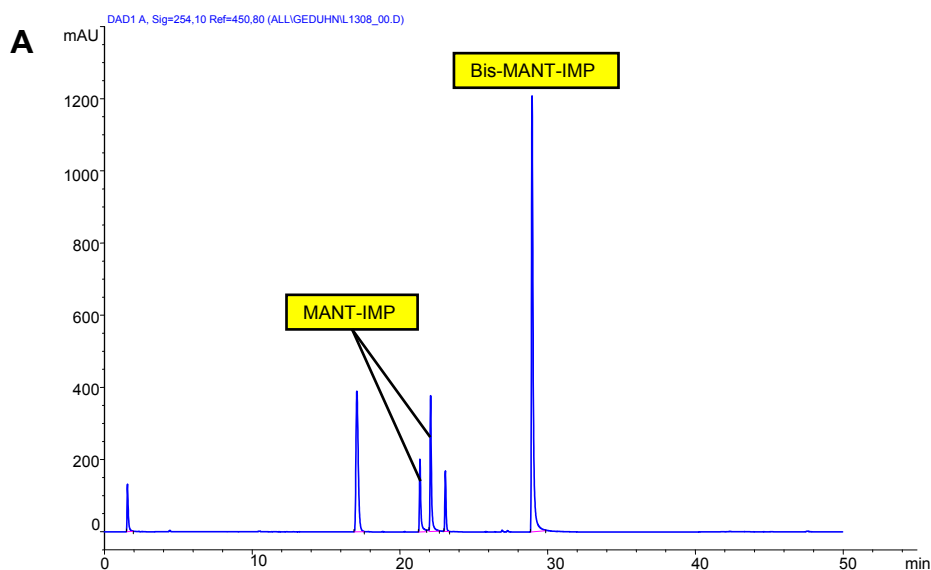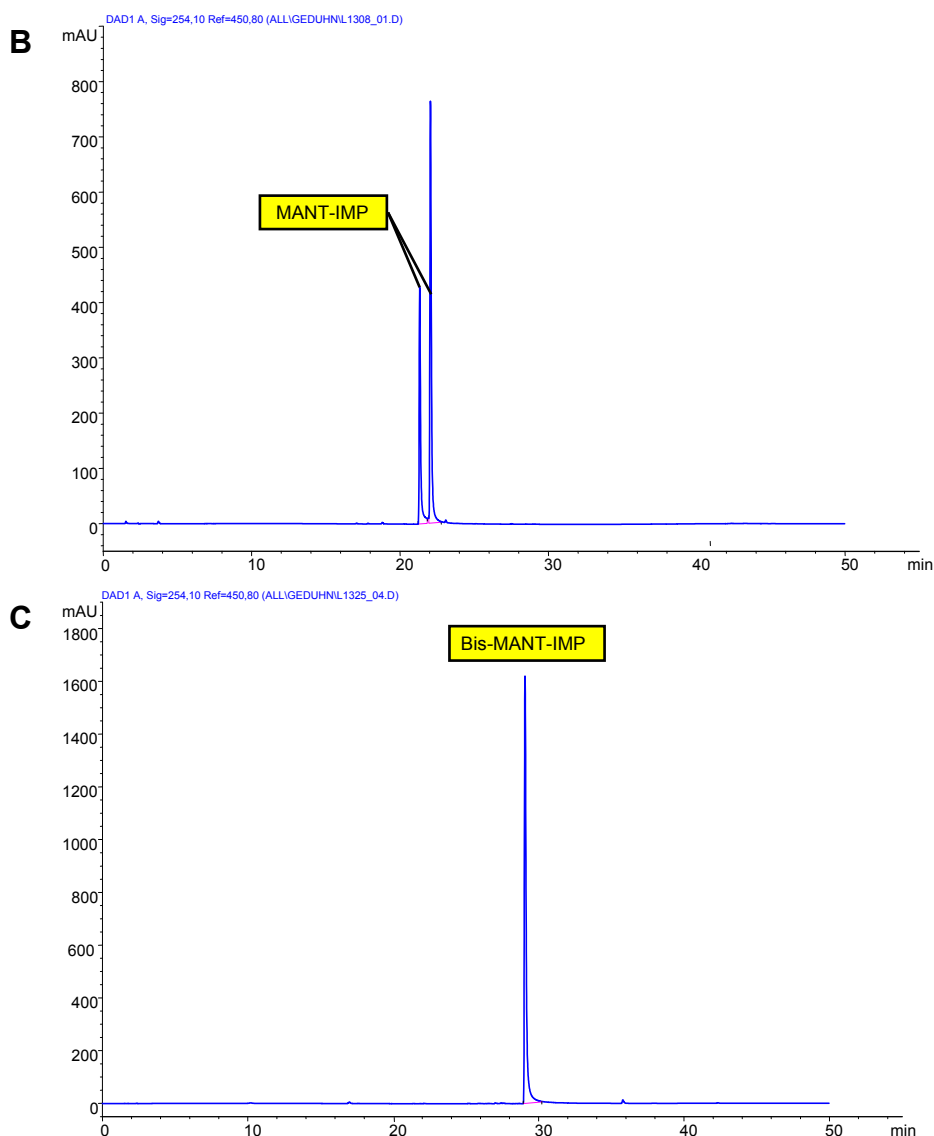
Chromatograms of MANT-IMP of the crude reaction mixture (A), after purification (B), and Bis-MANT-IMP after purification (C) were recorded by analytical HPLC analysis. The conditions are described under "Experimental section". Purification by size exclusion chromatography revealed high purity (> 99 %) for MANT-IMP and Bis-MANT-IMP. The retention times were 21.4/22.0 min for MANT-IMP and 29 min for Bis-MANT-IMP. *mAU, milli absorbance unit.*

purification of monophosphate derivatives only size-exclusion chromatography was required yielding MANT-nucleotides of high purity of approximately 99 %.

The obvious constitution of bis-substituted MANT-nucleotides is represented by a 2-fold acylated IMP derivative of the two hydroxyl groups of the ribosyl ring. A convincing conformation for this assumption was delivered by the NMR spectroscopy. By one- and two-dimensional NMR measurements structure determination of Bis-MANT-IMP confirmed our suggestion of the second acylatated free hydroxyl group. Thus, proton spectrum showed two sets of signals for the two

methyl anthraniloyl groups (**Fig. 4**). Furthermore, HMBC spectrum definitely identified *3J* correlation between protons and quaternary carbons to ensure no substitution in the purine system of the nucleobase (data not shown).

However, NMR spectroscopy is a less sensitive method and requires relatively high amount of compound, compared to HPLC and LC/MS analysis. Because of the time-consuming and costly preparative HPLC purification of (M)ANT-NTPs, NMR spectroscopic data was performed only for the monophosphate derivative of Bis-MANT-IMP. Moreover, newly synthesized compounds displayed similar properties in analytical and preparative HPLC and were clearly identified by LC/MS online coupling. The small amounts of (M)ANT-nucleotides were valuable for pharmacological analysis and also demanded in other important projects.

Fig. 4. Proton spectrum of Bis-MANT-IMP
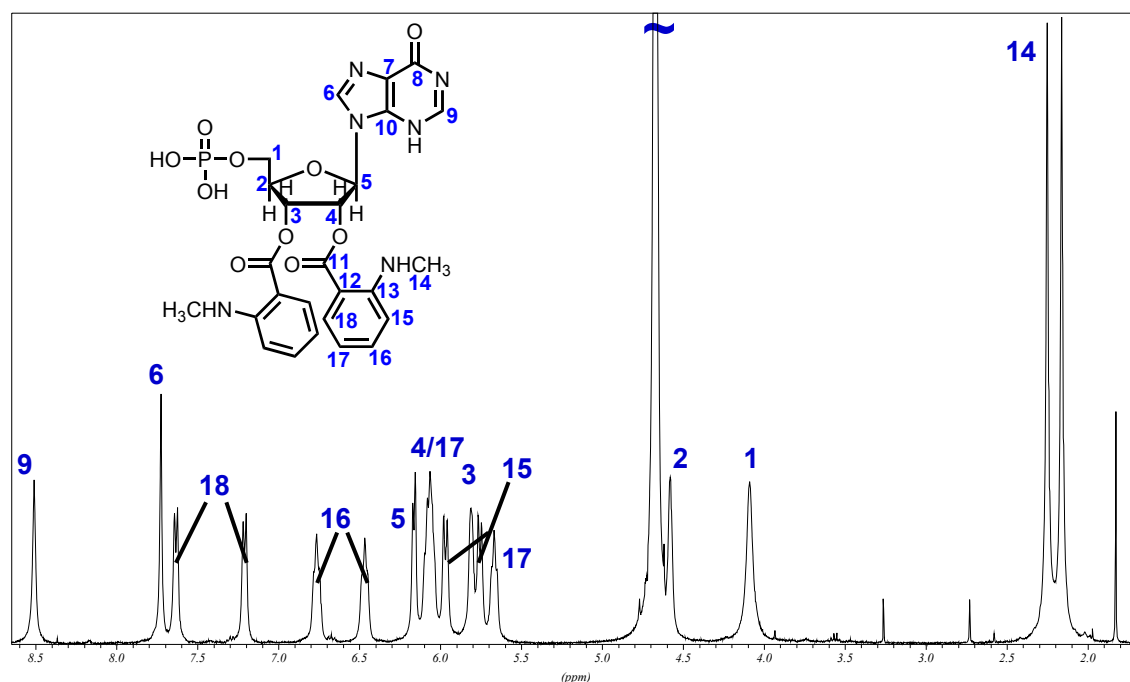
The structure determination of Bis-MANT-IMP was solved by NMR spectroscopy (details shown in Experimental section). The proton spectrum with the assignment of proton peaks is shown. The two anthraniloyl groups are represented by two signals for the methyl group of carbon **14** and according peaks of the phenyl group at position **15**, **16**, **17**, and **18**. The preserved purine base is indicated by the two protons of carbon **6** and **9**.

At the beginning of our MANT-NTP synthesis[14,15] we never observed the forming of bis-substituted MANT-nucleotides. After the discovery of Bis-MANT-IMP we addressed the question, why Bis-MANT-nucleotides did not arise for triphosphate derivatives. The standard purification procedure was performed by size-exclusion

chromatography for separation of starting materials. Non-reacted nucleotide and isatoic anhydride were removed by this method as a form of pre-cleaning. Unfortunately, bis-substituted MANT-nucleotides were lost by this separation as well. When we performed HPLC analysis of the crude reaction mixture without the pre-cleaning, similar peaks as for Bis-MANT-IMP appeared in the chromatogram (**Fig. 5**). Diode array detection and fluorescence detection for HPLC analysis supported the assignment of bis-substituted (M)ANT-nucleotide signals, because of similarity of spectroscopic properties to mono-substituted (M)ANT-nucleotides, especially of UV absorption.

Furthermore, the assignment of Bis-MANT-nucleotides was also confirmed by LC/MS online coupling. Under the basic reaction conditions degradation of the labile γ-phosphate always occurred for mono- and bis-substituted (M)ANT-nucleotides. Thus, preparative HPLC was applied for the separation of (M)ANT-NTPs and (M)ANT-NDPs. In general, the purification by this method offered the possibility to obtain four putative inhibitors simultaneously. However, due to the small retention time differences, the separation of diphosphate derivatives was more sensitive and the preparative HPLC conditions had to be chosen carefully to reach separation. Moreover, the (M)ANT-NDPs exhibited lower potencies in AC activity assay compared to (M)ANT-NTPs. Thus, purification of diphosphate derivatives were not carried out for all compounds. MANT-ATP and Bis-MANT-ATP displayed representative chromatograms for the preparative HPLC purification of mono- and bis-substituted (M)ANT-nucleotides in high purity (**Fig. 5**).

Fig. 5. Analysis of the synthesis of MANT-ATP/Bis-MANT-ATP

B

C
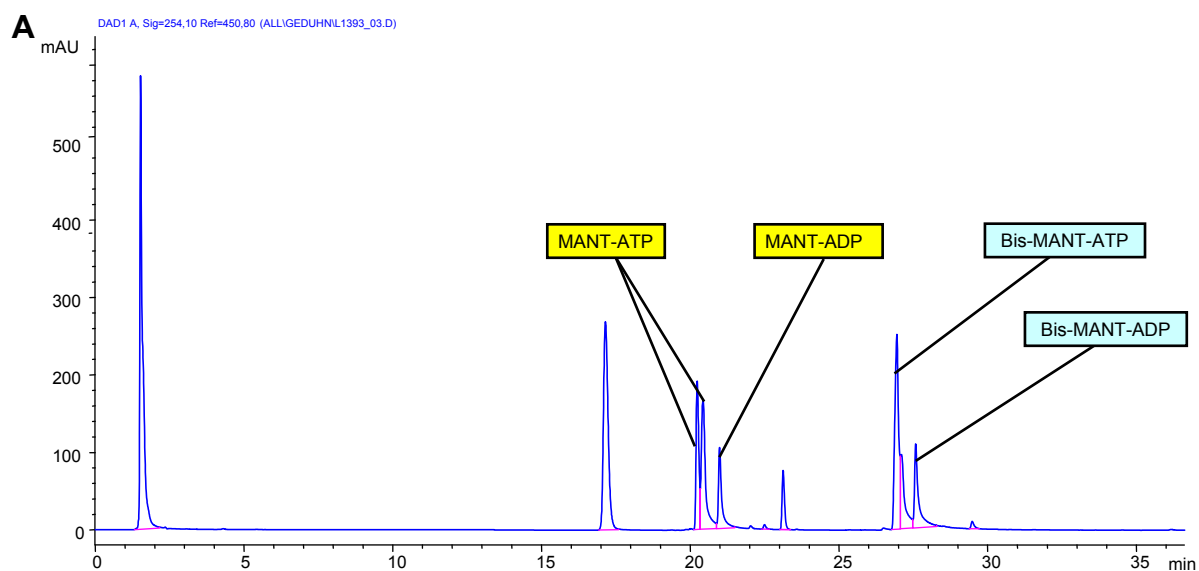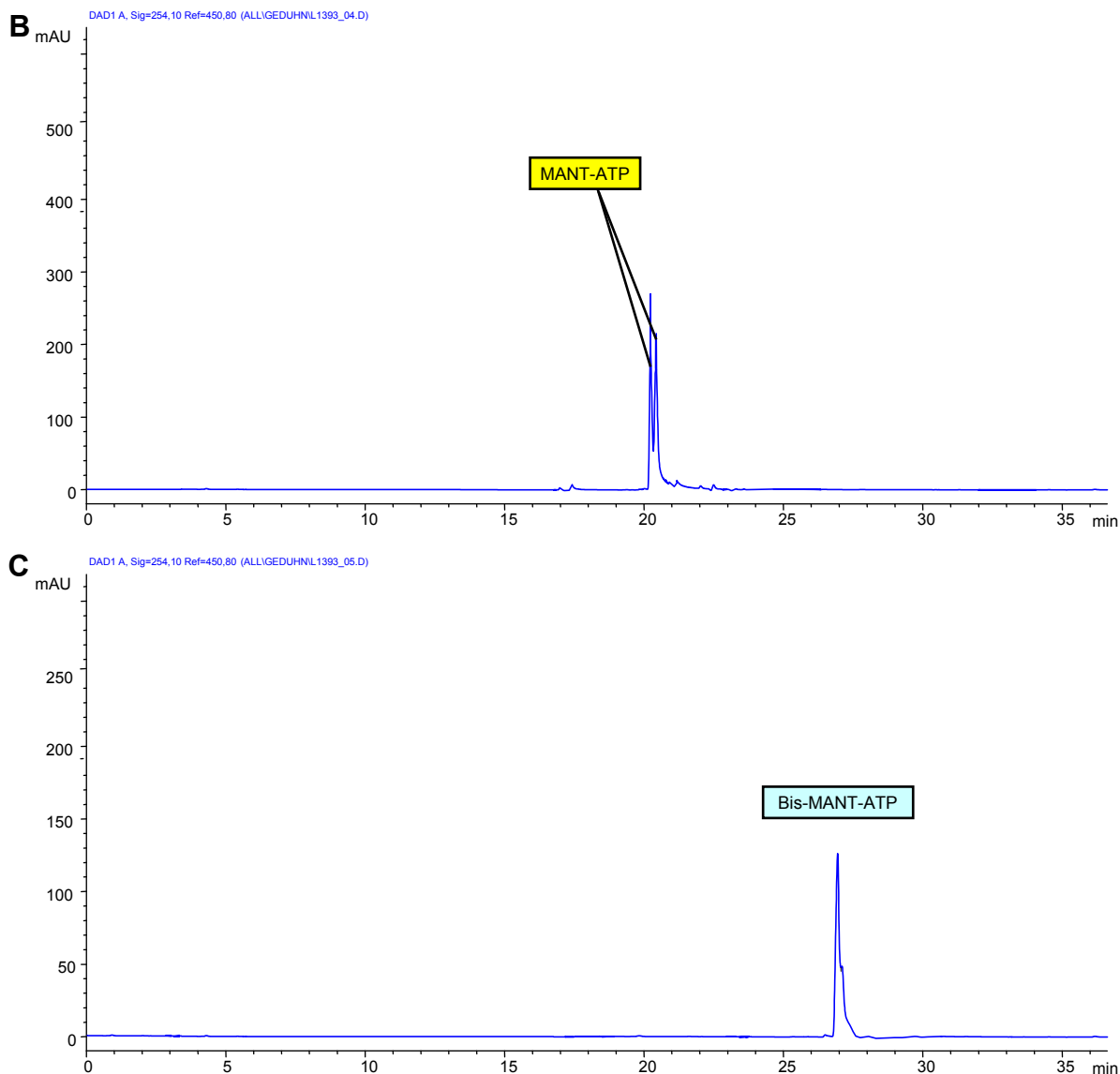
HPLC chromatograms of the crude reaction mixture of the synthesis of MANT-ATP/Bis-MANT-ATP (A), after preparative HPLC purification for MANT-ATP (B) and Bis-MANT-ATP (C) are shown. The typical peak system of MANT-ATP occurred at the retention times of 20.2 and 20.4 min and the signal for Bis-MANT-ATP appeared at later retention time of 27 min. The corresponding diphosphate derivatives followed shortly after (A). The crude reaction mixture contained still starting material of ATP (R_t < 2 min), methylisatoic anhydride (R_t ~17.3 min), and nucleoside (R_t ~23.1 min) (A). The chromatograms after purification by preparative HPLC are displayed for MANT-ATP (B) and Bis-MANT-ATP (C) as a representative result for mono- and bis-substituted (M)ANT-nucleotide separation. Both compounds were obtained simultaneously in high purity of 98 to 99 %. *mAU, milli absorption units.*

2.3 Cell culture and membrane preparation

Cell culture and membrane preparation were performed as previously described[17]. In brief, Sf9 cells were cultured in SF 900 II medium supplemented with 5 % (vol/vol) fetal bovine serum and 0.1 mg/ml gentamicin. High-titer baculoviruses for ACs 1, 2 and 5 were generated through two sequential amplification steps as previously described[17,18]. In each amplification step the supernatant fluid was harvested and stored under light protection at 4 °C. For membrane preparation Sf9 cells (3.0 x 10^6 cells/ml) were infected with corresponding baculovirus encoding different mammalian ACs (1:100 dilutions of high-titer virus) and cultured for 48 hours. Membranes expressing each construct and membranes from uninfected Sf9 cells were prepared as described[17]. Cells were harvested and cell suspensions were centrifuged for 10 min at 1,000 x g at 4 °C. Pellets were resuspended in 10 ml of lysis buffer (1 mM EDTA, 0.2 mM phenylmethylsulfonyl fluoride, 10 µg/ml leupeptine and 10 µg/ml benzamide, pH 7.4). Thereafter, cells were lyzed with 20 – 25 strokes using a Dounce homogenizer. The resultant cell fragment suspension was centrifuged for 5 min at 500 x g and 4 °C to sediment nuclei. The cell membrane-containing supernatant suspension was transferred into 30 ml tubes and centrifuged for 20 min at 30,000 x g and 4 °C. The supernatant fluid was discarded and cell pellets were resuspended in buffer consisting of 75 mM Tris/HCl, 12.5 mM $MgCl_2$, and 1 mM EDTA, pH 7.4. Membrane aliquots of 1 ml were prepared, stored at -80 °C and protein concentration for each membrane preparation was determined using the Bio-Rad DC protein assay kit (Bio-Rad, Hercules, CA).

2.4 AC activity assay

AC activity in Sf9 membranes expressing ACs 1, 2 or 5 was determined essentially as described in the literature[18]. Before starting experiments, membranes were sedimented by a 15 min centrifugation at 4 °C and 15,000 x g and resuspended in 75 mM Tris/HCl, pH 7.4. Reaction mixtures (50 µl, final volume) contained 20 - 40 µg of membrane protein, 40 µM ATP/Mn^{2+} plus 5 mM $MnCl_2$, 100 µM FS, 10 µM GTPγS and (M)ANT-nucleotides at concentrations from 0.1 nM to 1 mM as appropriate to obtain saturated inhibition curves. Following a 2 min pre-incubation at 37 °C, reactions were initiated by adding 20 µl of reaction mixture containing (final) 1.0 - 1.5 µCi/tube [α-^{32}P]ATP and 0.1 mM cAMP. AC assays were conducted in the

absence of an NTP-regenerating system to allow for the analysis of (M)ANT-NDPs that could otherwise be phosphorylated to the corresponding (M)ANT-NTPs[18]. Reactions were conducted for 20 min at 37 °C and were terminated by adding 20 µl of 2.2 N HCl.

For the determination of CyaA inhibition[15], assay tubes contained 10 µl of inhibitor at final concentrations from 1 nM to 100 µM and 20 µl of CyaA protein (final concentration, 10 pM) in 75 mM HEPES/NaOH, pH 7.4, containing 0.1 % (m/v) bovine serum albumin. After a 2 min pre-incubation at 25 °C reactions were initiated by the addition of 20 µl of reaction mixture consisting of the following components to yield the given final concentrations: 100 mM KCl, 10 µM free Ca^{2+}, 5 mM free Mn^{2+}, 100 µM EGTA, 100 µM cAMP and 100 nM calmodulin. ATP was added as nonlabeled substrate at a final concentration of 40 µM and as radioactive tracer [α-^{32}P]ATP (0.2 µCi/tube). For the determination of K_m and V_{max} values in kinetic studies, 10 µM to 2 mM ATP/Mn^{2+} were added, plus 5 mM free Mn^{2+}. To ensure linear reaction progress, tubes were incubated for 10 min at 25 °C and reactions were stopped by the addition of 20 µl of 2.2 N HCl. Denatured protein was precipitated by a 1 min centrifugation at 25 °C and 15,000 x g. Sixty µl of the supernatant fluid were applied onto disposable columns filled with 1.3 g neutral alumina. [^{32}P]cAMP was separated from [α-^{32}P]ATP by elution of [^{32}P]cAMP with 4 ml of 0.1 M ammonium acetate, pH 7.0. Recovery of [^{32}P]cAMP was ~80 % as assessed with [^{3}H]cAMP as standard. Blank values were approximately 0.02 % of the total added amount of [α-^{32}P]ATP; substrate turnover was < 3 % of the total added [α-^{32}P]ATP. Samples collected in scintillation vials were filled up with 10 ml of double-distilled water and Čerenkov radiation was measured in a Tri-Carb 2800TR liquid scintillation analyzer (PerkinElmer Life and Analytical Sciences).

Free concentrations of divalent cations were calculated with Win-MaxC (http://www.stanford.edu/_cpatton/maxc.html). Competition isotherms were analyzed by non-linear regression using the Prism 4.0 software (GraphPad, San Diego, CA). $K_{m;}$ values were 120 µM (AC1), 100 µM (AC2), 70µM (AC5) and were taken from Gille *et al.*[18] for mAC. K_m value for bacterial toxin CyaA was 45 µM and was determined in our previous studies[15].

2.5 Fluorescence spectroscopy

Experiments were conducted using a quartz UV ultra-micro cuvette from Hellma (Müllheim, Germany) (light path length, 3 mm; center, 15 mm; total volume, 70 µl; type 105.251-QS). Measurements were carried out in a Cary Eclipse fluorescence spectrometer (Varian, Inc., Palo Alto, CA, USA) at a constant temperature of 25 °C (scan rate, 120 nm/min; averaging time, 0.5 s; PMT voltage, 700 V, data interval, 1 nm; slit width, 5 nm). Initially, the cuvette contained 64 µl of 75 mM HEPES/NaOH buffer, 100 µM $CaCl_2$, 100 mM KCl and 5 mM $MnCl_2$, pH 7.4. Next, nucleotide, CyaA and CaM were added successively. The cuvette content was mixed after each addition to end up with a total volume of 70 µl. In direct fluorescence experiments, (M)ANT nucleotides were excited at 350 nm and steady-state emission spectra were recorded from 380 to 550 nm at low speed. For CyaA and CaM final concentrations of 2.4 µM were necessary to obtain sufficiently large increase in direct fluorescence. Basal fluorescence, consisting of buffer alone, was subtracted. (M)ANT-nucleotides were finally displaced from CyaA by 9-[2-(phosphonomethoxy)ethyl]adenine diphosphate (PMEApp) in concentrations of 100 nM to 3 µM. For an estimation of the hydrophobic properties of the binding site interacting with the MANT-group, direct fluorescence of mono- and bis-(M)ANT-nucleotides was determined with dimethyl sulfoxide ranging from 0 – 100 % (vol/vol). Fluorescence recordings were analyzed with the spectrum package of the Cary Eclipse software (Varian). Fluorescence polarization spectroscopy was conducted by a multifrequency luminescence spectrometer K2 from ISS using a quartz UV micro cuvette (Hellma, 10 x 2 mm).

2.6 Modeling of the nucleotide binding mode to CyaA

Docking studies were performed with the molecular modeling package SYBYL 7.3 (Tripos Inc., St. Louis, MO) on an Octane workstation (SGI, Mountain View, CA). An initial computer model of CyaA in complex with PMEApp was generated from the PDB crystal structure 1zot[29]. Hydrogens were added and AMBER_FF99 charges were assigned to the protein and the water molecules, followed by a rough preoptimization of the model (100 cycles) with the AMBER_FF99 force field[19] and fixed PMEApp. The three Mg^{2+} ions received formal charges of 2. Starting conformations of 3'-MANT-2'd-ATP and Bis-Br-ANT-ATP were derived from complexes of 3'-MANT-ATP and TNP-ATP with mammalian AC (PDB structures 2gvz

and 2gvd, respectively)[27,28]. PMEApp and the ligands 3'-MANT-2'd-ATP and Bis-Br-ANT-ATP were provided with Gasteiger-Hueckel charges. Initial docking positions resulted from superposition of roughly optimized conformations with PMEApp, allowing the modification of rotatable bonds, and from consideration of the fluorescence data (interaction of the MANT-group with Phe306). Water molecules in the catalytic site were removed. Each complex was refined in a stepwise approach. First, ~50 minimization cycles with fixed ligand (AMBER_FF99 force field, steepest descent method) were performed; second, ~100 minimization cycles of the ligand and the surrounding (distance up to 6 Å) protein residues (Tripos force field)[20], and, third, ~100 minimization cycles with fixed ligand (AMBER_FF99 force field, Powell conjugate gradient). The second and third steps were repeated with larger number of cycles until an root-mean-square force of 0.05 kcal/mol × Å^{-1} was approached. To avoid overestimation of electrostatic interactions, a distance-dependent dielectric constant of 4 was applied. Molecular surfaces and lipophilic potentials [protein variant with the new Crippen parameter table[21,22]] were calculated and visualized by the program MOLCAD (MOLCAD, Darmstadt, Germany) contained within SYBYL.

3.   Results and Discussion

3.1   Overview on nucleotide structures

We examined the inhibitory effect of 32 nucleotides on the catalytic activity of mammalian ACs 1, 2, 5 and bacterial CyaA toxin (**Table 1**). Nucleotides differed from each other in base of adenine, hypoxanthine, cytosine and in phosphate chain length of mono-, di- or triphosphate. Furthermore, nucleotides varied in mono- and bis-substitution at the 2', 3' position of the ribosyl ring by anthranilic acid groups. Mono-substituted compounds (**1 – 16**) undergo spontaneous isomerization under physiological pH between the 2'- and 3'- ribosyl position[23,24]. For bis-substituted nucleotides (**17 – 32**) both hydroxyl groups of the ribosyl cycle are replaced by anthranilic acid groups. The anthraniloyl (ANT) moiety differed by hydrogen, halogens of chlorine and bromine, and acetylated amino residue in 5 position of the phenyl ring system (**Fig. 2:R$_1$**). Moreover, substitution at the amino function of the ANT-group lead to methyl (MANT) and propyl (Pr-ANT) derivatives (**Fig. 2:R$_2$**). The potencies of the different nucleotides were determined in the AC activity assay in the presence of the cation Mn^{2+}.

3.2   Structure – activity relationships of mono-substituted (M)ANT-nucleotides for mAC

Recombinant ACs 1, 2, 5 showed different sensitivity to inhibition by (M)ANT-nucleotides (**Table 1**). In accordance with previous studies[18,25,26] AC2 constitutes the AC isoform with the lowest inhibitor affinity due to the exchange of Ala409Pro and Val1108Ile in AC1 and AC5 *versus* AC2[27]. (M)ANT-NTPs of the purine base hypoxanthine had the highest impact, especially MANT-ITP is the most potent inhibitor known so far for AC1 and AC5 with K_i values of 1 – 3 nM. The exchange of nucleobase adenine with cytosine displayed only marginal differences in potency (**1** and **3**). The halogenated ANT-ATP derivatives (**4** and **6**) showed in comparison to MANT-ATP (**1**) slightly more potent inhibition effect for mACs, but the corresponding inosine compounds (**5** and **7**) exhibited lower potency on a still high level. Substitution of bromine with chlorine of anthraniloyl inosine triphosphates induced 2-fold more potent inhibition for mAC (**7**→**5**). Elongation of the alkyl residue from *N*-methylated to *N*-propylated ANT-nucleotides lowered K_i values 3- to 8-fold (**1**→**8**,

Table 1. Inhibition of catalytic activity of recombinant ACs 1, 2, 5 and bacterial AC toxin CyaA by (M)ANT-nucleotides

	(M)ANT-nucleotide	AC 1 (nM)	AC 2 (nM)	AC 5 (nM)	CyaA (nM)
1	MANT-ATP	150 ± 40	330 ± 100	100 ± 30	4,300 ± 400
2	MANT-ITP	2.8 ± 0.9	13.5 ± 0.5	1.2 ± 0.1	600 ± 100
3	MANT-CTP	150 ± 30	690 ± 20	150 ± 30	1,100 ± 100
4	Cl-ANT-ATP	80 ± 4	490 ± 20	45 ± 1	350 ± 40
5	Cl-ANT-ITP	3.3 ± 0.3	8 ± 1	2.0 ± 0.2	700 ± 200
6	Br-ANT-ATP	120 ± 20	450 ± 40	70 ± 20	330 ± 30
7	Br-ANT-ITP	7.0 ± 0.1	22 ± 4	4.6 ± 0.4	920 ± 50
8	Pr-ANT-ATP	440 ± 20	1,100 ± 100	360 ± 60	820 ± 250
9	Pr-ANT-ITP	22 ± 1	68 ± 12	10 ± 2	3,800 ± 500
10	Ac-NH-ANT-ATP	6,800 ± 200	11,000 ± 1,000	3,400 ± 40	710 ± 40
11	Ac-NH-ANT-ITP	140 ± 30	390 ± 80	37 ± 7	4,800 ± 900
12	MANT-ADP	1,300 ± 200	2,900 ± 500	800 ± 200	12,000 ± 2,000
13	MANT-IDP	39 ± 12	86 ± 9	31 ± 12	11,000 ± 3,000
14	Br-ANT-ADP	560 ± 10	1,700 ± 100	280 ± 20	8,700 ± 1,300
15	MANT-IMP	4,600 ± 400	8,200 ± 800	3,400 ± 200	> 100,000
16	ANT-IMP	7,400 ± 1,200	7,500 ± 1,400	4,300 ± 600	> 100,000

17	Bis-MANT-ATP	700 ± 200	2,100 ± 600	430 ± 50	360 ± 10
18	Bis-MANT-ITP	310 ± 20	1,100 ± 200	140 ± 40	3,000 ± 400
19	Bis-MANT-CTP	620 ± 40	7,800 ± 100	750 ± 40	2,500 ± 500
20	Bis-Cl-ANT-ATP	1,700 ± 100	2,400 ± 100	1,600 ± 100	16 ± 1
21	Bis-Cl-ANT-ITP	66 ± 1	200 ± 10	65 ± 3	15 ± 1
22	Bis-Br-ANT-ATP	670 ± 50	1,100 ± 100	900 ± 90	12.6 ± 0.3
23	Bis-Br-ANT-ITP	21 ± 1	71 ± 2	15 ± 2	20 ± 2
24	Bis-Pr-ANT-ATP	18,000 ± 3,000	36,000 ± 3,000	18,000 ± 5,000	700 ± 200
25	Bis-Pr-ANT-ITP	440 ± 10	1,400 ± 100	250 ± 20	2,100 ± 100
26	Bis-Ac-NH-ANT-ATP	22,000 ± 1,000	7,000 ± 1,000	6,100 ± 1,300	280 ± 20
27	Bis-Ac-NH-ANT-ITP	1,700 ± 100	5,600 ± 300	480 ± 30	7,500 ± 100
28	Bis-MANT-ADP	700 ± 300	1,600 ± 300	510 ± 70	6,500 ± 800
29	Bis-MANT-IDP	1,000 ± 100	1,400 ± 100	700 ± 200	6,600 ± 900
30	Bis-Br-ANT-ADP	1,600 ± 300	3,300 ± 200	1,800 ± 200	91 ± 5
31	Bis-MANT-IMP	> 100,000	> 100,000	> 100,000	20,000 ± 3,000
32	Bis-ANT-IMP	> 100,000	> 100,000	> 100,000	12,000 ± 3,000

AC activity of bacterial toxin CyaA and in Sf9 membranes were determined as described in "Materials and Methods". Non-linear regression analysis was used for calculation of K_i values from IC_{50} values. Data are given in nanomolar and are the mean values ± SD of 4 – 5 independent experiments performed in triplicates with at least two different membrane preparations (for mACs).

2→9). A further decrease in potency was observed for the acetylated amino anthraniloyl nucleotides. The inhibition effect for Ac-NH-ANT-ATP (**10**) dropped into micromolar range and the corresponding inosine derivative (**11**) was 30- to 50-fold less potent than MANT-ITP (**2**). Interestingly, Ac-NH-ANT-ITP (**11**) displayed a 4-fold higher selectivity for AC5 than for AC1. Deletion of the γ-phosphate reduced inhibitor affinity 3- to 26-fold (**1→12**, **2→13**, **6→14**) and is in accordance with previous data. Mou *et al.* explained by crystallographic studies that the Mn^{2+} ion in the B-site coordinates with the γ-phosphate of MANT-nucleotides. The lack of this phosphate group destabilizes the polyphosphate chain in its binding site[27,28]. The deletion of the β-phosphate group of the MANT-NMP reduced inhibitor potency 120-fold (**13→15**). Exchange of the MANT-group with an ANT-group had only little effect on inhibitor affinity (**15→16**).

3.3 Structure – activity relationships of mono-substituted (M)ANT-nucleotides for CyaA

In principle, the inhibitor affinity of bacterial CyaA toxin for mono-substituted (M)ANT-NTPs was lower in comparison to mAC or reached maximally the affinity range of AC2. The general preference for a nucleobase was also less pronounced. MANT-ATP (**1**) was less potent than MANT-ITP (**2**), but at all other combinations of adenosine and inosine derivatives the corresponding ANT-ATPs exhibited higher inhibition potency (**4→5**, **6→7**, **8→9**, **10→11**). Recent studies from our laboratory showed that MANT-CTP (**3**) is the most potent MANT-nucleotide inhibitor of edema factor (EF) of the spore-forming bacterium *Bacillus anthracis* with the K_i value of 100 nM[14]. This preference for the nucleobase cytosine was not observed for CyaA[15]. Insertion of halogens in ANT-ATPs lead to a reduction of K_i values by 12- to 13-fold (**1→4**, **1→6**). However, the K_i values of the corresponding inosine derivatives remained almost constant (**2→5**, **2→7**). Pr-ANT-ATP (**8**) and Ac-NH-ANT-ATP (**10**) revealed still stable inhibition potency, but Pr-ANT-ITP (**9**) and Ac-NH-ANT-ITP (**11**) lost 6- to 8-fold inhibitor affinity compared to MANT-ITP (**1**). Deletion of γ-phosphate reduced inhibitor potency 3- to 20-fold and omission of γ- and β-phosphate reduced the inhibitory potency to the high micromolar range. Due to limitations of available material, the exact determination of low inhibition effects in millimolar range was avoided.

3.4 Structure – activity relationships of bis-substituted (M)ANT-nucleotides for mAC

Overall, bis-substituted (M)ANT-nucleotides exhibited lower inhibition potency for ACs 1, 2 and 5 than the corresponding mono-substituted derivatives. For the highest inhibition affinities of Bis-(M)ANT-NTPs the nucleotide inosine is still required. Bis-MANT-ATP (**18**) and Bis-MANT-CTP (**19**) inhibited AC1 and AC5 with almost equal potency. The preference for AC2 of this pair of compounds was 4-fold less pronounced by Bis-MANT-CTP (**19**). Bis-halogen-ANT-ITPs (**21** and **23**) showed impressive K_i values between 15 – 66 nM for AC1 and AC5, but the corresponding adenine nucleotides (**20** and **22**) exhibited 25- to 60-fold lower potency. *N*-propylated instead of *N*-methylated ANT-nucleotides lost affinity dramatically only for Bis-Pr-ANT-ATP (**24**) (17- to 42- fold) but not for Bis-Pr-ANT-ITP (**25**). Bis-Ac-NH-ANT-ATP (**26**) exhibited a low inhibition potency, but possessed 3-fold higher sensitivity for AC2 and AC5. Usually, the remaining inhibitors showed higher potencies at ACs 1 and 5 than AC2. Interestingly, Bis-MANT-ADP (**28**) was as potent as Bis-MANT-ATP (**17**) and Bis-MANT-IDP (**29**), Bis-Br-ANT-ADP (**30**) were only 1.3- to 5-fold less potent than the corresponding (M)ANT-NTPs. Bis-MANT-IMP (**31**) and Bis-ANT-IMP (**32**) showed almost no affinity for mACs.

3.5 Structure – activity relationships of bis-substituted (M)ANT-nucleotides for CyaA

Bis-substituted (M)ANT-NTPs exhibited a broad variety in potency by showing K_i values from the low nanomolar up to the micromolar range. In general, inhibition effects of compounds possessing the nucleobase adenine were more pronounced. Bis-MANT-CTP (**19**) and Bis-MANT-ITP (**18**) exhibited 7- and 8-fold lower inhibition potency than Bis-MANT-ATP (**17**). Interestingly, halogenated ANT-nucleotide derivatives (**20 – 23**) increased the inhibition affinity 20- to 240-fold compared to Bis-MANT-nucleotides (**16 – 19**). Most strikingly, Bis-Br-ANT-ATP (**22**) showed the lowest K_i value of 12.6 nM for CyaA. So far, the most potent inhibitor for bacterial CyaA toxin is PMEApp (K_i value: 1 – 25 nM)[15,29]. Thus, we found an inhibitor displaying similar potency. The remaining halogen-ANT-NTPs differed only slightly with K_i values between 15 – 20 nM. For the chlorine compounds (**20** and **21**) no preference of nucleobase was observable. The affinity of Bis-Pr-ANT-ATP (**24**) was decreased 2-fold compared to Bis-MANT-ATP (**17**). However, the corresponding

propylated inosine derivative (**25**) exhibited an increase in potency regarding Bis-MANT-ITP (**18**). The bulky acylated amino substituent afforded relatively stable inhibition affinities for Bis-Ac-NH-ANT-ATP and Bis-Ac-NH-ITP (**26** and **27**). Again, deletion of the γ-phosphate reduced potency of Bis-(M)ANT-NDPs (**28 – 30**). Although, Bis-(M)ANT-NMPs (**31** and **32**) constitute the end in rank order of affinity we paid, for the first time, attention to the couple MANT-IMP (**15**) and Bis-MANT-IMP (**31**) because of the significant increase in potency by connectivity of a second MANT-group[15]. Afterwards, we observed this phenomenon for most combinations of mono- and bis-substituted (M)ANT-NTPs and for all (M)ANT-NDPs. For our high potent halogen ANT-nucleotides esterification of the second hydroxyl group of the ribosyl residue exhibited 18- to 73-fold (**4 – 7→20 – 23**) increase in affinity. Bis-propylated ANT-nucleotides and Bis-Ac-NH-ANT-ATP displayed slight enhancement in potency (**8 – 10→24 – 26**). Exceptions of the rule were Bis-MANT-ITP (**17**), Bis-Ac-NH-ANT-ATP (**27**), and Bis-MANT-CTP (**19**) exhibiting lower affinity in comparison with the corresponding mono-substituted derivatives.

3.6   Selectivity aspects for bacterial CyaA

In previous studies[18] potent MANT-nucleotide inhibition for mAC was observed, but with lower affinity for bacterial CyaA toxin. In this study we found, for the first time, not only high potent (M)ANT nucleotide derivatives for CyaA inhibition, but also inhibitors with selectivity for CyaA *versus* ACs 1, 2, and 5. Bis-substituted halogenated ANT-nucleotides of adenosine demonstrated the best selectivity ratio. Bis-Cl-ANT-ATP (**20**) is the most interesting compound with a preference of 100- to 150-fold for CyaA. The most potent inhibitor Bis-Br-ANT-ATP (**22**) exhibited high selectivity as well (50- to 90-fold). However, Bis-halogen-ANT-ITPs (**21** and **23**) displayed similar potency for bacterial AC, but marginal selectivity. Interestingly, the more space filling propyl and acetylated amino group of ANT-ATPs implemented also selectivity aspects. Bis-Propyl-ANT-ATP (**24**) was 26- to 52-fold more selective for CyaA compared to mAC and Bis-Ac-NH-ANT-ATP (**26**) 20- to 80-fold. For acylated amino ANT-nucleotides even the mono-substituted derivative (**10**) yielded a 5- to 15-fold selectivity.

3.7 Analysis of the enzyme kinetics of CyaA

Historically, two classes of AC inhibitors are known, *i.e.* so-called P-site inhibitors: that are non-competitive (or uncompetitive) inhibitors and competitive inhibitors. P-site inhibitors are adenosine and adenine nucleotide analogues including an intact purine ring[30,31]. Most P-site inhibitors require a pyrophosphate (PP$_i$) as a cofactor and capture an AC-PP$_i$ conformation[32,33]. 2'-Deoxyadenosine or 2'-deoxy-3'-AMP, exhibited uncompetitive inhibition in presence of G$_{s\alpha}$ and Mg^{2+}, and non-competitive kinetics with Mn^{2+} [31]. However, β-L-2',3'-dd-5'-ATP including the triphosphate group in 5'-position leads to a competitive inhibition process[33]. Moreover, various nucleotides are competitive inhibitors for ACs[34] like ATPαS (R$_p$-diastereoisomer)[35,36]. The kinetic pattern of MANT-substituted nucleotides is also well understood. Specifically, MANT-nucleotides were observed as competitive AC inhibitors in S49 lymphoma cell membranes[37]. A validation for the competitive antagonism was achieved by further studies of the catalytical subunits C1/C2 of mACs[18].

Therefore, we expected for our newly synthesized mono- and bis-substituted (M)ANT-nucleotides identical behavior as for mono-substituted MANT-nucleotides. To prove our hypothesis enzyme kinetics of CyaA were conducted with two pairs of compounds: MANT-ATP (**1**) / Bis-MANT-ATP (**17**) and Br-ANT-ATP (**6**) / Bis-Br-ANT-ATP (**22**) (**Fig. 6**). Lineweaver-Burk double-reciprocal plotting of CyaA inhibition kinetics displayed competitive inhibition pattern for both types of substituted (M)ANT-nucleotides. The linear regression lines intersected at the y-axis, *i.e.* V$_{max}$ remained constant, whereas K$_m$ increased with rising inhibitor concentrations. These investigations are in accordance with recent literature data[14] according to which the bacterial AC toxin edema factor (EF) from *Bacillus anthracis* was inhibited competitively by MANT-nucleotides.

Fig. 6. Enzyme kinetics with mono- and bis-substituted (M)ANT-nucleotides
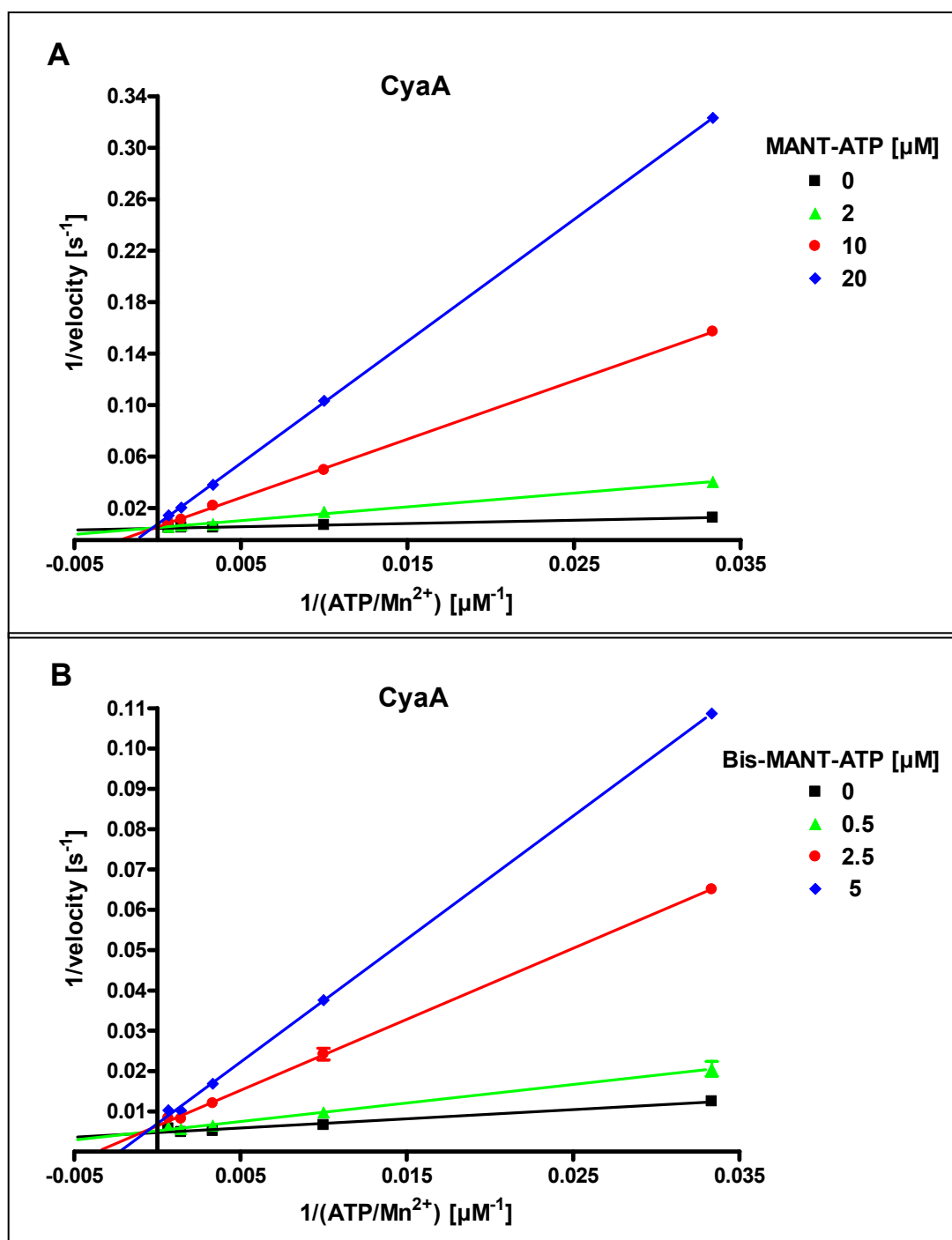
AC activity of bacterial CyaA toxin was determined as described under "Material and Methods" with the indicated concentrations of MANT-ATP (0 µM, 2 µM, 10 µM, 20 µM) (**A**) and Bis-MANT-ATP (0 nM, 0.5 µM, 2.5 µM, 5.0 µM) (**B**). Reaction mixtures contained 10 pM CyaA, 100 mM KCl, 10 µM free Ca^{2+}, 5 mM free Mn^{2+}, 100 µM EGTA, 100 µM cAMP, 100 nM calmodulin, 0.2 µCi/tube [α-^{32}P]ATP and unlabeled ATP/Mn^{2+} concentrations indicated in the graph. Data were plotted double reciprocally and analyzed by linear regression according to Lineweaver-Burk. The r^2 values of the regression lines were 0.97 – 0.99. Shown are the results of a representative experiment performed in triplicates. Similar results were obtained in at least two different experiments.
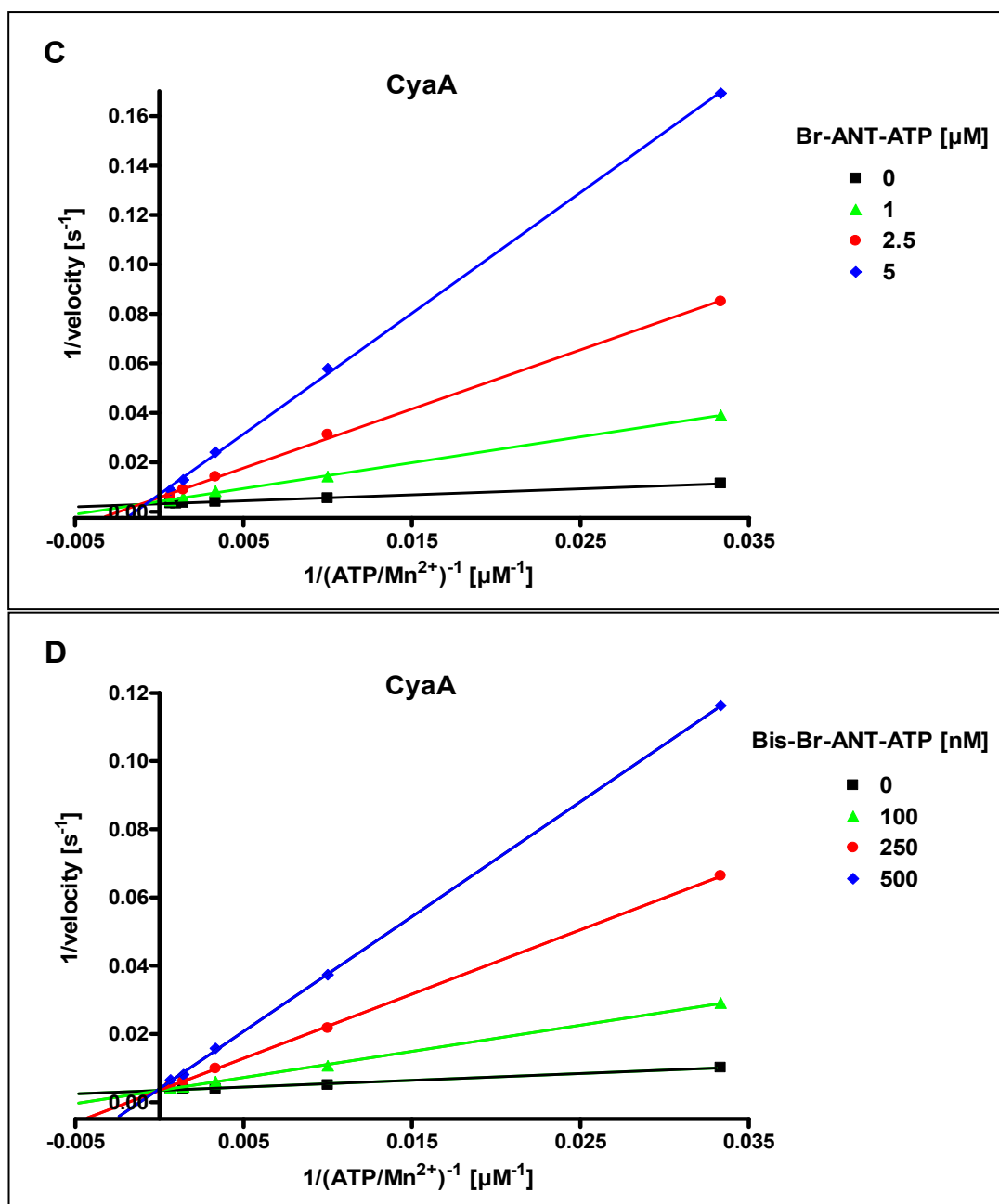
AC activity of bacterial CyaA toxin was determined as described under "Materials and Methods" with the indicated concentrations of Br-ANT-ATP (0 μM, 1 μM, 2.5 μM, 5 μM) (**C**) and Bis-Br-ANT-ATP (0 nM, 100 nM, 250 nM, 500 nM) (**D**). Reaction mixtures contained 10 pM CyaA, 100 mM KCl, 10 μM free Ca^{2+}, 5 mM free Mn^{2+}, 100 μM EGTA, 100 μM cAMP, 100 nM calmodulin, 0.2 μCi/tube [α-^{32}P]ATP and unlabeled ATP/Mn^{2+} concentrations indicated in the graph. Data were plotted double-reciprocally and analyzed by linear regression according to Lineweaver-Burk. The r^2 values of the regression lines were 0.96 – 0.99. Shown are the results of a representative experiment performed in triplicates. Similar results were obtained in at least two different experiments.

3.8 Fluorescence spectroscopy

FRET experiments

For fluorescence spectroscopic investigations of MANT-nucleotides two principal methods are under consideration[15,27,28,38], *i.e.* fluorescence resonance energy transfer (FRET) experiments and direct fluorescence spectroscopy. FRET experiments are an important tool for investigations of structure-response relationships of the catalytical AC binding site.

The approach of FRET analysis includes advantages compared to direct fluorescence studies[15]. For sufficient FRET recordings the final enzyme concentration for CyaA was reduced to 300 nM (direct fluorescence: 2.4 µM). Moreover, FRET can only occur directly in the catalytic binding pocket, because of the two tryptophan residues, Trp69 and Trp242, located 21 and 38 Å away from the catalytic site[29]. These distances allow FRET[38] from tryptophan (excitation wavelength, 280 nm; emission wavelength, 350 nm) to MANT (excitation wavelength, 350 nm; emission wavelength, ~450 nm). In previous studies[15] deoxygenated MANT-nucleotides like 2'-MANT-3'd-ATP exhibited significant FRET for CyaA, but for 2',(3') isomeric MANT-nucleotides the transfer of energy was absent or only minimal in fluorescence recordings. Thus, the isomerization of the MANT-group may impede energy capture of the fluorophore from tryptophan and tyrosine residues. Moreover, in this study newly synthesized mono-2',(3') isomeric (M)ANT-nucleotides revealed no significant energy transfer in fluorescence analysis, as well. Furthermore, addition of the second (M)ANT-group in bis-substituted (M)ANT-nucleotides did not change these fluorescence properties and exhibited no FRET, as well (**Fig. 7**). The labeled nucleotide was added first to the buffer and weak autofluorescence occurred without a maximum as a result of excitation at 280 nm (brown line). When CyaA was added, tryptophan and tyrosine fluorescence was detected at 350 nm (blue line). Upon addition of CaM, decrease in emission at 350 nm occurred clearly, but increase in emission at 430 nm did not arise significantly over the CyaA level (FRET; red line → blue line). Although, Bis-MANT-ATP was abounded (1 µM concentration) and CyaA saturation by the fluorophore is assumable, the FRET signal was weak and not significant over signal to noise ratio. Thus, we focused our measurements on direct fluorescence analysis.

Fig. 7. FRET analysis of Bis-MANT-ATP
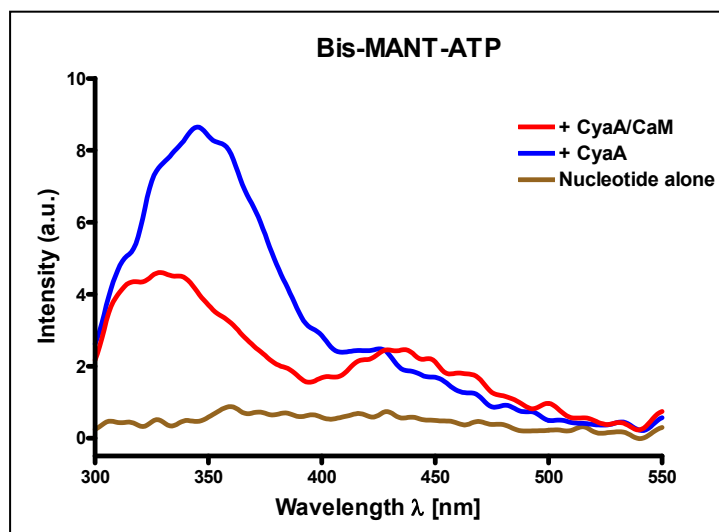
Monitoring of FRET with Bis-MANT-ATP as a representative bis-substituted (M)ANT-nucleotide binding to the catalytic site of CyaA. The assay buffer contained 75 mM HEPES/NaOH, 100 µM $CaCl_2$, 100 mM KCl, and 5 mM $MnCl_2$, pH 7.4. Bis-MANT-ATP was added to the buffer to yield a final concentration of 1 µM and emission was scanned from 300 nm to 550 nm at an excitation wavelength of 280 nm. CyaA and CaM were added successively to yield a final concentration of 300 nM. Shown are superimposed recordings of a representative experiment. Similar data were obtained with other bis-substituted (M)ANT-nucleotides. *a.u., arbitrary unit.*

Direct fluorescence experiments

In direct fluorescence experiments we observed important differences in the intrinsic fluorescence between mono- and bis-substituted (M)ANT-nucleotides. Although, nucleotides differ in mono-/bis-substiution and in diversified anthraniloyl groups wavelengths of absorption and emission spectra were similar. Nucleotides were excited at 350 nm and emission was scanned from 380 to 550 nm. As a representative experiment the pair of MANT-ATP and Bis-MANT-ATP was compared (**Fig. 8**). MANT-ATP was added first to the buffer, displaying high autofluorescence at λ_{em}= 449 nm (brown line). Addition of CyaA did not change the intrinsic fluorescence significantly (blue line). However, upon addition of CaM, fluorescence increased by approximately 36 % in accordance to our previous studies[15].

Interestingly, Bis-MANT-ATP revealed a nearly 20-fold lower autofluorescence (brown line) compared to MANT-ATP. The addition of CyaA into the cuvette containing Bis-MANT-ATP increased fluorescence by 4-fold. Moreover, emission maximum was shifted to shorter wavelength (blue shift). Thus, binding of MANT-nucleotides to CyaA transferred the MANT-group into a hydrophobic environment,

Fig. 8. Fluorescence emission of MANT-ATP (A) and Bis-MANT-ATP (B)
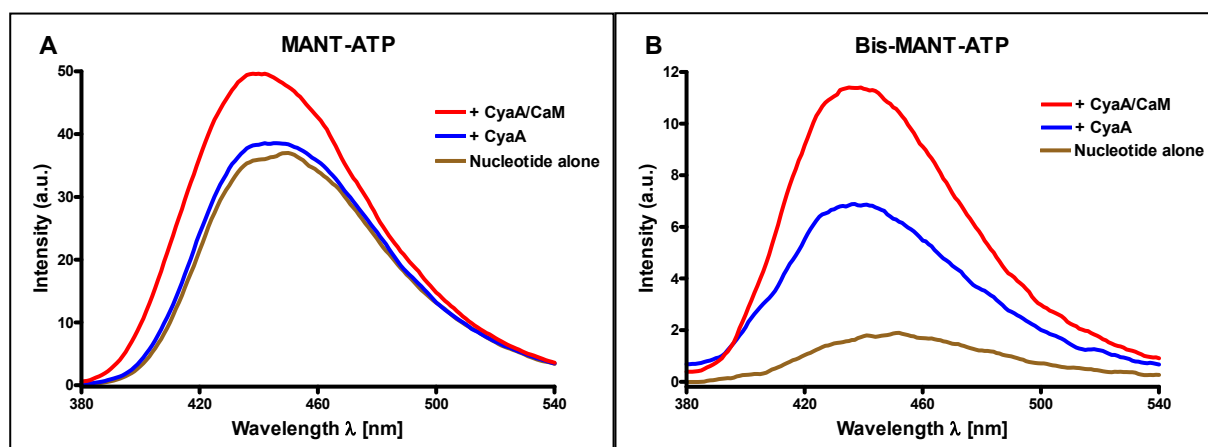
Monitoring of MANT-nucleotide binding to the catytic site of CyaA using direct fluorescence. The assay buffer contained 75 mM HEPES/NaOH, 100 µM $CaCl_2$, 100 mM KCl, and 5 mM $MnCl_2$, pH 7.4. MANT-ATP (A) and Bis-MANT-ATP (B) were added to the buffer to yield a final concentration of 2 µM and emission was scanned at an excitation wavelength of 350 nm. CyaA and CaM were added successively to yield a final concentration of 2.4 µM. Shown are superimposed recordings of a representative experiment. Similar data were obtained in three independent experiments. Fluorescence intensities are given in *a.u.* (*arbitrary unit*).

Fig. 9. Fluorescence changes of MANT-ATP and Bis-MANT-ATP in an hydrophobic environment
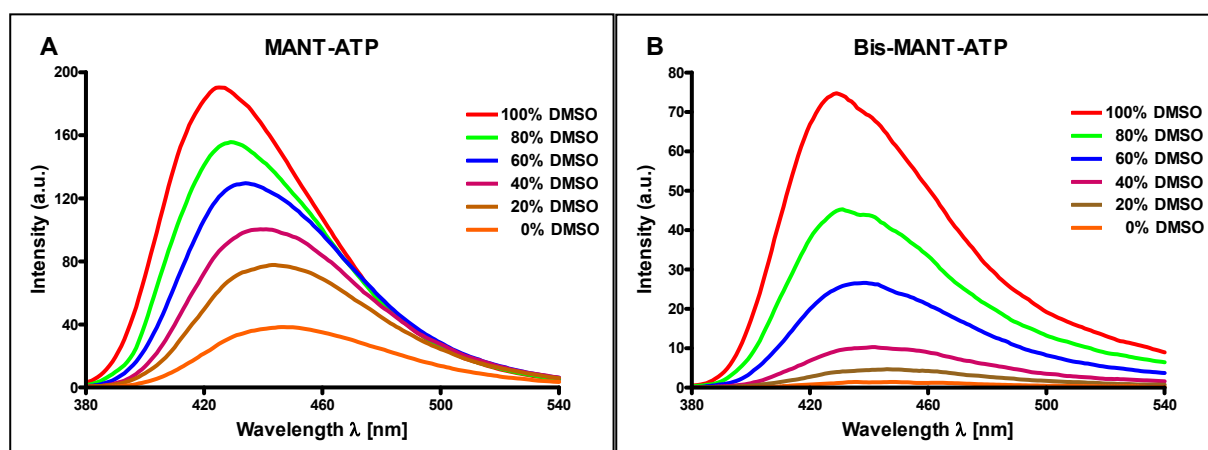
MANT-ATP (**A**) and Bis-MANT-ATP (**B**) were added to water-DMSO mixtures ranging from 0 – 100 % (vol/vol) to yield a final concentration of 2 µM. Nucleotides were directly excited at λ_{ex}= 350 nm to mimic binding of the MANT-group to a hydrophobic binding pocket. Shown are superimposed recordings of a representative experiment. Similar data were obtained in two independent experiments. *a.u.*, *arbitrary unit*.

probably facilitating interaction with Phe306[15,29], but without the activator CaM. Upon addition of CaM, Bis-MANT-ATP displayed full signal of fluorescence increase (6-fold higher compared to basal nucleotide fluorescence). For binding of mono-substituted

MANT-nucleotides to CyaA, binding of CaM is required. However, Bis-MANT-nucleotides revealed binding to CyaA without the activator CaM. In analogy, TNP-nucleotides are reported to display similar protein interaction with CyaA alone[15].

In comparison, direct fluorescence was determined in a gradient hydrophobic environment (**Fig. 9**). Experiments were conducted for MANT-ATP and Bis-MANT-ATP with dimethyl sulfoxide (DMSO) ranging from 0 – 100 % (vol/vol). Fluorescence of MANT-ATP increased from water environment to pure DMSO by only 5-fold. On the contrary, Bis-MANT-ATP exhibited fluorescence increase by ~40-fold. Thus, independently from a 12-fold higher potency for CyaA, Bis-MANT-ATP displayed an excellent signal to noise ratio for the fluorescence analysis of CyaA. Blue shifts were significantly detected for both classes of compounds (MANT-ATP: λ_{max}= 448 nm $\rightarrow$ 426 nm, Bis-MANT-ATP: λ_{max}= 445 nm $\rightarrow$ 429 nm). It should be noted, that the fluorescence intensities were 3- to 4-fold lower for Bis-MANT-ATP compared to MANT-ATP.

In kinetic experiments fluorescence was inhibited by the non-fluorescent nucleotide analog PMEApp[39] in a concentration dependent manner (**Fig. 10**). Due to the higher potency of PMEApp half-maximal displacement of 2 µM Bis-MANT-ATP occurred

Fig. 10. Competitive kinetic experiment with PMEApp
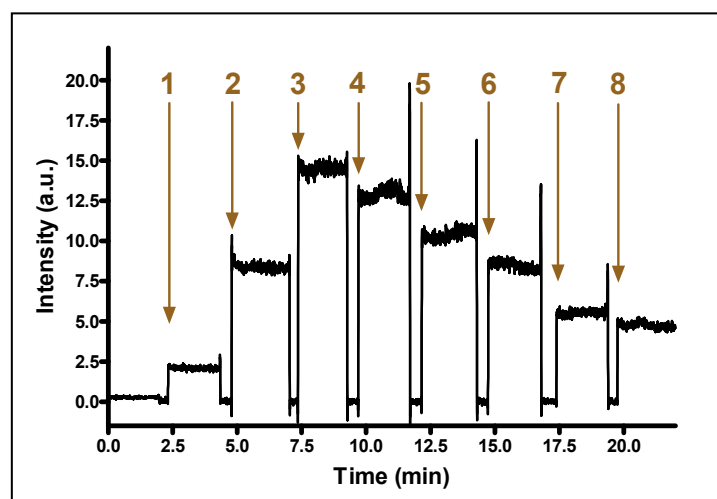
Time-resolved activation of CyaA by CaM and stepwise abolishment of direct fluorescence by PMEApp. Excitation wavelength was 350 nm and emission was detected at 440 nm over time. 2 µM Bis-MANT-ATP (1), 2.4 µM CyaA (2), 2.4 µM CaM (3), and PMEApp in the given concentrations (addition steps 4, 100 nM; 5, 500 nM; 6, 1 µM; 7, 2 µM; 8, 3 µM) were added in sequence. A recording of a representative experiment is shown. Similar data were obtained in three independent experiments. *a.u., arbitrary unit.*

at a PMEApp concentration of approximately 1 µM. Fluorescence change of CyaA stimulated by CaM and inhibition by PMEApp occurred within mixing time (a few seconds). These data show that direct fluorescence analysis was rapid, specific, and reversible. Because fluorescent nucleotides, *e.g.* Bis-MANT-ATP, were competitively displaced from CyaA by PMEApp, the affinity of nonlabeled inhibitors may also be estimated using this approach. Furthermore, the production of CyaA can be accomplished at large scale[16], and kinetics occur within seconds. Thus, fluorimetric high-throughput screening of potential novel inhibitors is feasible, avoiding the use of radioactive AC assays.

Experiments with two additional compound pairs, *i.e.* MANT-ITP/Bis-MANT-ITP and Br-ANT-ATP/Bis-Br-ANT-ATP showed similar fluorescence properties as with MANT-ATP/Bis-MANT-ATP. Control experiments were conducted to rule out false-positive fluorescence signals (data not shown): *e.g.* combination of CaM and fluorophore without CyaA caused no signal and denatured CyaA (10 min at 95 °C) reduced fluorescence to basal response.

Saturation experiments by direct fluorescence analysis

By determination of direct fluorescence with mono- and bis-MANT-derivatives at increasing concentrations after addition of CaM, saturation curves were obtained (**Fig. 11**). Final concentrations of nucleotide varied from 100 nM to 10 µM. Although saturation was not completely accomplished, higher inhibitor concentration measurements (>10 µM) were avoided to prevent intrinsic quenching of the fluorophore. K_D values were estimated to 6.4 µM for Bis-MANT-ITP and 4.5 µM for Bis-Br-ANT-ATP. Due to the high concentration of CyaA (protein concentration 2.4 µM) needed, saturation could not achieved for *e.g.* Bis-Br-ANT-ATP (K_i = 12 nM) in nanomolar range. Thus, K_d values exhibited only similarity for Bis-MANT-ITP, which showed also in AC activity assays only low potencies in the micromolar range. Exceptionally, MANT-ITP displayed similar fluorescence properties according to mono-substituted MANT-nucleotides, but with increasing concentrations of MANT-ITP the increase in direct fluorescence was not substantially different; thus, a recording of saturation was not possible (data not shown).

To address the issue of high protein concentration, we employed fluorescence polarization spectroscopy[40].

Fig. 11. Saturation curves of Bis-MANT-ATP and Bis-Br-ANT-ATP
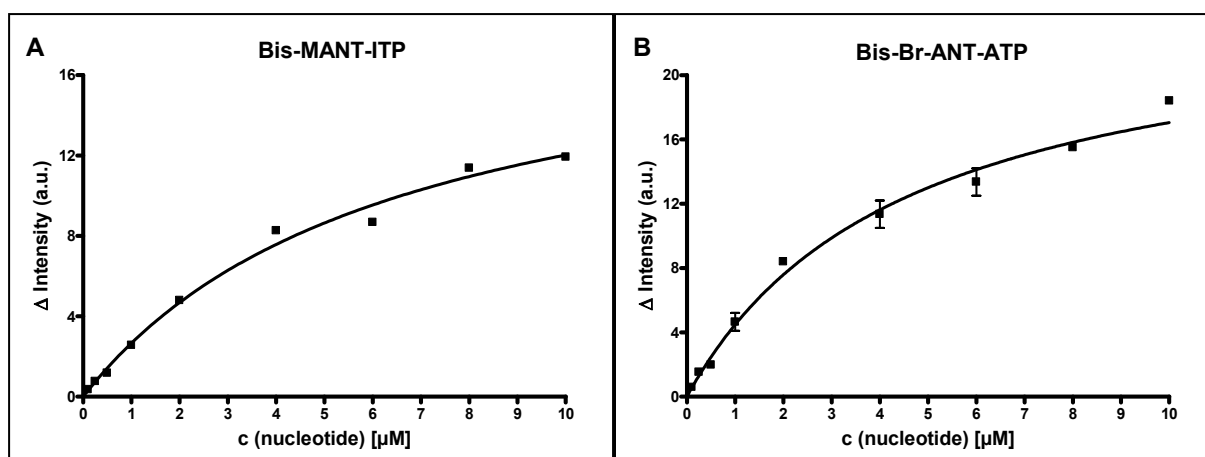
Representative saturation curves of Bis-MANT-ITP (A) and Bis-Br-ANT-ATP (B) binding to activated CyaA are shown. Each data point was determined in an independent experiment as described under "Materials and Methods". Final concentration of CyaA and CaM were 2.4 µM each. The fluorescence increase at 450 nm was calculated by subtraction of the autofluorescence at 450 nm from the maximal fluorescence at 450 nm after the addition of CyaA/CaM. Data were analyzed by nonlinear regression using the Prism 4.02 software. Similar data were obtained in three independent experiments. *a.u., arbitrary unit.*

Fluorescence polarization

The setup for fluorescence polarization measurements was similar to direct fluorescence analysis (details shown in Materials and Methods). In our previous observations bis-substituted (M)ANT-nucleotides exhibited low intensities in autofluorescence (**Fig. 8.**). For direct fluorescence spectroscopy the low intrinsic fluorescence was favorable due to an excellent signal to noise ratio, but for fluorescence polarization it was the exclusion criterion, because polarization values did not overcome signal to noise ratio for bis-substituted (M)ANT-nucleotides. Thus, only mono-substituted MANT-nucleotides were investigated for this type of analysis. First, (M)ANT-nucleotide at concentrations between 200 nM and 3.3 µM were added to the buffer and the basal polarization of free fluorophore in solution was determined. Second, addition of CyaA exhibited similar signals in polarization compared to fluorophore alone. Third, upon addition of CaM the polarization signal increased indicating bound fluorophore to the enzyme. CyaA and CaM were applied at a final concentration of 280 nM. By determination of fluorescence polarization at increasing concentrations of mono-substituted (M)ANT-nucleotides after addition of CaM, saturation curves were obtained (**Fig. 12**). Apparent K_d values were estimated

to be 300 nM for Br-ANT-ATP and 400 nM for MANT-ITP. Although, the change in polarization was low, saturation was clearly obtained in comparison to the direct fluorescence approach. Thus, by the use of fluorescence polarization we found a new alternative for the estimation of binding constants at least for one class of (M)ANT-derivatives. In future studies, this methodology should be considered for the characterization of new fluorophore labeled CyaA inhibitors.

Fig. 12. Saturation curves by fluorescence polarization
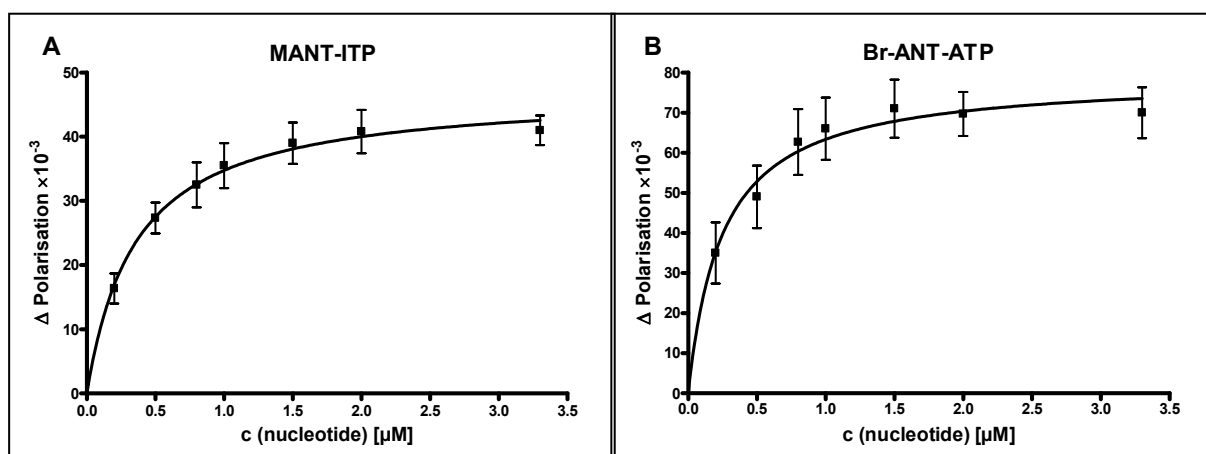
Saturation curves of MANT-ITP (A) and Br-ANT-ATP (B) binding to activated CyaA are shown. Each data point was determined in an independent experiment. Final concentrations of CyaA and CaM were 280 nM each. The fluorescence polarization increase was calculated by subtracting the fluorescence polarization of fluorophore from the fluorescence polarization after addition of CyaA/CaM. Data were analyzed by nonlinear regression using the Prism 4.02 software. Similar data were obtained in three independent experiments.

Comparison of binding constants by fluorescence analysis and AC assay

The high protein concentration of 2.4 µM for direct fluorescence analysis induced comparable results to AC assay only for inhibitors with affinity in the micromolar range (**Table 2**). Apparent K_d values for MANT-ATP and Bis-MANT-ITP from direct fluorescence were similar to K_i values of the functional AC assay (K_d 0.4 – 2 fold > K_i), but for more potent inhibitors, *e.g.* Bis-Br-ANT-ATP, the estimation by fluorescence spectroscopy produced higher K_d values due to the late saturation of the enzyme. Thus, we wished to address this issue by fluorescence polarization spectroscopy. In contrast to direct fluorescence, CyaA concentration was reduced by 9-fold for polarization measurements. The estimated K_d values for MANT-ITP and Br-ANT-ATP are in good agreement to the corresponding K_i values determined in AC

activity assay and reached nanomolar range. Overall, all types of fluorescence approaches showed limitations for determining of binding constants. FRET experiments are selected for deoxygenated MANT-nucleotides[15]; direct fluorescence analysis exhibited consistence with mono- and bis-substituted (M)ANT-nucleotides of low affinity, and fluorescence polarization is in agreement for mono-(M)ANT-nucleotides.

Table 2. Overview of spectroscopic data in comparison to AC assay

	Direct fluorescence	Fluorescence polarization	AC assay
c (CyaA)	2.4 µM	280 nM	10 pM
	K_d [nM]	K_d [nM]	K_i [nM]
MANT-ATP	5,800	n.d.	4,300
Bis-MANT-ATP	7,400	-	360
MANT-ITP	-	400	600
Bis-MANT-ITP	6,400	-	3,000
Br-ANT-ATP	2,400	300	330
Bis-Br-ANT-ATP	4,500	-	12.6

Comparison of determined K_d values by direct fluorescence and fluorescence polarization, and K_i values by AC activity assay. The CyaA concentration is given for each method. Due to low signal changes of activated CyaA at increasing nucleotide concentrations, the saturation curve for MANT-ITP could not be arranged. In fluorescence polarization experiments bis-substituted (M)ANT-nucleotides did not overcome signal to noise ration, because of the weak intrinsic fluorescence of these compounds. *n.d., not determined*.

3.9 Modeling of binding modes

The crystal structure of CyaA in complex with CaM and PMEApp[29] offered us the possibility of predicting the binding mode of mono- and bis-substituted (M)ANT-nucleotides. The AC domain of CyaA includes the catalytic site at the interface of two structural domains, C_A (Met1–Gly61, Ala187–Ala364) and C_B (Val62–Thr186). Compared with PMEApp, the substrate ATP and the fluorescent nucleotides are conformationally constrained because of the semirigid ribosyl moiety. However, the spacious cavity between C_A and C_B may accommodate the different scaffolds so that an alignment of the adenine base and the terminal phosphates is possible (**Fig. 6A**). Hydrophobic interactions, especially of the 3'-MANT-group with Phe306, significantly contribute to the binding of the mono-substitiuted MANT-nucleotide of adenine to CyaA. In fact, the mutant CyaA-Phe306Ala failed to increase the fluorescence signal of 3'-ANT-2'd-ATP[29].

How is the high affinity of PMEApp explained, compared to the potency of most MANT-NTPs, although the alignment of both indicates similar interactions? A reasonable superposition of the phosphates and the adenine bases is only possible if the conformation of the nucleotide moiety retains a certain strain of approximately 3 kcal/mol. A complete minimization would displace the adenine base and, in particular, the phosphate groups from their optimal positions. Therefore, the "true" fit must be a balance between conformational strain and binding energy. Moreover, the ethoxy oxygen of PMEApp strongly interacts with Glu301 and Asn304 via a water molecule, and the ethylene bridge is also in close contact with the edge of Phe306. The docking of 3'-MANT-2'-d-ATP into CyaA is represented in more detail by a stick model (**Fig.6B**). The desoxyribosyl ring adopts a 3'-exo conformation like the ribosyl moiety of MANT-ATP in complex with mammalian AC[28]. The three Mg^{2+} ions are in positions similar to those in the CyaA-PMEApp complex and form the same interactions. Two of them are coordinated with Asp188 and Asp190, one additionally with His298, and the third with the α- and β-phosphate. The imidazolyl-NH of His298 may be H-bonded with an oxygen of the α-phosphate. The γ-phosphate contacts the lysine residues Lys65 and Lys58 (O-N distances, ~2.8 Å). These interactions account for the higher inhibitory potencies of the triphosphates compared with the diphosphate and monophosphate analogs (**Table 1**). The adenine moiety is sandwiched between the side chains of Leu60, His298 and Asn304 whose amide NH_2 group may form an additional hydrogen bond with the desoxyribosyl ring oxygen.

The 6-amino substituent of the nucleobase is in proximity to the backbone oxygens of Val271, Gly299, and Thr300. However, the loop between Gly299 and Asn304 may align all of the nucleobases in similar position. In case of ITP derivatives backbone NH functions of, *e.g.* Gly299 and Val271, may serve as hydrogen donors for the carbonyl oxygens in 6 position, respectively. This diversity of possible interactions may account for inconsistent potency differences of nucleobase substitution. In addition, the affinity of each nucleotide may be affected by a specific arrangement of water molecules that cannot be simply transferred from the PMEApp-bound CyaA structure.

In our previous study[15] we observed high inhibition potency of 3'-MANT-2'-d-ATP and 2'-MANT-3'-d-ATP for CyaA. 3'-MANT-2'd-ATP adopted an ideal position for π-stacking of the phenyl rings of the inhibitor and Phe306. This stacking also accounts for the efficient fluorescence analysis. The axial position of the hydrogen atom corresponding to the 2'-OH group in 3'-MANT-ATP suggests that even the 2',3' bis-substituted MANT-ATP derivative will be potent because the 2'-MANT moiety may fit into a hydrophobic site consisting of Pro305 and Phe261. This site would also be occupied by the 2'-MANT group in 2'-MANT-3'-d-ATP if the desoxyribosyl ring adopts a 3'-exo conformation. However, similar potencies in AC assay of the positional isomers as well as similar magnitudes of fluorescence properties rather indicate analogous interactions between the MANT group and Phe306 in the complexes of CyaA with 2'-MANT-3'-d-ATP and 3'-MANT-3'-d-ATP, respectively. The docking of 2'-MANT-3'-d-ATP reproduced indeed the interaction pattern of 3'-MANT-2'-d-ATP. The only difference is a 3'-endo conformation of the desoxyribosyl moiety as is present, e.g., in A-DNA.

In our present study the docking of Bis-Br-ANT-ATP was based on the 3'-MANT-2'-d-ATP, since the position of the hydrogen atom corresponding to the 2'-OH group enables the second Br-ANT moiety to be accommodated outside of the active site and to form additional specific interactions with CyaA. The 3'-endo binding mode of 2'-MANT-3'-d-ATP does not provide the degree of freedom for an equatorial 3'-Br-ANT substituent. The previous guess that the second ANT-group may interact with Phe261 was not confirmed due to conformational restrictions of the ester moiety (clash with the adenine base)[15]. Instead of that, an energetically favorable conformation of Bis-Br-ANT-ATP is possible where the 2'-Br-ANT substituent can easily expand to Phe306 and where the binding mode of the rest of the molecule is

largely the same as in the case of 3'-MANT-2'-d-ATP. The bromo-anthraniloyl moieties enclose Phe306 from both sides (**Fig. 6C**). Obviously, bromine and chlorine substituents increase the hydrophobic interactions with Phe306, thus accounting for the high inhibitory activity of Bis-halogen-ANT-ATPs compared to their dehalogenated derivatives. Additional hydrophobic contacts are formed between the 2'-Br-ANT phenyl ring and the side chain of Leu60.

The stick model presents the putative binding mode of Bis-Br-ANT-ATP in more detail (**Fig. 6D**). The adenine base, the desoxyribosyl nucleus and the phosphate groups form the same interactions as described for 3'-MANT-2'-d-ATP (see above). The 3'-Br-ANT moiety is completely aligned with the phenyl ring of Phe306, whereas in the case of the 2'-Br-ANT-group only the bromine substituent contacts this residue. Not only the side chain, but also the backbone oxygen of Leu60 may interact with the 2'-Br-ANT group by forming a hydrogen bond with the amine. In the case of the 3'-substituents, generally an outer and an inner orientation of the free or substituted amino group is possible. An inner position like in Fig. 6D should be favorable due to a charge assisted hydrogen bond with the carboxylate of Glu308, but may be impossible when more bulky substituents are present. This may explain subtle activity differences between ANT, MANT, Pr-ANT and Ac-NH-ANT derivatives.

The lower substrate K_m and V_{max} values as well as the generally 5- to 40-fold higher activity of the inhibitors under Mn^{2+} conditions clearly point to considerably tighter binding when compared with the Mg^{2+} enzyme. This increase in the free energy of binding of up to ca. 2 kcal mol^{-1} should be mainly due to stronger Mn^{2+}-phosphate binding. No further conclusions can be drawn from the docking approaches based on force field methods and without a CyaA structure with Mn^{2+} instead of Mg^{2+}.

Fig. 13. Docking of mono- and bis-substituted (M)ANT-nucleotides
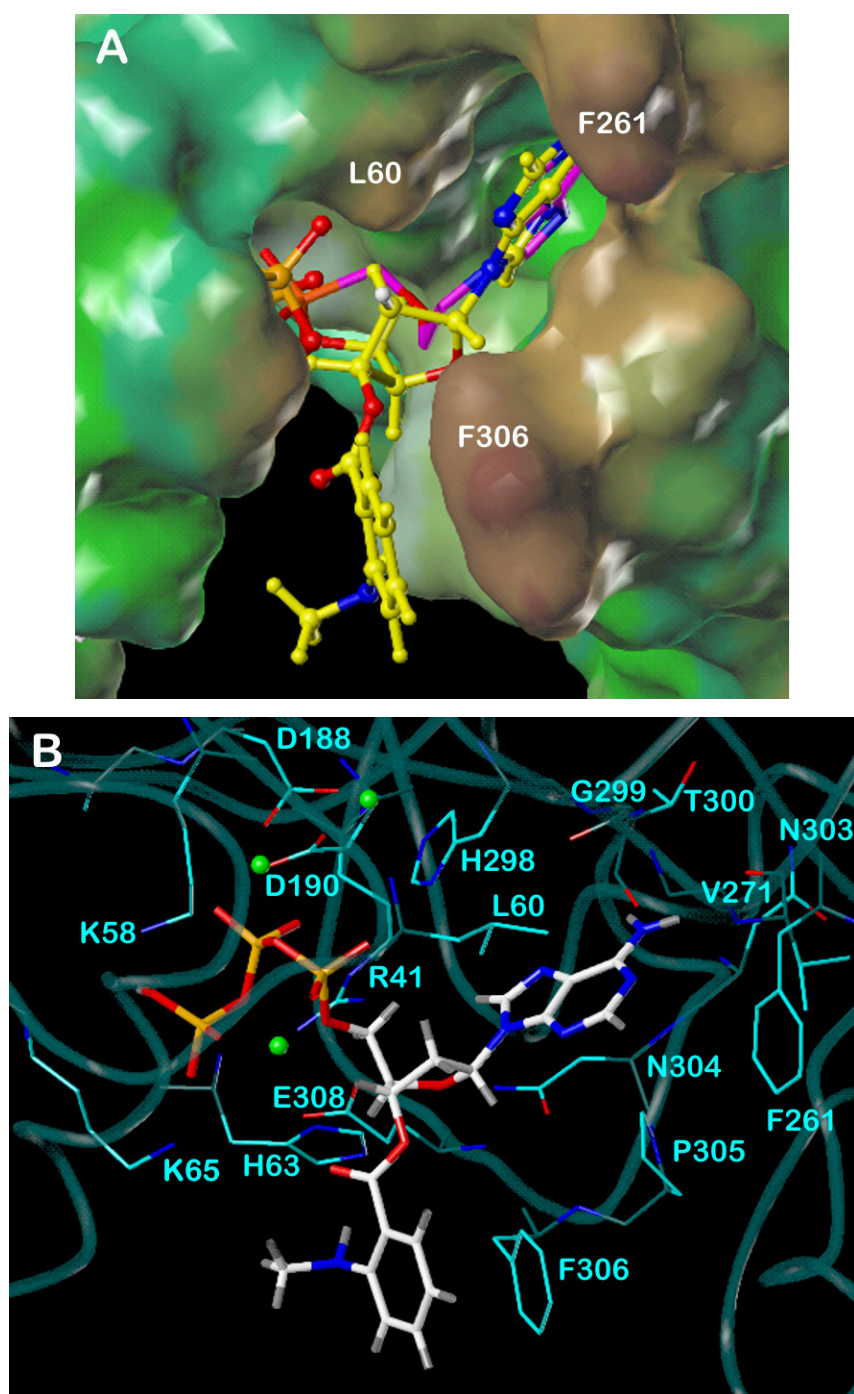
Docking of PMEApp (carbon atoms in magenta); 3'-MANT-2'd-ATP (carbon and hydrogen atoms in yellow) to CyaA (A). Overview of the binding site, represented by the lipophilic potential mapped onto a MOLCAD Connolly surface (brown, hydrophobic areas; green and blue, polar areas).The models are based on the crystal structure of CyaA in complex with PMEApp, PDB 1zot29. Colors of atoms, unless otherwise indicated: orange, phosphorus; red, oxygen; blue, nitrogen; white, carbon; gray, hydrogen; green spheres, magnesium. Docking of 3'-MANT-2'd-ATP[15] in the stick model (B). Amino acids within a sphere of ~3 Å around the ligand are labeled. The protein backbone is schematically represented by a tube. Carbon atoms of the backbone are colored in dark cyan; carbon atoms of the side chains are in light cyan.
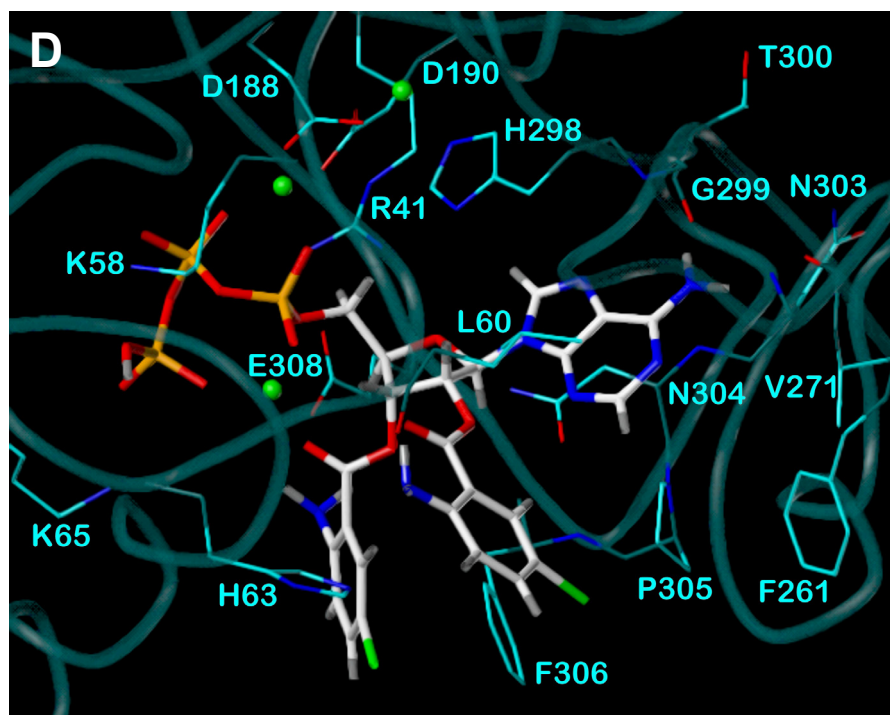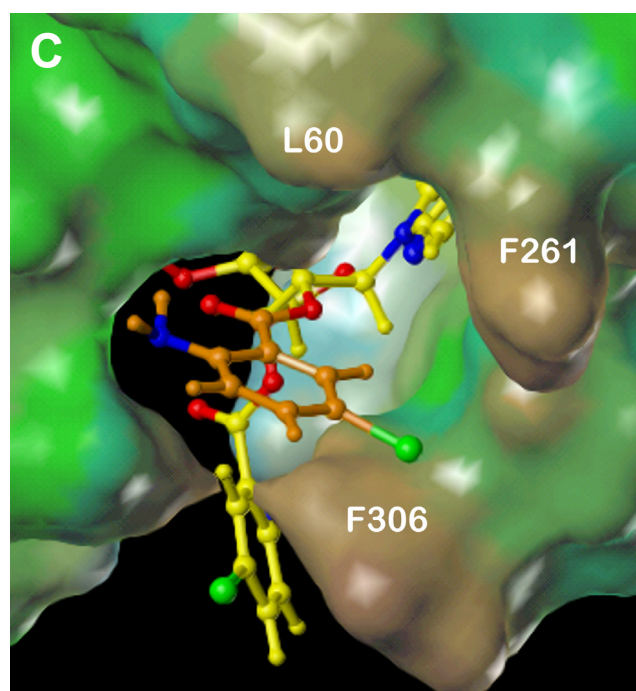
Docking of Bis-Br-ANT-ATP (C and D) to CyaA. The models are based on the crystal structure of CyaA in complex with PMEApp, PDB 1zot[29]. Colors of atoms, unless otherwise indicated: orange, phosphorus; red, oxygen; green, bromine; blue, nitrogen; white, carbon; gray, hydrogen; green spheres, magnesium. Overview of the binding site (C), represented by the lipophilic potential mapped onto a MOLCAD Connolly surface (brown, hydrophobic areas; green and blue, polar areas). Docked ligand: Bis-Br-ANT-ATP (carbon and hydrogen atoms in yellow; second Br-ANT group: carbon atoms in orange). D, docking of Bis-Br-ANT-ATP. Amino acids within a sphere of ~3 Å around the ligand are labeled. The protein backbone is schematically represented by a tube. Carbon atoms of the backbone are colored in dark cyan; carbon atoms of the side chains are in light cyan. For clarity, some labels are omitted (see B).

4. Conclusion

In our present study, we have shown that our newly synthesized (M)ANT-substituted nucleotides, especially the bis-substituted (M)ANT-nucleotides, exhibit unique pharmacological applications for bacterial CyaA with respect to inhibition potency, selectivity, and fluorescence spectroscopy.

For the first time we found inhibitors combining high inhibition potency for CyaA toxin with selectivity towards mammalian ACs. Bis-substituted halogen anthraniloyl-derived purine nucleotides inhibited CyaA in the nanomolar range in a competitive manner (**20 – 23**, K_i = 13 – 20 nM). Our prediction of accommodation bulky bis-substituted (M)ANT-nucleotides in the large cavity of the catalytic CyaA binding site, causing an increase in affinity, was confirmed experimentally. Moreover, bis-substituted halogen anthraniloyl-derived nucleotides of adenine (**20** and **22**) displayed not only high affinity to the bacterial AC, but also revealed high selectivity by 50- to 150-fold depending on the chosen mAC 1, 2 or 5 and purine derivative. In times of falling vaccine rates for whooping cough[41] and ineffective conventional antibiotic treatment due to toxemia or antibiotic-resistant strains, more effective drugs for the prophylaxis of whooping cough are needed. Thus, these nucleotide derivatives could serve as pharmacophores for finding new drugs against *Bordetella pertussis* broadening. For *in vivo* applications enzymatic degradation and high bioavailability of AC inhibitors may be achieved by recent prodrug strategies[42]. In analogy to antiviral drugs like PMEA, the lipophilic nucleotide prodrug is activated first by cleavage with esterases and then phosphorylated by specific kinases to obtain the active nucleoside 5'-triphosphate derivative.

Moreover, the expansion of pharmacological analysis with our nucleotide analogs may offer new potentials investigating other bacterial ACs. Thus, our newly synthesized compound library is analyzed for *Bacillus anthracis* AC toxin edema factor (EF) and AC of *Mycobacterium tuberculosis* in parallel projects.

In recent studies[14] EF displayed several structural homologies to CyaA. The *Bacillus anthracis* bears a phenylalanine residue close to the catalytic site. In comparison to Phe306 of CyaA, edema factor bears Phe586, resulting in fluorescence increases with MANT-nucleotides, as well. Nonetheless, the inhibitory profile of EF differs considerably from CyaA. In particular, MANT-ATP and MANT-CTP inhibit catalytic activity of CyaA with about 10-fold lower potency than catalysis by EF, respectively[14,15]. Based on these differences it is also reasonable to assume that the

enzymological analysis of EF with our new compound library will give different results than the analysis of CyaA. The knowledge about AC inhibition of *Mycobacterium tuberculosis* by MANT-nucleotides is very limited. Thus, the analysis of other ACs is feasible, but the success is not predictable.

Bis-substituted (M)ANT-nucleotides offered the advantage of excellent signal to noise ratio in fluorescence spectroscopy, compared to mono-substituted (M)ANT-nucleotides, with applications in HTS for assessment of non-fluorescent inhibitor potencies like PMEApp. The increase of direct fluorescence for Bis-(M)ANT-NTPs upon interaction with CyaA in the absence of the activator CaM indicates that the nucleotide binding site of CyaA is already functional in the catalytically inactive toxin. Similar results were obtained for TNP nucleotides with CyaA[15] and for MANT-nucleotides in combination with the catalytical subunits C1/C2 of mammalian AC in the absence of the activator forskolin[27,28]. The identification of the precise nature of this conformational change requires crystallization of CyaA complex with Bis-(M)ANT-nucleotide in the absence and presence of CaM. Another implication of the CaM-independent binding of bis-substituted (M)ANT-nucleotides to CyaA is that the catalytic site of CyaA possesses different binding properties than the site in the presence of CaM, offering additional possibilities for inhibitor design and increasing inhibitor selectivity. Comparison of inhibition profiles of non-fluorescent inhibitors on Bis-(M)ANT-NTP fluorescence bound to CyaA in the absence and presence of CaM is a feasible approach. With respect to catalysis, such comparison is impossible because enzymatic activity obligatorily depends on CaM[5,16].

Our present modeling study demonstrate an impression for the obvious alignment of the (M)ANT-nucleotide binding mode to CyaA. The docking of bis-substituted halogen anthraniloyl derivatives exposed additional hydrophobic interactions between enzyme and inhibitor causing higher potency for this class of compounds. Mammalian ACs offer a limitation in accommodation of the second bulky (M)ANT-substituent. Further dockings of the less potent binding of Bis-(M)ANT-NTPs to the catalytic site of C1/C2 for mACs are needed to explain its selectivity for CyaA.

5.   Experimental section

5.1 Synthesis procedures

General protocol of mono- and bis-(M)ANT-nucleotide synthesis

(M)ANT-nucleotides were synthesized according to Hiratsuka[43] with modifications. In general, mono- and bis-substituted (M)ANT-nucleotides could be achieved both in an one pot synthesis procedure. The nucleotide (0.33 mmol, 1 eq) was propounded in a small two-neck round flask and dissolved in a minimum amount of water (3 ml). Under continuous stirring a crystalline preparation of the appropriate isatoic anhydride derivative (0.5 mmol, 1.5 eq) was added. After heating to 38 °C the pH-value was adjusted to 8.6 and maintained by titration of 1 N NaOH solution for 2 hours. The reaction mixture was extracted three times by 20 ml chloroform (only for MANT-nucleotides). The aqueous phase was dry-frozen. The received foam showed white to brown color. The crude reaction mixture was purified by preparative reversed phase high pressure liquid chromatography. Especially for the sensitive separation of mono- and Bis-(M)ANT-NTPs from mono- and Bis-(M)ANT-NDPs this purification strategy was required. In case of monophosphate derivatives only size-exclusion chromatography with a long Sephadex® LH-20 column (85 x 2 cm) and subsequently elution with double-distilled water was applied. The desired product could be detected directly by its blue fluorescence in the collection tubes at λ_{ex} of 366 nm and by TLC. After final dry-freezing white to brown solid compounds (purity > 98 %) were obtained. For all derivatives yields were determined by analytical HPLC measurements of crude reaction mixtures and correlate with the maximal accessible yield. Because of the time consuming and costly preparative HPLC purification separation was stopped after obtaining approximate 5 mg pure compound.

Synthesis of isatoic anhydride precursors

For the propyl (**8**, **9**, **24**, **25**) and acetylated amino (**10**, **11**, **26**, **27**) ANT-nucleotide derivatives the corresponding isatoic anhydrides (**33**, **34**) were easily accessible by nucleophilic substitution[44] with propyliodide and for acetylation with acetic acid anhydride by standard protocol[45], respectively.

5.2 Analytical procedures

HPLC analysis of (M)ANT-nucleotides

The samples were filtered using a PTFE filter (Chromafil, O-20/15, organic, pore size 0.2 mm; Machery-Nagel, Düren, Germany). A 10 µL sample was analyzed using a HPLC model 1100 (Agilent Technologies, Waldbronn, Germany) fitted with a C18 analytical column (Phenomenex Luna, particle size 3 µm, 150 x 4.60 mm, Aschaffenburg, Germany) and DAD. Data were analyzed using a HPLC-3D ChemStation Rev. A.10.01 [1635]. Gradient elution was performed with 0.05 M ammonium acetate (solvent A) and acetonitrile (solvent B) at a constant flow rate of 1.0 ml/min. A gradient profile with the following proportions of solvent B was applied [t (min), % B]: [0, 5], [10, 5], [30, 45], [40, 80]. The chromatograms were monitored at 220 nm and 254 nm. In addition, a fluorescence detector was used for the analysis of the fluorescent anthraniloylic compounds at λ_{ex} of 350 nm and λ_{em} of 450 nm.

LC/MS online coupling

All samples were filtered using a PTFE filter and injected into a HPLC model 1100 (Hewlett-Packard, Waldbronn, Germany). The compound to be analyzed was separated by a C18 column (Phenomenex luna, particle size 3 µm, 150 x 2 mm, Aschaffenburg, Germany). A binary eluent mixture consisting of water (10 mM ammonium acetate) (eluent A) and acetonitrile (eluent B) was pumped with a constant flow of 0.3 ml/min. The following gradient profile was used t [min], % B: [0, 5], [10, 5], [30, 45], [40, 80]. The injected volume was 3 µl. The mass of the respective compound was determined using a triple stage mass spectrometer (Finnigan TSQ 7000; Thermo Fisher Scientific, Waltham, MA).

Preparative HPLC

Compound mixtures were dissolved in water (concentration: 30 - 50 mg/ml) and filtered using a PTFE filter. Compounds were separated using a HPLC model 1100 (Agilent Technologies, Waldbronn, Germany) fitted with a C18 preparative column (Phenomenex Luna, particle size 10 µm, 250 x 21.2 mm). Gradient elution was performed with 0.05 M ammonium acetate (solvent A) and acetonitrile (solvent B) at a constant flow rate of 21 ml/min. Due to the efficiency of separation injection

volumes differed from 10 µl to 60 µl for a run. The chromatograms were monitored at 220 nm and 254 nm.

NMR spectrometry

Bruker Avance 400 (^{1}H: 400.1 MHz, ^{13}C: 100.6 MHz, ^{31}P-NMR: 161.9 MHz, T = 300 K), Bruker Avance 300 (^{1}H: 300.1 MHz, ^{13}C: 75.5 MHz, T = 300 K). The chemical shifts are reported in δ [ppm] relative to external standards (solvent residual peak). The spectra were analyzed by first order, the coupling constants are given in Hertz [Hz]. Characterization of the signals: s = singlet, d = doublet, t = triplet, m = multiplet, dd = double doublet, ddd = double double doublet. Integration is determined as the relative number of atoms. Assignment of signals in ^{13}C-spectra was determined with DEPT-technique (pulse angle: 135 °) and given as (+) for CH or CH_3, (-) for CH_2 and (C_{quat}) for quaternary C. Error of reported values: chemical shift: 0.01 ppm for ^{1}H-NMR, 0.1 ppm for ^{13}C-NMR and 0.1 Hz for coupling constants. The solvent used is reported for each spectrum.

Spectroscopy

Absorption spectroscopy was performed using a Varian Cary BIO 50 UV/VIS/NIR spectrometer with a 1 cm quartz cuvette (Hellma) and Uvasol solvents (Merck or Baker). IR spectra were recorded by a Bio-Rad FTS 2000 MX FT-IR. Further mass spectrometry measurements with electron ionization technique were applied by a Varian CH-5.

Miscellaneous

Melting Points were determined by a Tottoli micro melting point apparatus and are uncorrected. TLC analyses were conducted on silica gel 60 F-254 with a 0.2 mm layer thickness.

5.3 Newly synthesized compounds
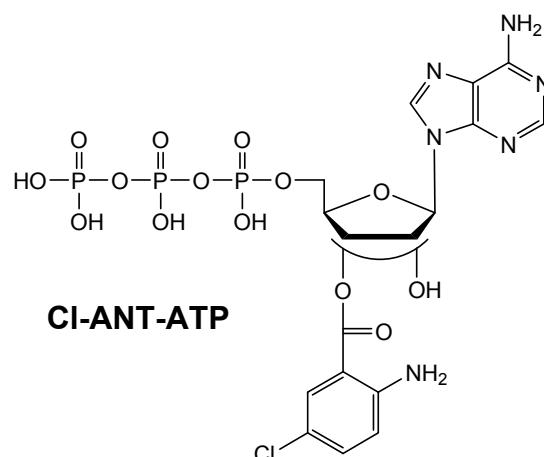
CI-ANT-ATP

CI-ANT-ATP (2'(3')-*O*-5-chloroanthraniloyl-adenosine-5'-triphosphate) or [(2R,3S, 4R,5R)-5-(6-aminopurin-9-yl)-4(3)-hydroxy-2-[[hydroxy-(hydroxyl-phosphonooxy-phosphoryl)oxyphosphoryl]oxymethyl]oxolan-3(4)-yl]2-amino-5-chlorobenzoate (**4**).

For the procedure see general prescription. 100 mg (0.18 mmol) introduced disodium salt of ATP yielded 61 mg (92 µmol, 51 %) pure product after purification. R_f = 0.26 (1-propanol:H_2O:NH_3 (32 %) = 2:1:1). HPLC (analytic): R_t = 21.35 min; k = 12.91; LC/MS (ESI, H_2O/CH_3CN): *m/z* = 678.0 [M+NH_4^+] (R_t = 18.89 min, 100 %), 660.8 [M+H^+] (R_t = 18.89 min, 10 %); (-ESI, H_2O/CH_3CN): *m/z* = 659.1 [M-H^-] (R_t = 18.89 min, 100 %); HPLC (preparative), gradient (t [min], % B: [0, 14], [6, 14], [11, 37], [15, 40], [20, 80]): R_t = 10.15 min; UV/Vis (H_2O) λ_{max} (log ε) = 255 nm (16,000), 343 nm (3,500); empirical formula: $C_{17}H_{20}ClN_6O_{14}P_3$; MW = 660.75
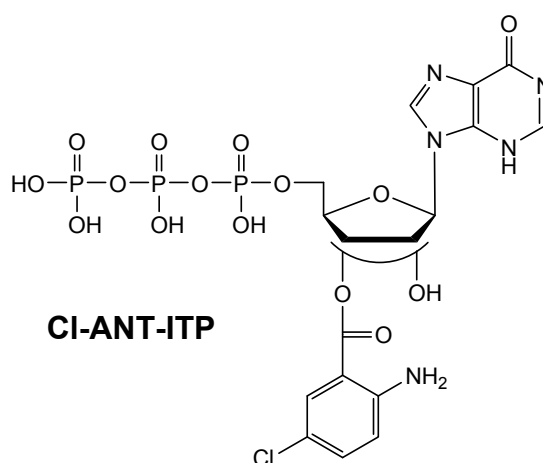
CI-ANT-ITP

CI-ANT-ITP (2'(3')-*O*-5-chloroanthraniloyl-inosine-5'-triphosphate) or [(2R,3S, 4R,5R)- 5-(6-oxo-1H-purin-9-yl)-4(3)-hydroxy-2-[[hydroxy-(hydroxyl-phosphonooxy-

phosphoryl)oxyphosphoryl]oxymethyl]oxolan-3(4)-yl]2-amino-5-chlorobenzoate (**5**).

For the procedure see general prescription. 100 mg (0.17 mmol) introduced disodium salt of ITP yielded 47 mg (71 µmol, 42 %) pure product after purification. R_f = 0.27 (1-propanol:H_2O:NH_3 (32 %) = 2:1:1). HPLC (analytic): R_t = 20.59 min, 20.84 min; k = 13.24, 13.39; LC/MS (ESI, H_2O/CH_3CN): m/z = 696.0 [M+$NH_3NH_4^+$] (R_t = 16.77 min, 100 %), 679.0 [M+NH_4^+] (R_t = 16.77 min, 90 %), 662.1 [M+H^+] (R_t = 16.77 min, 5 %); (-ESI, H_2O/CH_3CN): m/z = 660.1 [M-H^-] (R_t = 16.77 min, 100 %); HPLC (preparative), gradient (t [min], % B: [0, 14], [6, 14], [15, 38], [20, 80]): R_t = 7.71 min, 8.44 min; UV/Vis (H_2O) λ_{max} (log ε) = 255 nm (14,600), 348 nm (4,500); empirical formula: $C_{17}H_{19}ClN_5O_{15}P_3$; MW = 661.73
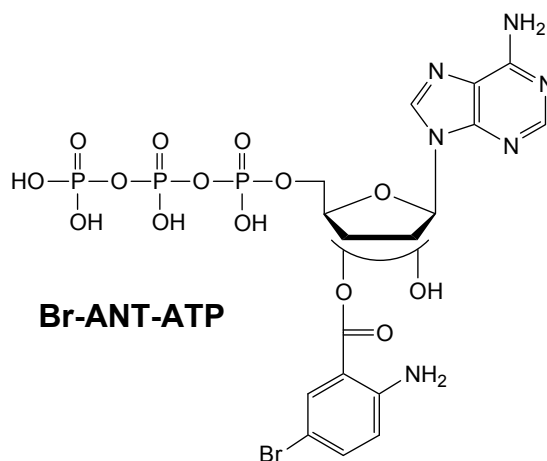
Br-ANT-ATP

Br-ANT-ATP (2'(3')-*O*-5-bromoanthraniloyl-adenosine-5'-triphosphate) or [(2R,3S, 4R,5R)-5-(6-aminopurin-9-yl)-4(3)-hydroxy-2-[[hydroxy-(hydroxyl-phosphonooxy-phosphoryl)oxyphosphoryl]oxymethyl]oxolan-3(4)-yl]2-amino-5-bromobenzoate (**6**).

For the procedure see general prescription. 100 mg (0.18 mmol) introduced disodium salt of ATP led to 36 mg (50 µmol, 28 %) pure product after purification. R_f = 0.24 (1-propanol:H_2O:NH_3 (32 %) = 2:1:1). HPLC (analytic): R_t = 20.24 min, 20.39 min; k = 12.18, 12.28; LC/MS (ESI, H_2O/CH_3CN): m/z = 724.1 [M+NH_4^+] (R_t = 21.21 min, 100 %), 741.2 [M+NH_3+NH_4^+] (R_t = 21.21 min, 40 %); (-ESI, H_2O/CH_3CN): m/z = 705.1 [M-H^-] (R_t = 21.21 min, 100 %); HPLC (preparative), gradient (t [min], % B: [0, 17], [8, 17], [10, 25], [15, 38], [20, 80]): R_t = 6.32 min; UV/Vis (H_2O) λ_{max} (log ε) = 256 nm (16,400), 332 nm (3,300); empirical formula: $C_{17}H_{20}BrN_6O_{14}P_3$; MW = 705.20
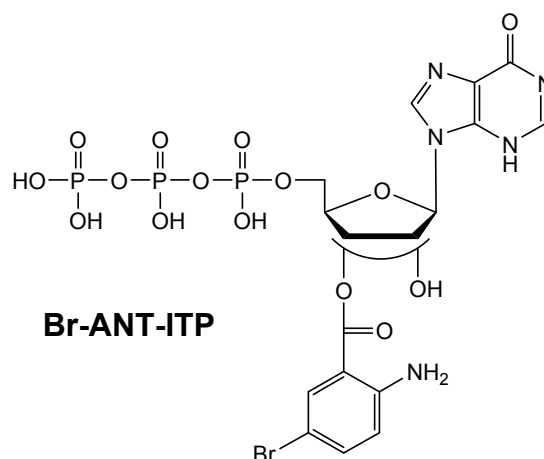
Br-ANT-ITP

Br-ANT-ITP (2'(3')-*O*-5-bromoanthraniloyl-inosine-5'-triphosphate) or [(2R,3S, 4R,5R)-5-(6-oxo-1H-purin-9-yl)-4(3)-hydroxy-2-[[hydroxy-(hydroxyl-phosphonooxy-phosphoryl)oxyphosphoryl]oxymethyl]oxolan-3(4)-yl]2-amino-5-bromobenzoate (**7**).

For the procedure see general prescription. 100 mg (0.17 mmol) introduced disodium salt of ITP yielded 48 mg (68 μmol, 40 %) pure product after purification. R_f = 0.25 (1-propanol:H_2O:NH_3 (32 %) = 2:1:1). HPLC (analytic): R_t = 21.16 min, 21.45 min; k = 13.63, 13.83; LC/MS (ESI, H_2O/CH_3CN): *m/z* = 725.1 [M+NH_4^+] (R_t = 18.81 min, 100 %), 742.2 [M+NH_3+NH_4^+] (R_t = 18.81 min, 35 %); (-ESI, H_2O/CH_3CN): *m/z* = 706.1 [M-H$^-$] (R_t = 18.81 min, 100 %); HPLC (preparative), gradient (t [min], % B: [0, 18], [15, 38], [20, 80]): R_t = 4.27 min, 4.53 min; UV/Vis (H_2O) λ_{max} (log ε) = 248 nm (15,000), 328 nm (4,300); empirical formula: $C_{17}H_{19}BrN_5O_{15}P_3$; MW = 706.18
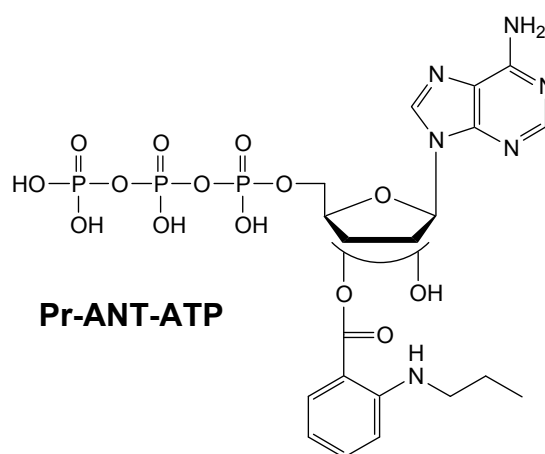
Pr-ANT-ATP

Pr-ANT-ATP (*N*-propyl-2'(3')-*O*-anthraniloyl-adenosine-5'-triphosphate) or [(2R,3S, 4R,5R)-5-(6-aminopurin-9-yl)-4(3)-hydroxy-2-[[hydroxy-(hydroxy-phosphonooxy-phosphoryl)oxyphosphoryl]oxymethyl]oxolan-3(4)-yl]2-propylaminobenzoate (**8**).
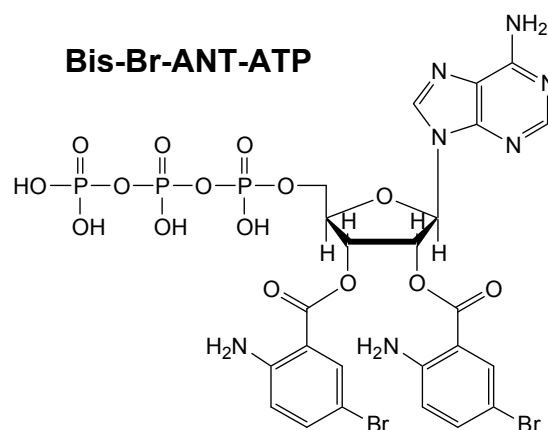
For the procedure see general prescription. 100 mg (0.18 mmol) introduced disodium salt of ATP yielded 29 mg (43 µmol, 24 %) pure product after purification. R_f = 0.31 (1-propanol:H_2O:NH_3 (32 %) = 2:1:1). HPLC (analytic): R_t = 24.93 min, 25.67 min; k = 15.29, 15.78; LC/MS (ESI, H_2O/CH_3CN): *m/z* = 669.0 [M+H$^+$] (R_t = 23.12 min, 100 %), 686.0 [M+NH$_4$$^+$] ($R_t$ = 23.12 min, 15 %); (-ESI, H_2O/CH_3CN): *m/z* = 667.0 [M-H$^-$] (R_t = 23.12 min, 100 %); HPLC (preparative), gradient (t [min], % B: [0, 5], [20, 45], [25, 80]): R_t = 13.33 min; UV/Vis (H_2O) λ_{max} (log ε) = 257 nm (17,500), 359 nm (4,600); empirical formula: $C_{20}H_{27}N_6O_{14}P_3$; MW = 668.38

Pr-ANT-ITP

Pr-ANT-ITP   (*N*-propyl-2'(3')-*O*-anthraniloyl-inosine-5'-triphosphate)   or   [(2R,3S, 4R,5R)-5-(6-oxo-1H-purin-9-yl)-4(3)-hydroxy-2-[[hydroxy-(hydroxy-phosphonooxy-phosphoryl)oxyphosphoryl]oxymethyl]oxolan-3(4)-yl]2-propylaminobenzoate (**9**).

For the procedure see general prescription. 100 mg (0.17 mmol) introduced disodium salt of ITP yielded 25 mg (37 µmol, 22 %) pure product after purification. R_f = 0.32 (1-propanol:H_2O:NH_3 (32 %) = 2:1:1). HPLC (analytic): R_t = 24.73 min, 25.16 min; k = 16.10, 16.40; LC/MS (ESI, H_2O/CH_3CN): *m/z* = 687.0 [M+NH$_4$$^+$] ($R_t$ = 22.87 min, 100 %), 669.8 [M+H$^+$] (R_t = 22.87 min, 20 %); (-ESI, H_2O/CH_3CN): *m/z* = 668.0 [M-H$^-$] (R_t = 22.87 min, 100 %); HPLC (preparative), gradient (t [min], % B: [0, 5], [20, 45], [25, 80]): R_t = 13.12 min; UV/Vis (H_2O) λ_{max} (log ε) = 257 nm (17,500), 359 nm (4,600); empirical formula: $C_{20}H_{26}N_5O_{15}P_3$; MW = 669.37
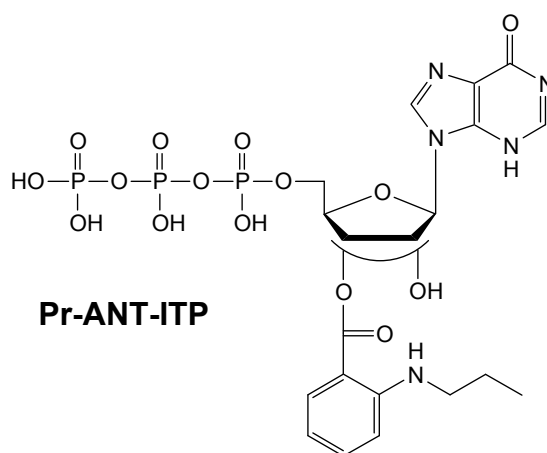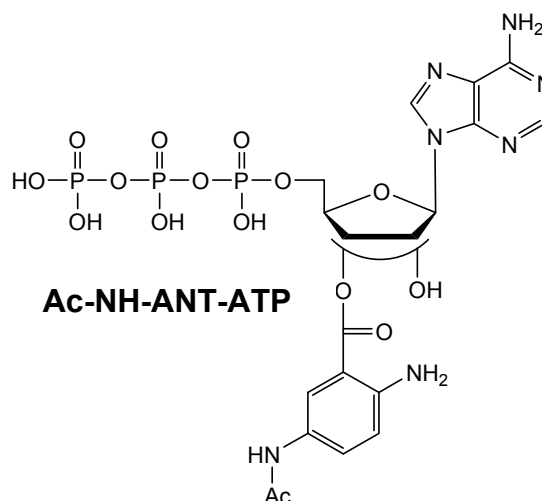
Ac-NH-ANT-ATP

Ac-NH-ANT-ATP (2'(3')-*O*-5-acetylaminoanthraniloyl-adenosine-5'-triphosphate) or [(2R,3S,4R,5R)-5-(6-aminopurin-9-yl)-4(3)-hydroxy-2-[[hydroxy-(hydroxyl-phosphono-oxyphosphoryl)oxyphosphoryl]oxymethyl]oxolan-3(4)-yl]2-amino-5-acetylamino-benzoate (**10**).
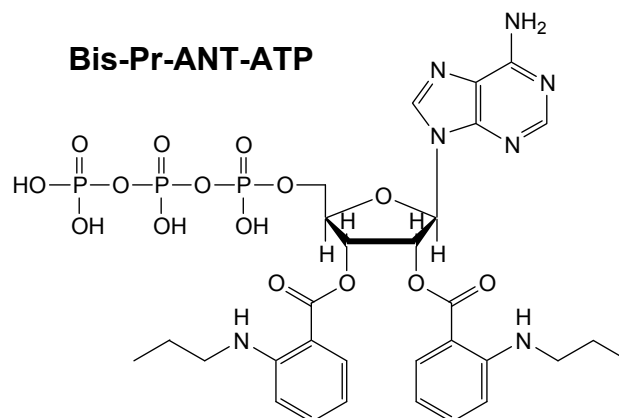
For the procedure see general prescription. 100 mg (0.18 mmol) introduced disodium salt of ATP yielded 57 mg (84 µmol, 46 %) pure product after purification. R_f = 0.21 (1-propanol:H_2O:NH_3 (32 %) = 2:1:1). HPLC (analytic): R_t = 8.39 min, 8.75 min; k = 4.48, 4.72; LC/MS (ESI, H_2O/CH_3CN): *m/z* = 683.9 [M+H$^+$] (R_t = 3.34 min, 100 %), 701.0 [M+NH$_4^+$] (R_t = 3.34 min, 70 %); (-ESI, H_2O/CH_3CN): *m/z* = 682.0 [M-H$^-$] (R_t = 3.34 min, 100 %); HPLC (preparative), gradient (t [min], % B: [0, 6], [5, 7], [23, 14], [24, 80], [29, 80]): R_t = 12.06 min; UV/Vis (H_2O) λ_{max} (log ε) = 259 nm (17,200), 349 nm (3,100); empirical formula: $C_{19}H_{24}N_7O_{15}P_3$; MW = 683.35
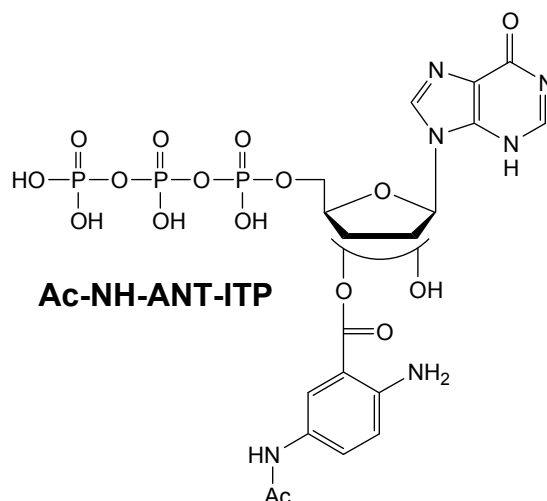
Ac-NH-ANT-ITP

Ac-NH-ANT-ITP (2'(3')-*O*-5-acetylaminoanthraniloyl-inosine-5'-triphosphate) or [(2R,3S,4R,5R)-5-(6-oxo-1H-purin-9-yl)-4(3)-hydroxy-2-[[hydroxy-(hydroxy-phosphonooxyphosphoryl)oxyphosphoryl]oxymethyl]oxolan-3(4)-yl]2-amino-5-acetyl-aminobenzoate (**11**).

For the procedure see general prescription. 100 mg (0.17 mmol) introduced disodium salt of ITP yielded 60 mg (88 µmol, 52 %) pure product after purification. R_f = 0.22 (1-propanol:H_2O:NH_3 (32 %) = 2:1:1). HPLC (analytic): R_t = 7.63 min, 7.99 min; k = 4.28, 4.53; LC/MS (ESI, H_2O/CH_3CN): *m/z* = 702.0 [M+NH_4^+] (R_t = 1.91 min, 100 %), 719.0 [M+NH_3+NH_4^+] (R_t = 1.91 min, 40 %), 684.9 [M+H^+] (R_t = 1.91 min, 25 %); (-ESI, H_2O/CH_3CN): *m/z* = 683.0 [M-H^-] (R_t = 1.91 min, 100 %); HPLC (preparative), gradient (t [min], % B: [0, 5.8], [11, 5.8], [12, 10], [18, 13], [20, 80]): R_t = 9.50 min; UV/Vis (H_2O) λ_{max} (log ε) = 248 nm (11,400; shoulder), 345 nm (2,500); empirical formula: $C_{19}H_{23}N_6O_{16}P_3$; MW = 684.34
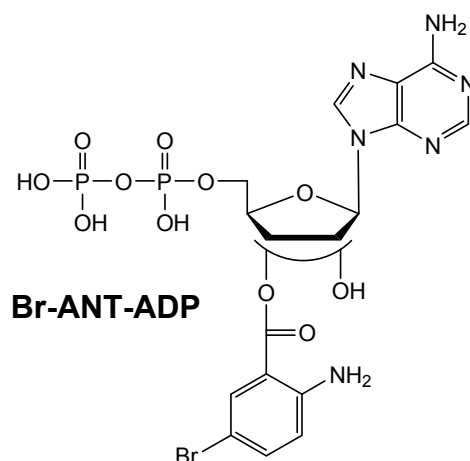
Br-ANT-ADP

Br-ANT-ADP (2'(3')-*O*-5-bromoanthraniloyl-adenosine-5'-diphosphate) or [(2R,3S, 4R,5R)-5-(6-aminopurin-9-yl)-4(3)-hydroxy-2-[(hydroxy-phosphonooxyphosphoryl) oxymethyl]oxolan-3(4)-yl]2-amino-5-bromobenzoate (**14**).

For the procedure see general prescription. 100 mg (0.18 mmol) introduced disodium salt of ATP yielded 9 mg (14 µmol, 8 %) pure product after purification. R_f = 0.27 (1-propanol:H_2O:NH_3 (32 %) = 2:1:1). HPLC (analytic): R_t = 20.86 min, 21.16 min; k = 12.59, 12.79; LC/MS (ESI, H_2O/CH_3CN): *m/z* = 644.1 [M+NH_4^+] (R_t = 22.09 min, 100 %), 627.2 [M+H^+] (R_t = 22.09 min, 80 %); (-ESI, H_2O/CH_3CN): *m/z* = 625.1 [M-H^-] (R_t = 22.09 min, 100 %); HPLC (preparative), gradient (t [min], % B: [0, 16], [10, 16], [15, 50], [17, 51.5], [20, 80]): R_t = 9.94 min, 10.99 min; UV/Vis (H_2O) λ_{max} (log ε) = 255 nm (12,700), 328 nm (3,400); empirical formula: $C_{17}H_{19}BrN_6O_{11}P_2$; MW = 625.25
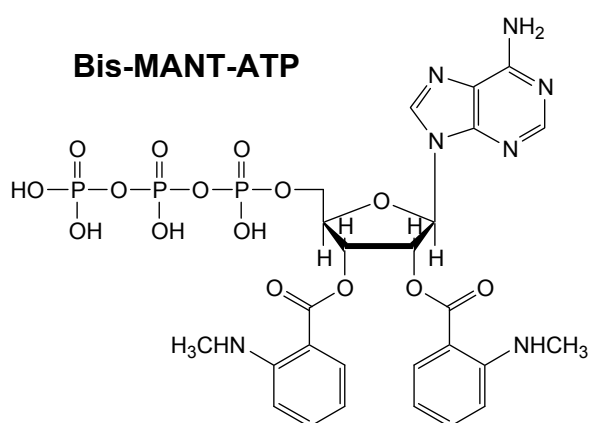
Bis-MANT-ATP
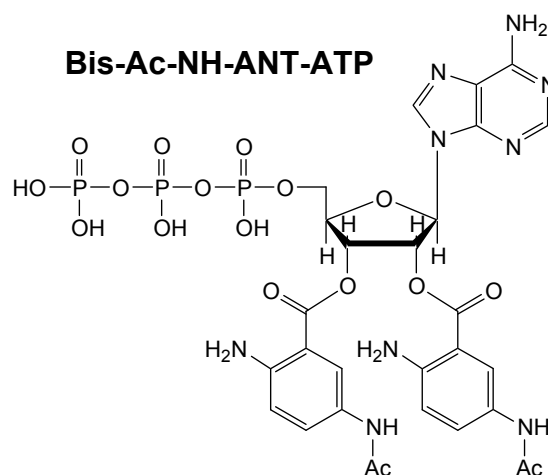
Bis-MANT-ATP (*N*-methyl-2',3'-bis-*O*-anthraniloyl-adenosine-5'-triphosphate) or [(2R,3S,4R,5R)-5-(6-aminopurin-9-yl)-2-[[hydroxy-(hydroxy-phosphonooxy-phosphoryl)oxyphosphoryl]oxymethyl]oxolan-3,4-bis-yl]2-methylaminobenzoate (**17**).

For the procedure see general prescription. 100 mg (0.18 mmol) introduced disodium salt of ATP led over all purification steps to 21 mg (27 µmol, 15 %) pure product. R_f = 0.32 (1-propanol:H_2O:NH_3 (32 %) = 2:1:1). HPLC (analytic): R_t = 26.95 min; k = 16.61; LC/MS (ESI, H_2O/CH_3CN): *m/z* = 791.2 [M+NH_4^+] (R_t = 28.58 min, 100 %), 774.2 [M+H^+] (R_t = 28.58 min, 40 %); (-ESI, H_2O/CH_3CN): *m/z* = 772.3 [M-H^-] (R_t = 28.58 min, 100 %); HPLC (preparative), gradient (t [min], % B: [0, 11], [2, 11], [5, 30], [15, 31.5], [18, 80]): R_t = 9.91 min; UV/Vis (H_2O) λ_{max} (log ε) = 255 nm (18,000), 359 nm (7,300); empirical formula: $C_{26}H_{30}N_7O_{15}P_3$; MW = 773.48
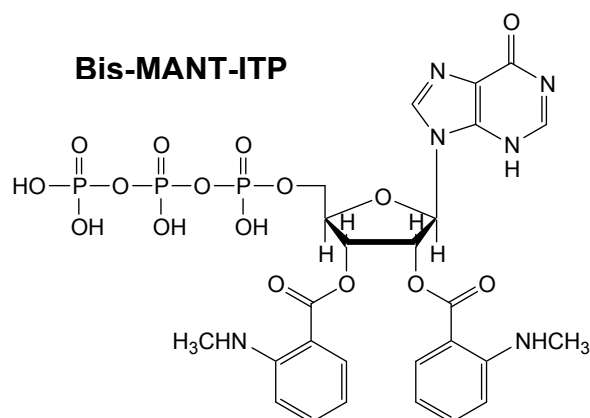
Bis-MANT-ITP (*N*-methyl-2',3'-bis-*O*-anthraniloyl-inosine-5'-triphosphate) or [(2R,3S, 4R,5R)-5-(6-oxo-1H-purin-9-yl)-2-[[hydroxy-(hydroxy-phosphonooxyphosphoryl) oxyphosphoryl]oxymethyl]oxolan-3,4-bis-yl]2-methylaminobenzoate (**18**).
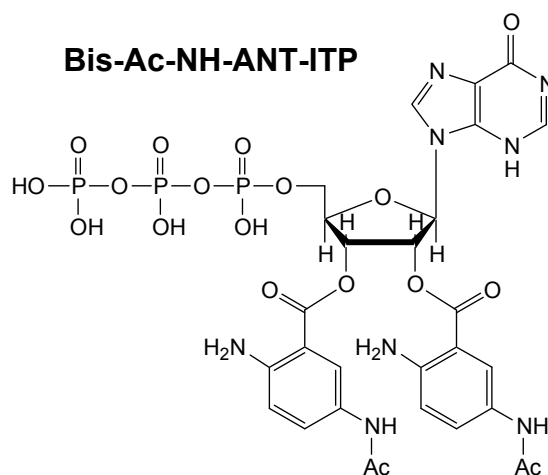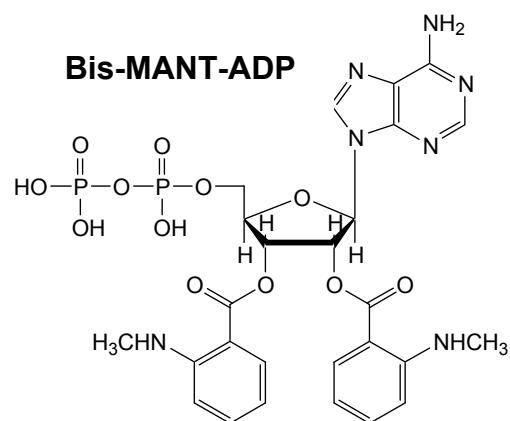
For the procedure see general prescription. 100 mg introduced disodium salt of ITP (0.17 mmol) yielded over all purification steps 18 mg (23 µmol, 14 %) pure product. R_f = 0.33 (1-propanol:H_2O: NH_3 (32 %) = 2:1:1) HPLC (analytic): R_t = 26.74 min; k = 16.52; LC/MS (ESI, H_2O/CH_3CN): *m/z* = 792.3 [M+NH_4^+] (R_t = 28.02 min, 100 %), 775.2 [M+H^+] (R_t = 28.58 min, 15 %); (-ESI, H_2O/CH_3CN): *m/z* = 773.3 [M-H^-] (R_t = 28.08 min, 100 %); HPLC (preparative), gradient (t [min], % B: [0, 11], [2, 11], [5, 30], [15, 31.5], [18, 80]): R_t = 9.72 min; UV/Vis (H_2O) λ_{max} (log ε) = 251 nm (16,400), 358 nm (6,400); empirical formula: $C_{26}H_{29}N_6O_{16}P_3$; MW = 774.46
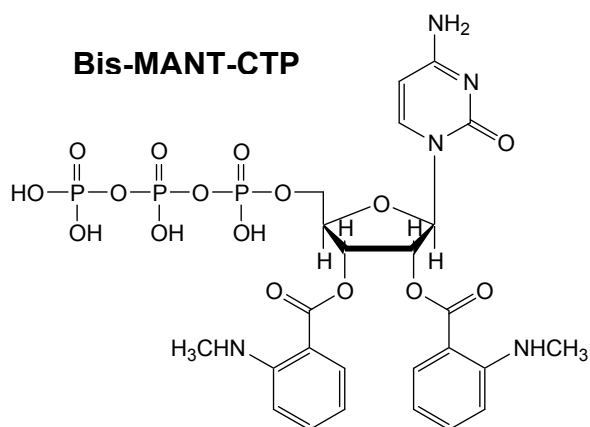
Bis-MANT-CTP

Bis-MANT-CTP (*N*-methyl-2',3'-bis-*O*-anthraniloyl-cytosine-5'-triphosphate) or [(2R,3S,4R,5R)-5-(4-amino-2-oxopyrimidin-1-yl)-2-[[hydroxy-(hydroxy-phosphonooxy-phosphoryl)oxyphosphoryl]oxymethyl]oxolan-3,4-bis-yl]2-methylaminobenzoate (**19**).

100 mg introduced trisodium salt of CTP (0.18 mmol) yielded 35 mg (46 µmol, 26 %) pure product. R_f = 0.29 (1-propanol:H_2O:NH_3 (32 %) = 2:1:1). HPLC (analytic): R_t = 26.83 min; k = 16.60; LC/MS (ESI, H_2O/CH_3CN): *m/z* = 750.0 [M+H$^+$] (R_t = 25.37 min, 100 %), 767.1 [M+NH$_4^+$] (R_t = 25.37 min, 10 %); (-ESI, H_2O/CH_3CN): *m/z* = 748.0 [M-H$^-$] (R_t = 25.37 min, 100 %); HPLC (preparative), gradient (t [min], % B: [0, 14], [6, 14], [11, 35], [15, 40], [20, 80]): UV/Vis (H_2O) λ_{max} (log ε) = 253 nm (14,500), 359 nm (6,600); R_t = 13.19 min; empirical formula: $C_{25}H_{30}N_5O_{16}P_3$; MW = 749.45
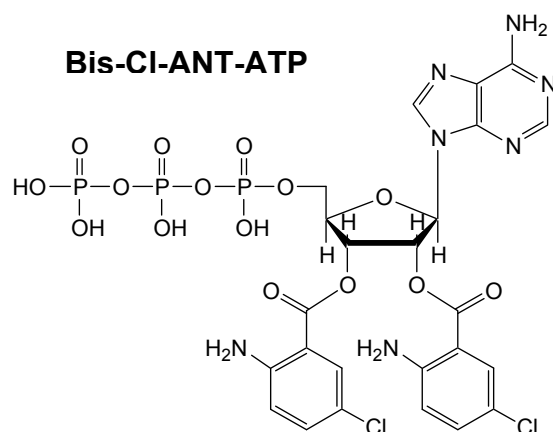
Bis-Cl-ANT-ATP

Bis-Cl-ANT-ATP (2',3'-bis-*O*-5-chloroanthraniloyl-adenosine-5'-triphosphate) or [(2R, 3S,4R,5R)-5-(6-aminopurin-9-yl)-2-[[hydroxy-(hydroxy-phosphonooxyphosphoryl) oxyphosphoryl]oxymethyl]oxolan-3,4-bis-yl]2-amino-5-chlorobenzoate (**20**).

For the procedure see general prescription. 100 mg (0.18 mmol) introduced disodium salt of ATP yielded 31 mg (38 µmol, 21 %) pure product after purification. R_f = 0.32

(1-propanol:H_2O:NH_3 (32 %) = 2:1:1). HPLC (analytic): R_t = 27.79 min; k = 17.10; LC/MS (ESI, H_2O/CH_3CN): *m/z* = 831.0 [M+NH_4^+] (R_t = 26.24 min, 100 %), 814.1 [M+H^+] (R_t = 26.24 min, 10 %); (-ESI, H_2O/CH_3CN): *m/z* = 812.0 [M-H^-] (R_t = 26.24 min, 100 %); HPLC (preparative), gradient (t [min], % B: [0, 14], [6, 14], [11, 37], [15, 40], [20, 80]): R_t = 13.26 min; UV/Vis (H_2O) λ_{max} (log ε) = 255 nm (16,900), 350 nm (5,100); empirical formula: $C_{24}H_{24}Cl_2N_7O_{15}P_3$; MW = 814.31

Bis-Cl-ANT-ITP
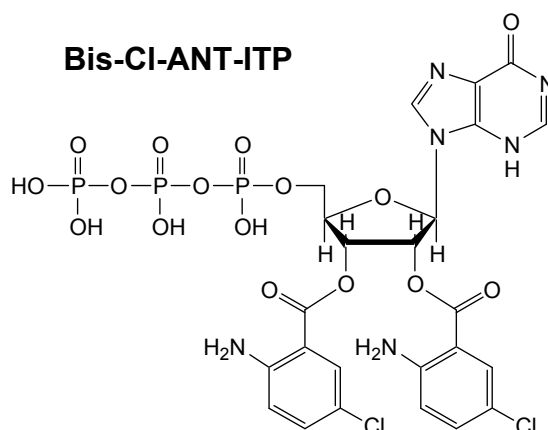
Bis-Cl-ANT-ITP (2',3'-bis-*O*-5-chloroanthraniloyl-inosine-5'-triphosphate) or [(2R,3S, 4R,5R)-5-(6-oxo-1H-purin-9-yl)-2-[[hydroxy-(hydroxy-phosphonooxyphosphoryl) oxyphosphoryl]oxymethyl]oxolan-3,4-bis-yl]2-methyl-5-chloroaminobenzoate (**21**).
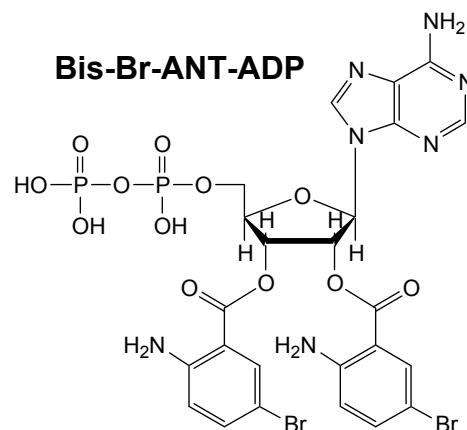
For the procedure see general prescription. 100 mg introduced disodium salt of ITP (0.17 mmol) yielded over all purification steps 30 mg (37 µmol, 22 %) pure product. R_f = 0.35 (1-propanol:H_2O:NH_3 (32 %) = 2:1:1). HPLC (analytic): R_t = 27.46 min; k = 17.99; LC/MS (ESI, H_2O/CH_3CN): *m/z* = 849.1 [M+NH_4^+] (R_t = 25.90 min, 100 %), 832.0 [M+H^+] (R_t = 25.90 min, 90 %); (-ESI, H_2O/CH_3CN): *m/z* = 830.0 [M-H^-] (R_t = 25.90 min, 100 %); HPLC (preparative), gradient (t [min], % B: [0, 14], [6, 14], [15, 38], [20, 80]): R_t = 15.65 min; UV/Vis (H_2O) λ_{max} (log ε) = 249 nm (19,700), 350 nm (6,200); empirical formula: $C_{24}H_{23}Cl_2N_6O_{16}P_3$; MW = 815.30

Bis-Br-ANT-ATP

Bis-Br-ANT-ATP (2',3'-bis-*O*-5-bromoanthraniloyl-adenosine-5'-triphosphate) or (2R, 3S,4R,5R)-5-(6-aminopurin-9-yl)-2-[[hydroxy-(hydroxy-phosphonooxyphosphoryl) oxyphosphoryl]oxymethyl]oxolan-3,4-bis-yl]2-amino-5-bromobenzoate (**22**).

For the procedure see general prescription. 100 mg introduced disodium salt of ATP yielded 18 mg (20 µmol, 11 %) pure product after purification. R_f = 0.31 (1-propanol:H_2O:NH_3 (32 %) = 2:1:1). HPLC (analytic): R_t = 26.72 min; k = 16.41; LC/MS (ESI, H_2O/CH_3CN): *m/z* = 920.9 [M+NH_4^+] (R_t = 26.24 min, 100 %), 904.0 [M+H^+] (R_t = 26.24 min, 10 %); (-ESI, H_2O/CH_3CN): *m/z* = 901.9 [M-H^-] (R_t = 26.24 min, 100 %); HPLC (preparative), gradient (t [min], % B: [0, 17], [8, 17], [10, 25], [15, 38], [20, 80]): R_t = 16.14 min; UV/Vis (H_2O) λ_{max} (log ε) = 255 nm (14,600), 348 nm (4,500); empirical formula: $C_{24}H_{24}Br_2N_7O_{15}P_3$; MW = 903.21
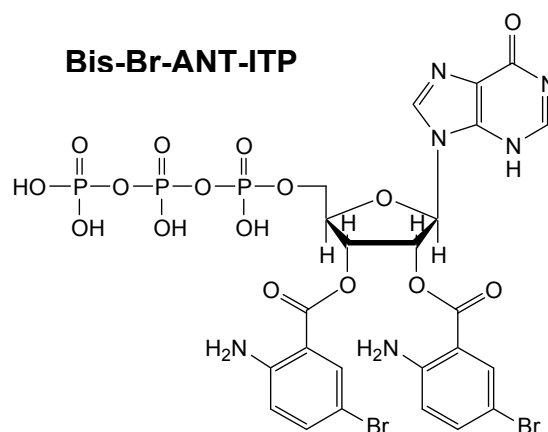
Bis-Br-ANT-ITP

Bis-Br-ANT-ITP (2',3'-bis-*O*-5-bromoanthraniloyl-inosine-5'-triphosphate) or [(2R,3S, 4R,5R)-5-(6-oxo-1H-purin-9-yl)-2-[[hydroxy-(hydroxy-phosphonooxyphosphoryl) oxyphosphoryl]oxymethyl]oxolan-3,4-bis-yl]2-methyl-5-bromoaminobenzoate (**23**).

For the procedure see general prescription. 100 mg introduced disodium salt of ITP (0.17 mmol) yielded over all purification steps 32 mg (36 µmol, 21 %) pure product.

R_f = 0.33 (1-propanol:H_2O:NH_3 (32 %) = 2:1:1). HPLC (analytic): R_t = 28.16 min; k = 18.47; LC/MS (ESI, H_2O/CH_3CN): *m/z* = 921.9 [M+NH_4^+] (R_t = 25.89 min, 100 %), 905.0 [M+H^+] (R_t = 25.89 min, 15 %); (-ESI, H_2O/CH_3CN): *m/z* = 903.0 [M-H^-] (R_t = 25.89 min, 100 %); HPLC (preparative), gradient (t [min], % B: [0, 18], [15, 38], [20, 80]: R_t = 12.39 min; UV/Vis (H_2O) λ_{max} (log ε) = 249 nm (19,000), 348 nm (5,600); empirical formula: $C_{24}H_{23}Br_2N_6O_{16}P_3$; MW = 904.20

Bis-Pr-ANT-ATP   (*N*-propyl-2',3'-bis-*O*-anthraniloyl-adenosine-5'-triphosphate)   or [(2R,3S,4R,5R)-5-(6-aminopurin-9-yl)-2-[[hydroxy-(hydroxy-phosphonooxy phosphoryl)oxyphosphoryl]oxymethyl]oxolan-3,4-bis-yl]2-propylaminobenzoate (**24**).

For the procedure see general prescription. 100 mg introduced disodium salt of ATP (0.18 mmol) yielded over all purification steps 21 mg (25 µmol, 14 %) pure product. R_f = 0.34 (1-propanol:H_2O:NH_3 (32 %) = 2:1:1). HPLC (analytic): R_t = 33.04 min; k = 20.59; LC/MS (ESI, H_2O/CH_3CN): *m/z* = 830.2 [M+H^+] (R_t = 30.63 min, 100 %), 847.2 [M+NH_4^+] (R_t = 30.63 min, 30 %); (-ESI, H_2O/CH_3CN): *m/z* = 828.1 [M-H^-] (R_t = 30.63 min, 100 %); HPLC (preparative), gradient (t [min], % B: [0, 5], [20, 45], [25, 80]): R_t = 20.14 min; UV/Vis (H_2O) λ_{max} (log ε) = 255 nm (16,800), 359 nm (5,800); empirical formula: $C_{30}H_{37}N_6O_{16}P_3$; MW = 829.58
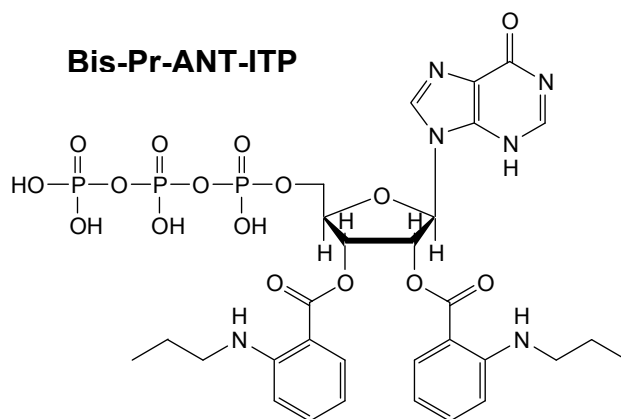
Bis-Pr-ANT-ITP

Bis-Pr-ANT-ITP (*N*-propyl-2',3'-bis-*O*-anthraniloyl-inosine-5'-triphosphate) or [(2R, 3S,4R,5R)-5-(6-oxo-1H-purin-9-yl)-2-[[hydroxy-(hydroxy-phosphonooxyphosphoryl) oxyphosphoryl]oxymethyl]oxolan-3,4-bis-yl]2-propylaminobenzoate (**25**).

For the procedure see general prescription. 100 mg introduced disodium salt of ITP (0.17 mmol) yielded over all purification steps 15 mg (19 µmol, 11 %) pure product. R_f = 0.35 (1-propanol:H_2O:NH_3 (32 %) = 2:1:1). HPLC (analytic): R_t = 30.57 min; k = 20.14; LC/MS (ESI, H_2O/CH_3CN): *m/z* = 848.1 [M+NH_4^+] (R_t = 30.60 min, 100 %), 831.1 [M+H^+] (R_t = 30.60 min, 20 %); (-ESI, H_2O/CH_3CN): *m/z* = 829.1 [M-H^-] (R_t = 30.60 min, 100 %); HPLC (preparative), gradient (t [min], % B: [0, 5], [20, 45], [25, 80]): R_t = 19.58 min; UV/Vis (H_2O) λ_{max} (log ε) = 255 nm (14,600), 359 nm (5,300); empirical formula: $C_{30}H_{37}N_6O_{16}P_3$; MW = 830.57

Bis-Ac-NH-ANT-ATP

Bis-Ac-NH-ANT-ATP (2',3'-bis-*O*-5-acetylaminoanthraniloyl-adenosine-5'-triphosphate) or [(2R,3S,4R,5R)-5-(6-aminopurin-9-yl)-2-[[hydroxy-(hydroxy-phosphonooxyphosphoryl)oxyphosphoryl]oxymethyl]oxolan-3,4-bis-yl]2-amino-5-acetylaminobenzoate (**26**).

For the procedure see general prescription. 100 mg introduced disodium salt of ATP (0.18 mmol) yielded over all purification steps 27 mg (32 µmol, 18 %) pure product. R_f = 0.27 (1-propanol:H_2O:NH_3 (32 %) = 2:1:1). HPLC (analytic): R_t = 20.05 min; k = 12.10; LC/MS (ESI, H_2O/CH_3CN): *m/z* = 860.1 [M+H$^+$] (R_t = 16.79 min, 100 %), 877.2 [M+NH$_4$$^+$] ($R_t$ = 16.79 min, 30 %); (-ESI, H_2O/CH_3CN): *m/z* = 858.1 [M-H$^-$] (R_t = 16.79 min, 100 %); HPLC (preparative), gradient (t [min], % B: [0, 6], [5, 7], [23, 14], [24, 80], [29, 80]): R_t = 21.49 min; UV/Vis (H_2O) λ_{max} (log ϵ) = 261 nm (23,500), 350 nm (5,700); empirical formula: $C_{28}H_{32}N_9O_{17}P_3$; MW = 859.53

Bis-Ac-NH-ANT-ITP

Bis-Ac-NH-ANT-ITP   (2',3'-bis-*O*-5-acetylaminoanthraniloyl-inosine-5'-triphosphate) or   [(2R,3S,4R,5R)-5-(6-oxo-1H-purin-9-yl)-2-[[hydroxy-(hydroxy-phosphonooxy-phosphoryl)oxyphosphoryl]oxymethyl]oxolan-3,4-bis-yl]2-amino-5-acetylamino-benzoate (**27**).

For the procedure see general prescription. 100 mg introduced trisodium salt of ITP (0.17 mmol) yielded over all purification steps 16 mg (19 µmol, 11 %) pure product. R_f = 0.29 (1-propanol:H_2O:NH_3 (32 %) = 2:1:1). HPLC (analytic): R_t = 18.80 min; k = 12.00; LC/MS (ESI, H_2O/CH_3CN): *m/z* = 878.1 [M+NH$_4$$^+$] ($R_t$ = 8.85 min, 100 %), 895.1 [M+NH$_3$+NH$_4$$^+$] ($R_t$ = 8.85 min, 35 %), 861.1 [M+H$^+$] (R_t = 8.85 min, 30 %); (-ESI, H_2O/CH_3CN): *m/z* = 859.1 [M-H$^-$] (R_t = 8.85 min, 100 %); HPLC (preparative), gradient (t [min], % B: [0, 5.8], [11, 5.8], [12, 10], [18, 13], [20, 80]): R_t = 18.43 min; UV/Vis (H_2O) λ_{max} (log ϵ) = 259 nm (14,300; shoulder), 348 nm (5,200); empirical formula: $C_{28}H_{31}N_8O_{18}P_3$; MW = 860.51

Bis-MANT-ADP

Bis-MANT-ADP (*N*-methyl-2',3'-bis-*O*-anthraniloyl-adenosine-5'-diphosphate) or [(2R,3S,4R,5R)-5-(6-aminopurin-9-yl)-2-[(hydroxy-phosphonooxyphosphoryl) oxymethyl]oxolan-3,4-bis-yl]2-methylaminobenzoate (**28**).

For the procedure see general prescription. 100 mg (0.18 mmol) introduced disodium salt of ATP yielded over all purification steps 7 mg (11 µmol, 6 %) pure product. R_f = 0.35 (1-propanol:H_2O:NH_3 (32 %) = 2:1:1). HPLC (analytic): R_t = 27.10 min; k = 16.78; LC/MS (ESI, H_2O/CH_3CN): *m/z* = 711.3 [M+NH_4^+] (R_t = 28.85 min, 100 %), 694.3 [M+H$^+$] (R_t = 28.85 min, 90 %); (-ESI, H_2O/CH_3CN): *m/z* = 692.2 [M-H$^-$] (R_t = 28.83 min, 100 %); HPLC (preparative), gradient (t [min], % B: [0, 11], [2, 11], [5, 30], [15, 31.5], [18, 80]): R_t = 11.71 min; UV/Vis (H_2O) λ_{max} (log ε) = 255 nm (16,000), 359 nm (6,200); empirical formula: $C_{26}H_{29}N_7O_{12}P_2$; MW = 693.50

Bis-MANT-IDP

Bis-MANT-IDP (*N*-methyl-2',3'-bis-*O*-anthraniloyl-inosine-5'-diphosphate) or [(2R,3S, 4R,5R)-5-(6-oxo-1H-purin-9-yl)-2-[(hydroxy-phosphonooxyphosphoryl)oxymethyl] oxolan-3,4-bis-yl]2-methylaminobenzoate (**29**).

For the procedure see general prescription. 100 mg (0.17 mmol) trisodium salt of ITP yielded 6 mg (9 µmol, 5 %) pure product. R_f = 0.36 (1-propanol:H_2O:NH_3 (32 %) =

2:1:1). HPLC (analytic): R_t = 27.48 min; k = 16.94; LC/MS (ESI, H_2O/CH_3CN): *m/z* = 712.3 [M+NH$_4$$^+$] ($R_t$ = 28.76 min, 100 %), 695.4 [M+H$^+$] (R_t = 28.76 min, 10 %); (-ESI, H_2O/CH_3CN): *m/z* = 693.3 [M-H$^-$] (R_t = 28.76 min, 100 %); HPLC (preparative), gradient (t [min], % B: [0, 11], [2, 11], [5, 30], [15, 31.5], [18, 80]): R_t = 11.24 min; UV/Vis (H_2O) λ_{max} (log ε) = 252 nm (15,800), 359 nm (6,000); empirical formula: $C_{26}H_{28}N_7O_{13}P_2$; MW = 694.48
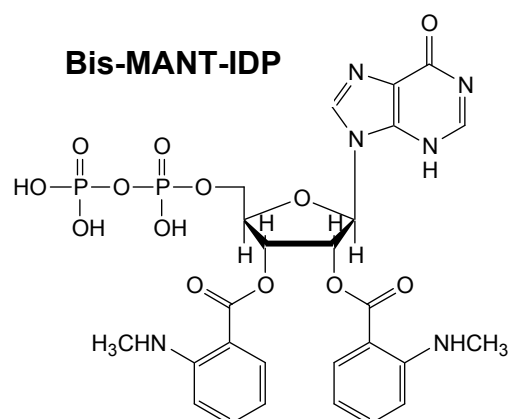
Bis-Br-ANT-ADP (2',3'-bis-*O*-5-bromoanthraniloyl-adenosine-5'-diphosphate) or [(2R,3S,4R,5R)-5-(6-aminopurin-9-yl)-2-[(hydroxy-phosphonooxyphosphoryl) oxymethyl]oxolan-3(4)-yl]2-amino-5-bromobenzoate (**30**).

For the procedure see general prescription. 100 mg (0.18 mmol) introduced disodium salt of ATP yielded 6 mg (7 µmol, 4 %) pure product after purification. R_f = 0.35 (1-propanol:H_2O:NH_3 (32 %) = 2:1:1). HPLC (analytic): R_t = 27.39 min; k = 16.85; LC/MS (ESI, H_2O/CH_3CN): *m/z* = 823.9 [M+H$^+$] (R_t = 27.73 min, 100 %), 840.9 [M+NH$_4$$^+$] ($R_t$ = 27.73 min, 20 %); (-ESI, H_2O/CH_3CN): *m/z* = 821.9 [M-H$^-$] (R_t = 27.73 min, 100 %); HPLC (preparative), gradient (t [min], % B: [0, 17], [8, 17], [10, 25], [15, 38], [20, 80]): R_t = 16.68 min; UV/Vis (H_2O) λ_{max} (log ε) = 255 nm (14,100), 348 nm (4,000); empirical formula: $C_{24}H_{23}Br_2N_7O_{12}P_2$; MW = 823.23
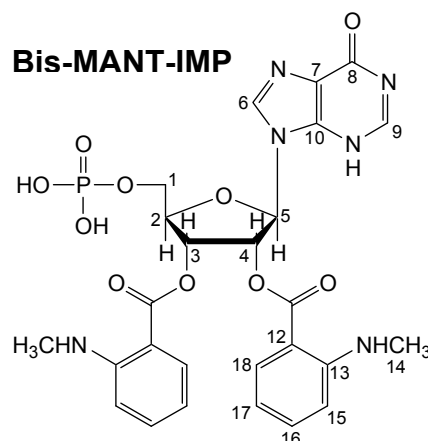
Bis-MANT-IMP

Bis-MANT-IMP   (*N*-methyl-2',3'-bis-*O*-anthraniloyl-inosine-5'-monophosphate)   or [(2R,3S,4R,5R)-5-(6-oxo-1H-purin-9-yl)-4(3)-hydroxy-2-[phosphonooxymethyl]oxolan-3,4-bis-yl]2-methylaminobenzoate (**31**).

The disodium salt of IMP (100 mg, 0.26 mmol) yielded 80 mg (130 μmol, 50 %) pure product after size-exclusion chromatography. R_f = 0.28 (1-propanol:H_2O:NH_3 (32 %) = 2:1:1). HPLC (analytic): R_t = 28.95 min, k = 17.56; LC/MS (ESI, H_2O/CH_3CN): *m/z* = 632.2 [M+NH_4^+] (R_t = 30.28 min,100 %); (-ESI, H_2O/CH_3CN): *m/z* = 613.2 [M-H$^-$] (R_t = 30.28 min, 100 %), 673.2 [M+CH_3COO^-] (R_t = 30.28 min, 70 %); ^{1}H-NMR (400 MHz, D_2O): δ = 2.16 (s, 3 H, HMBC: 14a-H), 2.25 (s, 3 H, HMBC: 14b-H), 4.09 (s, 2 H, COSY: 1-H), 4.58 (s, 1 H, COSY: 2-H), 5.67 (t, 1 H, COSY, HSQC: 17a-H), 5.75 (d, ^{3}J = 8.35 Hz, 1 H, COSY, HSQC: 15a-H), 5.81 (s, 1 H, COSY, HSQC: 3-H), 5.96 (d, ^{3}J = 8.38 Hz, 1 H, COSY, HSQC: 15b-H), 6.08 (m, 2 H, COSY, HSQC: 4-H, 17b-H), 6.16 (d, ^{3}J = 6.21 Hz, 1 H, COSY, HMBC: 5-H), 6.47 (s, 1 H, COSY: 16a-H), 6.77 (s, 1 H, COSY: 16b-H), 7.22 (d, ^{3}J = 7.52 Hz, 1 H, COSY, HSQC: 18a-H), 7.63 (d, ^{3}J = 7.49 Hz, 1 H, COSY, HSQC: 18b-H), 7.72 (s, 1 H, HSQC: 9-H), 8.51 (s, 1 H, HMBC: 6-H); ^{13}C-NMR (100.6 MHz, D_2O): δ [ppm] = 28.6 (1 C, HSQC, HMBC: 14-C), 28.8 (1 C, HSQC, HMBC: 14-C), 64.0 (1 C, HSQC: 1-C), 72.1 (1 C, HSQC: 3-C), 73.8 (1 C, HSQC: 4-C), 84.4 (1 C, HSQC: 2-C), 85.2 (1 C, HSQC, HMBC: 5-C), 107.5 (1 C, HMBC: 12a-C), 108.1 (1 C, HMBC: 12b-C), 110.54 (1 C, HSQC, HMBC: 15a/b-C),113.7 (1 C, HSQC, HMBC: 17a-C), 114.1 (1 C, HSQC, HMBC: 17b-C), 123.3 (1 C, HMBC: 10-C), 131.0 (1 C, HSQC: 18a-C), 131.3 (1 C, HSQC: 18b-C), 134.9 (2 C, HSQC, HMBC: 16a/b-C), 139.7 (1 C, HMBC: 6-C), 146.0 (1 C, HSQC, HMBC: 9-C), 148.9 (1 C, HMBC: 7-C), 151.7 (1 C, HMBC: 13a-C), 151.8 (1 C, HMBC: 13b-C), 158.1 (1 C, HMBC: 8-C), 166.7 (1 C, HMBC: 11a-C), 167.2 (1 C,

HMBC: 11b-C); ^{31}P-NMR (161.9 MHz, D_2O): δ = 3.3; UV/Vis (H_2O) λ_{max} (log ε) = 250 nm (16,200), 359 nm (6,500); empirical formula: $C_{26}H_{27}N_6O_{10}P_3$; MW = 614.50
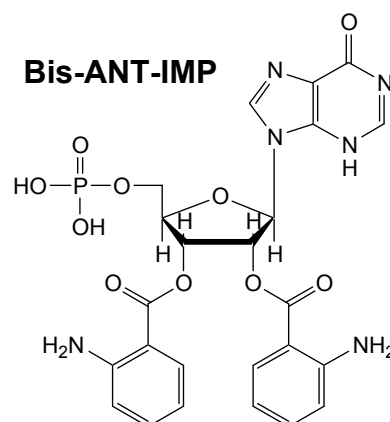
Bis-ANT-IMP (2',3'-bis-*O*-anthraniloyl-inosine-5'-monophosphate) or [(2R,3S, 4R,5R)-5-(6-oxo-1H-purin-9-yl)-2-[phosphonooxymethyl]oxolan-3,4-bis-yl]2-amino-benzoate (**32**).

The disodium salt of IMP (100 mg, 0.26 mmol) yielded 82 mg (140 µmol, 54 %) pure product after size-exclusion chromatography. R_f = 0.28 (1-propanol:H_2O:NH_3 (32 %) = 2:1:1). HPLC (analytic): R_t = 25.03 min, k = 15.41; LC/MS (ESI, H_2O/CH_3CN): *m/z* = 604.3 [M+NH$_4^+$] (R_t = 26.15 min, 100 %); (-ESI, H_2O/CH_3CN): *m/z* = 585.3 [M-H$^-$] (R_t = 26.15 min, 80 %), 645.3 [M+CH$_3$COO$^-$] (R_t = 26.15 min, 100 %); UV/Vis (H_2O) λ_{max} (log ε) = 250 nm (23,600), 333 nm (7,600); empirical formula: $C_{24}H_{23}N_6O_{10}P$; MW = 586.45
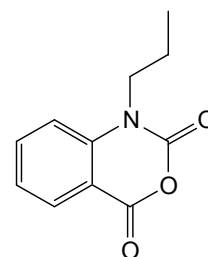
N-propylisatoic anhydride or 1-propyl-1,3-benzoxazine-2,4-dione (**33**).

Isatoic anhydride (1.0 g, 6.1 mmol) was dissolved in a minimum amount of dry dimethylformamide (10 ml) and 177 mg (7.35 mmol, 1.2 eq) sodiumhydrid (60 %) was added stepwise in small portions accompanied by vigorous gas evolution. After five minutes of stirring 1.2 g iodopropane (6.74 mmol, 1.1 eq) were added dropwise to the pacified solution. The reaction mixture was stirred for 24 h and then

precipitated in 100 ml cold water to give a white powder. After filtration and washing the product was dried over phosphorpentoxide under vacuum to yield 988 mg (4.8 mmol, 79 %).

^{1}H-NMR (300 MHz, CDCl$_3$): δ = 1.04 (t, ^{3}J = 8.1 Hz, 3 H, CH$_3$), 1.78 (m, 2 H, CH$_2$), 4.02 (t, ^{3}J = 7.7 Hz, 2 H, CH$_2$), 7.16 (d, ^{3}J = 8.5 Hz, 1 H, C8-H), 7.28 (ddd, ^{3}J = 7.9 Hz, ^{3}J = 7.4 Hz, ^{4}J = 1.0 Hz, 1 H, C6-H), 7.76 (ddd, ^{3}J = 8.6 Hz, ^{3}J = 7.4 Hz., ^{4}J = 1.7 Hz, 1 H, C7-H), 8.13 (dd, ^{3}J = 7.9 Hz, ^{4}J = 1.7 Hz, 1 H, C5-H); ^{13}C-NMR (75.5 MHz, CDCl$_3$): δ = 11.0 (+), 20.2 (–), 46.4 (–),111.7 (C$_{quat}$, phenyl), 114.0 (+), 123.9 (+), 130.9 (+), 137.3 (+), 141.4 (C$_{quat}$, phenyl), 147.8 (C$_{quat}$, anhydride), 158.6 (C$_{quat}$, anhydride); MS (EIMS, 70 eV): m/z = 205.0 [M$^{+•}$] (100 %), 161.1 [M$^{+•}$-CO$_2$] (20 %); IR (KBr): [cm^{-1}] = 3094, 2964, 2936, 2875, 1770, 1724, 1603, 1477, 1326, 1022, 766; Mp: 94 °C; UV/Vis (ACN) λ_{max} (log ε) = 245 (8,500), 320 nm (4,000); empirical formula: C$_{11}$H$_{11}$NO$_3$; MW = 205.21
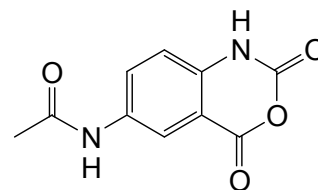
5-acetylaminoisatoic anhydride or _N_-(2,4-dioxo-1,4-dihydro-benzo[1,3] oxazin-6yl)-acetamide (**34**).

Acetic acid (2 ml) and acetic anhydride (63 mg, 0.61 mmol, 1.1 eq) was propounded in a small flask. Under stirring 5-aminoisatoic anhydride (100 mg, 0.56 mmol) was added and heated to 60 °C for 4 hours. After cooling to room temperature; 10 ml water was added dropwise. The brown colored product was precipitated by ice-cooling followed by filtration and washing with ice-cold water. The precipitate was dried over phosphorpentoxide under vacuum to yield 110 mg (0.5 mmol, 90 %).

^{1}H-NMR (300 MHz, CDCl$_3$): δ = 2.05 (s, 3 H, CH$_3$), 7.10 (d, ^{3}J = 8.8 Hz, 1 H, C8-H), 7.80 (dd, ^{3}J = 8.8 Hz, ^{4}J = 2.5 Hz, 1 H, C7-H), 8.24 (d, ^{4}J = 2.5 Hz, 1 H, C5-H), 10.17 (s, 1 H, N-H), 11.66 (s, 1 H, N-H); ^{13}C-NMR (75.5 MHz, CDCl$_3$): δ = 23.8 (+), 110.1 (C$_{quat}$, phenyl), 115.7 (+), 117.5 (+), 128.1 (+), 134.9 (C$_{quat}$, phenyl), 136.7 (C$_{quat}$, phenyl), 146.9 (C$_{quat}$, anhydride), 159.8 (C$_{quat}$, anhydride), 168.4 (C$_{quat}$, acetyl); MS (EIMS, 70 eV): m/z = 176.0 [M$^{+•}$-CO$_2$] (100 %), 161.1 [M$^{+•}$] (80 %); IR (KBr): [cm^{-1}] = 3117, 2843, 2936, 2735, 1788, 1725, 1645, 1510, 1336, 1264, 911; Mp: 259 °C;

UV/Vis (MeOH) λ_{max} (log ε) = 270 nm (15,500), 350 nm (5,600); empirical formula: $C_{10}H_8N_2O_4$; MW = 220.18

6. References

[1] Versteegh, F. G. A.; Schellekens, J. F. P.; Fleer, A.; Roord, J. *Rev. Med. Microbiol.* **2005**, *16*, 79

[2] Mattoo, S.; Foreman-Wykert, A. K.; Cotter, P. A.; Miller, J. F. *Front Biosci.* **2001**, *6*, e168

[3] Confer, D. L.; Eaton, J. W. *Science*, **1982**, *217*, 948

[4] Hewlett, E. L.; Gordon, V. M.; McCaffery, J. D.; Sutherland, W. M.; Gray, M. C. *J. Biol. Chem.* **1989**, 264, 19379

[5] Ladant, D.; Ullmann, A. *Trends Microbiol.* **1999**, *7*, 172

[6] (a) Mock, M.; Ullmann, A. *Trends Microbiol.* **1993**, *1*, 187; (b) Ahuja, N.; Kumar, P.; Bhatnagar, R. *Crit. Rev. Microbiol.* **2004**, *30*, 187

[7] (a) Boyd, A. P.; Ross P. J.; Conroy, H.; Mahon, N.; Lavelle, E. C.; Mills, K. H. *J. Immunol.* **2005**, *175*, 730; (b) Carbonetti, N. H.; Artamonova, G. V.; Andreasen, C.; Bushar, N. *Infect. Immun.* **2005**, *73*, 2698; (c) Hewlett, E. L.; Donato, G. M.; Gray, M. C. *Mol. Microbiol.* **2006**, *59*, 447

[8] Soelaiman, S.; Wei, B. Q.; Bergson, P.; Lee, Y. S.; Shen, Y.; Mrksich, M.; Shoichet, B. K.; Tang, W. J. *J. Biol. Chem.* **2003**, *278*, 25990

[9] Hanoune, J.; Defer, N.; *Annu. Rev. Pharmacol. Toxicol.* **2001**, *41*, 45

[10] Hiratsuka, T.; *J. Biol. Chem.* **1982**, *257*, 13354

[11] Gille, A.; Guo, J.; Mou, T. C.; Doughty, M. B; Lushington, G. H.; Seifert, R. *Biochem. Pharmacol.* **2005**, *71*, 89

[12] Wang, J. L.; Guo, J. X.; Zhang, Q. Y.; Wu, J. J.; Seifert, R.; Lushington, G. H. *Bioorg. Med. Chem.* **2007**, *15*, 2993

[13] Sarfati, R. S.; Kansal, V. K.; Munier, H.; Glaser, P.; Gilles, A. M.; Labruyere, E.; Mock, M.; Danchin, A.; Barzu, O. *J. Biol. Chem.* **1990**, *265*, 18902

[14] Taha, H.; Schmidt, J.; Göttle, M.; Suryanarayana, S.; Shen, Y.; Tang, W. J.; Gille, A.; Geduhn, J.; König, B.; Dove, S.; Seifert, R. *Mol. Pharmacol.* **2009**, *75*, 693

[15] Göttle, M.; Dove, S.; Steindel, P.; Shen, Y.; Tang, W. J.; Geduhn, J.; König, B.; Seifert, R. *Mol. Pharmacol.* **2007**, *72*, 526

[16] Shen, Y.; Lee, Y. S.; Soelaiman, S.; Bergson P.; Lu, D.; Chen, A.; Beckingham, K.; Grabarek, Z.; Mrksich, M.; Tang, W. J. *EMBO J.* **2002**, *21*, 6721

[17] Seifert, R.; Lee, T. W.; Lam, V. T.; Kobilka, B. K. *Eur. J. Biochem.* **1998***, 255,* 369

[18] Gille, A.; Lushington, G. H.; Mou, T. C.; Doughty, M. B.; Johnson, R. A.; Seifert, R. *J. Biol. Chem.* **2004**, *279*, 19955

[19] Cornell, W. D.; Cieplak, P.; Bayly, C. I.; Gould I. R.; Merz, K. M. J.; Ferguson, D. M.; Spellmeyer, D. C.; Fox, T.; Caldwell, J. W.; Kollman, P. A. *J. Am. Chem.* **1995**, *117*, 5179

[20] Clark, M.; Cramer, R. D. III.; Van Opdenbosch, N. *J. Comp. Chem. Soc.* **1989**, *10*, 982

[21] Heiden, W.; Moeckel, G.; Brickmann, J. *J. Comput. Aided Mol. Des.* **1993**, *7*, 503

[22] Ghose, A. K.; Viswanadhan, V. N.; Wendoloski, J. J. *J. Phys. Chem.* **1998**, *102*, 3762

[23] Jameson, D. M.; Eccleston, J. F. *Methods Enzymol.* **1997**, *278,* 363

[24] Gille, A.; Seifert, R. *Life Sciences* **2003**, *74*, 271

[25] Johnson, R. A.; Desaubry, L.; Bianchi, G.; Shoshani, I.; Lyons, E., Jr.; Taussig, R.; Watson, P. A.; Cali, J. J.; Krupinski, J.; Pieroni, J. P.; Iyengar, R. *J. Biol. Chem.* **1997**, *272*, 8962

[26] Onda, T.; Hashimoto, Y.; Nagai, M.; Kuramochi, H.; Saito, S.; Yamazaki, H.; Toya, Y.; Sakai, I.; Homcy, C. J.; Nishikawa, K.; Ishikawa, Y. *J. Biol. Chem.* **2001***, 276*, 47785

[27] Mou, T. C.; Gille, A.; Fancy, D. A.; Seifert, R.; Sprang, S. R. *J. Biol. Chem.* **2005**, *280*, 7253

[28] Mou, T. C.; Gille, A.; Suryanarayana, S.; Richter, M.; Seifert, R.; Sprang, S. R. *Mol. Pharmacol.* **2006**, *70*, 878

[29] Guo, Q.; Shen, Y.; Lee, Y. S.; Gibbs, C. S.; Mrksich, M.; Tang, W. J. *EMBO J.* **2005**, *24,* 3190

[30] Tesmer; J. J.; Dessauer, C. W.; Sunahara, R. K.; Murray, L. D.; Johnson, R. A.; Gilman, A. G.; Sprang, S. R. *Biochemistry* **2000**, *39*, 14464

[31] Dessauer; C. W.; Tesmer, J. J.; Sprang, S. R.; Gilman, A. G. *Trends Pharmacol. Sci.* **1999**, *20*, 205

[32] Johnson, R. A.; Shoshani, I. *J. Biol. Chem.* **1990**, *265*, 11595

[33] Shoshani, I.; Laux, W. H.; Perigaud, C.; Gosselin, G.; Johnson, R. A. *J. Biol. Chem.* **1999**, *274*, 34742

[34] Tao, M.; Huberman, A. *Arch. Biochem. Biophys.* **1970**, *141*, 236

[35] Tesmer, J. J.; Sunahara, R. K.; Johnson, R. A.; Gosselin, G.; Gilman, A. G.; Sprang, S. R. *Science*, **1999**, *285*, 756

[36] Eckstein, F.; Romaniuk, P. J.; Heideman, W.; Storm, D. R. *J. Biol. Chem.* **1981**, *256*, 9118

[37] Gille, A.; Seifert, R. *J. Biol. Chem.* **2003**, *278*, 12672

[38] Lakowicz, J. R. *Principles of Fluorescence Spectroscopy* Kluwer Academic/ Plenum, New York, **1999**

[39] Shen, Y.; Zhukovskaya, N. L.; Zimmer, M. I.; Soelaiman S.; Bergson, P.; Wang, C. R.; Gibbs, C. S.; Tang, W. J. *Proc. Natl. Acad. Sci. USA* **2004**, *101,* 3242

[40] Smith; D. S.; Eremin, S. A.; *Anal. Bioanal. Chem.* **2008**, *391*, 1499

[41] http://www.auswaertiges-amt.de/diplo/de/Laenderinformationen/01-Laender /Gesundheitsdienst/Symposien/XIII/Uebersicht.html; XIII. Symposium Reise- und Impfmedizin-Internationale Gesundheit im Auswärtigen Amt am 25./26. April **2008**, Dr. Martina Littmann, Pertussis – wieder ein Thema?

[42] Laux, W. H. G.; Pande, P.; Shoshani, I.; Gao, J. Y.; Boudou-Vivet, V.; Gosselin, G.; Johnson, R. A. *J. Biol. Chem.* **2004**, *279*, 13317

[43] Hiratsuka, T. Biochim. Biophys. Acta **1983**, 742, 496

[44] Barbuch, R. J.; Peet, N. P. *Org. Mass Spectrom.* **1988**, *23*, 816

[45] Hünig, S.; Märkl, G.; Sauer, J. *Einführung in die apparativen Methoden in der Organischen Chemie*, 2nd Edition, Würzburg, Regensburg, **1994**; Author collective, *Organikum*, 17th Edition, VEB Deutscher Verlag der Wissenschaften, Berlin, **1988**

IV. Transition metal complexes of some azamacrocycles and their use in molecular recognition[ω][φ]

1. Introduction

The field of coordination chemistry of polyazamacrocycles has undergone immense growth since the publication of seminal articles by *Curtis*[1] and *Thompson* and *Busch*[2] in the early 1960s. Especially two cyclic tetraamines have played a key role in this field, namely 1,4,7,10-tetraaza-cyclododecane ([12]aneN$_4$ or cyclen) and 1,4,8,11-tetraaza-cyclotetradecane ([14]aneN$_4$ or cyclam). The fit between the size of the metal ion and the cavity provided by the macrocycle is crucial for the design of metal complexes. On complexation with transition metals, the stereo-electronic requirements must also be taken into account[3-4]. As the cavity of the 12-membered cyclen is smaller than that of 14-membered cyclam, the macrocycle tends to fold around metal ions with octahedral coordination geometry adopting a *cis* conformation[4-6]. In general, tetraazamacrocycles exhibit high basicity in the first two protonation steps and rather low basicity in the last two steps. The critical protonation constants (log K^H_i) for cyclen and cyclam and stability constants (log $K_{M_mH_hL_l}$) of their complexes with several metal ions are reported in **Table 1**.

Table 1. Protonation constants (log K^H_i) for cyclen and cyclam and stability constants (log $K_{M_mH_hL_l}$) of their complexes with selected metal ions. T = 25 °C.

Ion	Equilibrium constant	Cyclam	Cyclen
H$^+$	[HL]/[L] x [H]	11.58,[a] 11.3[b]	10.97[h]
	[H$_2$L]/[HL] x [H]	10.62,[a] 10.23[b]	9.87[h]
	[H$_3$L]/[H$_2$L] x [H]	1.61,[a] 1.43[b]	1.6[i]
	[H$_4$L]/[H$_3$L] x [H]	2.42,[a] 2.27[b]	0.8[i]
	[H$_4$L]/[L] x [H]^4	26.23,[a] 25.23[b]	23.24[h,i]
Ni^{2+}	[ML]/[M] x [L]	22.2,[c] 20.1[d]	16.4[j]
Cu^{2+}	[ML]/[M] x [L]	26.5,[b] 27.2[e]	23.29,[b] 24.8[e]
Zn^{2+}	[ML]/[M] x [L]	15.0,[e] 15.5[f]	16.2[f]
	[ML(H$_2$O)]/[ML(OH)] x [H]	9.77[g]	8.02[g]

Cd^{2+}	[ML]/[M] x [L]	11.23[b]	14.3[f]
Pb^{2+}	[ML]/[M] x [L]	10.83[b]	15.9[f]
Co^{2+}	[ML]/[M] x [L]	12.7[i]	
Hg^{2+}	[ML]/[M] x [L]	23.0[k]	25.5[k]

[a] I = 0.5 mol dm^{-3} KNO_3 [7]; [b] I = 0.1 mol dm^{-3} $NaNO_3$[8]; [c] I = 0.1 mol dm^{-3} NaOH[9]; [d] I = 0.5 mol dm^{-3} NaCl[10]; [e] I = 0.2 mol dm^{-3} KNO_3[11,12]; [f] I = 0.2 mol dm^{-3} $NaClO_4$[13]; [g] I = 0.2 mol dm^{-3} KNO_3[14]; [h] I = 0.5 mol dm^{-3} KNO_3[15]; [i] I = 0.2 mol dm^{-3} $NaClO_4$[16]; [j] I = 0.1 mol dm^{-3} $NaNO_3$[17]; [k] I = 0.2 mol dm^{-3} KNO_3[18]

In this review the role of metal complexes of 1,4,7-triaza-cyclononane ([9]aneN$_3$ or TACN), 1,5,9-triaza-cyclododecane ([12]aneN$_3$), 1,4,7,10-tetraaza-cyclododecane ([12]aneN$_4$ or cyclen) and 1,4,8,11-tetraaza-cyclotetradecane ([14]aneN$_4$ or cyclam) as molecular binding sites is discussed (**Fig. 1**). Many metal complexes of azamacrocycles have in addition to the azamacrocycle ligand additional reversibly coordinated ligands. Their binding and exchange can be used in molecular recognition, if reversible and rapid. In the following review we discuss the current literature available for such binding situations. Reported X-ray structure analyses of TACN, cyclen and cyclam metal complexes which coordinate additional ligands and the literature on solution studies involving coordination to [9]aneN$_3$, [12]aneN$_3$, cyclen and cyclam are summarized and discussed.

Fig. 1. The parent structure [9]aneN$_3$, [12]aneN$_3$, cyclen and cyclam.

1
[9]aneN$_3$

2
[12]aneN$_3$

3
[12]aneN$_4$
cyclen

4
[14]aneN$_4$
cyclam
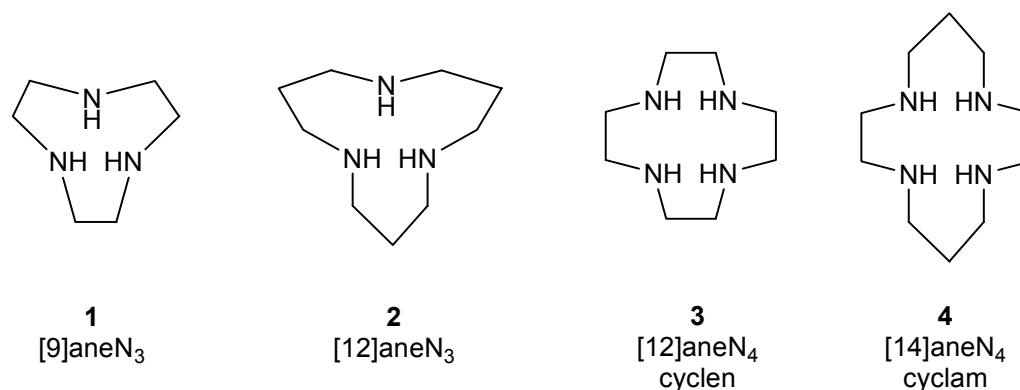
In order to be considered, the parent structure needs to complex a metal, thereby coordinating to all nitrogens (3 in the case of [9]aneN$_3$ and 4 in the case of [12]aneN$_4$ and [14]aneN$_4$) in the azamacrocycle. Alkyl, phenyl and aryl substitution at any position (carbon or nitrogen substitution) is allowed provided such substitution does not affect the geometry of the parent structure nor introduce additional ligands which

coordinate to the metal and thus induce a change in the coordination geometry. Such metal complexes needed to undergo an intermolecular coordination with another molecule. Only metal coordination to halogens, sulfates, perchlorates, cyanides, isothiocyanides, azides, nitrates, nitrites, carbonates and solvent molecules (DMF, DMSO, H_2O) are excluded. In general the guest molecule should be an organic entity which can coordinate to the host, ideally under physiological conditions.

2. Structures of 1,4,7,10-tetraaza-cyclododecane ([12]aneN$_4$ or cyclen) complexes in solid state

2.1. Co(III) complexes

[Co(cyclen)-(X)Y]$^{n+}$ species exhibit exclusive *cis* stereochemistry, but exist as various isomeric forms depending on the orientation (*syn* or *anti*) of the *sec*-NH protons at the two equatorial sites[19]. The X-ray structure analysis of [Co(cyclen)(O$_2$C$_2$O$_2$)]$^+$ (**Fig. 2**) shows the oxalate coordinated with a *cis* stereochemistry with the Co(III) atom adopting a distorted octahedral geometry which is typical for Co(III) cyclen complexes[20-23]. Similar complexes such as [Co(cyclen)-(O$_2$CCH$_2$CO$_2$)]$^+$ [19], show the same geometry.

Fig. 2. Structure of *syn,anti*-[Co(cyclen)(O$_2$C$_2$O$_2$)]$^+$ in the crystal. Thermal ellipsoids are drawn at the 50 % probability level.
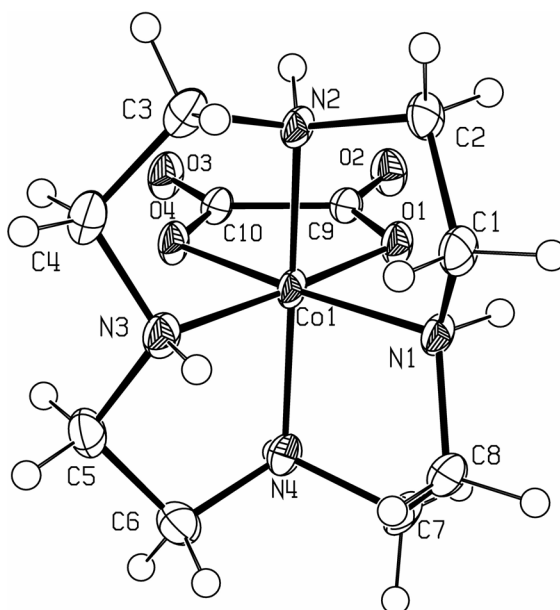
On coordination with a monodentate ligand such as a phosphite anion, Co(III) cyclen maintains its octahedral geometry by also coordinating a water molecule (**Fig. 3**)[24].

Fig. 3. Structure of *syn*(OP(H)(O)$_2$),*anti*(OH$_2$)-[Co(cyclen)(OH$_2$){OP(H)(O)$_2$}]$^+$ in the solid state. Thermal ellipsoids are drawn at the 50 % probability level.
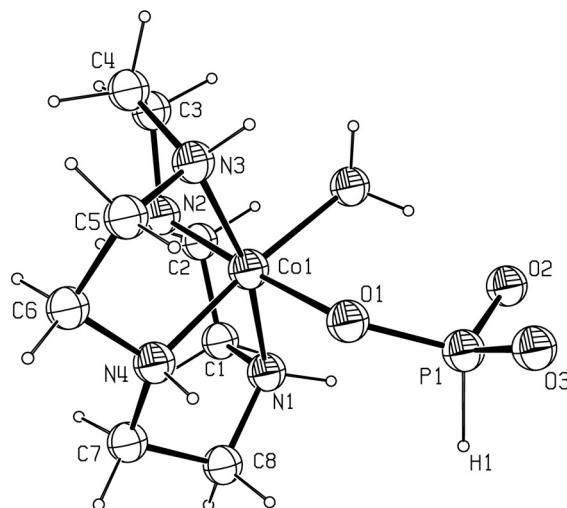
Co(III) complexes of cyclen also coordinate diamines, such as ethylenediamine, 2-(aminomethyl)pyridine, (*R*)-1,2-propanediamine, (*R*,*R*)-1,2,-diaminocyclohexane, trimethylenediamine or 2-methyl-1,3-diaminopropane[25,26]. In addition the coordination of amino acids such alanine to Co(III) complexes have been reported[20,27]. The X-ray structure of the Co(III) complex of (2R,5R,8R,11R)-2,5,8,11-tetraethyl-1,4,7,10-tetraaza-cyclododecane bound to (S)-alanine is shown in **Fig. 4**. The macrocycle coordinated in a folded manner leaves space available for the coordination of the bidentate ligand. The stereochemistry of the amino acid is maintained upon coordination to Co(III) ion[28].

Fig. 4. The crystal structure of the Co(III) complex of (2R,5R,8R,11R)-2,5,8,11-tetraethyl-1,4,7,10-tetraaza-cyclododecane bound to (S)-alanine.
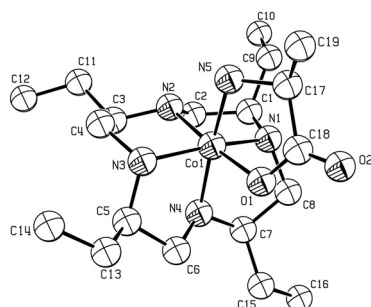
2.2 Cu(II) complexes

Several structures of Cu(II) complexes of cyclen have been reported[29,30]. X-ray analyses show that copper is coordinated in a square pyramidal geometry with the four nitrogens of cyclen[31]. However no relevant molecular recognition of such complexes has been reported.

2.3 Ni(II) complexes

Ni(II) cyclen complexes have an octahedral coordination sphere by coordinating two water molecules in a *cis* orientation that only slowly exchange with other ligands[32,33]. An N-methylated Ni(II) cyclen derivative leads to the $[Ni_2(Me_2\text{-cyclen})_2ox]^{2+}$ binuclear cation (where ox = oxalate anion)[34]. The oxalate dianion acts a tetradentate bridging ligand between two Ni(II) cyclen complexes.

A Ni(II) cyclen complex containing imidazole has also been reported. The X-ray structure analysis shows the Ni(II) ion in a distorted octahedral coordination geometry consisting of four nitrogen atoms from cyclen as donor atoms, one nitrogen atom from the imidazole and one oxygen atom from one of the perchlorate ions[35]. The same distorted octahedral geometry is also illustrated in the following example where a Ni(II) cyclen complex binds an acetate anion (**Fig. 5**)[36].

Fig. 5. Structure of $[Ni(cyclen)(\eta^2\text{-}CH_3CO_2)]^+$ cation in the solid state. Hydrogen atoms are omitted for clarity. Probability ellipsoids are 30%.
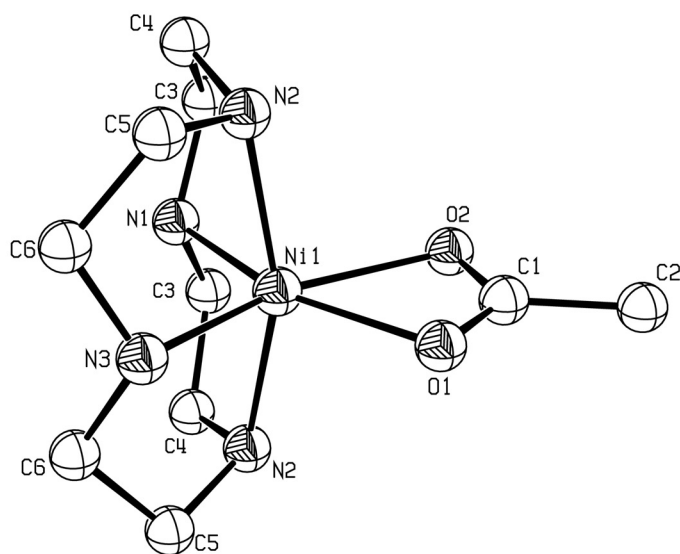
Ni(II) cyclen complexes also coordinate phenanthroline (phen) (**Fig. 6**)[37] and 7,7,8,8-tetracyanoquino-dimethane (TCNQ)[30] as additional ligands giving distorted octahedral coordination geometry consisting of four nitrogen atoms from cyclen and two nitrogens atoms from the heteroaromatic ligand.

Fig. 6. Molecular structure of [Ni(cyclen)(phen)](ClO$_4$)$_2$.
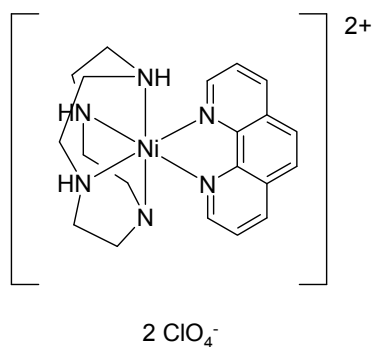
2.4 Zn(II) complexes

Zn(II) cyclen complexes interact with uridine (U) and thymidine (T) nucleotides by specific Zn(II)-imide N$^-$ coordination (**Fig. 7**)[38]. Additional stabilization of this structure by hydrogen bonds between amine N-H of the cyclen ligand and the carbonyl groups of the heterocycle have been proposed, but solid evidence is missing.

Fig. 7. Zn(II) cyclen complexes selectively coordinate the imide group in nucleosides, such as 3'-azido-3'-deoxythymidine (AZT).
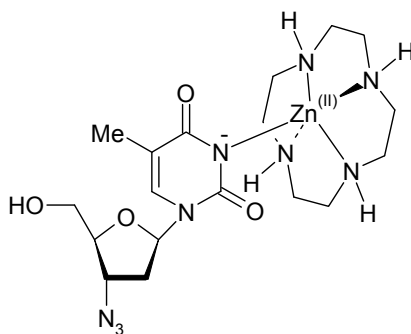
The X-ray structure analysis of [Zn(cyclen)(AZT)](ClO$_4$)·2H$_2$O reveals a distorted square pyramidal N$_5$-coordination geometry for the Zn(II) ion (**Fig. 8**)[38].

Fig. 8. Structure of [Zn(cyclen)(AZT)](ClO$_4$)·2H$_2$O, (AZT = 3'-azido-3'-deoxythymidine) in the crystal. A perchlorate anion and two water molecules are omitted for clarity (ellipsoids are 50%).
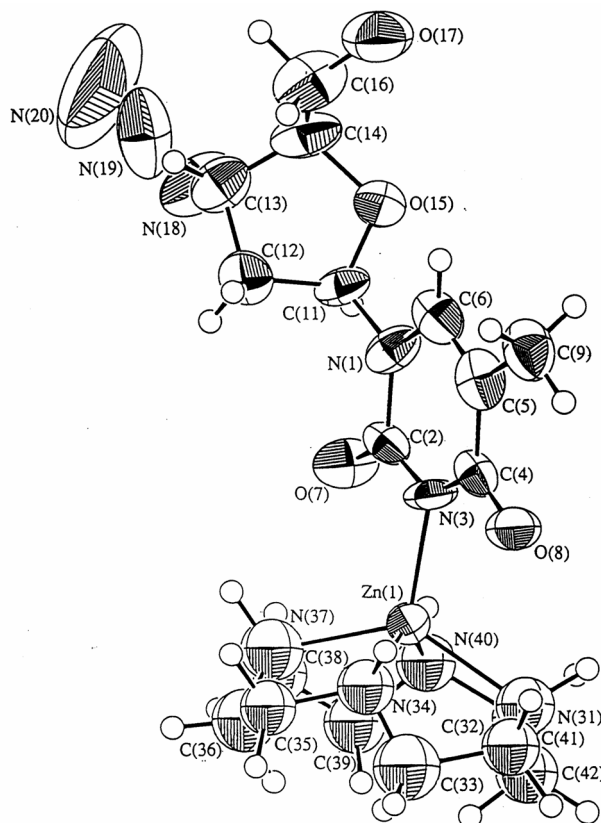
A further example for such an imide recognition repetitiving the distorted square pyramidal geometry is the coordination of the important metabolite creatinine to the Zn(II) cyclen[39]. In general the binding affinity of imides correlates with the decreasing of the pk$_a$ value of the imide nitrogen.

Zn(II) cyclen complexes coordinated with phosphate anions as additional ligands have been described and characterized by X-ray analysis (**Fig. 9**)[40]. The *para*-nitro phenyl ester of phosphate (NPP^{2-}) forms a complex with three Zn(II) cyclen moieties. The three oxygen atoms of the phosphate anion act as the fifth ligand for the Zn(II) ions coordinated by the cyclen ligand.

Fig. 9. Structure of Zn(cyclen)]$_3$-NPP^{2-} in the solid state. All hydrogen atoms, perchlorate anions and water molecules are omitted for clarity. Probability ellipsoids are 30%.
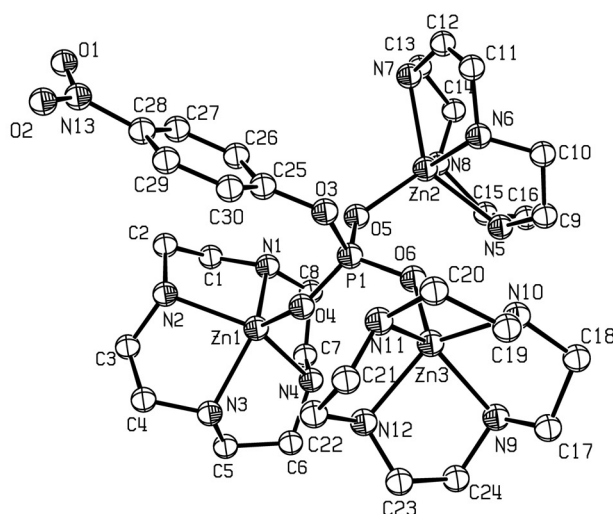
An imidazolate anion can act as a bridging ligand for two Zn(II) cyclen units. The X-ray structure analysis (**Fig. 10**) shows the two Zn(II) ions with distorted square pyramidal coordination geometry composed of four nitrogen atoms from cyclen ligand and one nitrogen atom from the bridging imidazolate ion[35].

Fig. 10. Structure of [Zn(cyclen)]$_2$-im (im = imidazolate) in the solid state.
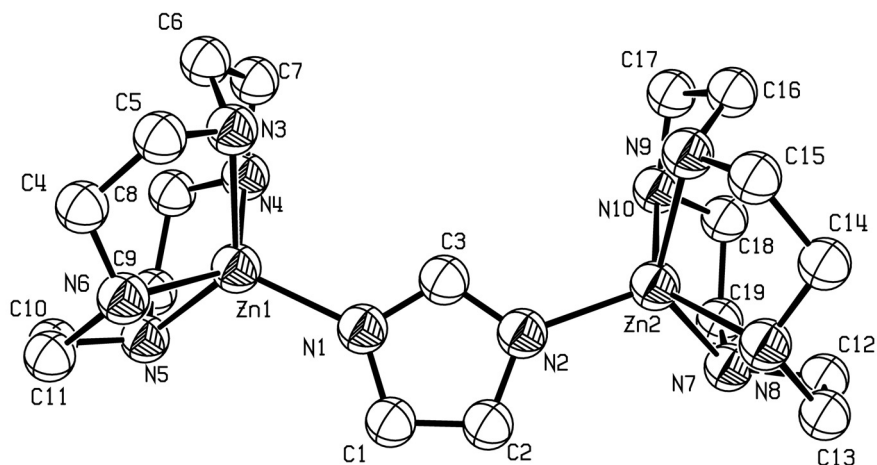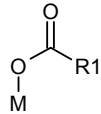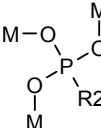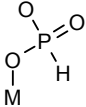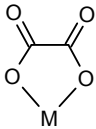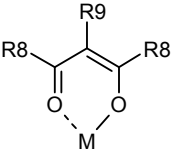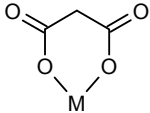
Bis-Zn(II) cyclen complexes coordinate barbital[41] as well as thymidine and uridine nucleosides, such as thymidine 5'-monophosphate (5'-dTMP)[42]. The aggregates have a 2:2 stoichiometry and consist of a macrocyclic arrangement. Tris-Zn(II) cyclen variations have also been reported to coordinate organic phosphate dianions[40].

3. Structures of 1,4,7,10-tetraaza-cyclododecane([12]aneN$_4$ or cyclen) complexes in solid state (tabulated)

Table 2 summarizes all X-ray structures registered at the Cambridge Crystallographic Database according to the selection criteria previously mentioned.

Table 2. Structurally characterized metal complexes of 1,4,7,10-tetraaza-cyclododecane ([12ane]N$_4$ or cyclen) with additional ligand coordinated to the metal ion in solid state.

Structure of the additional ligand	Metal ions				
	Zn^{2+}	Ni^{2+}	Co^{3+}	Rh^{3+}	Ru^{2+}
(carboxylate structure)	(1)See ref. [43]				
(phosphate bridging structure)	(2)See ref. [40, 44]				
(phosphonate structure with H)			(3)See ref. [24]		
(oxalate structure)			(4)See ref. [19]		
(enolate structure R8, R9)		(5)See ref. [45]	(6)See ref. [46]		
(malonate structure)			(7)See ref. [19]		

(8)See ref.
[47]
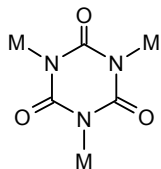
(9)See ref.
[48]
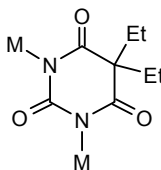
(10)See ref.
[49]
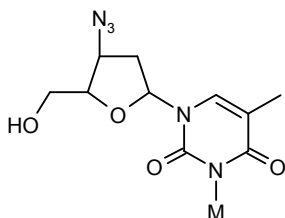
(11)See ref.
[38]
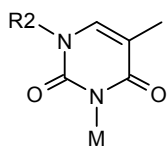
(12)See ref.
[50, 51]
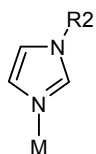
(13)See ref.   (14)See ref.
[35]   [35]
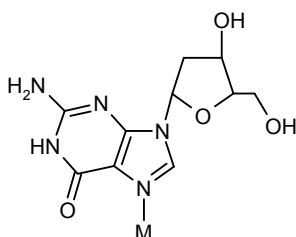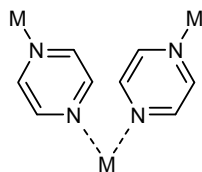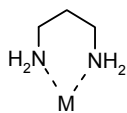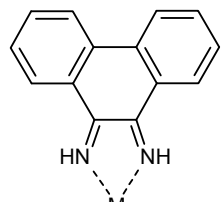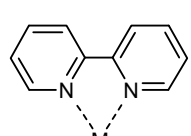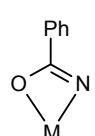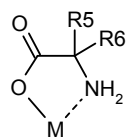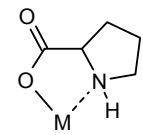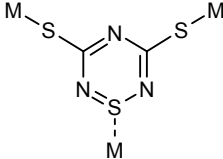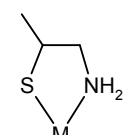
(15)See ref.
[50]

(16)See ref.
[52]

(17)See ref.
[26]

119
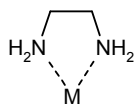
(18)See ref.
[26]

(19)See ref.
[53]

(20)See ref.
[37, 54]

(21)See ref.
[21]

(22)See ref.   (23)See ref.
[55]   [20,56-65]

(24)See ref.
[66]

(25)See ref.
[67]

(26)See ref.
[68]

(1) Substitution – n-aryl; R1 = aryl; (2) a) Substitution – none; R2 = *p*-nitrophenolate; (2) b) Substitution – n-alkyl; R2 = O; (3) Substitution – none; (4) Substitution – none; (5) Substitution – n-alkyl (cage); R8 = CH_3, R9 = H; (6) a) Substitution – none; R8 = CH_3, R9 = H; (6) b) Substitution – none; R8 = CH_3, R9 = Br; (7) Substitution – none; (8) Substitution – none; (9) Substitution – none; (10) Substitution – none; (11) Substitution – none; (12) Substitution – n-aryl; R2 = CH_3; (13) Substitution – none; R2 = metal; (14) Substitution – none; R2 = H; (15) Substitution – n-aryl; (16) Substitution – none; (17) Substitution – none; (18) Substitution – none; (19) Substitution – none; (20) Substitution – none; (21) Substitution – n-alkyl; (22) Substitution – n-alkyl; R5 = H, R6 = CH_3 (alanine); (23) a) Substitution – c-alkyl; R5 = H, R6 = CH_3 (alanine); (23) b) Substitution – c-alkyl; R5 = COOH, R6 = CH_3; (23) c) Substitution – c-alkyl; R5 = H, R6 = CH_2OH (serine); (23) d) Substitution – c-alkyl; R5 = CH_3, R6 = CH_2OH (methylserine); (23) e) Substitution – c-alkyl; R5 = H, R6 = H (glycine); (23) f) Substitution – c-alkyl; R5 = H, R6 = -$CH_2CH_2SCH_3$; (23) g) Substitution – c-alkyl; R5 = H, R6 = $CH(OH)CH_3$ (threonine); (23) h) Substitution – c-alkyl; R5 = CH_3, R6 = CH_2PhOH(methyltyrosine); (24) Substitution – none; (25) Substitution – none; (26) Substitution – none.

4. Molecular recognition of 1,4,7,10-tetraaza-cyclododecane ([12]aneN4 or cyclen) complexes in solution

4.1 Co(III) complexes

The optically active Co(III) complex of (2*R*,5*R*,8*R*,11*R*)-2,5,8,11-tetraethyl-1,4,7,10-tetraaza-cyclododecane was found to react with several neutral amino acids at pH 8 to form the corresponding amino acidato complexes[56]. The stereochemistry of the amino acid was retained on complexation with the macrocycle.

4.2 Cd(II) complexes

The Cd(II) complex of cyclen containing 7-amino-4-trifluoromethylcoumarin, **5** was designed as a fluorescent reporter[69]. Particular phosphate and citrate anions are bound by the metal complex, thus displacing the aromatic amino group of the coumarin and causing a change of the excitation spectrum (**Fig. 11**).

Fig. 11. Sensoric principle of phosphate ion sensing with **5**.

5 (M = Cd²⁺)
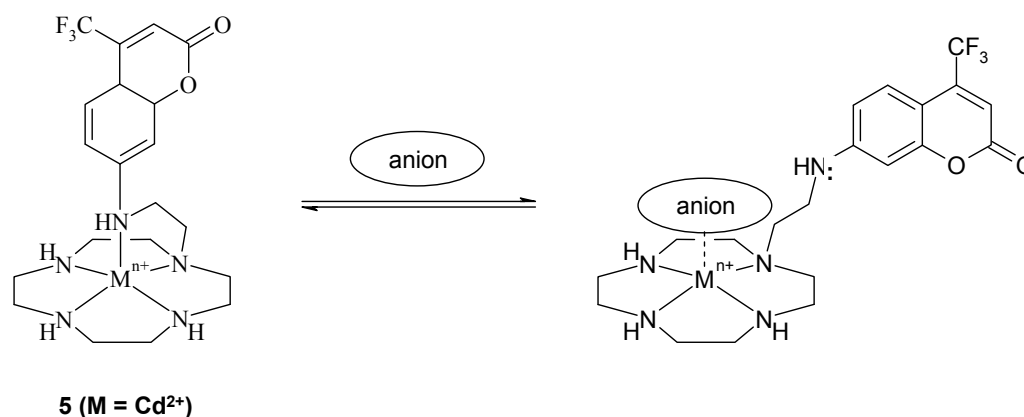
The metal complex detects pyrophosphate and citrate with high selectivity, whilst no response was shown for fluoride or perchlorate. Organic anions such as ATP and ADP also gave strong signals whilst cAMP showed little response (**Table 3**). The sensing mechanism was shown to be reversible.

Table 3. Apparent dissociation constants (K_d) of sensor **5** for anions in 100 mM HEPES Buffer (pH 7.4).

Anion	K_d (M)
Pyrophosphate	7.5×10^{-5}
Citrate	9.0×10^{-5}
Phosphate	1.5×10^{-2}
ATP	1.4×10^{-5}
ADP	2.6×10^{-5}
GMP	4.8×10^{-5}
AMP	4.4×10^{-4}
UMP	1.7×10^{-3}
UMP	1.7×10^{-3}
cAMP	*a*

a K_d is too large to be calculated.

4.3 Zn(II) complexes

The prevalence of Zn(II) ions in biological systems has led to a large number of Zn(II) complexes as models for such systems. A comprehensive review on the molecular interactions of Zn(II) cyclen and its derivatives was recently published[70]. On complexation with cyclen, the acidity of the Zn(II) ion is reinforced, which results in a lowering of the pK_a value of the Zn(II)-bound water from 9.0 to 7.9 at 25 °C[38]. Zn(II) cyclen also forms 1:1 complexes with deprotonated sulfonamides at neutral pH, despite the weak acidity of sulfonamides with pK_a values of 7-10 (**Fig. 12**)[71, 72].

Fig. 12. Reversible coordination of sulfonamide anions to Zn(II) cyclen.

6a (X = H_2O)
6b (X = OH^-)

7
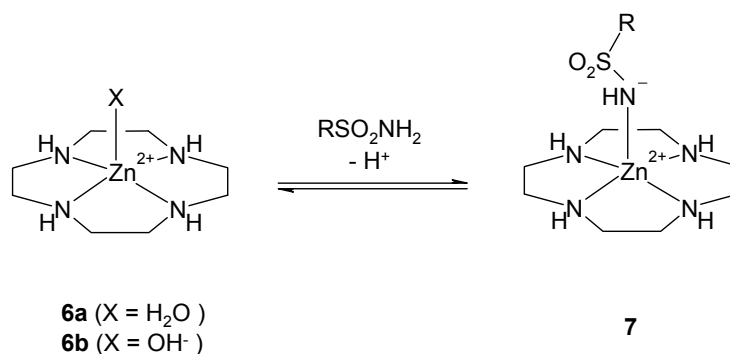
Following a similar principle Zn(II) cyclen complexes have been applied to the molecular recognition of nucleobases, thymine (dT) and uracil (U), which possess similarly weak acidic (pK$_a$ around 10) protons at their 'imide' groups[73]. The centrosymmetric linear arrangement of the three-point functional groups in **8** comprises the acidic Zn(II) acting to yield the 'imide' anion to form a stable Zn(II)-N(3)$^-$ bond and the two hydrogens attached to cyclen nitrogens to form two complementary hydrogen bonds with each of the 'imide' carbonyls. This specific Zn^{2+}-imide N$^-$ coordination allows the reversible coordination of flavin derivates, which are important cofactors of flavoproteins[74-76] and photolyases[77]. These electronic and structural fittings also permit formation of extremely strong 1:1 complexes of **8** with dT, AZT, U, Ff (5-fulorouracil) and riboflavin (**Fig. 13**). Zn(II) cyclen complexes appended with polyaromatic rings were shown to selectively bind to T- or U-rich sequences in double stranded DNA (or RNA) to denature them[50,78]. It does not interact with the other DNA nucleosides (i.e. dG, dA and dC), making the reversible coordination highly selective.

UV radiation leads to the formation of photolesions in DNA, which compromise the genetic information and can induce cell death or skin cancer. Especially dimeric Zn(II) cyclen complexes containing xylyl spacers inhibit efficiently photo[2+2]cycloaddition of thymidilyl(3′-5′)thymidine (d(TpT)) and promote the photosplitting of the corresponding photoproduct *cis-syn*-cyclobutane thymine dimer (T[c,s]T)[77,78].

Fig. 13. Zn(II) cyclen complex coordination to molecules bearing acidic imide groups.
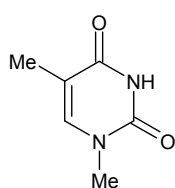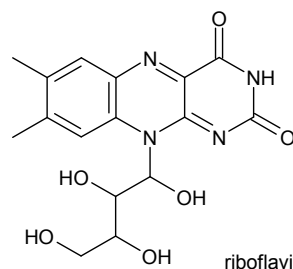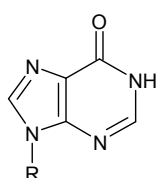
Zn(II) cyclen complexes reversibly coordinate phosphate dianions such as HPO_4^{2-}, phenyl phosphate (PP^{2-}) and 4-nitrophenyl phosphate (NPP^{2-}) as monodentate ligands to yield 1:1 complexes **9** in solution (**Fig. 14**). The observed binding affinities in neutral aqueous solution are in the millimolar range. Furthermore metal cyclen complexes added with fluorescent ligands are used for sensing anions by twisted intramolecular charge transfer (TICT)[79].

Fig. 14. Zn(II) cyclen coordinating monodentate phosphate dianions.

9a : R^1 = H, R^2 = ⟨benzene⟩–NO_2

9b : R^1 = H, R^2 = ⟨benzene⟩
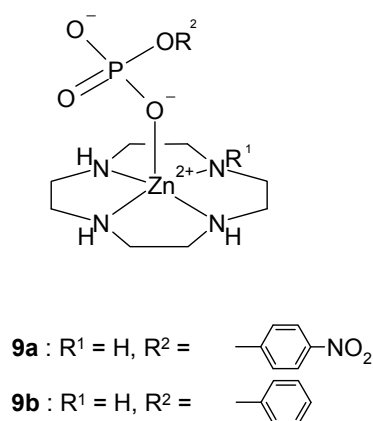
The dianions of phosphate monoesters, RPO_3^{2-} are potential bidentate donors and bridge two Zn(II) ions (**Fig. 15**). A bis-Zn(II) cyclen complex linked with a *meta*-xylene spacer forms a stable complex with NPP^{2-} with log K_s of 4.0 in aqueous solution (I = 0.1 $NaClO_4$ at 25 °C)[41].

Fig. 15. Bis-Zn(II) cyclen complexes bind phosphate monoesters in a bidentate fashion.

10
$Zn_2L^3(H_2O)_2$
meta-xylyl-bis(Zn^{2+}-cyclen)

11
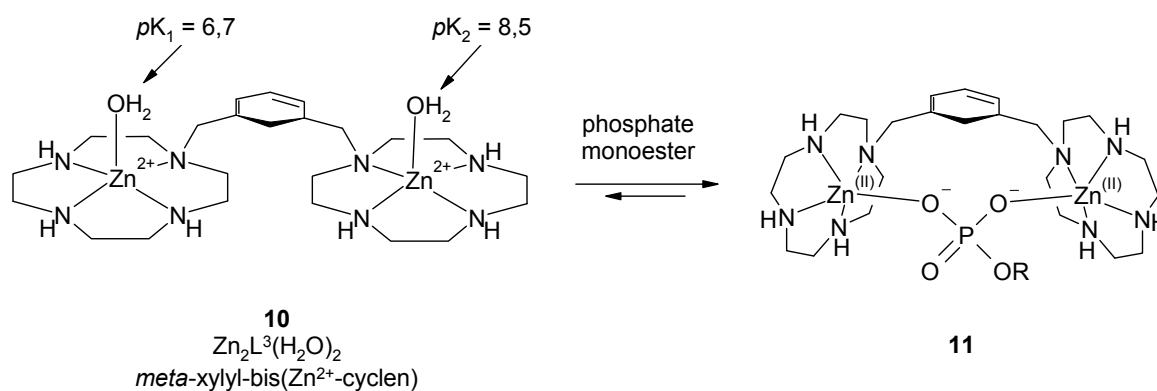
Fig. 16. The C_3-symmetric tris-Zn(II) cyclen complex **12**.

12
$Zn_3L^5(H_2O)_3$
$tris(Zn^{2+}\text{-cyclen})$
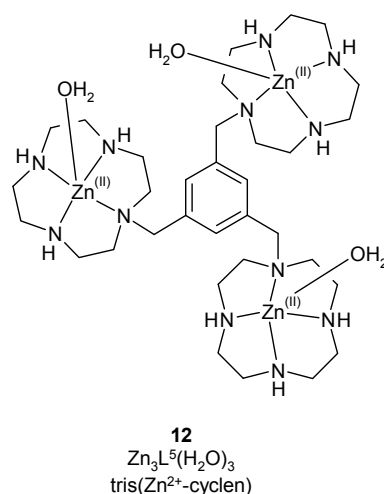
A yet higher binding constant could be achieved for tris-Zn(II) cyclen complexes (**Fig. 16**)[40]. A summary of the phosphate affinity constants of Zn(II) cyclen, bis-Zn(II) cyclen and tris-Zn(II) cyclen is shown in **Table 4**.

Table 4. Phosphate (phosphonate) affinity constants (log K_s)[2] of Zn(II) cyclen **9**, *m*-bis(Zn(II) cyclen) **10** and tris(Zn(II) cyclen) **12**, for NPP⁻, PP²⁻, phenyl phosphonate (PhP²⁻), and α-D-glucose 1-phosphate (α-Glu-P²⁻) at 25 °C and I = 0.10 (NaNO₃)[80].

Phosphate (phosphonate)	(pK_2'[b])	Log K_s[a]		
		9	**10**	**12**
NPP^{2-}	(5.2)	3.1	4.0	5.8
PP^{2-}	(5.9)	3.5	4.6	6.6
$\alpha\text{-Glu-P}^{2-}$	(6.1)			7.0
PhP^{2-}	(7.0)			7.9

[a]K_s = [ZnL^1-RPO$_3^{2-}$ complex] / [ZnL^1][RPO$_3^{2-}$] (M^{-1}) for **9**, [Zn$_2$L^3-RPO$_3^{2-}$ complex] / [Zn$_2$L^3][RPO$_3^{2-}$] (M^{-1}) for **10**, or [Zn$_3$L^5-RPO$_3^{2-}$ complex] / [Zn$_3$L^5][RPO$_3^{2-}$] (M^{-1}) for **12**.

[b]K_2' = - log ([RPO$_3^{2-}$]a_H + / [RPO$_3$H⁻]) obtained by pH titration at 25 °C with I = 0.10 (NaNO₃).

The bis-[Zn(II) cyclen] complexes **10** and **14** (**Fig. 17** and **18**) can bind imide-containing nucleotides. **Table 5** compares the apparent complexation constants of **13**, **10** and **14**[80]. Recent investigations have shown a dramatical acceleration of plasmid DNA cleavage by derivatives of bis[Zn(II) cyclen] complexes[81].

Fig. 17. Zn(II) benzylcyclen **13** and *p*-xylyl-bis-[Zn(II) cyclen] **14**.

13
ZnL(H$_2$O)
Zn^{2+}-benzylcyclen

14
Zn$_2$L^4(H$_2$O)$_2$
para-xylyl-bis(Zn^{2+}-cyclen)
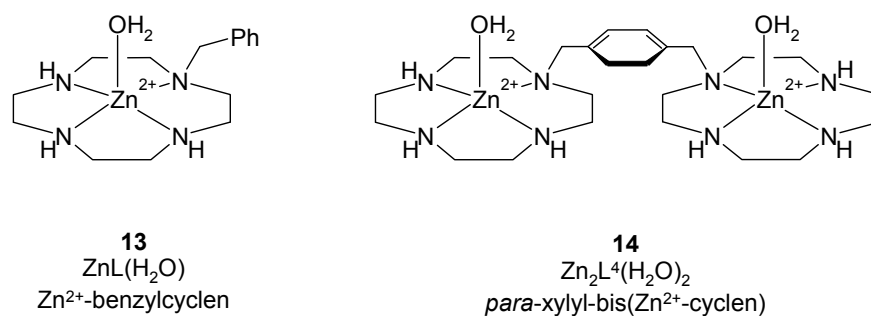
Fig. 18. The binding of **14** to 5'-dTMP and 5'-dTDP respectively, showing the NOE interactions.

NOE 1%

14-(5'-dTMP) complex

NOE 2%

14-(5'-dTDP) complex
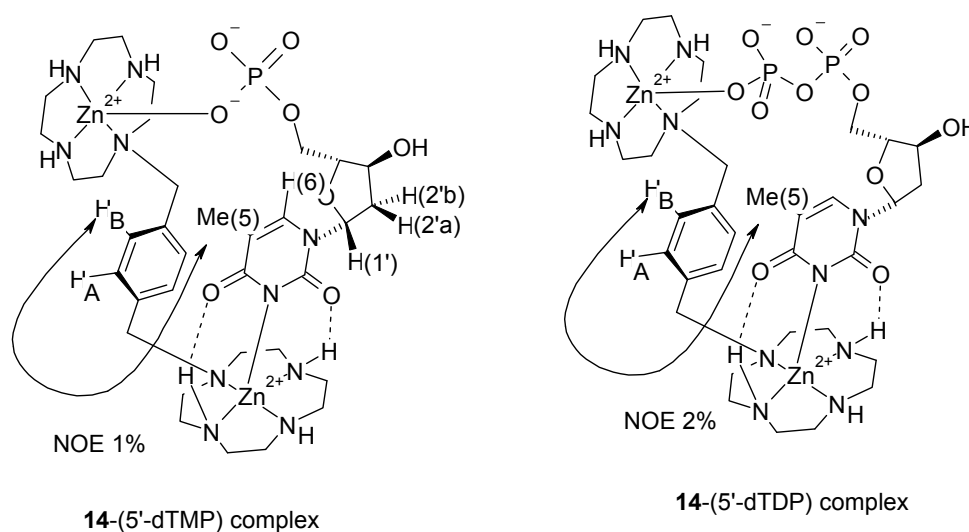
Table 5. Apparent complexation constants (log K_{app}) for imide-containing nucleotides with Zn(II) cyclen complexes at pH 7.6 and 25 °C.

	13	10	14
dT	3.2[a] (5.7)[d]	3.2, 3.2[b]	
	3.4[c]	(**10**:dT = 1:2)	
c-dTMP	3.3[c]	3.5, 3.5[b]	
		(**10**:c-dTMP = 1:2)	
5'-CMP	3.3[a] (3.7)[d]	3.2[a] (4.3)[d]	
	3.3[b]	3.4[b]	
3'-dTMP		5.2[a] (8.6)[d]	5.9[a] (8.9)[d]
		5.3[b]	5.8[b,e]

		$5.4^{c,f}$	$5.8^{c,f}$
5'-dTMP	$3.4, 3.4^b$	5.5^a $(9.3)^d$	6.4^a $(9.6)^d$
	(**13**:5'-dTMP = 2:1)	5.5^b	$> 6^{b,e}$
		$5.7^{c,f}$	$> 6^{c,f}$
2'-UMP		5.7^b	
3'-UMP		4.8^a $(7.8)^d$	5.5^a $(8.5)^d$
		$5.2^{c,f}$	$5.7^{c,f}$
5'-UMP		5.4^a $(8.3)^d$	6.2^a $(8.8)^d$
		$5.5^{c,f}$	$> 6^b$
			$> 6^{c,f}$
5'-dTDP		5.6^b	$> 6^b$
		$5.5^{c,f}$	$> 6^{c,f}$
5'-dTTP		5.0^b	5.6^b
5'-AZTMP		5.5^b	$> 6^{b,e}$
		$5.7^{c,f}$	$> 6^{c,f}$
5'-AZTDP		5.3^b	5.9^b
		5.5^c	$> 6^{c,f}$

[a] Determined by potentiometric pH titration.
[b] Determined by isothermal titration calorimetry (50 mM HEPES buffer).
[c] Determined by UV titration in 50 mM HEPES buffer with $I = 0.1$ (NaNO$_3$).
[d] For the intrinsic complexation constants K_s, see reference.
[e] Titrations were carried out at [5'-dTMP] = 0.2 mM and 0.1 mM and the average values were listed.
[f] Titrations were carried out at [nucleotide] = 0.1 mM and 50 μM and the average values were listed.

A recent publication has exposed a further approach of recognition with the tris-[Zn(II)cyclen] **12**[82]. The (Zn$_3$L^3)$_3$ forms a stable 1:1 complex with *cis,cis*-1,3,5-cyclohexanetriol triphosphate (CTP$_3$), a model compound for inositol 1,4,5-triphospate (IP$_3$) (**Fig. 19**). IP$_3$ is an important second messenger in the intracellular signaling pathway released by a phospholipase C (PLC), which induces an increase of Ca^{2+} concentrations in living cells. CTP$_3$ has a similar Ca^{2+}-releasing activity, but it is readily available. A luminescent chemical sensing system can be achieved by a ruthenium(II)-templated assembly of three molecules of a bis-[Zn(II)cyclen] complex containing a bipyridyl linker[82].

Fig. 19. 1:1 complex of tris-[Zn(II)cyclen] and CTP$_3$.

= Zn(II)cyclen
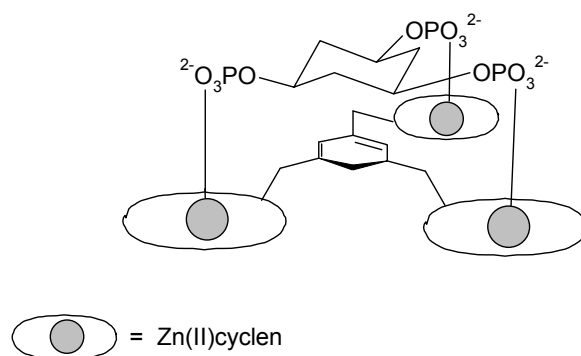
The search for small molecules that interact with RNA is currently attracting great interest for drug discovery in AIDS therapeutics[83]. The transcription of HIV-1 genome is facilitated by a HIV-1 regulatory protein Tat which activates the synthesis of full-length HIV-1 mRNA by its binding to a TAR (*trans*-activation responsive) element RNA[84]. The TAR element comprising the first 59 nucleotides of the HIV-1 primary transcript adopts a hairpin structure with a uracil (U)-rich bulge (UUU or UCU), which is the Tat binding site. Linear tris-[Zn(II) cyclen] complexes inhibit HIV-1 TAR RNA-Tat peptide binding due to its strong binding to the UUU bulge[83,85]. **Fig. 20** shows the coordination of dT$^-$ pdT$^-$ pdT$^-$ with a linear tris-[Zn(II) cyclen] complex **15**.

Fig. 20. The binding of tris-[Zn(cyclen)] **15** to dT$^-$pdT$^-$pdT$^-$.

dT$^-$pdT$^-$pdT$^-$ - **15** complex
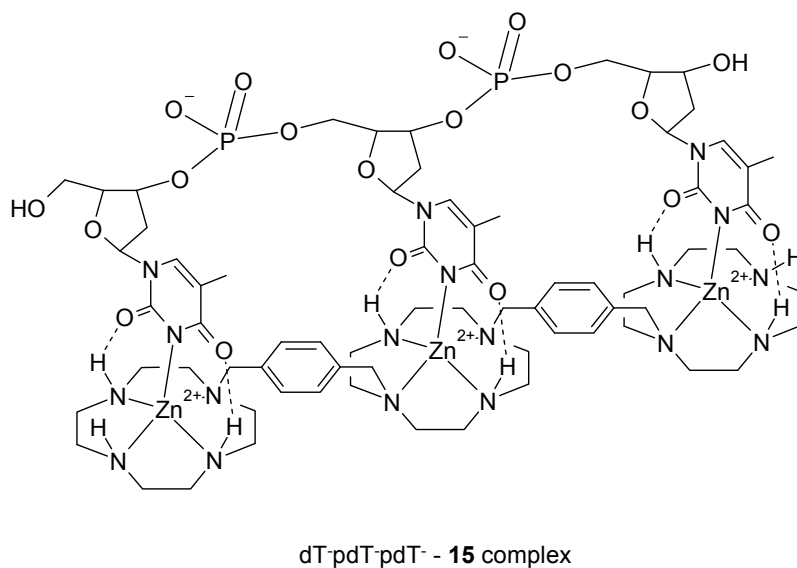
5. Immobilized 1,4,7,10-tetraaza-cyclododecane ([12]aneN4 or cyclen) complexes in solid state

Zn(II) complexes

Zn(II) cyclen complexes have been bound to polymers and used to extract riboflavin from aqueous solutions. The reversible recognition of Zn(II) cyclen complexes to flavin imide moieties allowed the quantitative and selective extraction (and release from the polymer) of vitamin B2 (riboflavin) from a mixture of compounds at physiological pH (**Fig. 21**)[86].

Fig. 21. Binding equilibrium of Zn(II) cyclen polymer with riboflavin (R = ribityl) or its tetraacetate [R = $CH_2CH(OAc)CH(OAc)CH(OAc)CH_2OAc$].
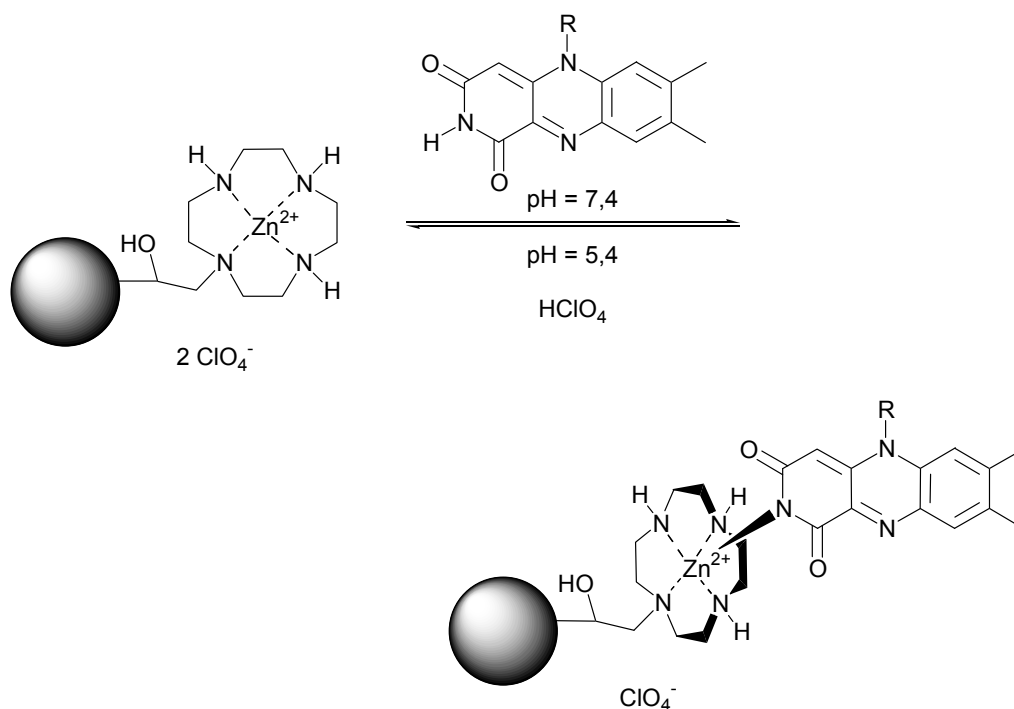
A molecular imprinted polymer (MIP) from polymerizable Zn(II) cyclen complexes and ethylene glycol dimethyl acrylate has been prepared[39]. Creatinine was used as the template molecule which was reversibly coordinated to the Zn(II) complex (**Fig. 22**). The imprinted polymer reverses the binding selectivity of Zn(II) cyclen for creatinine and thymine from 1:34 in homogenous solution to 3.5:1 in the MIP.

Fig. 22. Preparation of a stoichiometric template Zn(II) cyclen-creatinine monomer salt and copolymerization of **17** with ethylene glycol dimethyl acrylate (EDGMA).
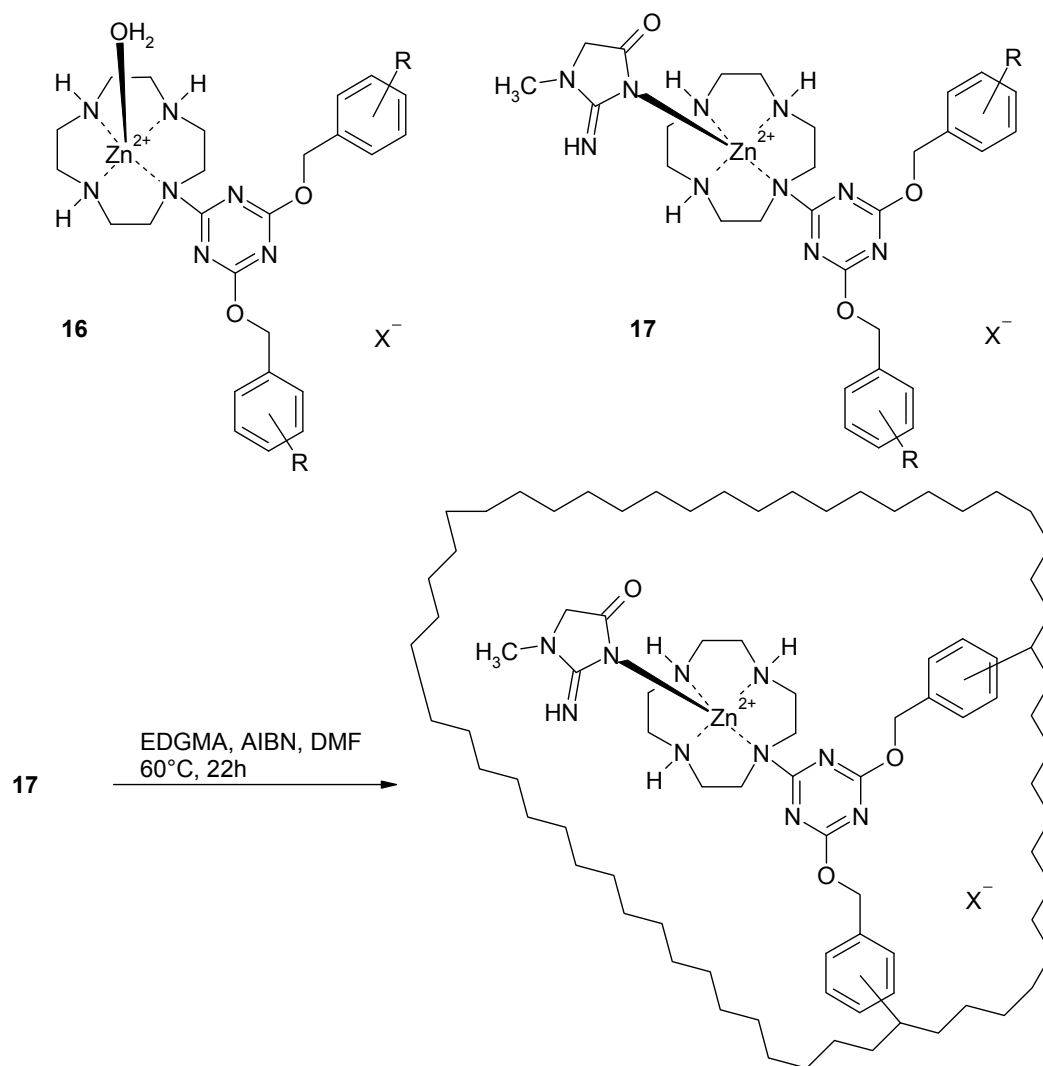
A similar MIP polymer was prepared for the selective recognition and separation of phosphates[87]. Here again a polymerizable Zn(II) cyclen complex (ZnL^2) was copolymerized with ethylene glycol dimethyl acrylate. The polymer interacts selectively with phosphomonoester dianions such as deoxyadenosine 5'-monophosphate (5'-dAMP) and 4-nitrophenyl phosphate (4-NPP) over deoxyadenosine (dA) and adenosine 3',5'-cyclic-monophosphate (3',5'-cAMP). The apparent complexation constants for the 1:1 complex of ZnL^2 on the MIP and 5'dAMP and 4-NPP, log K_{app}(ZnL-S^{2-}) (S^{2-} = phosphomonoester dianion), at pH 7.0 and 25 °C were determined as 4.1.

6. Structures of 1,4,8,11-tetraaza-cyclotetradecane ([14]aneN4 or cyclam) complexes in solid state

6.1 Zn(II) complexes

Zn(II) cyclam complexes can coordinate carboxylates as additional ligand. The X-ray structure of a Zn_2-xylyl-bicyclam with an acetate anion is shown (**Fig. 23**)[88]. Both cyclam units adopt the *cis*-V configuration (according to the nomenclature of *Bosnich*[89]) with chelation by acetate on one cyclam face and twofold H-bonding on the other.

Fig. 23. X-ray crystal structure of $[Zn_2$-xylyl-bicyclam$(OAc)_2](OAc)_2 \cdot 2CH_3OH$. CH_3OH is not shown for clarity.
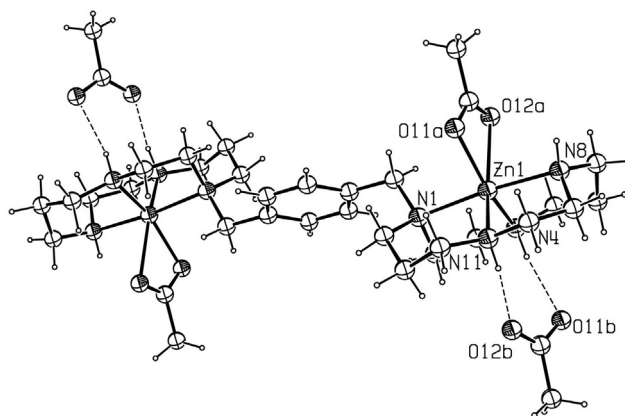
The Zn(II) complex of 1,4,8,11-tetraazacyclotridecane-5-one, a closely related cyclam derivative, can coordinate glycine by glycine amine-Zn(II) coordination[90]. The X-ray structure (**Fig. 24**) shows a distorted square pyramidal geometry. The Zn atom has an irregular five-coordinate geometry, with the donors being three nitrogen atoms and one oxygen atom from the azamacrocycle and one coordinated chloride.
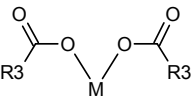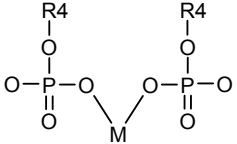
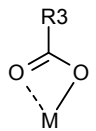**Fig. 24.** Structure of Zn(II) complex of 1,4,8,11-tetraazacyclotridecane-5-one in the crystal.
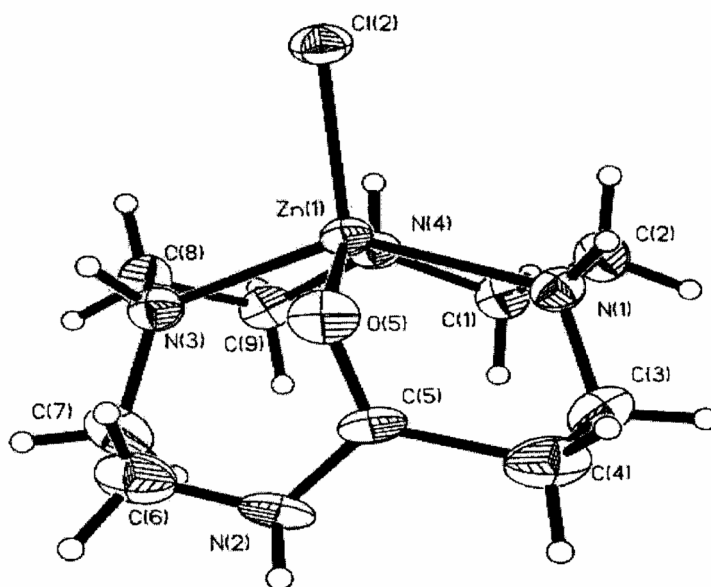
6.2 Ni(II) complexes

Cyclam forms compared to zinc the thermodynamically and kinetically more stable complexes with copper and nickel, where the cyclic amine is arranged in a strain-free conformation with the metal atom located in the plane defined by the four nitrogen atoms of the cyclam[4-6]. There is some evidence that Ni(II)-cyclam can bind benzoates and that the metal free cyclams preorganize the ligands. The X-ray structure (**Fig. 25**) of Ni(*O*-benzoato)$_2$(cyclam) quite closely parallels that of nickel free (4-*t*-butylbenzoato)$_2$(cyclamH$_2$). The X-ray structure of the Ni(II) cyclam distinctly shows that a Ni-O bond is formed in the case of Ni(*O*-benzoato)$_2$(cyclam).

Fig. 25. Structure of (4-*t*-butylbenzoato)$_2$(cyclamH$_2$) and Ni(*O*-benzoato)$_2$(cyclam) respectively, in the solid state.
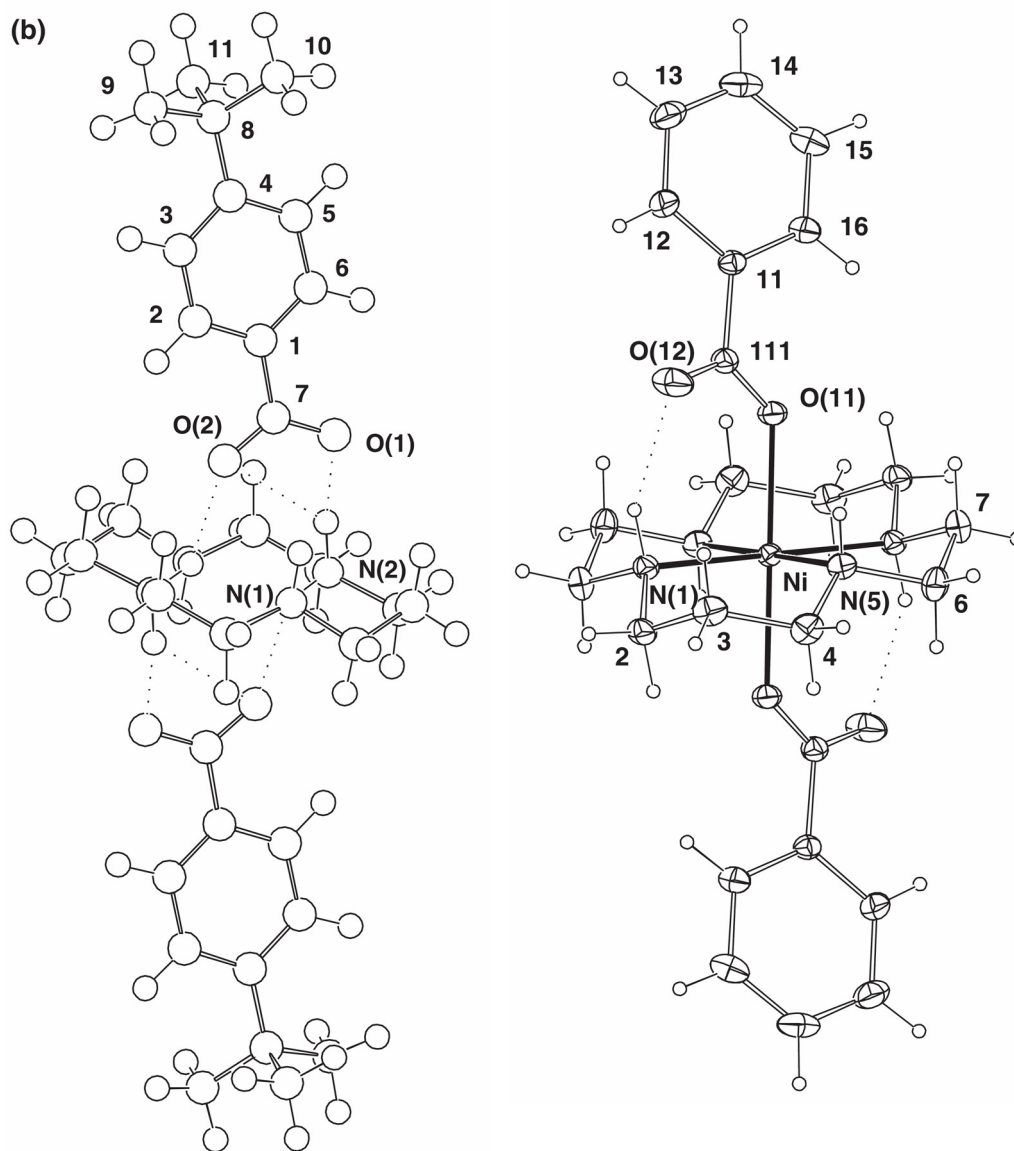
Similar geometries were found for the corresponding Cu(II) complexes. However in the case of copper, the two carboxylate anions remain hydrogen bound to the (coordinated) cyclam ligand, and do not take part in the metal's inner coordination sphere and no Cu-O bond is formed[91].

The Ni(II) complex of 1,4,7,10-tetraazacyclododecane-2,9-dione coordinates the dipeptide glycine-glycine[92]. The X-ray structure of $[Ni(DOTA)_2](ClO_4)_2$ (**Fig. 26**) shows a octahedral coordination geometry. The Ni(II) has a regular six-coordinate geometry, with the donors being four nitrogen atoms and two oxygen atoms from two macrocyclic ligands.
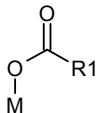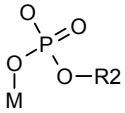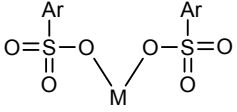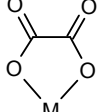
Fig. 26. Structure of Ni(II) complex of 1,4,7,10-tetraazacyclododecane-2,9-dione) in the crystal.
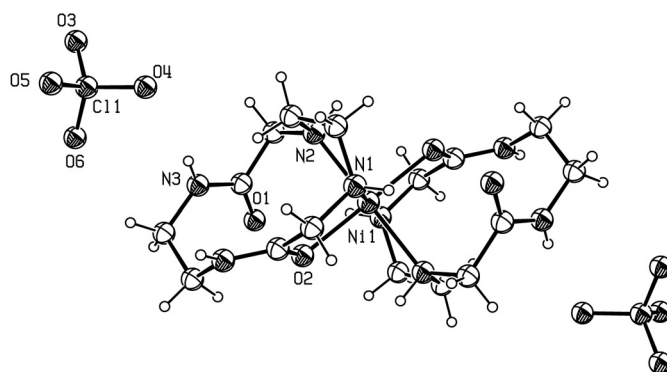
7. Structure of 1,4,8,11-tetraaza-cyclotetradecane ([14]aneN$_4$ or cyclam) complexes in solid state (tabulated)

Table 6 summarizes all X-ray structures registered at the Cambridge Crystallographic Database according to the selection criteria previously mentioned.

Table 6. Structurally characterized metal complexes of 1,4,8,11-tetraaza-cyclotetradecane ([14ane]N_4 or cyclam) with additional ligand coordinated to the metal ion in solid state.

Structure of the additional ligand	Metal ions									
	Ga^{3+}	Zn^{2+}	Cd^{2+}	Cu^{2+}	Ni^{2+}	Co^{3+}	Fe^{2+}	Ru^{2+}	Mn^{3+}	Cr^{3+}
(carboxylate, R1)					(1)See ref. [93]					
(phosphate, O—R2)	(2)See ref. [94, 95]			(3)See ref. [94, 95]		(4)See ref. [96]				
(dicarboxylate, R3)		(5)See ref. [97-99]		(6)See ref. [93, 100]	(7)See ref. [91, 101-106]				(8)See ref. [107]	
(diphosphonate, R4)					(9)See ref. [108]					
(disulfonate, Ar)			(10)See ref. [109]	(11)See ref. [110]	(12)See ref. [111]					
(oxalate)					(13)See ref. [112]					(14)See ref. [113]

(15)See ref. [114-116]
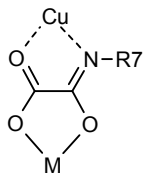
(16)See ref. [117]
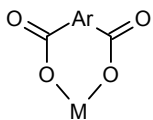
(17)See ref. [118]

(18)See ref. [119]
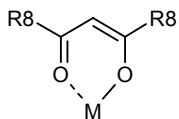
(19)See ref. [120-122]

(20)See ref. [123]

(21)See ref. [124]

(22)See ref. [45, 125-127]
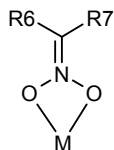
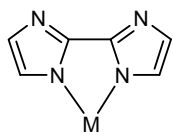(23)See ref. [128]

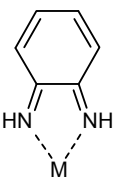(24)See ref. [129]

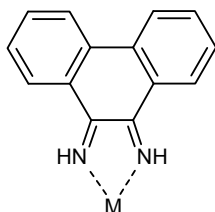(25)See ref. [129, 130]

(26)See ref. [131]
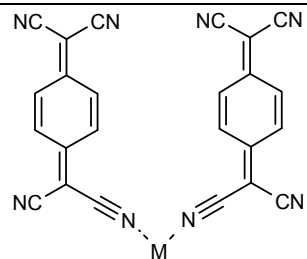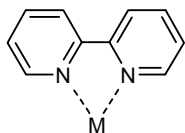
(27)See ref. [132]
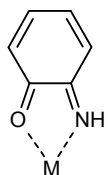
(28)See ref.
[133]

(29)See ref.
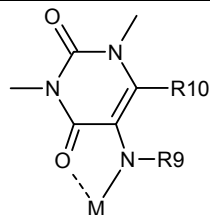[134]

(30)See ref.
[135]

(31)See ref.
[136]

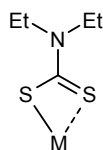(32)See ref.
[136]

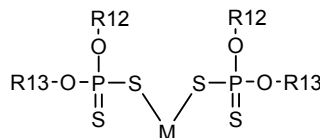(33)See ref.
[137]

(34)See ref.
[138]

(35)See ref.
[139, 140]

(36)See ref.
[141-143]

(37)See ref.
[144]

(38)See ref.   (39)See ref.
[145]   [145]

[1] Substitution – n-alkyl; R1 = CH_3; [2] a) Substitution – none; R2 = Ga^{3+}; [3] Substitution – none; R2 = Ga^{3+}; [4] Substitution – c-alkyl; R2 = Al^{3+}; [5] a) Substitution – none; R3 = Ar; [5] b) Substitution – none; R3 = OMe; [6] a) Substitution – none; R3 = Ar; [6] b) Substitution – none; R3 = OMe; [7] a) Substitution – none; R3 = Ar; [7] b) Substitution – none; R3 = cyclohexane; [8] Substitution – none; R3 = pyridine; [9] Substitution – none; R4 = H; [10] Substitution – none; [11] Substitution – none; [12] Substitution – none; [13] Substitution – c-alkyl; [14] Substitution – none; [15] a) Substitution – c-alkyl; R3 = aryl; [15] b) Substitution – c-alkyl; R3 = pyridine; [16] Substitution – c-alkyl; R3 = aryl; [17] Substitution – c-alkyl; R7 = alkyl or aryl; [18] Substitution – c-alkyl; [19] a) Substitution – none; [19] b) Substitution – c-alkyl; [20] a) Substitution – c-alkyl; [21] Substitution – c-alkyl; [22] a) Substitution – n-alkyl (caged); R8 = CH_3; [22] b) Substitution – c-phenyl; R8 = CH_3; [23] Substitution – none; R8 = CH_3; [24] Substitution – n-alkyl; R6 = R7 = CH_3; [25] a) Substitution – c-alkyl; R6 = R7 = H, [25] b) Substitution – n-alkyl; R6 = H, R7 = CH_3; [25] c) Substitution – c-alkyl; R6 = R7 = CH_2CH_3; [26] Substitution – none; R1 = quinonedi-imine; [27] Substitution – n-alkyl; R1 = 2-cyanoethene-1,2-dithiolate; [28] Substitution – none; [29] Substitution – none; [30] Substitution – none; [31] Substitution – none; [32] Substitution – none; [33] Substitution – none; [34] Substitution – none; [35] Substitution – c-alkyl; R9 = O, R10 = NH-alkyl; [36] a)Substitution – c-alkyl; R11 = Ar; [36] b) Substitution – c-alkyl; R11 = $-SCH_2COO^-$; [36] c) Substitution – c-alkyl; R11 = $-SCH_2CH_2COO^-$; [37] Substitution – c-alkyl; [38] Substitution – c-alkyl; R12 = R13 = CH_2CH_2-Ph; [39] Substitution – c-alkyl; R12 = R13 = CH_2CH_2-Ph;

8. Structures of 1,4,8,11-tetraaza-cyclotetradecane ([14]aneN$_4$ or cyclam) complexes in solution

8.1 Zn(II) complexes

The bicyclam **18** (**Fig. 27**) is a very potent anti-HIV agent[146]. Entry of T-lymphotropic HIV-1 and HIV-2 strains is blocked by specific binding to the CXCR4 coreceptor[147]. Based on the strong propensity of the cyclam to bind carboxylic acid groups, receptor mutagenesis identified Asp171 and Asp262 as being essential for the ability of **18** to block the binding of the chemokine ligand stromal cell-derived factor (SDF)-1α and the binding of the receptor antibody 12G5[149]. Since the level of free Zn(II) in plasma is ca. 1 nM and cyclam and its alkylated derivates strongly bind Zn(II), it is reasonable to expect that the active compound in vivo is the Zn(II) complex[88].

Fig. 27. Molecular structure of xylyl-bicyclam **18**, 1,1'-[1,4-phenylenebis(methylene)]-bis(1,4,8,11-tetraazacyclotetradecane). The octa-HCl salt of the compound is registered as the anti-HIV drug AMD3100.

18
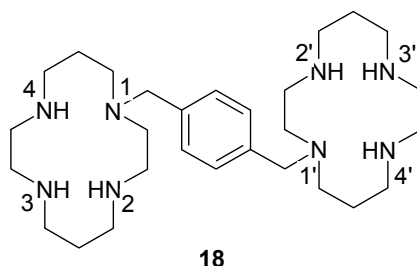
The interaction of the Zn(II) complex of xylyl-bis-cyclam, which is 10 times more active than **18** in its interaction with the CXCR4 receptor[148], with acetate was studied. In solution, acetate binds[149] to the Zn(II) bicyclam complex with a binding constant of log K = 2.75 ± 0.15, assuming the formation of 1:1 complexes of acetate with Zn-cyclam units and that the two Zn-cyclam units are independent[88]. Both in solution and in the solid phase the complex adopts a *cis*-V configuration (according to the nomenclature of *Bosnich*[89]) via chelation and second coordination sphere double H-bonding[88]. It was shown that only Zn(II) cyclams could bind acetates. Pd(II) cyclams do not coordinate acetates, as the acetate does not induce configurational changes of Pd(II) cyclam nor Pd(II)$_2$-xylyl-bicyclam, and Pd(II) cyclams can readily adopt a *cis*-V configuration[88,148].

Although Co(III) cyclams are known to bind strongly to carboxylates, and are capable of undergoing isomerizations from *cis* to *trans* configurations[150], Co(III)$_2$-xylyl-bicyclam has a very low activity towards CXCR4[148]. This is most likely attributable to the kinetic inertness of Co(III) cyclams[151].

The Zn(II) complex of 1,4,8,11-tetraaza-cyclotridecane-5-one was found to be extremely efficient in the recognition of glycine in aqueous solution (**Fig. 28**)[90].

Fig. 28. Zn(II) complex of 1,4,8,11-tetraaza-cyclotridecane-5-one can bind glycine.
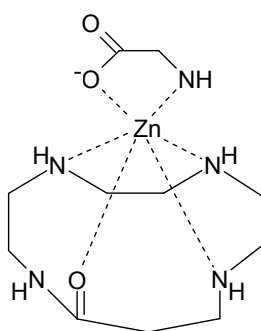
19

The carboxylate group is capable of forming a coordinative bond to the Zn(II) ion, while the H-atom of the amide on the macrocycle may also favor aggregate formation. **Table 7** shows the stability constants for the Zn(II) 1,4,8,11-tetraazacyclotridecane-5-one glycine complex **19**.

Table 7. Stability constants for Zn(II) 1,4,8,11-tetraaza-cyclotridecane-5-one (L) glycine complex **19** (µ = 0.10 M KCl, 25 °C).

Stoichiometry				Quotient *K*	log *K*
(L)	Zn	Glycine	H		
1	1	0	0	[LZn] / [L][Zn]	9.33
1	1	0	1	[LZnH] / [LZn][H]	6.44
1	1	0	2	[LZnH$_2$] / [LZn][H]^2	6.65
1	1	1	0	[LZnGly⁻] / [LZn][Gly⁻]	12.25
1	1	1	1	[LZnGlyH] / [LZnH][Gly]	2.58
1	1	1	-1	[LZnGlyOH] / [LZnOH][Gly]	1.00
1	1	1	-2	[LZnGlyOH$_2$] / [LZnOH$_2$][Gly]	0.88

8.2 Ni(II) complexes

The Ni(II) complex of 1,4,7,10-tetraaza-cyclododecane-2,9-dione was found to be efficient in the recognition of the dipeptide glycine-glycine in aqueous solution (**Fig. 29**)[92].

Fig. 29. Ni(II) complex of 1,4,7,10-tetraaza-cyclododecane-2,9-dione **20** can recognize the dipeptide glycine-glycine (GG).
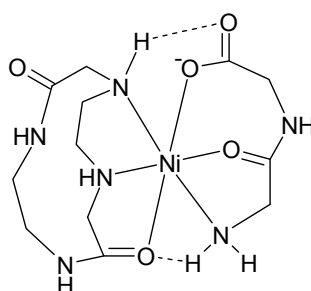
20

The formation of a stable ternary complex, L-Ni(II)-Gly-Gly⁻ leads to a very high binding constant of log K = 19.20 (**Table 8**). The strong recognition may also be partially attributed to the formation of an H-bond between the macrocycle and the dipeptide.

Table 8. Stability constants for the Ni(II) 1,4,7,10-tetraaza-cyclododecane-2,9-dione (L) glycine-glycine (GG) complex **20** (μ = 0.10 M KCl, 25 °C).

Stoichiometry				Quotient K	log K
(L)	Ni	GG	H		
1	1	0	0	[LNi] / [L][Ni]	15.51
1	1	0	1	[LHNi] / [LNi][H]	4.50
1	1	0	2	[LH$_2$Ni] / [LHNi][H]	4.11
1	1	0	-1	[LNiOH] / [LNi][H]	6.31
1	1	0	-2	[LNiOH$_2$] / [LNiOH][OH]	-9.64
1	1	1	0	[LNiGG] / [LNi][GG]	19.20
1	1	1	-1	[LNiGGOH] / [LNiG][OH]	10.07
1	1	1	-2	[LNiGGOH$_2$] / [LNiGOH][OH$_2$]	0.29

8.3 Hg(II) complexes

Mallik et al. have shown that the Hg(II)-xylyl-bicyclam **21** (**Fig. 30**) could bind imidazole in DMSO (binding constants >> 100 M^{-1})[152,153].

Fig. 30. The Hg(II)-xylyl-bis-cyclam **21** bound to two imidazole units.

21
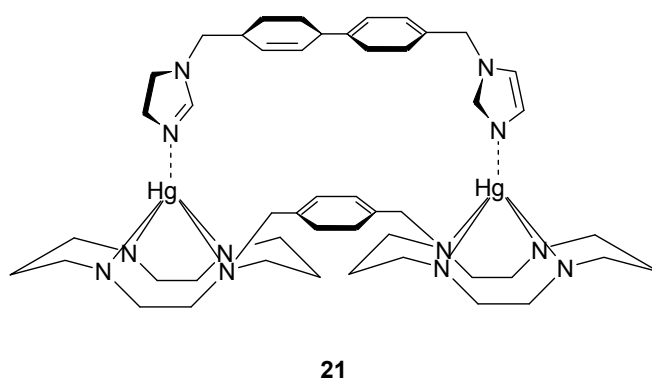
An improvement in imidazole binding is shown with the tris-cyclam ligand **22** which when complexed with Hg^{2+} has recognized a model histidine peptide **23** with a K > 10^5 M^{-1} in DMSO (**Fig. 31**)[154].

Fig. 31. A tris-cyclam **22** when complexed with Hg(II) recognizes the model tris-histidine peptide **23**, which is complementary in geometry.

22   **23**
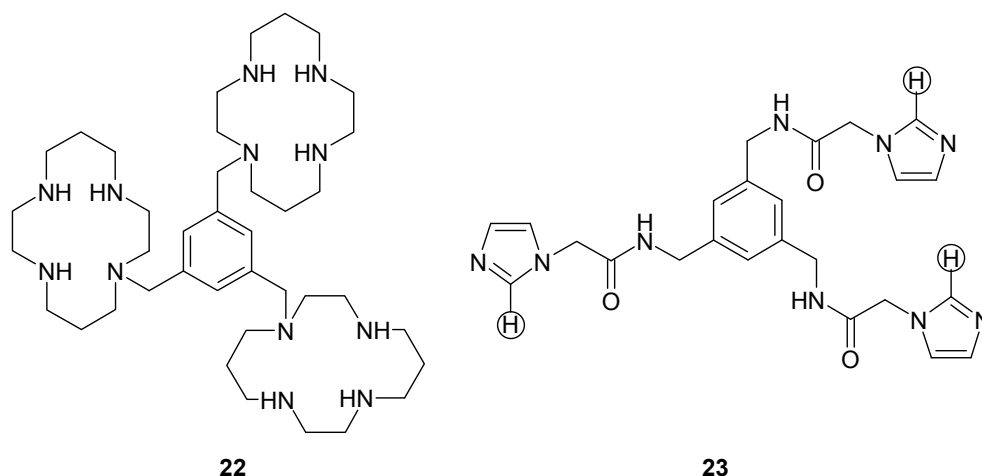
9. Immobilised 1,4,8,11-tetraaza-cyclotetradecane ([14]aneN₄ or cyclam) complexes

Ni(II) complexes

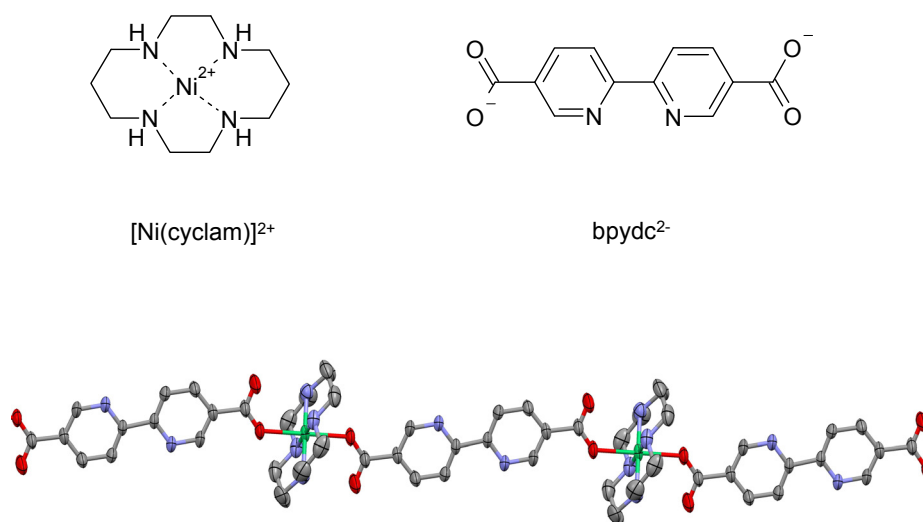A linear polymer containing Ni(II) cyclam and 2,2'-bipyridyl-5,5'-dicarboxylate (bpydc^{2-}) was synthesized (**Fig. 32**). The polymer binds guests in the order of ethanol ≈ phenol (formation constant, K_f = 42 M^{-1}) > pyridine (K_f = 13 M^{-1}) > benzene (K_f = 3 M^{-1}) in isooctane solution[155].

Fig. 32. Structure of the linear polymer containing Ni(II) cyclam and bpydc^{2-}.

[Ni(cyclam)]$^{2+}$ bpydc^{2-}

10. Structures of 1,5,9-triaza-cyclododecane ([12]aneN₃) complexes in solid state

Zn(II) complexes

Although the coordination of Zn(II) [12]aneN₃ to acetazolamide and sulfonamides has been reported in solution[14,71], no X-ray structures were found for their coordination in solid state. The X-ray structure of [Zn(12aneN₃)(OH₂)](ClO₄)₂ shows a zinc atom with slightly distorted tetrahedral coordination environment, with a bound water molecule (**Fig. 33**).

Fig. 33. Structure of [Zn(12aneN$_3$)(OH$_2$)](ClO$_4$)$_2$ in the crystal. Perchlorate anions and hydrogen atoms are omitted for clarity. Probability ellipsoids are 30%.
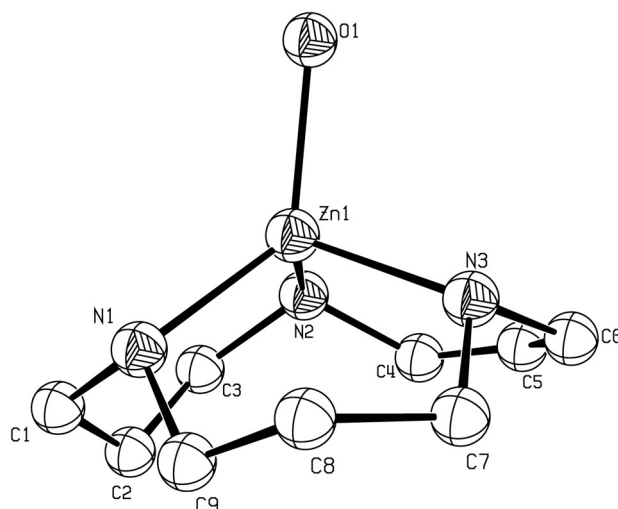
11. Molecular recognition of 1,5,9-triaza-cyclododecane ([12]aneN3) complexes in solution

Zn(II) complexes

The Zn(II) complex of the 12-membered triamine, [12]aneN$_3$ forms 1:1 complexes with acetazolamide and sulfonamides[14,71]. The intermolecular affinities of aromatic sulfonamides to Zn(II) [12]aneN$_3$ (ZnL) are summarized in the **Table 9**.

Table 9. Comparison of critical affinity constants of different inhibitors (I) and inhibitor-ZnL complexes, K_i (M^{-1}) and K [Zn(II) [12]aneN$_3$-I] (M^{-1})[71].

Inhibitor(I)	log K_i	log K[Zn(II) [12]aneN$_3$-I]
acetazolamide	3.6	4.9
4-nitrobenzenesulfonamide	2.6	4.8
p-toluenesulfonamide	2.4	5.7

Determined by inhibition kinetics at pH 8.4 (50 mM TAPS buffer), I = 0.10 and 25 °C.

Due to the poor solubility of the sulfonamides, the potentiometric pH titration method could not be used to determine the binding constants. The binding constants were measured by an inhibition kinetic method in the Zn(II) [12]aneN$_3$ complex promoted 4-nitrophenyl acetate hydrolysis, which is analogous to the procedure used to

determine sulfonamide binding to carbonic anhydrase (CA)[156]. The apparent binding constants are consistent with previous biochemical data reported for CA models which makes such Zn(II) [12]aneN$_3$ complexes good models for CA.

12. Immobilised 1,5,9-triaza-cyclododecane ([12]aneN$_3$) complexes

No reports on immobilized [12]aneN$_3$ complexes have been appeared in literature so far.

13. Structures of 1,4,7-triaza-cyclononane ([9]aneN$_3$ or TACN) complexes in solid state

Cu(II) complexes

The smallest azamacrocycle which forms metal complexes is [9]aneN$_3$. Its Cu(II) complex binds to the amino acid histidine, forming a square pyramidal Cu(II) coordination geometry[157]. The X-ray structure analysis confirms that the distorted square-pyramidal Cu(II) coordination sphere is comprised of three nitrogen donors from the [9]aneN$_3$ plus one carboxylate atom and the primary nitrogen from L-histidine (**Fig. 34**).

Fig. 34. The structure of [Cu(TACN)(histidine)]$^{2+}$(PF$_6$)$^-$ in the solid state.
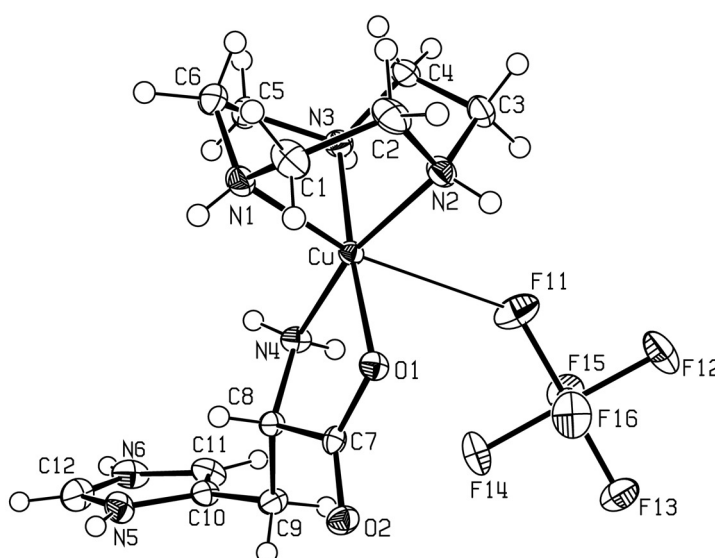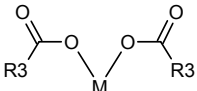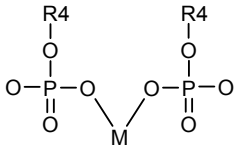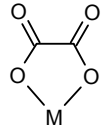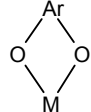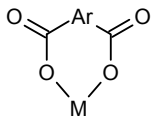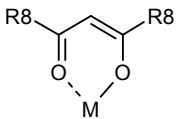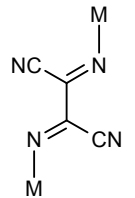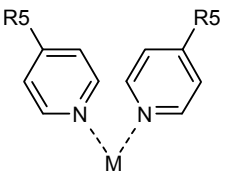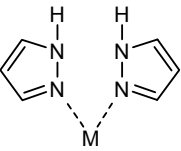
14. Structures of 1,4,7-triaza-cyclononane ([9]aneN$_3$ or TACN) complexes in solid state (tabulated)
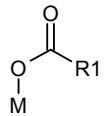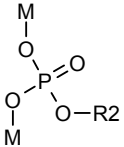
Table 10 summarizes all X-ray structures registered at the Cambridge Crystallographic Database according to the selection criteria previously mentioned.

Table 10. Structurally characterized metal complexes of 1,4,7-triaza-cyclononane ([9ane]N_3 or TACN) with additional ligand coordinated to the metal ion in solid state.

Structure of the additional ligand	Metal ions											
	Zn^{2+}	Cu^{2+}	Ni^{2+}	Co^{3+}	Rh^{3+}	Fe^{3+}	Fe^{2+}	Ru^{2+}	Mn^{3+}	Cr^{3+}	V^{3+}	Zr^{4+}
(carboxylate, R1)		[1]See ref. [158-160]										
(phosphate, O–R2)	[2]See ref. [161]											
(R3 dicarboxylate)	[3]See ref. [158, 162]											
(R4 diphosphate)	[4]See ref. [163]	[5]See ref. [161]										
(oxalate)		[6]See ref. [164, 165]	[7]See ref. [166]									
(Ar)		[8]See ref. [167, 168]				[9]See ref. [169, 170]				[10]See ref. [171]		

(11)See ref. [159]

(12)See ref. [172]

(13)See ref. [173]

(14)See ref. [173]

(15)See ref. [174]

(16)See ref. [175]

(17)See ref. [172, 176, 177]

(18)See ref. [178, 179]

(19)See ref. [180]

(20)See ref. [181]

(21)See ref. [182]

(22)See ref. [183]

(23)See ref. [184]
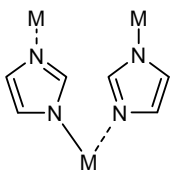
(24)See ref. [185, 186]
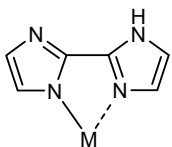
(25)See ref. [187, 188]
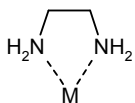
(26)See ref. [189]
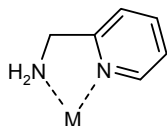
(27)See ref. [189]
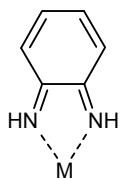
(28)See ref [190]
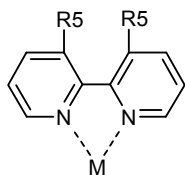
(29)See ref. [191, 192]
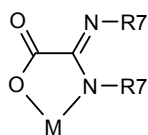
(30) See ref. [193, 194]
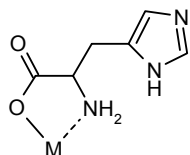
(31) See ref. [157]
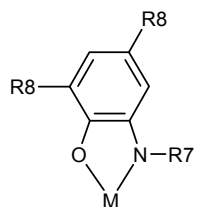
(32) See ref. [195]

(1) a) Substitution – none; R1 = aryl; (1) b) Substitution – n-alkyl; R1 = aryl; (2) Substitution – n-alkyl; R2 = Ph; (3) a) Substitution – n-alkyl; R3 = aryl; (3) b) Substitution – none; R3 = aryl; (4) Substitution – n-alkyl; R4 = CH$_2$Ph; (5) Substitution – n-alkyl; R4 = Ph; (6) Substitution – none; (7) a) Substitution – none; (8) a) Substitution – n-CH$_2$Ph; (8) b) Substitution – n-alkyl; (9) Substitution – n-alkyl; (10) Substitution – n-alkyl; (11) Substitution – n-alkyl; (12) Substitution – n-alkyl; R8 = CH$_3$; (13) Substitution – n-alkyl; R8 = Ph; (14) Substitution – n-alkyl; R8 = Ph; (15) Substitution – n-alkyl; R8 = CH$_3$; (16) Substitution – n-alkyl; R8 = CH$_3$; (17) Substitution – n-alkyl; R8 = CH$_3$; (18) Substitution – n-alkyl; R8 = CH$_3$; (19) Substitution – none; R8 = CH$_3$; (20) Substitution – n-alkyl; (21) Substitution – n-alkyl; (22) Substitution – none; R5 = pyridine; (23) Substitution – n-alkyl; (24) a) Substitution – none; (24) b) Substitution – n-alkyl; (25) Substitution – none; (26) Substitution – none; (27) Substitution – none; (28) Substitution – n-alkyl; (29) a) Substitution – n-alkyl; R5 = CH$_3$; (29) b) Substitution – n-alkyl; R5 = O-alkyl; (30) a) Substitution – n-alkyl; R7 = H; (30) b) Substitution – none; R7 = CH$_3$; (31) Substitution – none; (32) Substitution – n-alkyl; R7 = Ph, R8 = *tert*-butyl.

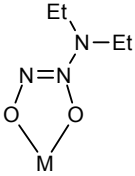# 15. Molecular recognition of 1,4,7-triaza-cyclononane ([9]aneN₃ or TACN) complexes in solution

Cu(II) complexes

TACN chelates Cu(II) strongly (log K = 15.5 at 25 °C)[196]. Above pH 8 one of the two equatorial coordination sites available on the copper atom is occupied by a hydroxide ion[197]. Above pH 9 glucose readily displaces water and hydroxide to form a ternary TACN-Cu(II)-glucose complex, which results in the net release of protons (**Fig. 35**). The measurement of this proton release by pH titration gives apparent binding constants of 35 M^{-1} at pH 10.25 to 1200 M^{-1} at pH 11.5 for the complexation of Cu(II) TACN with glucose[198]. The Cu(II) TACN complex exhibits considerable selectivity depending on the diol. At alkaline pH it can bind *cis*-diols 1,4-anhydroerythritol and glucose, while *trans*-diol sugar analogue and 1,4-anhydro-L-threitol cannot be coordinated.

Fig. 35. The Cu(II) TACN complex coordinates glucose at alkaline pH.
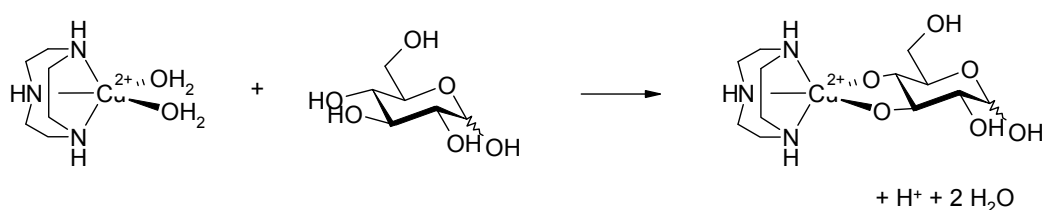
In addition recent investigations of a TACN cobalt complexe have shown interactions with calf-thymus DNA (CT DNA) by visometric and electrochemical studies[199]. The metal complex binds on the DNA surface with no possibility for partial intercalation interaction.

16. Immobilised 1,4,7-triaza-cyclononane ([9]aneN₃ or TACN) complexes

Cu(II) complexes

A polymerizable TACN-Cu(II)-glucopyranoside complex has been copolymerized with a cross linking monomer to form a porous polymer[198]. After washing to remove the template, a polymer which rebinds glucose and thereby releasing protons in to the surrounding solution was created (**Fig. 36**). The change in pH provides a convenient measure of glucose concentration over a clinically relevant range (0-25 mM) (**Fig. 37**).

Fig. 36. Preparation of a glucose sensing Cu(II) TACN containing polymer.
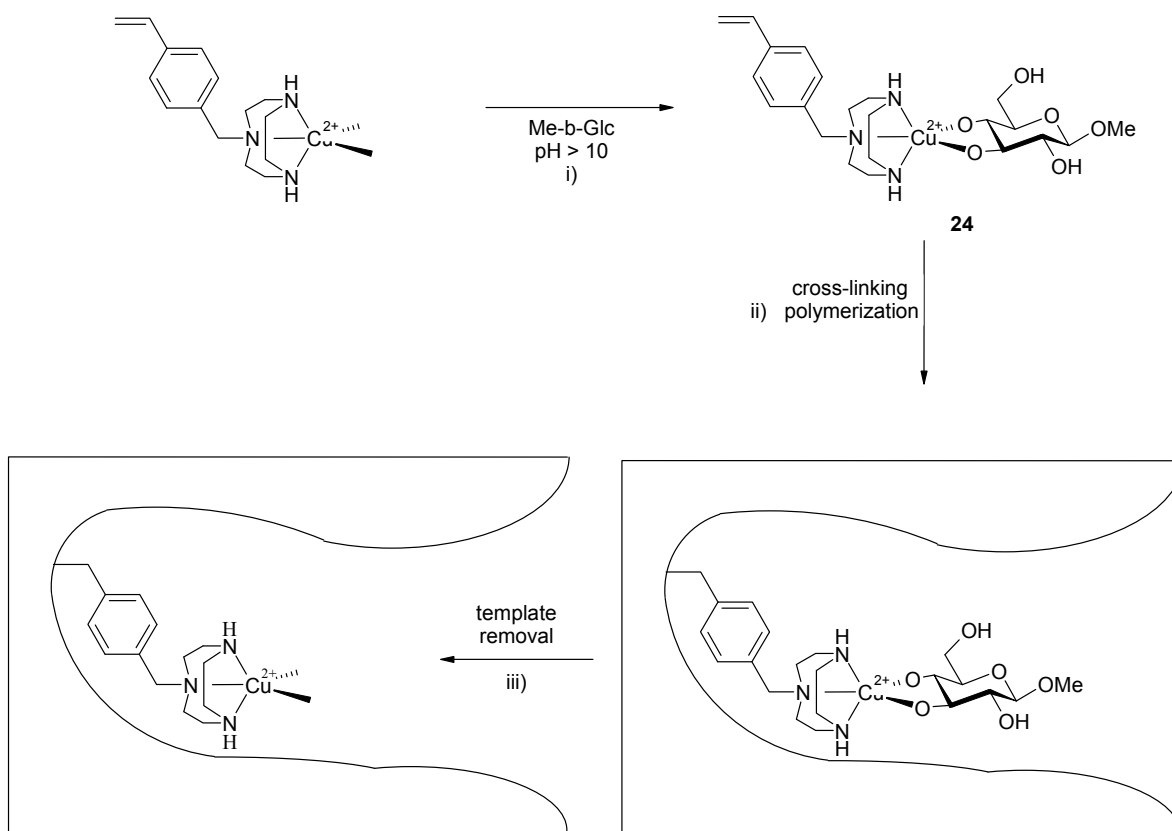
Fig. 37. Titration of methyl-ß-D-glucopyranoside-imprinted polymer (0.034 mmol Cu(II)) with D-glucose in 0.15 M NaCl, 25 °C at pH 10.25, 10.75 and 11.25 at constant pH.
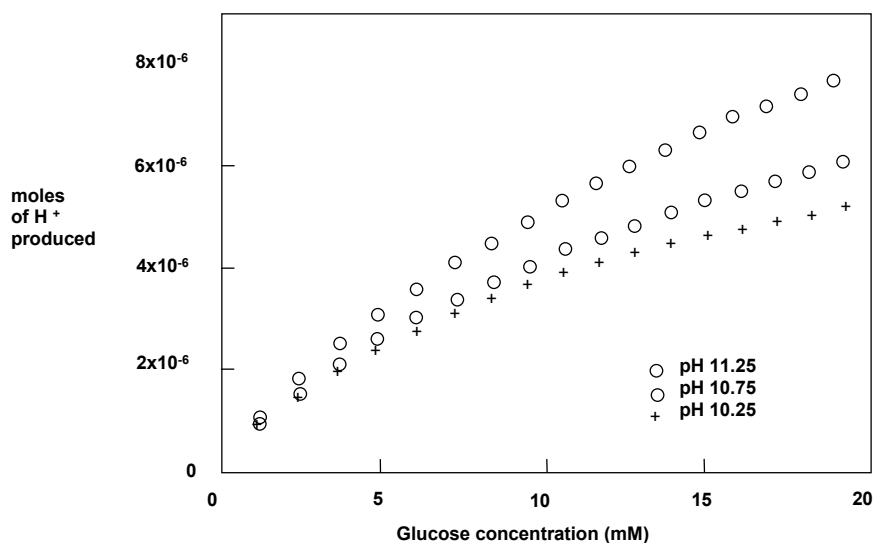
The high ratio of cross-linker in the polymer generates a microporous polymer which allows the small glucose molecules to bind, but hinders larger molecules such as glycosylated proteins which may otherwise also bind to the metal complex. The polymers ability to sense glucose is not impeded by the many potential competing species present in a complex biological sample such as porcine plasma (adjusted to pH 11.25)[200].

17. Conclusion

A variety of transition metal complexes from cyclen, cyclam to TACN reversibly coordinate additional donor molecules in the solid state, in solution or immobilized on polymer support. In many cases this coordination of an additional ligand is selective for a particular functional group. In solution binding affinities in the milli or micromolar range are observed, even at physiological conditions. This allows the selective molecular recognition of target molecules with high binding strength in biological media, a process which is difficult to achive using synthetic receptors based on hydrogen bonding. Therefore many transition metal complexes of azamacrocyclic ligands are ideally suited as molecular binding sites for analytes, and many applications in diagnostics, bioanaytics, biotechnology or material sciences may be envisaged.

18. References

[1]   Curtis, N. F. *J. Chem. Soc.* **1960**, 4409

[2]   Thompson, M. C.; Busch, D. H. *J. Am. Chem. Soc.* **1964**, *86*, 3651

[3]   Izatt, R. M.; Pawlak, K.; Bradshaw, J. S.; Bruening, R. L. *Chem. Rev.* **1995**, *95*, 2529

[4]   Bianchi, A.; Micheloni, M.; Paoletti, P. *Coord. Chem. Rev.* **1991**, *110*, 17

[5]   Boeyens, J. C. A.; Dobson, S. M. in *Sterochemical and Stereophysical Behaviour of Macrocycles*, ed. Bernal, I.; Elsevier, Amsterdam, , **1987**, Vol. *2*, pp. 1-102

[6]   Curtis, N. F.; in *Coordination Chemistry of Macrocyclic Compounds,* ed. Melson, G. A.; Plenum Press, **1979**, 219

[7]   Micheloni, M.; Sabatini, A.; Paoletti, P. *J. Chem. Soc., Perkin Trans. 2* **1978**, 828

[8]   Thöm, V. J.; Hosken, G. D.; Hancock, R. D. *Inorg. Chem.* **1985**, *24*, 3378

[9]   Hinz, F. P.; Margerum, D. W. *Inorg. Chem.* **1974**, *13*, 2941

[10]   Evers, A. Hancock, R. D. *Inorg. Chim. Acta* **1989**, *160*, 245

[11]   Kodama, M.; Kimura, E. *J. Chem. Soc., Dalton Trans.* **1977**, 1473

[12]   Kodama, M.; Kimura, E. *J. Chem. Soc., Dalton Trans.* **1978**, 1081

[13]   Kodama, M.; Kimura, E. *J. Chem. Soc., Dalton Trans.* **1977**, 2269

[14]   Kimura, E.; Shiota, T.; Moike, T.; Shiro, M.; Kodama, M. *J. Am. Chem. Soc.* **1990**, *112*, 5805

[15]   Leugger, A. P.; Hertli, L.; Kaden, T. A. *Helv. Chim. Acta* **1978**, *61*, 2296

[16]   Kodama, M.; Kimura, E. *J. Chem. Soc., Dalton Trans.* **1980**, 327

[17]   Thöm, V. J., Hanock, R. D. *J. Chem. Soc., Dalton Trans.* **1985**, 1877

[18]   Kodama, M.; Kimura, E. *J. Chem. Soc., Dalton Trans.* **1976**, 2335

[19]   Clarkson, A. J.; Blackman, A. G.; Clark, C. R. *J. Chem. Soc. Dalton Trans.* **2001**, 758

[20]   Buckingham, D. A.; Clark, C. R.; Rogers, A. J. *Aust. J. Chem.* **1998**, *51*, 461.

[21]   Kim, J. H.; Britten, J.; Chin, J. *J. Am. Chem. Soc.* **1993**, *115*, 3618

[22]   Iitaka, Y.; Shina, M.; Kimura, E. *Inorg. Chem.* **1974**, *13*, 2886

[23]   Loehlin, J. H.; Fleischer, E. B. *Acta Crystallogr.*, *Sect. B* **1976**, *32*, 3063

[24] Carrington, S. J.; Buckingham, D. A.; Simpson, J.; Blackman, A. G.; Clark, C. R. *J. Chem. Soc. Dalton Trans.* **1999**, 3809

[25] Nonoyama, M.; Kurimoto, T. *Polyhedron* **1985**, *4*, 471

[26] Clarkson, A. J.; Buckingham, D. A.; Rogers, A. J.; Blackman, A. G.; Clark, C. R. *Inorg. Chem.* **2000**, *39*, 4769

[27] Buckingham, D. A.; Clark, C. R.; Rogers, A. J. *J. Am. Chem. Soc.* **1997**, *119*, 4050

[28] Ajioka, M.; Yano, S.; Matsuda, K.; Yoshikawa, S. *J. Am. Chem. Soc.* **1981**, *103*, 2459

[29] Styka, M. C.; Smierciak, R. C.; Blinn, E. L.; DeSimone, R. S.; Passariello, J. V. *Inorg. Chem.* **1978**, *17*, 82

[30] Ballester, L.; Gutiérrez, A.; Perpiñán, M. F.; Sánchez, A. E.; Azcondo, M. T.; González, M. J. *Inorg. Chim. Acta* **2004**, *357*, 1054

[31] Clay, R. M.; Murray-Rust, P. Murray-Rust, J. *Acta Crystallogr., Sect. B.* **1979**, *35*, 1894

[32] Smierciak, R. C.; Passariello, J.; Blinn, E. L. *Inorg. Chem.* **1977**, *16*, 2646

[33] Plassman, W. H.; Swisher, R. G.; Blinn, E. L. *Inorg. Chem.* **1980**, *19*, 1101

[34] Bencini, A.; Bianchi, A.; Garcia-España, E.; Jeannin, Y.; Julve, M.; Marcelino, V.; Philoche-Levisalles, M. *Inorg. Chem.* **1990**, *29*, 963

[35] Pariya, C.; Chi, T.-Y.; Mishra, T. K.; Chung, C.S. *Inorg. Chem. Comm.* **2002**, *5*, 119

[36] Li, J.; Ren, Y.-W.; Zhang, J.-H.; Yang, P. *J. Chem. Cryst.* **2004**, *34*, 409

[37] Lin, Y.-C.; Lu, T.-H.; Liao, F.-L.; Chung, C.-S. *Anal. Sci.* **2003**, *19*, 967

[38] Shionoya, M.; Kimura, E.; Shiro, M. *J. Am. Chem. Soc.* **1993**, *115*, 6730

[39] Subat, M.; Borovik, A. S.; Koenig, B. *J. Am. Chem. Soc.* **2004**, *126*, 3185

[40] Kimura, E.; Aoki, S.; Koike, T.; Shiro, M. *J. Am. Chem. Soc.* **1997**, *119*, 3068

[41] Fujioka, H.; Koike, T.; Yamada, N.; Kimura, E. *Heterocycles* **1996**, *42*, 775

[42] Aoki, S.; Kimura, E. *J. Am. Chem. Soc.* **2000**, *122*, 4542

[43] Kimura, E.; Ikeda, T.; Shionoya, M.; Shiro, M. *Angew. Chem., Int. Ed.* **1995**, *34*, 663

[44] Koike, T.; Kajitani, S.; Nakamura, I.; Kimura, E.; Shiro, M. *J. Am. Chem. Soc.* **1995**, *117*, 1210

[45] Hubin, T. J.; Alcock, N. W.; Clase, H. J.; Busch, D. H. *Supramol. Chem.* **2001**, *13*, 261

[46] Matsumoto, N.; Hirano, A.; Hara, T.; Ohyoshi, A. *J. Chem. Soc., Dalton Trans.* **1983**, 2405

[47] Han, M.S.; Kim, D.H. *Supramol. Chem.* **2003**, *15*, 59

[48] Aoki, S.; Shiro, M.; Koike, T.; Kimura, E. *J. Am. Chem. Soc.* **2000**, *122*, 576

[49] Koike, T.; Takashige, M.; Kimura, E.; Fujioka, H.; Shiro, M. *Chem. Eur. J.* **1996**, *2*, 617

[50] Shionoya, M.; Ikeda, T.; Kimura, E.; Shiro, M. *J. Am. Chem. Soc.* **1994**, *116*, 3848

[51] Kimura, E.; Katsube, N.; Koike, T.; Shiro, M.; Aoki, S. *Supramol. Chem.* **2002**, *14*, 95

[52] Lau, V. C.; Berben, L. A.; Long, J. R. *J. Am. Chem. Soc.* **2002**, *124*, 9042

[53] Krotz, A. H.; Kuo, L. Y.; Barton, J. K. *Inorg. Chem.* **1993**, *32*, 5963

[54] Lu, T.-H.; Panneerselvam, K.; Chen, L.-H.; Lin, Y.-J.; Liao, F.-L.; Chung, C.-S. *Anal. Sci.* **2001**, *17*, 571

[55] Buckingham, D. A.; Clark, C. R.; Rogers, A. J.; Simpson, J. *Inorg. Chem.* **1995**, *34*, 3646

[56] Tsuboyama, S.; Sakurai, T.; Tsuboyama, K. *J. Chem. Soc., Dalton Trans.* **1987**, *4*, 721

[57] Tsuboyama, S.; Shiga, Y.; Takasyo, Y.; Chijimatsu, T.; Kobayashi, K.; Tsuboyama, K.; Sakurai, T. *J. Chem. Soc., Dalton Trans.* **1992**,1783

[58] Tsuboyama, S.; Takishima, T.; Sakurai, T.; Tsuboyama, K. *Nippon Kagaku Kaishi (Jap.) (J. Chem. Soc. Jpn.)* **1987**, 313

[59] Tsuboyama, S.; Tsuboyama, K.; Sakurai, T. *Acta Crystallogr., Sect.C: Cryst. Struct. Commun.* **1989**, *45*, 669

[60] Tsuboyama, S.; Tsuboyama, K.; Sakurai, T. *Acta Crystallogr., Sect.C: Cryst. Struct. Commun.* **1990**, *46*, 727

[61] Tsuboyama, S.; Miki, S.; Chijimatsu, T.; Tsuboyama, K.; Sakurai, T. *J. Chem. Soc., Dalton Trans.* **1989**, 2359

[62] Kobayashi, K.; Tsuboyama, S.; Tsuboyama, K.; Ito, T. *Anal. Sci.* **1996**, *12*, 821

[63] Kobayashi, K.; Tsuboyama, S.; Tabata, N.; Tsuboyama, K.; Sakurai, T. *Anal. Sci.* **1996**, *12*, 531

[64] Tsuboyama, S.; Kobayashi, K.; Tsuboyama, K.; Sakurai, T. *Anal. Sci.* **1995**, *11*, 707

[65] Kobayashi, K.; Takahashi, H.; Nishio, M.; Umezawa, Y.; Tsuboyama, K.; Tsuboyama, S. *Anal. Sci.* **2000**, *16*, 1103

[66] Tsuboyama, S.; Matsudo, M.; Tsuboyama, K.; Sakurai, T. *Acta Crystallogr., Sect.C: Cryst. Struct. Commun.* **1989**, *45*, 872

[67] Aoki, S.; Shiro, M.; Kimura, E. *Chem.-Eur. J.* **2002**, *8*, 929

[68] Kojima, M.; Nakabayashi, K.; Ohba, S.; Okumoto, S.; Saito, Y.; Fujita, J. *Bull. Chem. Soc. Jpn.* **1986**, *59*, 277

[69] Mizukami, S.; Nagano, T.; Urano, Y.; Odani, A.; Kikuchi, K. *J. Am. Chem. Soc.* **2002**, *124*, 3920

[70] Aoki, S.; Kimura, E. *Chem. Rev.* **2004**, *104*, 769

[71] Koike, T.; Kimura, E.; Nakamura, I.; Hashimoto, Y.; Shiro, M. *J. Am. Chem. Soc.* **1992**, *114*, 7338

[72] (a) Koike, T.; Watanabe, T.; Aoki, S.; Kimura, E.; Shiro, M. *J. Am. Chem. Soc.* **1996**, *118*, 12696; (b) Kimura, E.; Aoki, S.; Kikuta, M.; Koike, T. *Proc. Natl. Acad. Sci. U.S.A.* **2003**, *100*, 3731; (c) Aoki, S.; Kaido, S.; Fujioka, H.; Kimura, E. *Inorg. Chem.* **2003**, *42*, 1023; (d) Koike, T.; Abe, T.; Takahashi, M.; Ohtani, K.; Kimura, E.; Shiro, M. *J. Chem. Soc. Dalton Trans.* **2002**, 1764; (e) Kimura, E.; Koike, T. *Chem. Soc. Rev.* **1998**, *27*, 179; (f) Kimura, E. *S. Afr. J. Chem.* **1997**, *50*, 240; (g) Kimura, E.; Aoki, S. *BioMetals* **2001**, *14*, 191

[74] Koenig, B.; Pelka, M.; Zieg, H.; Ritter, T.; Bouas-Laurent, H.; Bonneau, R.; Desvergne, J.-P. *J. Am. Chem. Soc.* **1999**, *121*, 1681

[75] Koenig, B.; Pelka, M.; Reichenbach-Klinke, R.; Schelter, J.; Daub, J. *Eur. J. Org. Chem.* **2001**, 2297

[76] Reichenbach-Klinke, R.; Kruppa, M.; Koenig, B. *J. Am. Chem. Soc.* **2002**, *124*, 12999

[77] Wiest, O.; Harrison, C. B.; Saettel, N. J.; Cibulka, R.; Sax, M.; Koenig, B. *J. Org. Chem.* **2004**, *69*, 8183

[78] (a) Aoki, S.; Sugimura, C.; Kimura, E. *J. Am. Chem. Soc.* **1998**, *120*, 10094; b) Kimura, E.; Ikeda, T.; Aoki, S.; Shionoya, M. *J. Biol. Inorg. Chem.* **1998**, *3*, 259; (c) Kikuta, E.; Murata,M.; Katsube, N.; Koike, T.; Kimura, E. *J. Am. Chem. Soc.* **1999**, *121*, 5426; (d) Kikuta, E.; Katsube, N.; Kimura, E. *J. Biol. Inorg. Chem.* **1999**, *4*, 431; (e) Kimura, E.; Koike, T.; Kimura, E. *J. Inorg. Biochem.* **2000**, *79*, 253; (f) Kikuta, E.; Matsubara, R.; Katsube, N.; Koike, T.; Kimura, E. *J. Inorg. Biochem.* **2000**, *82*, 239; (g) Kimura, E.; Kikuta, E. *J. Biol. Inorg. Chem.* **2000**, *5*, 139; (h) Kimura, E.; Kitamura, H.; Ohtani, K.; Koike, T. *J. Am. Chem. Soc.* **2000**, *122*, 4668; (i) Kikuta, E.; Aoki, S.; Kimura, E. *J. Biol. Inorg. Chem.* **2002**, *7*, 473

[79] a) Koike, T.; Kimura, E. *J. Am. Chem. Soc.* **1991**, *113*, 8935. b) Aoki, S.; Kagata, D.; Shiro, M.; Takeda, K.; Kimura, E. *J. Am. Chem. Soc.* **2004**, *126*, 13377

[80] Aoki, S.; Kimura, E. *Rev. Mol. Biotechnol.* **2002**, *90*, 129

[81] Xiang, Q.-X.; Zhang, J.; Liu, P.-Y.; Xia, C.-Q.; Zhou, Z.-Y.; Xie, R.-G.; Yu, X.-Q. *J. Inorg. Biochem.* **2005**, *99*, 1661

[82] Aoki, S.; Zulkefeli, M; Shiro, M.; Kohsako, M.; Takeda, K.; Kimura, E. *J. Am. Chem. Soc.* **2005**, *127*, 9129

[83] Kikuta, E; Aoki, S.; Kimura, E. *J. Am. Chem. Soc* **2001**, *123*, 7911

[84] Jones, K. A.; Peterlin, B. M. *Annu. Rev. Biochem.* **1994**, *63*, 717

[85] Kimura, E.; Kikuchi, M.; Kitamura, H.; Koike, T. *Chem. Eur. J.* **1999**, *5*, 3113

[86] Koenig, B.; Gallmeier, H.-C.; Reichenbach-Klinke, R. *Chem Commun.* **2001**, 2390

[87] Aoki, S.; Jikiba, A.; Takeda, K.; Kimura, E. *J. Phys. Org. Chem.* **2004**, *17*, 489

[88] Liang, X.; Parkinson, J. A.; Weishaeupl, M.; Gould, R. O.; Paisey, S. J.; Park, H.; Hunter, T. M.; Blindauer, C. A.; Parsons, S.; Sadler, P. J. *J. Am. Chem. Soc.* **2002**, *124*, 9105

[89] Bosnich, B.; Poon, C. K.; Tobe, M. L. *Inorg. Chem.* **1965**, *4*, 1102

[90] Gao, J.; Martell, A. E.; Reibenspies, J. H. *Helv. Chim. Acta* **2003**, *86*, 196

[91] Lindoy, L. F.; Mahinay, M. S.; Skelton, B. W.; White, A. H. *J. Coord. Chem.* **2003**, *56*, 1203

[92] Gao, J.; Reibenspies, J. H.; Sun Y.; Martell, A. E. *Helv. Chim. Acta* **2003**, *86*, 563

[93] Kato, M.; Ito, T. *Bull. Chem. Soc. Jpn.* **1986**, *59*, 285

[94] Wragg, D. S.; Hix, G. B.; Morris, R.E. *J. Am. Chem. Soc.* **1998**, *120*, 68287

[95] Morris, R. E. *J. Mater. Chem.* **2001**, *11*, 513

[96] Wheatley, P. S.; Love, C. J.; Morrison, J. J.; Shannon, I. J.; Morris, R. E. *J. Mater. Chem.* **2000**, *12*, 477

[97] Liang, Xiangyang; Weishaupl, M.; Parkinson, J. A.; Parsons, S.; McGregor, P. A.; Sadler, P. J. *Chem. Eur. J.* **2003**, *9*, 4709

[98] Kato, M.; Ito, T. *Inorg. Chem.* **1985**, *24*, 509

[99] Kim, J. C.; Lough, A. J.; Park, H.; Kang, Y.C. *Inorg. Chem. Commun.* **2006**, *9*, 514

[100] Kim, J. C.; Jo, H.; Lough, A. J.; Cho, J.; Lee, U.; Pyun, S. Y. *Inorg. Chem. Commun.* **2003**, *6*, 474

[101] Glidewell, C.; Ferguson, G.; Gregson, R. M.; Lough, A. J. *Acta Crystallogr., Sect. C: Cryst. Struct. Commun.* **2000**, *56*, 174

[102] Suh, M. P.; Min, K. S.; Ko, J. W.; Choi, H. J. *Eur. J. Inorg. Chem.* **2003**, 1373

[103] Suh, M. P.; Choi, H. J.; So, S. M.; Kim, B. M. *Inorg. Chem.* **2003**, *42*, 676

[104] Zakaria, C. M.; Ferguson, G.; Lough, A. J.; Glidewell, C. *Acta Crystallogr., Sect. B: Struct. Sci.* **2002**, *58*, 78

[105] Zakaria, C. M.; Ferguson, G.; Lough, A. J.; Glidewell, C. *Acta Crystallogr., Sect. C: Cryst. Struct. Commun.* **2001**, *57*, 683

[106] Choi, K.-Y.; Ryu, H.; Lim, Y.-M.; Sung, N.-D.; Shin, U.-S.; Suh, M. *Inorg. Chem. Commun.* **2003**, *6*, 412

[107] Shaikh, N.; Panja, A.; Banerjee, P.; Kubiak, M.; Ciunik, Z.; Puchalska, M.; Legendziewicz, J.; Vojtisek, P. *Inorg. Chim. Acta* **2004**, *357*, 25

[108] Namouchi-Cherni, S.; Driss, A.; Jouini, T. *Acta Crystallogr., Sect. C: Cryst. Struct. Commun.* **1999***,55*, 345

[109] Chen, C.-H.; Cai, J.; Liao, C.-Z.; Feng, X.-L.; Chen, X.-M.; Ng, S. W.; *Inorg. Chem.* **2002**, *41*, 4967

[110] Cai, J.; Chen, C.-H.; Liao, C.-Z.; Yao, J.-H.; Hu, X.-P.; Chen, X.-M. *J. Chem. Soc., Dalton Trans.* **2001**, 1137

[111] Cai, J.-W.; Chen, C.-H.; Zhou, J.-S.; *Wuji Huaxue Xuebao (Chin.) (Chin. J. Inorg. Chem.)* **2003**, *19*, 81

[112] Tang, J.-K.; Gao, E.-Q.; Zhang, L.; Liao, D.-Z.; Jiang, Z.-H.; Yan, S.-P. *J. Coord. Chem.* **2002**, *55*, 527

[113] Choi, J.-H.; Suzuki, T.; Kaizaki, S. *Private Communication* to Cambridge Database **2002**

[114] Gao, E.-Q.; Zhao, Q.-H.; Tang, J.-K.; Liao, D.-Z.; Jiang, Z.-H.; Yan, S.-P. *J. Coord. Chem.* **2002**, *55*, 205

[115] Basiuk, E. V.; Basiuk, V. A.; Hernandez-Ortega, S.; Martinez-Garcia, M.; Saniger-Blesa, J.-M. *Acta Crystallogr., Sect. C: Cryst. Struct. Commun.* **2001**, *57*, 553

[116] Basiuk, E.V.; Basiuk, V. V.; Gomez-Lara, J.; Toscano, R. A. *J. Inclusion Phenom. Macrocyclic Chem.* **2000**, *38*, 45

[117] Toby, B. H.; Hughey, J. L.; Fawcett, T. G.; Potenza, J. A.; Schugar, H. J. *Acta Crystallogr., Sect. B: Struct. Crystallogr. Cryst. Chem.* **1981**, *37*, 1737

[118] Gao, E.-Q.; Tang, J.-K.; Liao, D.-Z.; Jiang, Z.-H.; Yan, S.-P.; Wang, G.-L. *Inorg. Chem.* **2001**, *40*, 3134

[119] Benelli, C.; Dei, A.; Gatteschi, D.; Pardi, L. *Inorg. Chem.* **1988**, *27*, 2831; Lemma, K.; Ellern, A.; Bakac, A. *Inorg. Chem.* **2003**, *42*, 3662

[120] Caneschi, A.; Dei, A.; Gatteschi, D.; Tangoulis, V. *Inorg. Chem.* **2002**, *41,* 3508

[121] Caneschi, A.; Dei, A.; de Biani, F. F.; Gutlich, P.; Ksenofontov, V.; Levchenko, G.; Hoefer, A.; Renz, F. *Chem. Eur. J.* **2001***, 7*, 3926

[122] Cador, O.; Dei, A.; Sangregorio, C. *Chem. Commun.* **2004**, 652

[123] Escuer, A.; Vicente, R.; Salah El Fallah, M.; Solans, X.; Font-Bardia, M. *Inorg. Chim. Acta* **1998**, *278*, 43

[124] Ito, H.; Ito, T. *Bull. Chem. Soc. Jpn.* **1985**, *58,* 2133

[125] Cook, D. F.; Curtis, N. F.; Gladkikh, O. P.; Weatherburn, D. C. *Inorg. Chim. Acta* **2003**, *355*, 15

[126] Curtis, N. F.; Swann, D. A.; Waters, T. N. *J. Chem. Soc., Dalton Trans.* **1973**, 1408

[127] Cook, D. F.; Curtis, N. F.; Rickard, C. E. F.; Waters, J. M.; Weatherburn, D. C. *Inorg. Chim. Acta* **2003**, *355*, 1

[128] Simon, E.; Haridon, P.L.; Pichon, R.; L'Her, M. *Inorg. Chim. Acta* **1998**, 282, 173

[129] Ito, H.; Ito, T. *Chem. Lett.* **1985**, 1251

[130] Ito, H.; Ito, T. *Bull. Chem. Soc. Jpn.* **1985**, *58*, 1755

[131] Oshio, H. *Inorg. Chem.* **1993**, *32*, 4123

[132] Nowicka, B.; Schmauch, G.; Chihara, T.; Heinemann, F.W.; Hagiwara, M.; Wakatsuki, Y.; Kisch, H. *Bull. Chem. Soc. Jpn.* **2002**, *75*, 2169

[133] Ballester, L.; Gil, A. M.; Gutierrez, A.; Perpinan, M. F.; Azcondo, M. T.; Sanchez, A. E.; Amador, U.; Campo, J.; Palacio, F. *Inorg. Chem.* **1997**, *36*, 5291

[134] Ballester, L.; Gutierrez, A.; Perpinan, M. F.; Amador, U.; Azcondo, M. T.; Sanchez, A. E.; Bellitto, C. *Inorg.Chem.* **1997**, *36*, 6390

[135] Tadokoro, M.; Sato, K.; Shiomi, D.; Takui, T.; Itoh, K. *Mol. Cryst. Liq. Cryst. Sci. Technol., Sect. A* **1997**, *306*, 49

[136] Chan, H.-L.; Liu, H.-Q.; Tzeng, B.-C.; You, Y.-S.; Peng, S.-M.; Yang, M.; Che, C.-M. *Inorg. Chem.* **2002**, *41*, 3161

[137] Sakai, K.; Yamada, Y.; Tsubomura, T. *Inorg. Chem.* **1996**, *35*, 3163

[138] Vasconcellos, L. C. G.; Oliveira, C. P.; Castellano, E. E.; Ellena, J.; Moreira, I. S. *Polyhedron* **2001**, *20*, 493

[139] Colacio, E.; Dominguez-Vera, J. M.; Escuer, A.; Kivekas, R.; Klinga, M.; Romerosa, A. *Inorg Chem.* **1994**, *33*, 3914

[140] Colacio, E.; Dominguez-Vera, J. M.; Escuer, A.; Kivekas, R.; Klinga, M.; Moreno, J.-M.; Romerosa, A. *J. Chem. Soc., Dalton Trans.* **1997**, 1685

[141] Hughey, J. L.; Fawcett, T. G.; Rudich, S. M.; Lalancette, R. A.; Potenza, J. A.; Schuguar, H. J. *J. Am. Chem. Soc.* **1979**, *101*, 2617

[142] John, E.; Bharadwaj, P. K.; Krogh-Jespersen, K.; Potenza, J. A.; Schugar, H. J. *J. Am. Chem. Soc.* **1986**, *108*, 5015

[143] John, E.; Bharadwaj, P. K.; Potenza, J. A.; Schugar, H.J. *Inorg. Chem.* **1986**, *25*, 3065

[144] Vicente, R.; Escuer, A.; Ribas, J.; Dei, A.; Solans, X.; Calvet, T. *Polyhedron* **1990**, *9*, 1729

[145] Xie, B.; Li, K.-B.; Zou, L.-K.; Mao, Z.-H.; Hong, Z. *Jiegou Huaxue (Chin.) (Chinese J. Struct. Chem.)* **2004**, *23*, 324

[146] (a) De Clercq, E.; Yamamoto, N.; Pauwels, R.; Baba, M.; Schols, D.; Nakashima, H.; Balzarini, J.; Debyser, Z.; Murrer, B. A.; Schwartz, D.; Thornton, D.; Bridger, G.; Fricker, S.; Henson, G.; Abrams, M.; Picker, D. *Proc. Natl. Acad. Sci. U.S.A.* **1992**, *89*, 5286; (b) Inouye, Y.; Kanamori, T.; Yoshida, T.; Bu, X.; Shionoya, M.; Koike, T.; Kimura, E. *Biol. Pharm. Bull.* **1994**, *17*, 243; (c) Inouye, Y.; Kanamori, T.; Sugiyama, M.; Yoshida, T.; Koike, T.; Shionoya, M.; Enomoto, K.; Suehiro, K.; Kimura, E. *Antiviral Chem. Chemother.* **1995**, *6*, 337; (d) Inouye, Y.; Kanamori, T.; Yoshida, T.; Koike, T.; Shionoya, M.; Fujioka, H; Kimura, E. *Biol. Pharm. Bull.* **1996**, *19*, 456; (e) De Clercq, E. *Mini-Rev. Med. Chem.* **2005**, *5*, 805

[147] De Clercq, E. *Mol. Pharmacol.* **2000**, *57*, 833

[148] a) Esté, J. A.; Cabrera, C.; De Clercq, E.; Struyf, S.; Van Damme, J.; Bridger, G.; Skerlj, R. T.; Abrams, M. J.; Henson, G.; Gutierrez, A.; Clotet, B.; Schols, D. *Mol. Pharmacol.* **1999**, *55*, 67; b) Liang, X., Parkinson, J. A.; Weishäupl, M.; Gould, R. O.; Paisey, S. J.; Park, H.; Hunter, T. M.; Blindauer, C. A.; Parsons, S.; Sadler, P. J. *J. Am. Chem. Soc.* **2002**, *124*, 9105

[149] Gerlach, L. O.; Skerlj, R. T.; Bridger, G. J.; Schwartz, T. W. *J. Biol. Chem.* **2001**, *276*, 14153

[150] (a) Hung, Y.; Martin, L. Y.; Jackels, S. C.; Tait, A. M.; Busch, D. H. *J. Am Chem. Soc.* **1977**, *99*, 4029; (b) Hung, Y.; Busch, D. H. *J. Am Chem. Soc.* **1977**, *99*, 4977

[151] Cooksey, C. J.; Tobe, M. L. *Inorg. Chem.* **1978**, *17*, 1558

[152] Mallik, S.; Johnson, R. D.; Arnold, F. H. *J. Am. Chem. Soc.* **1994**, *116*, 8902

[153] Mallik, S.; Johnson, R. D.; Arnold, F. H. *J. Am. Chem. Soc.* **1993**, *115*, 2518

[154] Sun. S.; Saltmarsh, J.; Mallik, S.; Thomasson, K. *Chem. Commun.* **1998**, 519

[155] Lee, E. Y.; Suh, M. P. *Angew. Chem. Int. Ed.* **2004**, *43*, 2798

[156] Pocker, Y.; Stone, J. T. *Biochemistry* **1967**, *6,* 668

[157] Graham, B.; Hearn, M. T. W.; Spiccia, L.; Skelton, B. W.; White, A. H. *Aust. J. Chem.* **2003**, *56*, 1259

[158] Wang, Q.-L.; Xie, C.-Z.; Liao, D.-Z.; Yan, S.-P.; Jiang, Z.-H.; Cheng, P. *Transition Met. Chem.* **2003**, *28*, 16

[159] Chaudhuri, P.; Oder, K.; Wieghardt, K.; Gehring, S.; Haase, W.; Nuber, B.; Weiss, J. *J. Am. Chem. Soc.* **1988**, *110*, 3657

[160] Burger, K.-S.; Chaudhuri, P.; Wieghardt, K.; Nuber, B. *Chem. Eur. J.* **1995**, *1*, 583

[161] Fry, F. H.; Jensen, P.; Kepert, C. M.; Spiccia, L. *Inorg. Chem.* **2003**, *42*, 5637

[162] Chaudhuri, P.; Stockheim, C.; Wieghardt, K.; Deck, W.; Gregorzik, R.; Vahrenkamp, H.; Nuber, B.; Weiss, *J. Inorg.Chem.* **1992**, *31*, 1451

[163] Gross, F.; Muller-Hartmann, A.; Vahrenkamp, H. *Eur. J. Inorg. Chem.* **2000**, 2363

[164] Zhang, L.; Yan, H.-L.; Yan, S.-P.; Jiang, Z.-H.; Liao, D.-Z.; Wang, G.-L. *Pol. J. Chem.* **1999**, *73*, 391

[165] Zhang, L.; Bu, W.-M.; Yan, S.-P.; Jiang, Z.-H.; Liao, D.-Z.; Wang, G.-L. *Polyhedron* **2000**, *19*, 1105

[166] Bencini, A.; Bianchi, A.; Paoli, P.; Garcia-Espana, E.; Julve, M.; Marcelino, V. *J. Chem. Soc., Dalton Trans.* **1990**, 2213

[167] Berreau, L. M.; Mahapatra, S.; Halfen, J. A.; Houser, R. P.; Young Junior, V. G.; Tolman, W. B. *Angew. Chem., Int. Ed.* **1999**, *38*, 207

[168] Gallert, S.; Weyhermuller, T.; Wieghardt, K.; Chaudhuri, P. *Inorg. Chim. Acta* **1998**, *274*, 111

[169] Justel, T.; Muller, M.; Weyhermuller, T.; Kressl, C.; Bill, E.; Hildebrandt, P.; Lengen, M.; Grodzicki, M.; Trautwein, A. X.; Nuber, B.; Wieghardt, K. *Chem. Eur. J.* **1999**, *5*, 793

[170] Jo, D.-H.; Que Junior, L. *Angew. Chem., Int. Ed.* **2000**, *39*, 4284

[171] Shiren, K.; Tanaka, K. *Inorg. Chem.* **2002**, *41*, 5912

[172] Bossek, U.; Haselhorst, G.; Ross, S.; Wieghardt, K.; Nuber, B. *J. Chem. Soc., Dalton Trans.* **1994**, 2041

[173] Muller, M.; Weyhermuller, T.; Bill, E.; Wieghardt, K. *J. Biol. Inorg. Chem.(JBIC)* **1998**, *3*, 96

[174] Schneider, R.; Weyhermuller, T.; Wieghardt, K.; Nuber, B. *Inorg. Chem.* **1993**, *32*, 4925

[175] Wieghardt, K.; Pohl, K.; Bossek, U. *Z. Naturforsch., B: Chem. Sci.* **1988**, *43*, 1184

[176] Bossek, U.; Wieghardt, K.; Nuber, B.; Weiss, J. *Angew. Chem., Int. Ed.* **1990**, *29*, 1055

[177] Niemann, A.; Bossek, U.; Haselhorst, G.; Wieghardt, K.; Nuber, B. *Inorg. Chem.* **1996**, *35*, 906

[178] Knopp, P.; Wieghardt, K.; Nuber, B.; Weiss, J.; Sheldrick, W. S. *Inorg. Chem.* **1990**, *29*, 363

[179] Knopp, P.; Weighardt, K.; Nuber, B.; Weiss, J. *Z. Naturforsch., B: Chem. Sci.* **1991**, *46*, 1077

[180] Jeske, P.; Wieghardt, K.; Nuber, B.; Weiss, J. *Inorg. Chim. Acta* **1992**, *193*, 9

[181] Schneider, J. L.; Young Junior, V. G.; Tolman, W. B. *Inorg. Chem.* **1996**, *35*, 5410

[182] Shores, M. P.; Long, J. R. *J. Am. Chem. Soc.* **2002**, *124*, 3512

[183] Xu, J.-Y.; Gu, W.; Bian, H.-D.; Bian, F.; Yan, S.-P.; Cheng, P.; Liao, D.-Z.; Jiang, Z.-H.; Shen, P.-W. *Inorg. Chem. Commun.* **2003**, *6*, 513

[184] Sudfeld, M.; Sheldrick, W. S. *Z. Anorg. Allg. Chem.* **2002**, *628*, 1366

[185] Chaudhuri, P.; Karpenstein, I.; Winter, M.; Lengen, M.; Butzlaff, C.; Bill, E.; Trautwein, A. X.; Florke, U.; Haupt, H.-J. *Inorg. Chem.* **1993**, *32*, 888

[186] Chaudhuri, P.; Karpenstein, I.; Winter, M.; Butzlaff, C.; Bill, E.; Trautwein, A. X.; Florke, U.; Haupt, H. H. *Chem. Commun.* **1992**, 321

[187] Tadokoro, M.; Toyoda, J.; Isobe, K.; Itoh, T.; Miyazaki, A.; Enoki, T.; Nakasuji, K. *Chem. Lett.* **1995**, 613

[188] Tadokoro, M.; Isobe, K.; Miyazaki, A.; Enoki, T.; Nakasuji, K. *Mol. Cryst. Liq. Cryst. Sci. Technol., Sect. A* **1996**, *278*, 199

[189] Derwahl, A.; Dickie, A. J.; House, D. A.; Jackson, W. G.; Schaffner, S.; Svensson, J.; Turnbull, M. M.; Zehnder, M. *Inorg. Chim. Acta* **1997**, *257*, 179

[190] Justel, T.; Bendix, J.; Metzler-Nolte, N.; Weyhermuller, T.; Nuber, B.; Wieghardt, K. *Inorg. Chem.* **1998**, *37*, 35

[191] Cheng, W.-C.; Yu, W.-Y.; Zhu, J.; Cheung, K.-K.; Peng, S.-M.; Poon, C.-K.; Che, C.-M. *Inorg. Chim. Acta* **1996**, *242*, 105

[192] Yu, W.-Y.; Fung, W.-H.; Zhu, J.-L.; Cheung, K.-K.; Ho, K.-K.; Che, C.-M. *J. Chin. Chem. Soc.(Taipei)* **1999**, *46*, 341

[193] Florke, U.; Haupt, H.-J.; Karpenstein, I.; Chaudhuri, P. *Acta Crystallogr., Sect. C: Cryst. Struct. Commun.* **1993**, *49*, 1625

[194] Giesbrecht, G. R.; Shafir, A.; Arnold, J. *Chem. Commun.* **2000**, 2135

[195] Chaudhuri, P.; Verani, C. N.; Bill, E.; Bothe, E.; Weyhermuller, T.; Weighardt, K. *J. Am. Chem. Soc.* **2001**, *123*, 2213

[196] Yang, R.; Zompa, L. J. *Inorg. Chem.* **1976**, *14*, 1499

[197] Martell, A. E.; Motekaitis, R. J. *Determination and use of stability constants*, 2nd Ed., VCH Publishers Inc. **1992**

[198] Chen, C.-T.; Chen, G.; Guan, Z.; Lee, D.; Arnold, F. H. *Polymer Reprints* **1996**, *37*, 216

[199] Tamil Selvi, P.; Stoeckli-Evans, H.; Palaniandavar, M. *J. Inorg. Biochem.* **2005**, *99*, 2110

[200] Chen, G.; Sundaresan, V.; Arnold, F. H. Polym. Mat. Sci. Eng. **1997**, *76*, 378

V. Appendix

1. ABBREVIATIONS

AC	adenylyl cyclase		GTP	guanosine 5'-triphosphate
Ac	acetyl		GTPγS	guanosine 5'-(γ-thio) triphosphate
ANT	anthraniloyl			
ATP	adenosine 5'-triphosphate		HEPES	4-(2-hydroxyethyl)-piperazine-1-ethane sulfonic acid
AU	arbitrary unit			
CaM	Calmodulin		HMBC	heteronuclear multiple bond coherence
cAMP	adenosine 3',5'-cyclic monophosphate		HPLC	high performance liquid chromatography
CTP	cytidine 5'-triphosphate		HSQC	heteronuclear single quantum coherence
CyaA	exotoxin AC of *Bordetella pertussis*		IC_{50}	half-maximal inhibition concentration
d-	deoxy		IR	infrared spectroscopy
DAD	diode array detector		IMP	inosine 5'-monophosphate
DNA	deoxyribonucleic acid		ITP	inosine 5'-triphosphate
EDTA	ethylene diaminetetraacetic acid disodium salt		ITPγS	inosine 5'-(γ-thio) triphosphate
EF	edema factor		J	coupling constant
EGTA	ethylene glycol tetraacetic acid		k	capacity factor
EI	electronic ionisation		K_d	dissociation constant
eq	equivalents		K_i	inhibition constant
ESI	electronic spray ionisation		K_m	Michaelis Menten constant
Fig.	figure		KO	knockout
FRET	fluorescent resonance energy transfer		LC	liquid chromatography
FS	forskolin		LTP	long-term potentiation
GPCR	G-protein coupled receptor		mAC	membranous adenylyl cyclase

166

MANT	methyl anthraniloyl		TLC	thin layer chromatography
mAU	milli absorbance unit		UTP	uridine 5'-triphospate
Mp	melting point		UV	ultraviolet
mRNA	messenger ribonucleic acid		Vis	visible
MS	mass spectroscopy		V_{max}	maximal velocity
MW	molecular weight		vol/vol	volume/volume
n. d.	not determined		*vs*	*versus*
NDP	nucleoside 5'-diphosphate		XTP	xanthosine 5'-triphospate
NMP	nucleoside 5'-mono phosphate			
NMR	nuclear magnetic resonance			
NOE	nuclear overhauser effect			
NTP	nucleoside 5'-triphosphate			
PDB	protein data bank			
PKA	protein kinase A			
PKC	protein kinase C			
PMEapp	9-[2-(phosphonomethoxy) ethyl]adenine diphosphate			
PMT	photomultiplier			
PP_i	pyrophosphate			
Pr	propyl			
PTFE	polytetrafluorethylene			
R_f	retention factor			
R_t	retention time			
sAC	soluble adenylyl cyclase			
SD	standard deviation			
Sf	*Spodoptera frugiperda*			
TNP	2,4,6 trinitrophenyl			

2. PUBLICATIONS

- Hübner, M.; Geduhn, J.; Pinto, C.; Mou, T. C.; König, B.; Sprang, S. R.; Seifert, R. 2',3'-(*O*)-(*N*-Methyl)anthraniloyl-inosine 5'-triphosphate is the Most Potent Adenylyl Cyclase 1 and 5 Inhibitor Known so far and Effectively Promotes Catalytic Subunit Assembly in the Absence of Forskolin, *Mol. Pharmacol.* **2009** (*in revision*)

- Geduhn, J.; Shen, Y.; Tang, W. J.; Dove, S.; Seifert, R.; König, B. Bis-substituted anthraniloyl-derived nucleotides as potent and selective *Bordetella pertussis* Adenylyl Cyclase Inhibitors (*in preparation*)

- Göttle, M.; Geduhn, J.; König, B.; Höcherl, K.; Seifert, R. Characterization of Mouse Heart Adenylyl Cyclase *J. Pharmacol. Exp. Ther.* **2009** (accepted)

- Taha, H.; Schmidt, J.; Göttle, M.; Suryanarayana, S.; Shen, Y.; Tang, W. J.; Gille, A.; Geduhn, J.; König, B.; Dove, S.; Seifert, R. *Mol. Pharmacol.* **2009**, *75*, 693-703

- Göttle, M.; Dove S.; Steindel, P.; Shen, Y.; Tang, W. J.; Geduhn, J.; König, B.; Seifert, R. Molecular Analysis of the Interaction of *Bordetella pertussis* Adenylyl Cyclase with Fluorescent nucleotides, *Mol. Pharmacol.* **2007**, *72*, 526-535

- Geduhn, J.; Walenzyk, T.; König, B. Transition Metal Complexes of some Azamacrocycles and their Use in Molecular Recognition, *Curr. Org. Synth.* **2007**, *4*, 390-412

3. CONFERENCES

Oral Poster Presentations

- *Transport of adenylyl cyclase inhibitors by lipophilic Zinc(II) – cyclen complexes into living cells* – Workshop Meeting of the graduate colleges GRK 760 and GRK 677 of the German Research Foundation (DFG), Nuremberg, **2007**

- *Transport of adenylyl cyclase inhibitors by lipophilic Zinc(II) – cyclen complexes into living cells* – European Science Foundation (ESF – COST) High level research conference, Inorganic Chemistry: Metal – nucleic acid interactions, Athens, Greece, **2006**

- *Development of New Adenylyl Cyclase Inhibitors* – Workshop of the graduate college "Medicinal Chemistry" (GRK 760), Windberg, **2005**

Poster Presentations

- Symposium "Signal transduction – innovative fount for Pharmacology" Hanover Medical School, Hanover, **2008**

- 49th Annual conference of the German Society of Pharmacology and Toxicology (DGPT), Mainz, **2008**

- Annual Meeting "Frontiers in Medicinal Chemistry" of the German Chemistry Society (GDCh), Frankfurt **2006**, Berlin **2007**, Regensburg **2008**

- Summer School "Medicinal Chemistry", EU-ASIA-Link Medicinal Chemistry, SIOC, Shanghai, China, **2005**

- 2nd/3rd/4th Summer School "Medicinal Chemistry", University of Regensburg, **2004/ 2006/2008**

4. CURRICULUM VITAE

Personal Details

Name:	Jens Geduhn
Date of birth:	04.03.1976
Place of Birth:	Cloppenburg
Status:	married, one daughter, born 08.07

Tertiary Education

03.05 – 04.09	PhD in Organic Chemistry under Prof. Dr. Burkhard König and Pharmacology under Prof. Dr. R. Seifert at the University of Regensburg.
03.04 – 12.04	Diploma-Thesis in Organic Chemistry under Prof. Dr. Burkhard König at the University of Regensburg, thesis on the "Synthesis of chiral azamacrocyclic Metal complexes and their interaction with Thalidomide".
11.99 – 02.04	Chemistry studies at the University of Regensburg.

School Education

06.95	Abitur, majors in Chemistry and Maths
09.92 – 06.95	Gymnasium (grammar school) in Cloppenburg

Internships

08.02 – 09.02	Internship at Bayer Cropscience AG, Department for chemical research, Monheim
02.00 – 03.00	Internship at Remmers Bauchemie GmbH, research lab, Löningen

Professional Experience

04.05 – 07.08   Scientific assistant for student lab courses at the
                       University of Regensburg
07.99 – 09.99   Employment as chemical lab technician, Remmers
                       Bauchemie GmbH, Löningen
08.96 – 07.99   apprenticeship chemical lab technician, Remmers
                       Bauchemie GmbH, Löningen

Academic continuing education

01.06 – 05.08   "Certified project manager in chemical economics"
                       of the German Chemistry Society (GDCh), Prof. J.
                       Leker, Westfälische Wilhelms-University of Münster
04.08   Competence in genetic engineering law, Prof. S.
                       Modrow, University of Regensburg

Scholarship

03.05 – 02.08   Scholarship of the graduate college "Medicinal
                       Chemistry" (GRK 760)